Cortical contributions to landmark integration in the rodent head direction system

James Spencer Street

Institute of Behavioural Neuroscience, UCL

supervised by

Professor Kate Jeffery

Submitted in partial fulfilment of the requirements

for the degree of Doctor of Philosophy at

University College London

September 2019

Declaration

I, James Spencer Street, confirm that the work presented in this thesis is my own. Where information is derived from other sources, I confirm that this has been indicated in the thesis.

James Spencer Street

September 2019

0.1 Abstract

Head direction (HD) cells in the rodent brain can use visual information about surrounding landmarks to 'reset' their represented orientation, to keep it aligned with the world (a process called landmark anchoring). This implies HD cells receive input from the visual system about the surrounding panorama and its landmarks.

Which features in a panorama are used by the HD system? Can HD cells integrate raw luminance input from across the panorama, as might be subserved by subcortical visual processing? Alternatively, do HD cells need discretised landmarks with features, requiring more elaborate visual landmark processing and recognition?

I present work addressing how visual information reaches the HD circuit in rats. In the first experiment, we ask whether HD cells require discrete landmarks to anchor to visual panoramas. We record HD cells in a landmark anchoring paradigm using a visual panorama containing a single gradient shifting gradually from black to grey to black. Although there was evidence HD cells could integrate information from this scene, cue control was weak and less reliable than anchoring to visual landmarks with edges. In the second experiment, I present HD cell recordings in rats with lesions of the lateral geniculate nucleus, the thalamic relay of the cortical visual pathway, to test whether subcortical vision is sufficient for landmark-anchoring. HD cells in these animals showed impaired anchoring to cue cards, and lesion extent correlated with the severity of the impairment.

Together, these findings indicate that the cortical visual pathway is necessary for intact and stable landmark anchoring to visual cues. Although this process can use entire visual panoramas, it may be more precise if distinct features are available in the scene. Landmark processing in the brain may be complex, and further work could probe whether direct projections from visual cortex provide this information to the HD circuit.

0.2 Impact statement

Maintaining a consistent sense of direction necessitates that we integrate information from a variety of sources, including using information about the surrounding visual scene to keep our representations of spatial orientation aligned with the external world. It is through maintaining coherent and stable representations of direction (and place) that we are able to perform cognitive tasks necessitating navigation through our environment. This process seems to often be disrupted in disease. For example, navigation in familiar spaces is frequently impaired as the neurodegenerative pathologies of dementia progress, leading to sufferers often finding themselves lost in daily life. Understandably, impairments in navigating lead to large reductions in quality of life metrics, and put undue stress on both the patient and their primary carers.

Although in its (relative) infancy, it is an overarching aim of neuroscience that understanding how the brain represents space (and how these representations are used) can help to guide therapeutic interventions for those who suffer from disease or disability.

Here, we investigate how vision is integrated into neural representations of spatial orientation in the rat brain. We find that, although these representations can use visual scenes without discrete landmarks, they are able to integrate vision more precisely when the visual panorama contains discontinuities in contrast, such as edges. We also provide evidence that one of the two visual pathways in the rat brain (the cortical visual pathway) is important in extracting landmark information from the visual scene, as damage to this pathway was correlated with impairments in the use of visual landmarks by the direction system in the rat brain.

A thorough understanding of how visual scenes are integrated into a single sense of direction could help to guide work in a number of fields. Understanding which features of a visual panorama are weighted most strongly in this process could help architects and urban planners design spaces that help people to stay oriented while navigating spaces – especially if they are unfamiliar with these places. Technological interventions, utilising an understanding of how vision is used for navigating, could be designed to provide aid to visually impaired people, or to help sufferers of cognitive impairments (e.g. early stages of dementia) navigate better. These interventions could, in principle, help patients remain independent for longer, maintaining greater dignity and reducing the burden of care on close family and healthcare services.

0.3 Table of contents

0.4 List of figures

0.5 List of tables

0.6 List of Abbrieviations

ADN	Antero-dorsal thalamic nucleus
AMN	Antero-medial thalamic nucleus
API	Application programming interface
ATI	Anticipatory time interval
ATN	Anterior thalamic nuclei
AVN	Antero-ventral thalamic nucleus
CA1/2/3	Cornus ammonis 1/2/3 (hippocampal subfields)
DIC	Directional information content
DTG	Dorsal tegmental nucleus
KL	Kullback-Liebler
LGN	Lateral geniculate nucleus
LMN	Lateral mammillary nucleus
LPN	Lateral posterior nucleus
mEC	Medial entorhinal cortex
NMDA	N-methyl-D-aspartic acid
NPH	Nucleus prepositus hypoglossi
HD	Head direction
HPC	Hippocampus
ParaS	Parasubiculum
PFD	Preferred firing direction
PFR	Peak firing rate
ParaS	Parasubiculum
POR	Postrhinal cortex
PoS	Postsubiculum
PrS	Presubiculum
RGC	Retinal ganglion cell
RSC	Retrosplenial cortex
SC	Superior colliculus
Sub	Subiculum
TLP	Tractatus logico-philosophicus
V1	Primary visual area
V2	Secondary visual area
V2M	Medial secondary visual area
V2L	Lateral secondary visual area

0.7 Acknowledgements

First and foremost, I would like to thank Kate Jeffery for the fantastic supervision and guidance she has provided throughout my doctorate. It is thanks to her insight, enthusiasm, and patience that I have become the scientist I am today. Similarly, I would like to thank every PI in the IBN – Dan Bendor, Sam Solomon, Aman Saleem, and Hugo Spiers – for always being so happy to proffer advice, and for the innumerable interesting discussions, often impromptu around the corridors of the offices and the unit.

To the IBN in general: you are all wonderful people, and these years would never have been so much fun without you all. There are too many of you to list here, but I have to extend particular gratitude to Han Cheng, Ningyu Zhang and Merlin Williams – the KateLab student gang. Thank you all for sharing the highs and lows of the PhD with me – and for all the (inebriated) science conversations! To Gioia and Zita: it is because of you two I was integrated into this group – thank you for being such glorious socialites. To Marta and Margot: I will miss distracting you at your desks! Thank you both for always being there; talking to you always cheers me up on a bad day. I must also thank Roddy Grieves, Ele Duvelle, Stefano Zucca, and Giulio Casali – not only for our social times together – but for all of the time and effort they have put into teaching and advising me and others. To Stefano especially, thank you for being the supportive and caring person you are; thank you for being the sort of person who always finds time to care for others when they need it; and thank you for being that person towards me when you saw that I needed it most.

To Elliot – thank you for putting up with me for all of these years. Evenings with you stopped me from going insane, and I will always love you. To Seb – thank you for going insane by my side for these few years. And to my parents – thank you for your unconditional support from the day I was born until now! I would not be here were it not for your unending love, pride, and enthusiasm in everything I do.

Finally – and most importantly – thank you, rats! Every one of you was your own individual, and each one of you was loved and appreciated.

Chapter 1

Introduction to Navigation

Die Welt ist alles, was der Fall ist.

The world is everything that is the case.

TLP 1; Ludwig Wittgenstein

1.1 Ubiquity of navigation

Mobile animals are presented throughout their lives with daily challenges to their survival: the need to forage for food, to discover new shelter, to escape to a known safe place. These challenges frequently share a common element to them: each of these physiological needs necessitates the (successful) traversal and navigation through space. That so many animal species, from insects to humans, navigate throughout their lives demonstrates how fundamental cognitive behaviour regarding space is (Tolman, 1948). Similarly, the extreme behavioural impairments and phenomenological distress seen when these navigation systems fail, and the deterioration in quality of life in cases of neurodegenerative disease causing permanent impairments in navigation (American Psychiatric Association, 2013), demonstrate the importance of navigation in our collective lives.

This thesis will be concerned with how neural populations within the rat brain, which are presumed to underlie many of these cognitive behaviours, function in order to maintain an animal's sense of orientation within an environment. In particular, we address how vision is used by these neural systems to maintain a consistent representation of direction, as vision is known to be an important source of information for navigation from both behavioural (Foo et al., 2005; Youngstrom and Strowbridge, 2012) and electrophysiological (Taube et al., 1990b) evidence. In particular, we ask two questions: (1) can these populations use large visual

panoramas to reorient their directionality and remain oriented in the environment? (2) Which visual areas of the rat brain are involved in processing landmarks to be integrated into neural representations of head direction? We believe these findings add to the growing literature on sensory integration within navigation circuits in the rodent brain.

1.2 Orientation behaviour

1.2.1 Path integration

An animal that navigates away from its home base (e.g. in search of a source of food) will inevitably have to return to its starting point. An intuitive notion is that, if the animal can keep track of how far it moves (or its speed) and in which directions, then it can calculate the route back to its starting point. This process has been called 'path integration', or 'dead reckoning' (Etienne and Jeffery, 2004).

The idea that navigation can rely on a path integrative strategy to solve tasks such as homing was suggested by Darwin:

> We must bear in mind that neither a compass, nor the north star, nor any other such sign, suffices to guide a man to a particular spot through an intricate country, or through hummocky ice, when many deviations from a straight course are inevitable, unless the deviations are allowed for, or a sort of "dead reckoning" is kept.
>
> (Darwin (1873))

Although this process can be largely non-reliant on landmarks and beacons (using senses internal to the animal, such as motor efference copy and the vestibular sense), it has been proposed that during homing tasks animals could use landmarks as reference directions, so as to keep track of their updated heading direction. Examples of such landmarks include the use of the sun by ants or polarised light by bees (Menzel et al., 2005; Kraft et al., 2011; Philippides et al., 2011; Schwarz et al., 2017).

A general diagram demonstrating path integration over a simple path is shown in Figure 1.1A. An animal is initially at home, and makes three straight-line trajectories while searching for food. After finding the food, it is seen to return home along a near-optimal single trajectory – a homing vector. This indicates that the animal has maintained a representation of its direction (relative to home) while navigating, so as to orient itself optimally when returning. This is known as path integration. Most models of path integration will generalise this process, including extending it to arbitrarily large numbers of steps with arbitrarily small temporal extension, so as to enable homing behaviour following large and complex paths (Figure 1.1B).

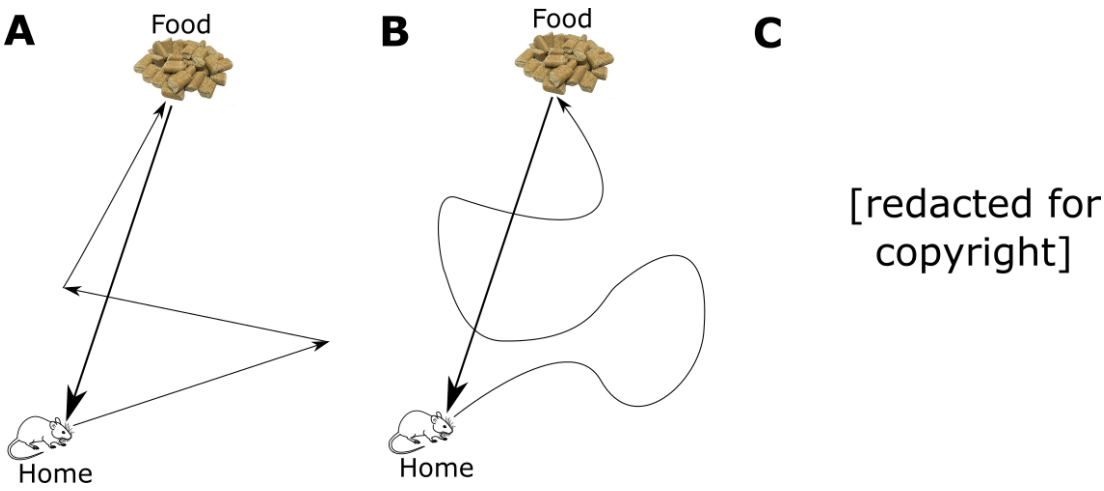

Figure 1.1: Path integration in animals. A: A rodent that makes an outbound journey from its home to food will frequently make a bee-line when returning on its inbound journey to home, rather than returning via the outbound route. This suggests that the rodent has maintained a representation of its bearing (relative to home), and updated this as it moves through space. In this case, the animal's movement consists of three trajectories (thin lines); adding these vectors together gives a 'total' trajectory that can be used to compute the homing vector (thick line). B: Extending this model to allow infinitesimal vectors means that the homing vector (thick line) can be computed from an arbitrarily long and complex route (represented here as a single thin curved line) by taking the path integral along the curve. C: These sorts of homing behaviours have been observed in numerous species, including ants. Here, an ant that has foraged for food (thin lines) is seen to return home along a near-optimal vector (thick line), indicating it has path integrated along its foraging trajectories. Adapted from (Wehner, 2003).

This sort of homing behaviour is remarkably well-described by the general model, and has been observed in numerous species, such as the ant (shown in Figure 1.1C. from Wehner (2003)).

Path integration as an ongoing process is error accumulative: that is, small errors in estimates of speed and direction change at each timestep will tend to accumulate, over many timesteps, to a significant size. This could lead to estimates of, for example, home location, that are far away from its true location, and more complex or longer paths will lead to more substantial errors. Consistent with this, data from the hamster show that animals can navigate more accurately back to a home nest following an outward journey to food if the journey is direct and contains fewer turns and less linear distance (Séguinot et al. (1993), although hamsters remained well-oriented in general throughout this experiment).

As such, information about the external world – such as prominent landmarks that may provide a reference direction for the path integrative model – can be used to keep a representation of direction anchored and to minimise drift. Again, rodents appear to behaviourally utilise distal cues that provide directional information when performing homing tasks (see Section 1.2.2), and computational models can similarly integrate external (visual) information and self-motion cues (Page and Jeffery, 2018). However, how this integration occurs in the brain is unknown, and this thesis will address how visual information about the world is combined with abstract

representations of direction in the rat brain.

1.2.2 Rodent orienting behaviour

Rodents are an example taxonomic family that reliably demonstrate good path integrative behaviours. Following a period of exploration on an arena, after which an animal will be displaced from its home nest, the animal will tend to take a direct 'bee-line' path back to its home nest. This can occur in the absence of external cues provided through vision and olfaction (Etienne, 1980; Etienne et al., 1985), and is true for numerous rodents, including rats (Benhamou, 1997), mice (Alyan and Jander, 1994), gerbils (Mittelstaedt and Mittelstaedt, 1980), and hamsters (Séguinot et al., 1993). Rodents maintain the ability to path integrate back to home following passive transportation to a displaced location, as opposed to actively locomoting there (Bovet, 1984; Etienne et al., 1986). Disruption of the vestibular sense impairs path integrative behaviours in the rat (Wallace et al., 2002), indicating that this sense may be one source of internal self-motion information for the maintenance of a sense of direction.

As would be expected from a useful path integrative model (Etienne and Jeffery, 2004), when solving homing tasks rodents do not solely rely on an internally-updated path integration estimate, but also use external cues such as visual landmarks to remain oriented and minimise accumulated error (Etienne et al., 1985). Hamsters navigating to their home nest following foraging for food tended to orient their homing trajectories relative to a distal light cue (Etienne et al., 1990). However, this only occurred when the orientation implied by the cue was not in substantial conflict with the animal's path integrative estimate; if so, the animal ignored the light and relied on an internally maintained sense of direction. This suggests that the animal is integrating information about the distal visual scene, where useful, into its representation of direction.

These findings led to the conclusion that rodents maintain a representational sense of direction as a sort of 'compass' (Etienne, 1980), influenced by both internal (e.g. vestibular, Wallace et al. (2002)) and external (e.g. visual, Etienne et al. (1990)) information and which may be used to navigate.

1.3 Neural correlates of navigation

That neural activity of the brain underlies cognitive processes such as navigation and reorientation discussed above is a central tenet of modern neuroscience research (Bennett and Hacker, 2003). This in part arises from the observation that damage to restricted areas of the brain in various species results in characteristic deficits in performance on spatial tasks (see Section

Figure 1.2: (REDACTED FOR COPYRIGHT) Schematic of a recording setup for single-unit recordings. The rat with implanted electrodes is able to freely explore an arena, and is plugged into a headstage. Neural signals are propagated through a pre-amplifier circuit, into a system unit (for digitisation and alignment with behavioural readouts, such as position tracking from a camera), and into a computer for analysis. Taken from Jeffery et al. (2018).

1.4.3).

With the advent of chronic electrophysiology, in which animals are implanted *in vivo* with microelectrodes targeted to a brain region of interest, neuroscience saw a shift in methods towards finding behavioural correlates of brain activity. These methods allowed the activity of single neurons to be recorded, and correlated with the behaviour of the implanted animal. Figure 1.2, from Jeffery et al. (2018), shows a typical chronic electrophysiology setup, and Chapter 3 contains a more detailed description of the technique.

Within the field of spatial navigation, a paradigm shift of sorts occurred following the observation of cells in the rat hippocampus that only fired action potentials when the animal was positioned in a specific part of an environment it was exploring (O'Keefe and Dostrovsky, 1971). These 'place cells' triggered decades of ongoing research into the discovery, characterisation, and modelling of representations of space and orientation in the brain, with an aim to formulate a description of how the brain transforms sensory information about oneself and the world into abstract representations that could underlie a cognitive sense of place or direction.

Some of the neural correlates found and categorised will be briefly reviewed here, before the representation of heading direction in the brain will be described in more detail. Although discussions here will be limited to the main spatial cells discovered over the past few decades, many other cells have been discovered that may comprise the cognitive map in various species – including the egocentric border cell (Alexander et al., 2019; Laurens et al., 2019), centre-bearing cell (LaChance et al., 2019), object vector cell (Wang et al., 2018; Høydal et al., 2019), and goal vector cell (Sarel et al., 2017). However, the relationship of these cells to directional representations in the brain is unclear, and they will not be discussed here in detail. A recent and thorough review of the diverse representations of space in the animal brain can be found in Grieves and Jeffery (2017).

1.3.1 Neural correlations of orientation: head direction cells

> The manner in which the sense of direction is sometimes suddenly disarranged in very old and feeble persons, and the feeling of strong distress which, as I know, has been experienced by persons when they have suddenly found out that they have been proceeding in a wholly unexpected and wrong direction, leads to the suspicion that some part of the brain is specialised for the function of direction.

(Darwin (1873))

As well as representing where it is, an animal should also have a cognitive representation of the direction it is facing. Without something to provide directional information to the animal, orienting correctly to navigate, for instance, home, would be difficult in any non-trivial environment.

Head direction (HD) cells represent, as a population, the direction an animal's head faces in an environment. An individual HD cell is characterised by its tuning curve – an activity profile of the cell's average firing rate at each direction on the azimuth plane. The cell's firing rate is maximal when the animal faces a specific direction – the cell's preferred firing direction (PFD) – and drops to zero as the animal faces further from the PFD. As such, each HD cell displays a unimodal tuning curve, an example of which is shown in Figure 5.7C.

This figure shows an example HD cell, recorded by the author, from a rat exploring a flat plane inside a cylinder. The tuning curve of this HD cell indicates that this cell fired preferentially when the animal was facing the 'North-West' of the environment, when the top of the image is arbitrarily defined as 'North' (in spite of this nomenclature, there is little evidence that HD cells encode information in a global Earth-centric reference frame). This corresponds to a PFD of 117°, where (following mathematical nomenclature) 0° corresponds to East, and anti-clockwise is positive. When the animal faced any other direction, the cell was (near) silent, and fired few action potentials.

The HD cell signal is thought to be generated by the integration of a vestibular angular head velocity signal (see Section 1.4.4). This is similar to the transformations seen in path integration models that update using self-motion cues (Etienne and Jeffery, 2004), and so the HD cell provides a plausible neural substrate for a 'neural compass' that encodes and maintains an animal's sense of direction as it explores. Just as path integration models can also maintain a representation of orientation relative to a prominent landmark in the environment, HD cells also integrate allothetic information about the external world, and are influenced by the presence of visual and olfactory landmarks. However, HD cells are not dependent on these inputs, and generally continue to fire in complete darkness.

HD cells (or directional neurons) have been observed in a large number of species from various taxonomic classes, consistent with the idea that representing heading direction is an evolutionarily basic requirement for locomoting species. These species include numerous rodents (rats: Taube et al. (1990a,b), mice: Khabbaz et al. (2000); Yoder and Taube (2009), gerbils: Mankin et al. (2019)), bats (Egyptian fruit bats: Finkelstein et al. (2018), big brown bats: Rubin et al. (2014)), non-human primates (rhesus macaques: Robertson et al. (1999)), humans, and insects (flies: Seelig and Jayaraman (2015), locusts: Pegel et al. (2019)).

1.3.1.1 Attractor architecture of the HD system

Each individual HD cell possesses its own PFD. In an area of the brain containing HD cells, there will be a large population of these neurons, each with its own PFD; the PFDs of different HD cells will be different, and are uniformly circularly distributed. As such, all possible directions on the azimuth plane are represented by the HD system: some HD cells will be active whenever the animal faces a given direction (as this direction is their PFD), and the remainder will be silent. Theoretically, if one could observe the activity of many HD neurons simultaneously, one could decode from their population activity the direction of the animal's head at any given time (Peyrache et al., 2015).

It is a well-observed phenomenon of HD cells that the population behaves coherently: that is, if one HD cell shifts its PFD by n° (perhaps due to the rotation of a prominent landmark, Yoganarasimha et al. (2006)), all other cells in the population shift by the same angle[1]. Work that has co-recorded multiple HD cells at the same time has found that this coherent relationship between HD cells is maintained even during sleep (Peyrache et al., 2015), when other spatial cells lose coherence (such as place cells, see Section 1.3.3.1, Yoganarasimha et al. (2006)), and before eye-opening in rat pups (Bjerknes et al., 2015).

These findings have led to the description of the HD system as a 1-dimensional ring attractor (Skaggs et al., 1995; Redish et al., 1996; Zhang, 1996; Boucheny et al., 2005; Song and Wang, 2005). As differences between proposed attractor models are beyond the scope of this thesis, attractor models will not be reviewed here in detail. However, most models are similar in their basic construction (see Sharp et al. (2001a) for an early discussion); the fundamental principle of these models is that the set of HD cells are organised as a 'ring', as shown in Figure 1.3, taken from Skaggs et al. (1995). Here, each HD cell is positioned on the ring according to its PFD (note that there is no evidence that the HD cells are physically organised in this way, or display any sort of topography in the rat brain). The cells are recurrently connected such that 'nearby' cells (those with similar PFDs) excite one another, and 'distant' cells (with very different PFDs) inhibit one another.

Even in the absence of external inputs, this architecture is self-stabilising (Zhang, 1996), causing only a subset of HD cells with similar PFDs to be active at a given time (the attractor's 'activity packet')[2]. Any 'unstable' configuration – such as two cells with opposite PFDs being active simultaneously – will quickly evolve over time (as the cells will inhibit one another) into

[1] A corollary of this is that recording a single HD cell is sufficient to infer the activity of the entire population of HD cells.

[2] That only a restricted manifold on the population's state space is 'stable', and all other points in the state space are unstable and will evolve towards a stable point over time, is the defining characteristic of attractor models. In the case of HD cells, the stable manifold is defined by a 1-dimensional line through the state space (Burgess, 2006).

Figure 1.3: (REDACTED FOR COPYRIGHT) An attractor network model of the HD system. HD cells (light grey) are organised in a 'ring', such that each direction is encoded by an active subpopulation of these cells. Recurrent connections excite nearby cells, and inhibit far away cells, such that this activity packet is stable and localised on the ring. Input from visual cells (dark grey) onto a subpopulation of HD cells can, if strong enough, draw the activity packet to the cells receiving this visual input. If this input is provided from (e.g.) a visual ring encoding a familiar landmark, this orients the HD attractor to align with the known environment. As the animal turns, vestibular input drives a different 'rotation' ring (white cells), akin to the observed HDxAHV cells. A rotation ring exists for each turn direction, and these rings input onto the HD ring, connecting with the HD cells nearby their own preferred direction. The effect of this is to drag the activity packet clockwise if the animal turns clockwise, or anticlockwise if it turns anticlockwise. As such, idiothetic information about self-motion can be used to maintain a representation of head-direction. Figure taken from Skaggs et al. (1995).

a stable state in which only one of these two cells remains active, and thus as a population the ring will code for a single azimuth direction.

External inputs can be used to shift the activity packet of the attractor network. Self-motion inputs, that in principle could arrive from the vestibular system, could shift the activity packet on the ring left or right as the animal makes left or right head turns; this would be akin to integrating representations of angular head velocity into a representation of angular direction (Sharp et al., 2001a). Indeed, a number of cells with behavioural correlates similar to those predicted to drive this transformation have been observed (see Section 1.4.4.1). Similarly, external inputs about the directions of prominent landmarks in the world that project into the attractor ring can shift the activity packet (and thus reorient the whole attractor) to be in alignment with a learned external world (Boucheny et al., 2005; Page et al., 2014).

With this architecture, the model emulates known properties of the HD system such as network coherence between individual cells (Zhang, 1996), path integration of angular movements (Stringer et al., 2002; Laurens and Angelaki, 2018; Page et al., 2018), and integration of external allothetic information into its representation of direction (such as input from 'visual cells', Boucheny et al. (2005); Page et al. (2014); Jeffery et al. (2016)).

1.3.2 Neural correlates of orientation: Non-HD cells

Besides the traditional HD cell, numerous cells have been identified that are directionally modulated, but do not display the stereotypical unimodal tuning curve.

One such recorded neuron is the bi-directional cell – a neuron that exhibits a tuning curve with two opposed peaks at 180° apart (Jacob et al., 2017). These cells were recorded from an environment consisting of two rotationally symmetric compartments, each with a cue card attached to the wall. It has been proposed that these neurons represent a sort of 'local directionality', in which the local visual scene in each compartment is associated with an azimuth direction; the rotational symmetry of the compartments then generates the 180° separation of

the two tuning curve peaks. These cells are discussed further in Sections 1.4.1.2.1 and 2.6.

A different directional neuron that has been described is the axis cell in subiculum (Olson et al., 2016), which was seen to encode the current axis of travel of a rat exploring a branching T-maze. These neurons display bimodal tuning curves similar to the bi-directional cell, such that the cell will fire whenever the animal faces a direction or the opposite direction on the T-maze.

That these more complex representations of direction exist demonstrate the complexity of landmark integration that may occur in the brain, with neurons learning to encode conjunctions of geometry, boundaries and directions.

1.3.3 Neural correlates of location

1.3.3.1 Place cells

The first spatial neuron recorded from the rodent brain was the place cell (5.7A), traditionally found in the pyramidal layers of hippocampal fields CA1, CA2, CA3 and the dentate gyrus. These cells exhibit location-specific firing, such that the cell only fires when the animal is located inside a restricted portion of the environment (its 'place field') and is near silent elsewhere (O'Keefe and Dostrovsky, 1971). As such, an entire environment is represented by a population of place cells, with different populations of cells representing different environments. This finding led to the argument that neural correlates of location in the hippocampus underlies (in part) the behavioural 'cognitive map' of an animal that needs to cognitively represent this space (O'Keefe and Nadel, 1978),

Functional characteristics of place cells have been intricately studied and will not be reviewed here. However, similar to the HD cell population, the activity of place cells has been shown to be influenced by a variety of allothetic and idiothetic information. The location of the place field is partially determined by distal visual cues and landmarks in an environment (Yoganarasimha et al., 2006), although place cells retain place-specific firing in the dark (Save et al., 2000). A review of the numerous sensory modalities integrated into the abstract representation of place in the rodent hippocampus can be found in Jeffery (2007). Numerous models of place cell firing have been proposed that can generate restricted firing fields in space (some of which are discussed in Grieves and Jeffery (2017)), including from grid cells (Section 1.3.3.2) and boundary-related cells (Section 1.3.3.3). Both of these types of cells are thought to require inputs from HD cells.

Outside of the hippocampus cells have been recorded that display place fields qualitatively similar to those of traditional place cells. These 'place-like' cells have been recorded in a number of HD areas (see Section 1.4.1), but also in numerous other brain structures including

the claustrum (Jankowski and O'Mara, 2015) and dorsal lateral geniculate nucleus (Hok et al. (2018), see Chapter 2).

1.3.3.2 Grid cells

Another form of representation of location exists in the grid cells, which have been proposed to provide a form of odometric encoding of distance (Solstad et al., 2006). Rather than solely be active within a single place field, these cells fire whenever the animal is within one of multiple firing fields organised in a hexagonal lattice over the environment (see Figure 5.7B). These cells, found in mEC (Fyhn et al. (2004); Hafting et al. (2005), see Section 1.4.1.2.2) and subicular cortices (Sharp and Green (1994); Sharp (1999); Boccara et al. (2010), see Section 1.4.1.1), may drive place cell activity in hippocampus, with a single place field generated by combining inputs from grid cells with different spacings between their grid fields (Solstad et al., 2006). However, empirical evidence may question this model of place cell activity (Bush et al., 2014), with place cells still exhibiting location-specific firing following the inactivation of grid cells (Koenig et al., 2011; Brandon et al., 2014).

1.3.3.3 Border cells

Border cells, that fire when an animal is in proximity to a particular barrier or border in an environment, have also been described (Solstad et al., 2008; Lever et al., 2009). These cells, notably found in the mEC (Solstad et al. (2008), see Section 1.4.1.2.2) and subicular cortices (Lever et al. (2009), see Section 1.4.1.1), may be related to boundary vector cells modelled as a theoretical generative input for place cell firing (Burgess and O'Keefe, 1996; O'Keefe and Burgess, 1996).

Indeed, boundary vector cells were predicted to exist before first detailed report of their experimental existence was published (Barry et al., 2006). However, it has been argued that boundary vector cells and border cells behave differently following, for example, the addition or removal of a barrier (Stewart et al., 2014), and so these cells may belong to two distinct populations with different computational or cognitive functions (Derdikman, 2009). The explicit relationship between border and HD cells is unknown, but it is generally believed that boundary vector cells require an intact HD signal, and in general rotational shifts of boundary vector cell representations correlate with rotations of the HD signal (Stewart et al., 2014) and the encoding of allocentric boundaries provides a plausible model to explain some place cell phenomena such as place field repetition across multiple visually similar compartments (Grieves et al., 2018).

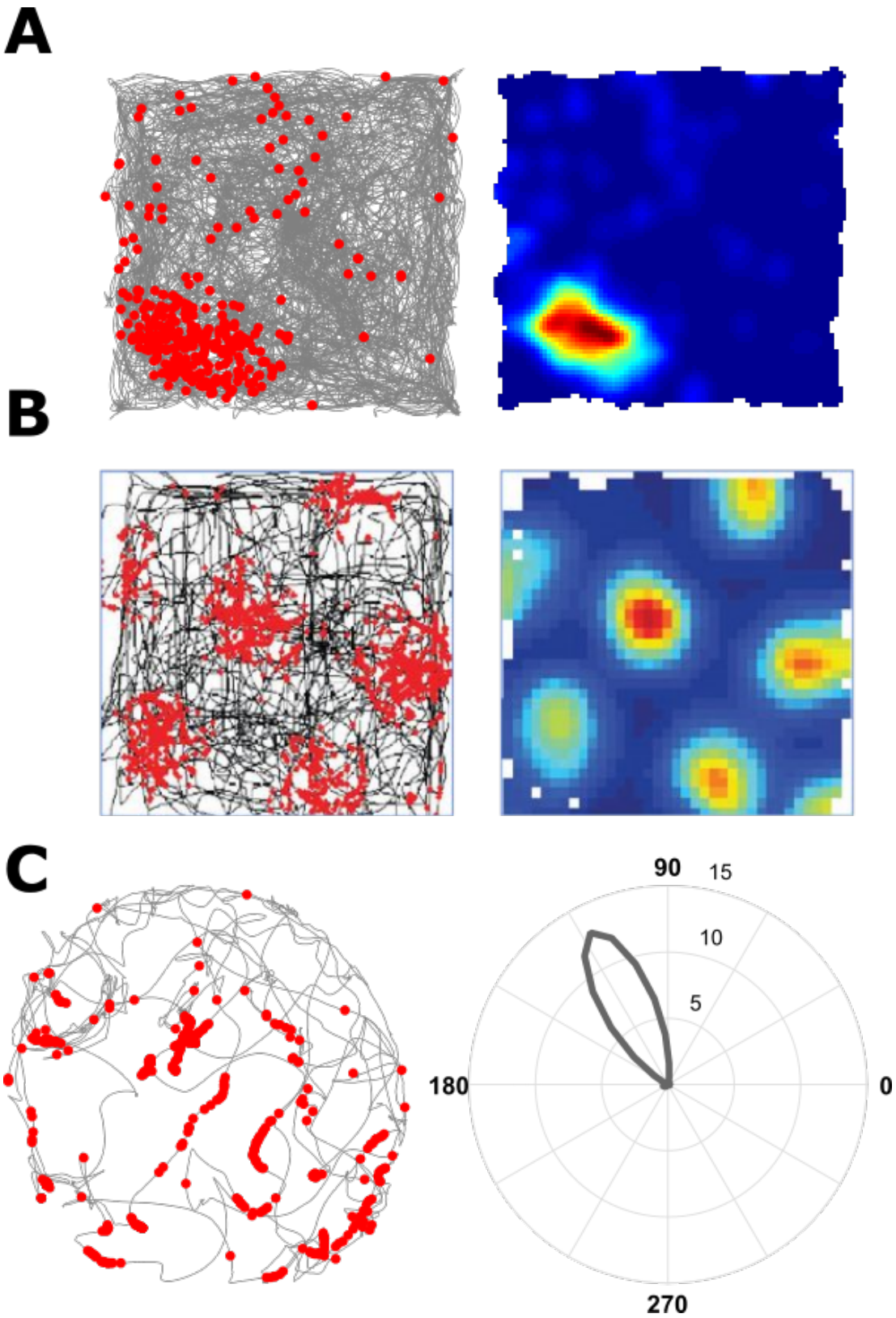

Figure 1.4: Examples of spatial cells recorded in the rodent. Each plot shows the cell spikes in red, overlayed with on the animal's path (left), alongside the corresponding ratemap (for cells A and B) and directional tuning curve (for cell C) A: An example hippocampal place cell (recorded by Roddy Grieves). B: An example entorhinal grid cell (taken from Moser et al. (2015)). C: An example postsubicular HD cell, recorded by the author.

1.4 Head direction cells in the rodent brain

1.4.1 Electrophysiology in areas of the HD system

HD cells were first discovered in the postsubiculum (PoS) of the rat (Taube et al., 1990a,b). Over the following decades, HD cells were subsequently discovered in numerous interconnected regions around the rat brain, including within cortex, thalamus, and brainstem.

This section will review some of the regions in which HD cells have been reported in terms of the functional characteristics of HD cells and other spatial cells recorded there. Subsequently, evidence for the functional connectivity of the HD circuit will be discussed.

1.4.1.1 Subicular cortices

The subicular cortex is a parahippocampal region with strong connections to the hippocampus proper (Hopkins, 2005), although some authors have claimed the subicular complex is a part of the hippocampal formation in light of it receiving a substantial portion of the hippocampal output (Amaral and Witter, 1995).

In this thesis the nomenclature of van Groen and Wyss (1990c) will be adopted, in which the rat subicular cortex will be segmented into four distinct regions: the postsubiculum (PoS), alongside the parasubiculum (ParaS), (ventral) presubiculum (PreS) and subiculum proper (the authors recognise that the prosubiculum, although present in some mammals, is not evident in the rat). The subiculum proper, in particular, has sometimes been categorised separated from other parahippocampal regions (O'Mara et al., 2009), in light of its role as the main projection target of efferents from hippocampal CA1 (Amaral et al., 1991).

The distinction between the PoS and PreS in the rat has historically been a matter of some debate, with some early authors considering the PoS to be synonymous with the dorsal extent of PreS (Krieg, 1946). However, distinct histological landmarks exist within the PoS that are not present within the PreS: layer II of PoS contains dense 'islands' of neuron bodies, and layer III is parallel to the pia mater bordering the ventricle. Further, the functional connectivity of the PoS differs from that of its neighbouring PreS (van Groen and Wyss, 1990c).

HD cells have been reported in all subregions of the subicular cortices: the postsubiculum (Taube et al., 1990a), presubiculum (Boccara et al., 2010), parasubiculum (Taube, 1995b; Boccara et al., 2010), and subiculum (Muller et al., 1991; Sharp and Green, 1994). These areas frequently also contain cells with spatial correlates: including the discovery of place-like cells in subiculum (Muller et al., 1991; Sharp and Green, 1994), parasubiculum (Taube, 1995b) and pre-/post-subiculum (Cacucci et al., 2004), grid cells in pre-/parasubiculum (Boccara et al.,

2010), and border cells in subiculum (Lever et al., 2009; Stewart et al., 2014). The dense interconnectedness between these regions, and the rich variety of spatial cells found here, implies that the subicular cortices play an important role in the processing and routing of spatial information throughout the hippocampal formation.

1.4.1.1.1 PoS

The PoS is well connected with numerous areas of both the HD circuit and in the wider (para)hippocampus. It is known to receive substantial inputs from (granular) retrosplenial cortex, and anterodorsal, anteroventral and laterodorsal thalamus – all areas within the HD circuit (see below). The subiculum, entorhinal cortex, CA1, and visual cortex also project to PoS. These inputs frequently display a layer-specific topography, and are summarised in Figure 1.6.

The PoS sends heavy projections to the anterior and laterodorsal thalamic nuclei, as well as to retrosplenial cortex (most strongly to granular b cortex), perirhinal cortex, entorhinal cortex, and the lateral mammillary bodies. Smaller efferent projections may also terminate in the dorsal tip of the thalamic reticular nucleus and nucleus reuniens. Most efferent projections from the PoS have been observed to be ipsilateral, although projections to entorhinal and perirhinal cortices may be bilateral (van Groen and Wyss, 1990c). The location and connectivity of the PoS make it a candidate region to distribute the HD signal to areas containing other spatial cells – such as the grid cells of entorhinal cortex (see Section 1.4.4.5).

Although beyond the scope of this review, the PoS has been well characterised electrophysiologically *ex vivo* (Funahashi and Stewart, 1997a,b; Abbasi and Kumar, 2013; Simonnet et al., 2013), with spiking properties and morphological characteristics defining up to seven distinct cell types which are frequently distributed within the PoS in a layer-specific fashion (Abbasi and Kumar, 2013). One unsupervised clustering method applied to morphological and action potential properties of PoS and PreS neurons recorded *ex vivo* identified three clusters corresponding to neurons in layers II/III, layer IV, and layers V/VI (Simonnet et al., 2013). This maps well to anatomical tracing experiments that show the PoS/PreS projections to mEC arise from layers II/III (Huang et al., 2017), layer IV projects to LMN, and layers V/VI project to the ATN (Yoder and Taube, 2011; Huang et al., 2017), all areas within the canonical HD circuit. This is summarised in Figure 1.7, taken from Huang et al. (2017).

The HD cell was first reported in the PoS (Taube et al., 1990a,b). 25.5% (61/239) of cells recorded from the PoS were classified as HD cells, which displayed a mean peak firing rate of 35.7 Hz, and on average displayed a 83.4° tuning curve width (Taube et al., 1990a), although these characteristics frequently vary between reports (for example, see Lozano et al. (2017)).

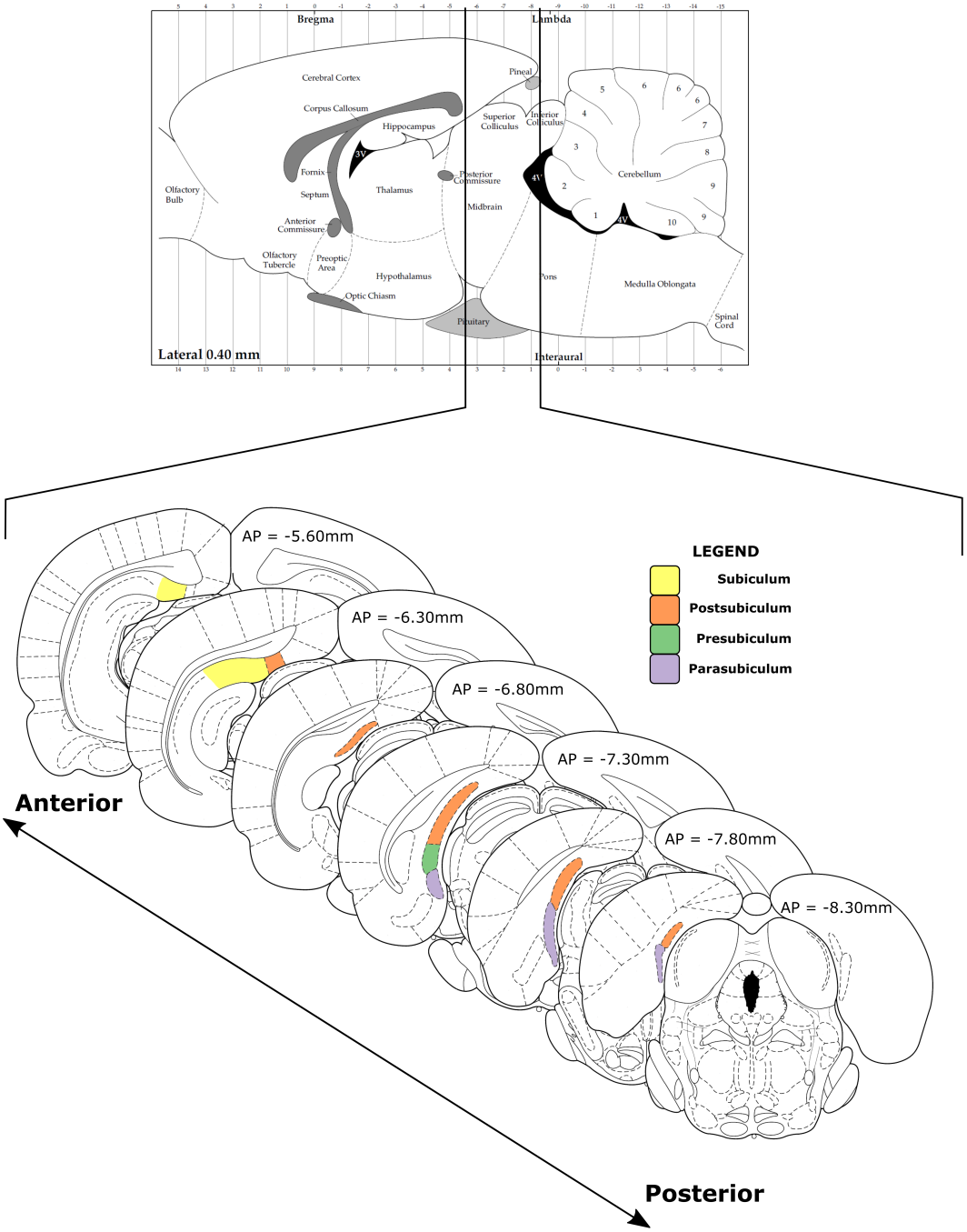

Figure 1.5: Schematic showing the extent of areas of the subicular cortex through the rat brain. Upper: A sagittal atlas plate through a rat brain, with vertical lines detailing the approximate anteroposterior extent of the coronal slices below. Bottom: 6 coronal atlas plates with subregions of the subicular complex.

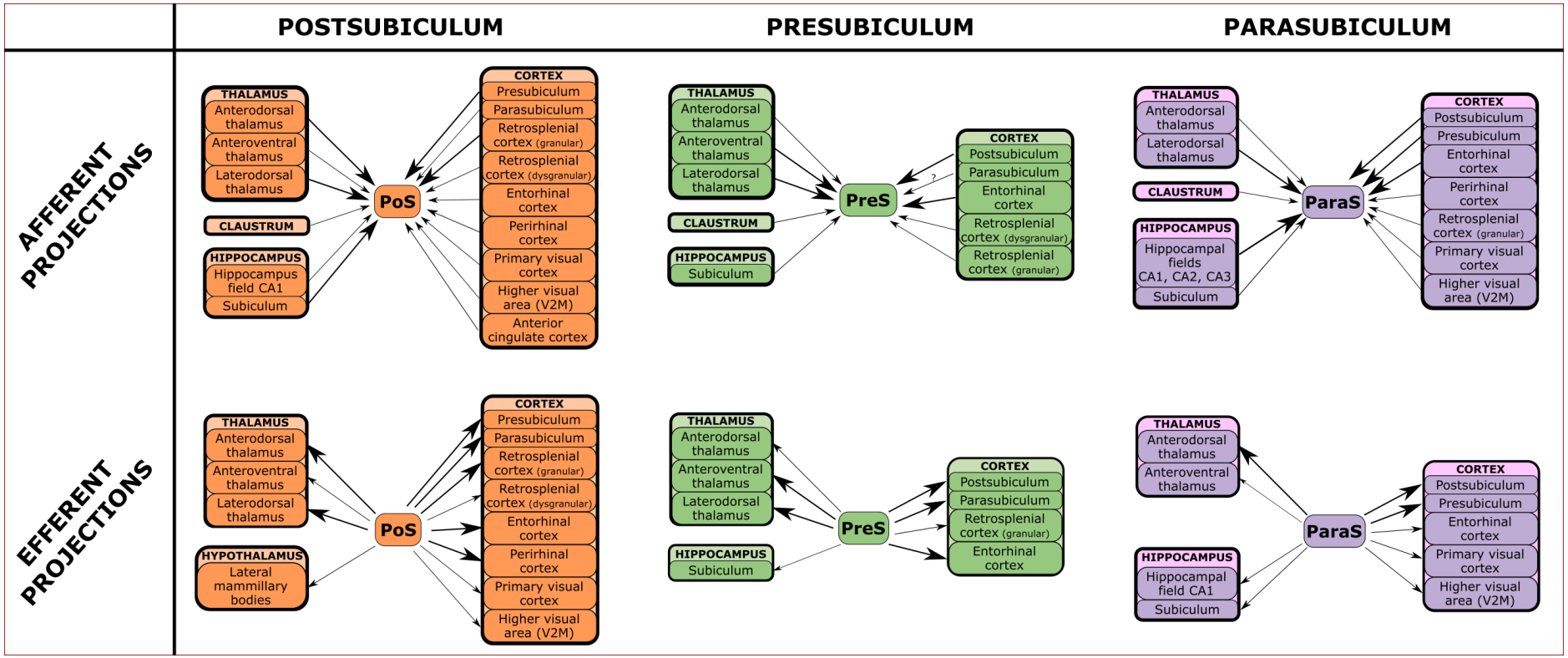

Figure 1.6: Summary of connections of subregions of the subicular complex. Constructed from van Groen and Wyss (1990c,a).

Figure 1.7: (REDACTED FOR COPYRIGHT) Summary of projection neurons in the presubiculum. Neurons targeting the mEC arise from Layers II and III; neurons in Layer II also target the contralateral RSC and presubicular cortices. Layer IV sends projections to LMN, and Layers V/VI send efferents to the anterior thalamus. Figure from Huang et al. (2017).

The directionality of HD cells was stable both within and between trials, and was consistent across multiple days. The distribution of HD cell PFDs was not found to be significantly different from uniform, indicating that all directions were represented equally. That these were not visual cells, that might encode when the animal's visual input matches a remembered viewpoint, is suggested by the persistence of directional firing after the removal of visual cues (Taube et al., 1990b), and in darkness or blindfolded (Goodridge et al., 1998). A HD cell recorded in one environment is directional in a different and visually distinct environment (see, for example, Lozano et al. (2017)), indicating that these cells are encoding abstract head direction and not only a conjunction of allothetic directional cues.

Although analyses in early papers found some limited evidence that PoS HD cell firing rates are also modulated by the animal's position (Taube et al., 1990a), geometric confounds that restricted complete directional sampling in certain places (such as near walls) prevented detailed analysis. With more nuanced analysis pipelines, there is now good evidence that a subpopulation of HD cells in the PoS (and PreS/ParaS) are modulated by position and therefore carry true spatial information (Sharp and Green, 1994; Sharp, 1999; Cacucci et al., 2004; Boccara et al., 2010; Peyrache et al., 2017). Whereas the firing rates of classical HD cells in the PoS are not modulated by theta oscillations in the local field potential, conjunctive place-by-HD cells identified in the PoS appear to display significantly greater theta-modulation (Cacucci et al., 2004). Interestingly, in mice, the non-theta-modulated HD cells appear to be more driven by landmarks than theta-modulated HD cells (see Section 1.4.5, Kornienko et al. (2018)). This leads to the plausible interpretation that some HD cells in PoS conjunctively code for heading direction and vision, and are not constrained by the attractor dynamics of the HD system.

A number of PoS spatial neurons may conjunctively code for HD and proximity to environmental boundaries (Peyrache et al., 2017), similar to border cells seen within the subiculum (Lever et al. (2009); Stewart et al. (2014)) and medial entorhinal cortex (Solstad et al., 2008; Savelli et al., 2008). There also exists a grid cell population in the PoS, although this was lower than the proportions found in the neighbouring ParaS and mEC (Boccara et al. (2010), see Section 1.4.1.2.2).

That neurons in the PoS encode a variety of spatial, directional and temporal correlates solidifies the important position of the area within spatial circuitry of the brain. However,

various other areas also contain neural codes for direction, creating a densely connected network underlying the neural correlates of orientation (see Section 1.4.4). In particular, spatial and directional representations in the ParaS and PreS are similar to those in the PoS (Cacucci et al., 2004; Boccara et al., 2010), with these areas all containing qualitatively similar HD cells, grid cells, border cells and conjunctions of these representations.

1.4.1.2 Other cortical areas

1.4.1.2.1 RSC

Chronic implants in the posterior cortex of the rat discovered HD cells in numerous regions of cortex, including in the retrosplenial cortex (RSC; Chen et al. (1994b,a); Cho and Sharp (2001)). These papers reported that approximately 10% of cells displayed significant directionality (as per the Rayleigh vector length) whilst rats foraged in a radial arm maze. This percentage is consistent with subsequent studies recording RSC HD cells (Jacob et al. (2017): 9%).

The RSC is divided histologically into a granular and an agranular region (gRSC and aRSC respectively, (Mitchell et al., 2018)), with HD cells being observed in both areas. Although the majority of connections in the RSC originate in the RSC itself, it is also well situated within spatial circuits, with interconnections with the hippocampus, parahippocampal cortex, and spatial thalamus (Mitchell et al., 2018). Appropriately, single-unit electrophysiological work has found numerous correlates of place, direction, speed, angular head velocity, and conjunctions of these encoded in the RSC (see Mitchell et al. (2018) for review).

HD cells in the RSC are qualitatively similar to those seen in the PoS, with clear unimodal tuning curves. However, the peak firing rates of RSC HD cells are generally higher than those seen in the PoS (22.4 ± 2.6 Hz in the RSC versus 8.1 ± 0.6 Hz in the PoS), and there is evidence that HD tuning curves are slightly wider in the RSC ($49.3 \pm 1.3°$) than those in the PoS ($43.7 \pm 1.1°$, Lozano et al. (2017)). RSC HD cells displayed an ATI of approximately 48 ± 4 ms. This was significantly greater than the ATI of PoS HD cells (14 ± 8 ms), which itself was not significantly different from zero. This indicates that the RSC HD signal leads the PoS signal, with the anticipatory firing in RSC being comparable to that of the thalamus (see Section 1.4.1.3). HD cell ATI values have been used to argue the direction of information flow through the HD system (see Taube and Muller (1998)), and so may indicate that the RSC HD system provides some information to the HD cells.

The rat gRSC is also known to contain a population of cells that encode head direction within local subspaces, as opposed to the global heading direction represented by traditional HD cells (Jacob et al., 2017). These neurons display firing patterns that are dominated by local visual landmark configurations, and as such display a bi-directional tuning curve when

recorded from a box containing two rotationally symmetrical compartments. These cells are independent from the traditional HD cells observed in the RSC, and showed slightly lower peak firing rates on average than HD cells from the region (bi-directional cells: 5.1 ± 0.4 Hz, HD: 7.6 ± 0.9 Hz). Two categories of bi-directional cell were described by the author: one group of neurons displayed a unimodal tuning curve in each compartment (similar to HD cells), but which flipped its PFD 180° between compartments, resulting in a bi-directional tuning curve on average (the 'between-compartment bidirectional cells'). The second group maintained a bi-directional firing pattern in each compartment (the 'within-compartment bi-directional cell').

As these cells encode information about the direction of landmarks within local spaces, bi-directional cells have been proposed as a putative integrative input of landmark information into the HD system (Page and Jeffery, 2018).

1.4.1.2.2 mEC

HD cells are also observed in the medial entorhinal cortex (mEC), the area where grid cells were first recorded (Fyhn et al., 2004; Hafting et al., 2005). mEC HD cell firing has been shown to be correlated more strongly with heading direction than movement direction (Raudies et al., 2015), in spite of the significant odometric encoding by the area. Interestingly, although populations of 'pure' HD or grid cells exist, these representations are frequently conjunctive – one cell may exhibit grid-like spatial firing and directional selectivity. Conjunctive grid-by-HD cells show similar strength in their directional tuning as pure HD cells (Sargolini et al., 2006). Unlike true HD cells, grid-by-HD cell PFDs are not uniformly distributed across the whole horizontal plane, but are tuned preferentially to directions in 36° increments. This suggests that conjunctive neurons may underlie different computations than pure HD cells, and in particular the periodicity in PFDs of grid-by-HD cells is consistent with path integrative models that update grid cell representations using inputs from 10 sheets of conjunctive neurons (Keinath, 2016).

Whereas grid cells are found within layer II (and deeper layers) of mEC, directional neurons (HD and conjunctive cells) are only found in deeper layers, with 71% (273/385) of neurons recorded from layers III-VI found to exhibit directional firing correlates (Sargolini et al., 2006). mEC HD cells have similar properties to those recorded in other cortical areas: mean tuning curve widths of approximately 55° (angular standard deviation) and firing rates in the range of 5-40 Hz (Sargolini et al., 2006). Layer III HD cells show a topography of directional precision: more dorsal neurons show more precise tuning (higher resultant vector length) than ventral neurons, consistent with dorsal neurons displaying narrower tuning widths (Giocomo et al., 2014). This topography is not present in HD cells from layers V/VI, but is similar to that of

grid modules, in which the distance between individual firing fields of grid cells increases across the dorsal-ventral axis of the mEC (Stensola et al., 2012).

Many cells in mEC also display correlates with animal speed. Most HD cells (70%, 153/220), and most grid (94%, 141/150) and conjunctive (85%, 45/53) cells also displayed positive correlations between firing rate and linear animal speed (Sargolini et al., 2006). There also appears to be a dedicated population distinct from the grid, HD and conjunctive populations that code exclusively for speed in a linear, positive fashion (Kropff et al., 2015).

Other spatial codes exist within the mEC. Border cells, which are only active when the animal is in the proximity of a boundary of an environment, have been recorded from the area, although they appear to be a small and sparse population (Solstad et al., 2008; Savelli et al., 2008). Indeed, unbiased statistical methods (that do not prescribe 'categories' as conventional HD or grid cell analyses do) show that the majority of cells in the mEC (77%, 617/794) code for some combination of spatial or temporal predictors in a heterogeneous and dynamic manner (Hardcastle et al., 2017).

The conjunctive coding of head-direction, speed and position provides a plausible substrate for the derivation of an estimate of the animal's odometry by integrating linear speed in a given direction. Principal neurons in deeper layers, such as the conjunctive grid-by-HD cells, may project to layer II into the pure grid cell population.

1.4.1.2.3 PrCM

HD cells have recently been reported in the medial precentral cortex (Mehlman et al., 2019b), a region associated with motor control and more specifically with the generation of horizontal head movements during orienting behaviours. For instance, electrical stimulation of the PrCM elicited head turns, usually contraversive to the stimulated hemisphere (Sinnamon and Galer, 1984), and unilateral inactivation of the region impaired contraversive orienting responses in a stimulus-response orienting task containing a delay between stimulus offset and motor response epoch (Erlich et al., 2011).

PrCM HD cells displayed similar properties to other HD cells in the cortex and thalamus, with comparable tuning widths ($117 \pm 5^\circ$) to HD cells in other cortical or thalamic areas, although the cells displayed significantly higher peak firing rates (65 ± 7 Hz) than cells recorded in the thalamus or other cortical areas (Mehlman et al., 2019b). AHV cells were also recorded from the area.

1.4.1.2.4 V2M

Of notable interest, HD cells have been recorded in areas of rat posterior cortex traditionally associated with higher vision: the medial extrastriate cortex (V2M, Chen et al. (1994b,a)). The putative role of this cortical region in visual processing is discussed in Chapter 2. The discovery of HD cells in a visual area make this region a good candidate for integrating allothetic information from vision into a 'pure' HD representation as seen in other cortical HD areas (that are known to be connected to V2M).

However, these cells were quite rare: of 257 cells, only 7 (2.7%) were classified as HD cells. It is unclear whether this proportion is greater than that expected to be observed by chance. Interestingly, these cells were all classified by the authors as 'persistent' HD cells: they did not rotate their tuning curves to follow the rotation of a visual cue card (see Section 1.4.6), but maintained a consistent PFD relative to the first trial. These cells also continued to fire in the absence of a visual cue card. As such, vision did not appear to exert strong control over the firing properties of these HD cells. In contrast, the authors also recorded 'cue-dependent' cells, for which removal of the cue card disrupted or changed the directionality of the cell tuning curves.

These findings are consistent with more recent recordings finding HD, egocentric landmark-direction and allocentric landmark-direction (conjunctive HD-by-egocentric landmark) cells within V2M (Wilber et al. (2014), although the authors classify this cortical area as posterior parietal cortex: (Wilber et al., 2015)[3]). These authors found a notably larger proportion of HD cells at their implant co-ordinates (12%), which are believed to correspond to posteromedial, anteromedial and mediomedial visual areas (Wilber et al., 2014). In contrast, Chen et al. (1994b) have been reported as recording predominantly in the posteromedial area. Nevertheless, these visual areas inside V2M are known to project strongly to HD areas, including the retrosplenial cortex and presubicular cortices (Wang et al., 2012; Wilber et al., 2015), and therefore provide a plausible route for vision to reach directional representations (see Section 2.6).

1.4.1.2.5 S1

One recent study has identified populations of cells in the primary somatosensory area (S1) that display various spatial characteristics (Long and Zhang, 2018). Briefly, this paper recorded cells

[3]In spite of this, the implant co-ordinates these authors use is considered by others (e.g. Wang et al. (2012)) to fall inside V2M, and is classified in Paxinos and Watson (2007) as V2M. Numerous other spatial cells have been reported in (posterior) parietal cortex (e.g. cells that encode positions within subspaces of complex mazes: Nitz (2006, 2012)), but these are frequently recorded from sites anterior to V2M. For example, according to Paxinos and Watson (2007), cells recorded from Nitz (2006) and Nitz (2012) are anterior to those in Wilber et al. (2014), and fall inside the parietal association area.

in freely moving rats foraging in an open field arena, and generated shuffled distributions of spatial metrics against which spatial metrics of recorded cells were compared. This method revealed populations with a variety of spatial codes as seen in (para)hippocampal areas, including place cells, HD cells, grid cells, border cells, speed cells and conjunctive cells.

However, beyond classifying these cells using statistically derived thresholds, the authors do not characterise these cells or their behaviour: for instance, it is unknown whether any of these 'spatial' cells would be consistently spatial in multiple environments; are controlled by visual cues or cues of other modalities; fire action potentials in darkness. As cells are defined as spatial by a single threshold generated from a shuffle distribution over all cells, it is expected that some cells will pass this metric; the authors argue that more cells than expected pass the shuffle threshold criterion for all of these populations. However, it is known that shuffle methods can have high false positive rates (Barry and Burgess, 2017), and so it may be expected that more cells pass the threshold than the theoretical chance proportion. As such, it is unclear whether this report demonstrates a distinct and real population of spatial cells in S1, or if this is an epiphenomenon from the somatic codes in S1 or from the statistical analyses used.

1.4.1.3 Anterior thalamic nuclei

HD cells have also been reported in nuclei of the anterior thalamus (ATN) (Taube, 1995a), which show a similar unimodal tuning curve to those seen in the PoS.

The ATN is comprised of three nuclei: the anterodorsal (ADN), anteroventral (AVN) and anteromedial (AMN) thalamic nuclei, each of which have unique histochemical appearances and connectivity (Jankowski et al., 2013). The first HD cells recorded in the ATN (Taube, 1995a) were predominantly seen in the ADN, although some may have been located in the AVN. Although the ADN receives the most attention of the thalamic HD areas, cells have since been reported in many other nuclei, including the other two nuclei of the ATN.

1.4.1.3.1 ADN

The discovery of HD cells in the ADN quickly followed that of the PoS (Taube, 1995a). This is unsurprising given the direct reciprocal connections between the ADN and PoS (van Groen and Wyss, 1990c), which indicated a plausible role for the anterior thalamus in the generation of the HD signal.

Similarly to within the PoS, HD cells with similar PFDs may be located far away from each other within the ADN (Taube, 1995a), suggesting the representation of heading direction in the brain is not topographic.

Unlike PoS HD cells, ADN HD cells display an anticipatory element to their firing profile, in

Figure 1.8: (REDACTED FOR COPYRIGHT) Linear plots of HD cell tuning curves for the main areas in which HD cells have been recorded. The two overlayed curves show the separation angle of the HD cell PFDs when constructed separately for clockwise versus anti-clockwise turns. As is clear, the LMN contains the largest separation angle, and the PoS HD cell displays little to no separation angle. Figure taken from Sharp (2005).

which the firing rate of the cell is maximal shortly before the animal faces the PFD as defined by the trial-averaged tuning curve. This is revealed from plots of an HD cell tuning curve filtered for when the animal was moving clockwise or anti-clockwise only (Blair and Sharp, 1995) (see Figure 1.8 from Sharp (2005)). If the plots are superimposed, a non-zero separation angle can be seen between the PFDs of clockwise and anti-clockwise tuning curves of ADN HD cells, whereas no separation angle is present for PoS HD cells. Blair et al. (1998) showed that this angle was best described with a time-lag model: the faster the animal was turning its head, the larger the observed separation angle. This provided evidence that the ADN HD cells were anticipatory for the future heading direction of the rat, with an anticipatory time interval (ATI) of approximately 25ms in papers from the Sharp laboratory, and 40-50ms in papers from the Taube laboratory (Sharp, 2005). PoS HD cells displayed no anticipation, and may instead lag slightly behind current heading.

1.4.1.3.2 AVN

HD cells have also been observed and characterised in the anteroventral nucleus (AVN) of the thalamus (Yoganarasimha et al., 2006; Tsanov et al., 2011a), displaying similar characteristics to ADN HD cells in parameters of peak firing rate (ADN: 71 ± 26 , AVN/LDN: 80 ± 38) and tuning curve half-width (ADN: 50 ± 13 , AVN/LDN: 51 ± 14 , mean $\pm$ std, Yoganarasimha et al. (2006)). Tsanov et al. (2011a) more rigorously characterised directional cells within the AVN, classifying 69% of recorded neurons as HD cells.

The AVN, and its bordering AMN, have been characterised electrophysiologically as theta-rhythmic areas, with reports finding approximately 75% (39/52) of AVN neurons are theta-modulated in urethane-anaesthetised rats (Vertes et al., 2001; Albo et al., 2006). However, brain state may affect electrophysiological characteristics of neurons, and differences in analyses pipelines may effect classification rates. Subsequent work has found substantially fewer theta-rhythmic AVN neurons in freely moving rats (24% in Tsanov et al. (2011b), or 50% in Tsanov et al. (2011a)). In contrast, research has found no (Vertes et al., 2001) or very few (Albo et al., 2006; Tsanov et al., 2011a) theta-modulated cells in ADN or laterodorsal thalamus, and as such HD cells in this region are rarely theta-modulated.

1.4.1.3.3 AMN

Compared to the ADN/AVN, the AMN has received little attention in electrophysiological studies, in spite of its similar anatomical connectivity and the implications of ATN in spatial memories and orienting behaviour. An early paper reported a single neuron that appeared to encode "orienting and locomotor" activity, although this was not discussed in detail (Mink et al., 1983).

A more recent paper has shown the AMN to contain spatially selective cells, with approximately 10% of cells recorded being HD cells (36/371, Jankowski et al. (2015)). These cells displayed on average a lower firing rate than those in the neighbouring ADN/AVN (20 ± 4, mean *pm* SEM), and HD cell firing was not entrained to a theta rhythm. Although these cells anecdotally displayed a separation angle between the PFDs during clockwise versus anticlockwise movements, the difference was not significant.

The AMN was also seen to contain a number of other spatially selective cells, including place cells (6%) and border cells (0.5%), whilst a number of neurons also showed theta-rhythmic firing (11% total). Together, all three anterior nuclei of the thalamus contain HD cells, and may be situated as thalamic relays within the HD circuit (see Section 1.4.4).

1.4.1.4 Other thalamic nuclei

1.4.1.4.1 LDN

The lateral dorsal nucleus (LDN) of the thalamus also contains HD cells (Mizumori and Williams, 1993). Similarly to cells reported in previous regions, these cells show unimodal peaks in their firing when the rat faces one direction in the horizontal plane.

Mizumori and Williams (1993) recorded cells from the LDN whilst rats performed working memory task on a radial maze, in which all arms were rewarded such that the animal had to visit each arm and retrieve the reward to complete the trial (thus remembering the arms it had previously visited). In this task, some cells showed strong directional specificity, which appeared to correlate with the performance of the animal on the task. Interestingly, these cells were only directional when the room was illuminated; when animals were exposed to the environment in darkness (that is, carried into the room and placed in the environment in darkness), the cells did not establish directional specificity in their firing. If the lights were switched off part-way through a trial, the cells were frequently able to maintain some directionally specific firing, but their PFDs often drifted. This suggests that, unlike HD cells in other regions, HD cells in the LDN need visual input to establish a directional code in a new environment.

1.4.1.4.2 NRe

Nucleus reuniens (NRe) of the thalamus is a well-connected midline thalamic nucleus, known to interconnect HPC and medial prefrontal cortex, and which has been functionally implicated in contextual fear memory (Ramanathan et al., 2018) and long-term associations between objects and places (Barker and Warburton, 2018) in rats. These findings indicate a role for the NRe in the spatial network, although its precise role within the HD circuit remains unclear.

The NRe has been described electrophysiologically in a set of two papers exploring the spatial correlates of neurons in the area (Jankowski et al., 2014, 2015). Both papers found a population of HD cells within the region (9% in Jankowski et al. (2014), 11% in Jankowski et al. (2015)). These cells displayed similar characteristic unimodal tuning curves to that seen in other HD areas, and were not seen to be theta-modulated. Although not reported in the paper, the mean PFR of the subset of cells shown in Figure 1A of Jankowski et al. (2014) was 59 ± 4 (mean $\pm$ SEM), broadly comparable to the firing rates of HD cells in other thalamic nuclei. Although beyond the scope of this review, a number of place-modulated, border, and theta cells were also described in NRe (Jankowski et al., 2015), similar to those seen within AMN, that provide a plausible substrate for the laying down of spatial associative memory.

1.4.1.5 Tegmento-mammillary nuclei

1.4.1.5.1 DTG

The dorsal tegmental nucleus of Gudden (DTG), considered an important relay nucleus in the limbic system (Liu et al., 1984), was shown to contain HD cells (Sharp et al., 2001b), alongside correlates of angular head velocity (AHV) and conjunctive representations of HD-by-AHV (Bassett and Taube, 2001; Sharp et al., 2001b).

Fewer cells show HD tuning than in other areas: Sharp et al. (2001b) found only 12.5% 'classic' HD cells, whereas Bassett and Taube (2001) report 11%. The tuning curves for these cells were significantly wider than those in downstream HD areas; the mean tuning width of DTG HD cells was 109°, compared with 65° for PoS HD cells recorded by the same authors (Sharp et al. (2001b), compare with Table 3 of Cho and Sharp (2001)), whilst Bassett and Taube (2001) report even broader tuning ranges of approximately 200°.

HD cells recorded in the DTG frequently displayed symmetric tuning curves, although some were seen with notable skew in one circular direction (as can be seen in Figure 1.8). A subset of recorded HD cells were modulated by turning direction, for which ipsiversive turns generated a higher peak firing rate for the cell than contraversive turns. These HD-by-AHV cells have been predicted as a means of shifting the activity packet of the HD attractor in response to head

turns (Sharp et al., 2001a).

The DTG has also been reported to contain pure AHV cells (Bassett and Taube, 2001; Sharp et al., 2001b). The firing rates of these cells encode the current angular velocity of the animal's head as it makes a turn. These cells are substantially more numerous than the HD cell population, with $75-85\%$ of cells modulated by instantaneous head velocity of the animal.

Bassett and Taube (2001) separated AHV cells into two categories based on the shape of the cell tuning curves: asymmetric (aAHV) and symmetric (sAHV) cells The firing rates of aAHV cells are (mostly) positively correlated with head turn velocity in one direction only, and are either negatively correlated or uncorrelated with head turns in the opposite direction, whereas sAHV cells are positively correlated with the angular speed of the animal's head irrespective of turning direction. In general, aAHV cells preferred turns in the contraversive direction to the hemisphere in which the cell was recorded, although some cells were seen with preferences to ipsiversive turns.

Although the DTG is considered a vestibular nucleus and receives significant input from other vestibular nuclei (see Section 1.4.4.1), AHV cells in the DTG may integrate vestibular, motor and sensory cues into a representation of turning speed. Evidence for this comes primarily from the observation that asymmetric AHV cells are silent during passive rotations of the animal when restrained by an experimenter, and plausible anatomical routes have been identified which could carry motor efference copy from the striatum (Sharp et al., 2001b) and optic flow information from the nucleus prepositus hypoglossi (Lannou et al., 1984).

1.4.1.5.2 LMN

Recordings of single units in the lateral mammillary nuclei (LMN), an area densely reciprocally connected with the DTG, unveil a qualitatively similar population of HD cells to those recorded upstream (Stackman and Taube, 1998; Blair et al., 1998; Yoder et al., 2015). Approximately 25% of all recorded cells show modulation by head direction (Stackman and Taube, 1998; Yoder et al., 2015), comparable to the proportion of HD cells seen in the PoS. However, Blair et al. (1998) reported significantly more HD cells in LMN than these authors: 56% of neurons were directional, a number closer to the percentage of HD cells seen in ADN.

LMN HD cells tend to show significantly higher background firing rates and wider tuning curve widths in LMN HD cells than ATN or PoS HD cells (Blair et al., 1998; Stackman and Taube, 1998). Interestingly, Blair et al. (1998) found that the shape of the tuning curves of LMN HD cells are significantly modulated by turning direction, with neurons displaying narrower tuning widths during contraversive head turns, which may inherited from the asymmetry seen in DTG HD-by-AHV cells.

The effect of turning direction on HD cell activity may indicate that the LMN is involved in the integration of vestibular information coding for angular head velocity into the HD signal (see Section 1.4.4, as downstream ATN HD cells do not display similar asymmetries during clockwise versus anticlockwise head turns (Blair et al., 1998).

Consistent with this, other firing parameters of LMN HD cells may be modulated by turning direction. Although there was no difference in the mean PFR of HD cells when binned for clockwise versus anticlockwise turns (Blair et al., 1998), this analysis did not control for the implanted hemisphere. Other evidence suggests that the ratio of these PFRs may encode ipsi-/contraversive turns of the animal, with a given HD cell displaying a higher PFR when the animal makes a turn contraversive to the cell hemisphere (Stackman and Taube, 1998).

Together these findings provide evidence that neurons in the LMN are in general more sensitive to AHV correlates than in thalamic or cortical HD areas. This is supported by the presence of sAHV cells within the LMN, with 44% of non-HD cells modulated by head velocity (Stackman and Taube, 1998), along with cells responsive to head pitch angle, and a separate population of theta-rhythmic cells (Blair et al., 1998; Stackman and Taube, 1998). Theta cells in the LMN showed no clear relationship to any other behavioural correlate, and have been observed previously *in vitro* in the LMN (Llinas and Alonso, 1992) and in anaesthetised rats (Kirk and McNaughton, 1991; Kocsis and Vertes, 1994)

1.4.1.6 Dorsal striatum

HD cells have also been recorded from the dorsal striatum during foraging on a radial arm maze (Mizumori et al., 2000) and inside cylindrical (Mehlman et al., 2019b) and square (Wiener, 1993) open fields. Other spatial or movement correlates have been recorded from the dorsal striatum, including location and head movement (e.g. AHV) correlates (Mizumori et al., 2000; Kim et al., 2014), with HD cells being localised within the dorsomedial extent of the dorsal striatum (Mizumori et al., 2000).

HD cells displayed similar properties to those seen in limbic areas, with no significant differences in tuning curve width ($112 \pm 6°$) or peak firing rate ($37 \pm 4\,\text{Hz}$) to HD cells recorded from the ADN (Mehlman et al., 2019b). Like most other HD cells, the cells continued to fire in darkness, and consistently rotated to follow transformations of distal visual cues (Mizumori et al. (2000); Mehlman et al. (2019b) although Ragozzino et al. (2001) saw less consistent cue control). In general, HD cell PFDs rotated the same amount as location cells in dorsal striatum (Mizumori et al., 2000) or as place cells in hippocampus (when the place cells did not remap, Ragozzino et al. (2001)).

1.4.1.7 Interconnections and the HD circuit

As described in the above paragraphs, brain areas from which HD cells have been recorded are densely interconnected. As such, the natural questions emerge of where and how the HD signal is generated, and whether there are differences between areas in how information from multiple sensory modalities is integrated into the an abstract representation of direction. The dense recipricosity of projections between HD areas within the rat is summarised in Figure 1.9.

Much work has investigated how information about the external world is integrated into the HD signal, and numerous lesion studies have attempted to identify a hierarchical structure to the HD areas, and relate HD activity to behavioural correlates. The following sections will detail these fruitful areas of research.

1.4.2 Head direction cells and behaviour

HD cells are well-correlated with the behaviour of rats performing spatial tasks. Moreover, a plethora of behavioural evidence from lesion studies (reviewed briefly below in Section 1.4.3) demonstrates that damage to many of the brain regions containing HD cells results in behavioural deficits in orientation and spatial navigation.

However, demonstration of a causal relationship between HD cells and the animal's behavioural sense of direction has proven less fruitful. This section will briefly review papers exploring the correlative and causative relationships between HD cells and navigating behaviour, and briefly discuss the broad behavioural impairments seen following damage to HD areas in the rodent brain.

Early work recorded from LDN HD cells while rats performed a spatial working memory task (Mizumori and Williams, 1993). Rats explored a radial maze with four of eight arms exposed, and retrieved chocolate milk reward from the end of each arm; after this, all eight arms were exposed and the rat had to visit the remaining four arms. Optimal exploring would involve the rat not mistakenly re-visiting any arms already visited. The authors found that the directional specificity of the cells was correlated with task performance: the less directional the tuning curves of the recorded HD cells, the more arm revisits the rat made. Furthermore, LDN HD cells became more directional over the course of learning the task. This was an early indication that the HD system may be a cognitive representation of the rat's sense of direction, which may inform the rat's ongoing behaviours whilst navigating. Accordingly, inactivating the LDN impaired performance on this task, with rats making more errors following tetracaine injections into LDN (Mizumori et al., 1994).

Similarly, ATN and PoS HD cells were recorded in a radial maze while rats were trained

to approach the end of one arm, regardless of starting point (Dudchenko and Taube, 1997). Training occurred in a curtained environment with a salient visual cue. Rotations of the visual cue resulted in a corresponding rotation of the rat's arm choice, indicating that the animal used the landmark to orient itself within the maze and solve the task. Similarly, HD cells usually shifted their tuning curves to follow the rotation of the visual cue (see Section 1.4.5); as such, the rat's behavioural choice was strongly coupled to the orientation represented by the HD system. This was also true during error trials: when the rat selected the incorrect arm, this was frequently an arm in register with the heading direction implied by the HD system (that is, the error in directionality of the HD cell representation and in behaviour were correlated). This provides further evidence that the animal may rely on its internal representation of direction when navigating.

However, Golob et al. (2001) recorded ADN HD cells during a task in which rats had to approach the correct corner of an arena as designated by a prominent visual cue. Notably, in a number of trials, the HD cell PFDs were not consistent with the behavioural sense of direction inferred from the task. Moreover, when the arena was changed (but the cue card retained), most HD cells shifted their PFDs. However, the rats were still able to solve the navigation task, generalising the chosen corner to the new arena. This indicates that the representation of direction in the HD system may not be directly related to the behavioural response of the animal (although a form of beacon-navigation may have been used to solve the task, with the animal simply approaching the relevant corner of the cue).

In a path integration and homing tasks, ADN HD cell PFDs have been found to be closely correlated with the animal's trajectory to a homecage following a period of foraging, with homing trajectory errors individual trials correlating with PFD shifts (Valerio and Taube, 2012). Rotating the rat (at a velocity below the vestibular threshold) while eating reward caused a corresponding rotation in the homing box to which the rat returned (van der Meer et al., 2010), indicating that the animal largely uses idiothetic information while homing. Following rotations, the authors found that ADN and PoS HD cell PFDs shifted an angle that correlated well with the angular shift in the animal's behavioural response. In a similar task, one study (Butler et al., 2017) recorded HD cells during unilateral optogenetic inactivation of vestibular projections into the dorsal tegmental nucleus, an area that contains HD cells and is believed to be involved in generating the HD signal using vestibular information (see Section 1.4.4). This injected noise into the HD signal, which drifted over time (as a function of the cumulative head turns of the animal). Separately, this inactivation decreased performance in the homing task above, when performed in the dark, with animals taking less direct routes back to their homecage after foraging. However, the authors did not record HD cells during this task, and

relied on correlating task performance with neural activity recorded in a different apparatus.

A recent paper assessed whether HD cells maintain a single registration with the external environment across the course of a spatial task (Park et al., 2019). Rats were trained to avoid a restricted zone of a cylindrical platform, defined relative to the external reference frame of the room, with the platform either stationary or rotating. When the platform rotated, the rat had to additionally keep track of and avoid a second restricted portion of the platform, defined in the platform reference frame (so the second restricted area rotated with the platform).

mEC HD cells were stable during the trials when the platform was stationary, but their dirctionality degraded during the rotating trials (whether the HD activity was analysed relative to the room, or to the platform reference frames). This was not a degradation of the intrinsic dynamics of the HD system, as HD cell pairs maintained coherence. The authors note that these findings are difficult to reconcile with the traditional (map-based) navigation model, as the animals learn to avoid both restricted areas (and therefore maintain a sense of direction) in spite of a degraded representation of direction in the HD system. As such, how HD cell activity may underlie spatial behaviours such as navigating within two frames of reference is unclear (the authors propose an 'etak' model, which will not be discussed here but is in Park et al. (2019)).

1.4.3 Lesion models

Descriptions of the behavioural outcomes of brain damage have been recorded since ancient civilisations. The Edwin Smith Papyrus, an ancient Egyptian medical text from ca. 1600 BCE, described multiple cases of head and vertebral injuries alongside descriptions of their clinical manifestations (Mohamed, 2008). One case described contralateral paralysis of the arms and legs following a skull fracture – a finding consistent with modern knowledge of the contralateral control of muscles by each hemisphere of the brain. Later ancient writers describe cases of more specific deficits following localised head trauma: Valerius Maximus (ca.30 CE) describes a patient who "lost his memory of letters, [...] but retained his memory of everything else"; an early desription of alexia (Levin et al., 1982, p. 4).

Neuroscience has since utilised lesion models, in which a spatially localised region of brain is damaged ('lesioned') and its effects observed, throughout its history to explore localisation of behavioural functions within the brain (within 'modules'). Although the cognitive theory of modularity put forward in Fodor's Modularity of Mind (Fodor, 1983) has been brought into question (Cisek, 2012), along with its localisationist and internalist assumptions (Frisch, 2014), modularity has nonetheless influenced some work on spatial cognition (cf. the geometric module, Cheng (1986)), and lesion studies remain an important means of assessing the necessary neural

structures that underlie cognitive tasks.

Numerous methods for lesioning restricted areas of the brain have been developed, including aspiration of the target area, injection of a neurotoxin into the target area, and application of an electric current through electrodes in the target area. These methods frequently have different practical and theoretical considerations, and of note whereas aspiration and electrolytic lesions destroy all tissue in the selected area (neuron bodies, glia, and neuron fibres), injection of an excitotoxic neurotoxin (such as NMDA) will kill excitatory neurons in the region whilst leaving glia and fibres of passage intact (Kirby et al., 2012).

Unsurprisingly, in rodent models, damage to the brain, including to HD areas, is frequently accompanied by deficits of spatial navigation. This section will briefly review areas of the brain implicated in rodent orientation behaviours from such lesion studies.

1.4.3.1 Lesions of HD areas

A causal role in HD cells in orienting behaviours is difficult to show, as the cells are found in regions of the brain with a rich gamut of other spatial cells (Grieves and Jeffery (2017), as discussed in Section 1.4.1). However, lesions directed towards areas that contain HD cells frequently are associated with deficits in angular path integration, although these effects are inconsistent. A large body of literature exists on this, and therefore will not be reviewed in detail here. The mixed evidence for the behavioural significance of HD cells is well discussed in a recent review (Dudchenko et al., 2019).

Briefly, deficits of homeward path integration have been observed following disruption of the vestibular sense (Wallace et al., 2002), and, accordingly, damage to vestibular nuclei frequently ablates the HD signal (see Section 1.4.4.1). However, animals appear to perform above chance on a homing task following lesions of the dorsal tegmental nucleus, although they are impaired (Frohardt et al., 2006). Similarly, lesions of the lateral mammillary body generate only a transient deficit in learning a Morris water maze task, and have no effect on performance in a task requiring the rat to dig at a correct location defined at a direction relative to a salient visual landmark (Harland et al., 2015).

In contrast, it is well described that large lesions directed toward the anterior thalamus result in a large variety of spatial and non-spatial cognitive deficits (for review, see Aggleton and Nelson (2015)), including deficits in homing (Frohardt et al., 2006). However, this may be in part due to lesions including other portions of the anterior thalamus (e.g. combined lesions of the ADN and LDN, Aggleton et al. (1996); Wilton et al. (2001)) and restricted lesions to the ADN/AVN or AMN only mildly impairing performance on spatial tasks (Aggleton et al., 1996).

Whereas animals foraging for food on a large cylinder would typically return directly to their home nest at the edge, thermal lesions of the retrosplenial cortex impaired the ability of rats to orient towards their home nest after foraging in the dark (Elduayen and Save, 2014). This deficit was not present in the light (although no distal cues were present outside the arena), indicating that visual input can rescue this rotational inaccuracy. This could be due to animals using non-path integrative strategies (such as beacon navigation), or the lesions causing increased drift of directional cells in darkness that is corrected by an intact integration of allothetic visual landmarks into the system in the light (as ADN HD cells still exist following RSC lesions). This is consistent with correlative findings above that showed greater HD cell instability and poorer homing task performance, when vestibular input to the HD circuit is disrupted in darkness (Butler et al., 2017).

Lesions directed to other HD areas result in a similar deficit of path integration. Animals with lesions of the PPC or entorhinal cortex failed to return to their home nest after foraging on a similar circular arena in the light (with no distal cues visible to the animal, Parron and Save (2004)). The deficit was worse in animals with entorhinal lesions than those with parietal lesions, which may reflect the intimate connections between the entorhinal cortex and hippocampus. However, path integration experiments in humans have suggested that the entorhinal cortex and hippocampus are not necessary for successful angular estimates (Shrager et al., 2008).

Animals with excitotoxic or electrolytic lesions of the PoS less frequently selected the correct arms on a radial maze, although both lesion groups improved over the course of the experiment. Similarly, the animals were impaired on a Morris water maze task relative to the control groups, but were unimpaired on a similar task where the platform was cued with a striped flag (Taube et al., 1992). This is consistent with the animals being unable to utilise directional bearing information to solve a spatial task, and may suggest a role for the HD system in processing information for spatial behaviour. Rat with PoS lesions were not impaired on a water plus-maze task requiring the association of platform location with an allocentric direction (Peckford et al., 2014)

Further work has found inconsistent effects of PoS lesions on spatial behaviours in the rat. Peckford et al. (2014) trained rats on a homing task in which animals were trained to emerge from one of six hole around the edge of a circular arena, retrieve food from the centre, and return to the correct hole. This protocol is comparable to that described above in RSC/PPC/EC lesions (Parron and Save, 2004; Elduayen and Save, 2014). PoS-lesioned animals performed significantly worse than sham-operated controls in this task, with these animals more likely to return to a hole adjacent to the correct one (Peckford et al., 2014). In contrast with this, one study trained rats on a similar homing task on a large circular platform following excitotoxic

PoS lesions with ibotenic acid (Bett et al., 2012). In this experiment, lesioned and sham-operated rats did not perform significantly differently, indicating that the PoS may not be necessary for path integrative homing behaviours here. These inconsistent findings are difficult to reconcile, but may relate to lesion size, task parameters, or extra-maze information available to the animals.

In general, deficits in spatial orienting following lesions of HD areas indicate that there may be disruptions of neural representations of orientation and space following these lesions. However, this appears to depend to a large extent on lesion site, size, and task demands. In particular, effects are more pronounced on tasks requiring intact path integration – such as homing in darkness. Impairments in other tasks frequently are transient, or inconsistently reported. This indicate that rodents may be able to use alternate strategies to solve these tasks that do not depend on robust directional neural signals.

One synthesis of this complex collection of results proposes that two types of HD cell exist (Dudchenko et al., 2019): one more driven by vestibular inputs (a 'traditional' HD cell) and one more driven by sensory inputs (e.g. the directional cells seen in Olson et al. (2016); Jacob et al. (2017); Kornienko et al. (2018)). These cells may be distributed in different areas of the HD system, and so lesions of these different areas may cause different deficits in spatial navigation: lesions of more vestibular HD cells leading to deficits in tasks requiring path integration, and lesions of more sensory HD cells leading to deficits in tasks requiring associating external landmarks with allocentric directional responses. As such, further characterisation of HD cells may aid interpretation of the conflicting behavioural literature.

1.4.4 Generation and hierarchy of the HD system

Many areas from which HD cells have been recorded are known to be interconnected and send projections to other HD areas.

If directional information is propagated through the system via these connections, it is reasonable to suppose that this propagation is asymmetric, and defines a hierarchical structure to the distributed HD system. In such a system, the HD population signal would be generated in a subset of the HD areas and propagated through the system such that destruction of one area would ablate the HD signal i in all areas downstream, whilst (relatively) preserving the upstream code.

Generally, this pattern of results is observed across numerous lesion and inactivation studies. This section will review the work supporting the current model of the generation and propagation of the HD system through the rodent brain.

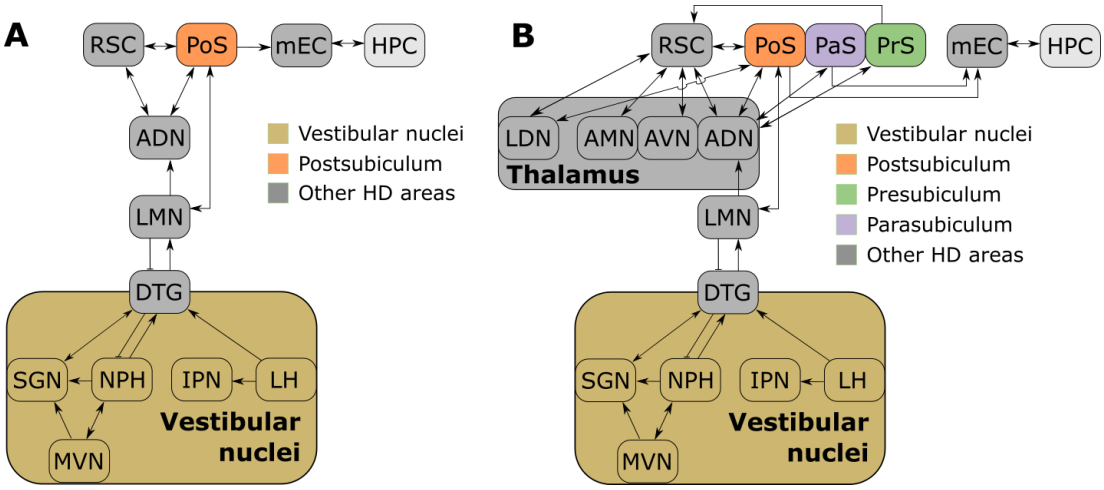

Figure 1.9: Schematics of the canonical HD circuit in the rodent brain. A: A simplified, traditional schematic showing the propagation of the HD signal from the DTG through to the cortical HD areas. Although it leaves out many areas known to also contain HD cells, this is the circuit typically shown in papers. See, for instance, Taube (2007); Clark et al. (2009); Clark and Taube (2012); Winter and Taube (2014); Yoder and Taube (2014); Peyrache et al. (2017). B: A more complete (but still incomplete!) schematic of the HD circuit. Notably, this schematic has added other nuclei of the anterior thalamus, and other subregions of the subicular complex.

1.4.4.1 Vestibular inputs to early HD nuclei

Observations that an HD cell is capable of maintaining a constant PFD in darkness, during fast passive rotations of the floor on which an animal forages, suggests that the HD signal can use vestibular information to remain oriented (Zugaro et al., 2000). Although allothetic cue information is processed and integrated into the HD signal (Taube et al., 1990b), generation of the signal is dependent on intact vestibular information from the organs of the inner ear. Although the anatomy of the inner ear will not be discussed here, the inner ear contains two sets of organs for detecting linear and rotational motion: the otolith organs and semicircular canals, respectively. The otoliths are comprised of the utricle and saccule, which detect acceleration in the linear forward/backward and vertical directions, respectively, and can also signal information about tilt orientation of the head when the head is still (Purves et al., 2001).

Accordingly, bilateral chemical labyrinthectomies in the rat via intratympanic injections of sodium arsanilate, which disrupt activity of the semicircular canals and utricle, result in the loss of directional tuning in the HD system (Stackman and Taube, 1997). The tuning curves of ATN HD cells post-lesion were non-directional, although the mean firing rate remained constant relative to pre-lesion recordings of the same neurons. These changes could not be attributed to differences in locomotion of the rat following lesions, and imply that the directional code of HD cells requires intact vestibular information about the animal's head movements, which may be integrated to generate a representation of current bearing.

This interpretation has been supported by additional work in mice: *tilted* mice, which lack

functional otolith organs, have significantly fewer HD cells in the ADN than wildtypes, and the directional signal encoded by these cells frequently degraded over the course of a trial (Yoder and Taube, 2009). Similarly, mice lacking intact horizontal semicircular canals (*epistatic circler* mice) have an impaired HD signal, with no 'true' HD cells being identified in the ADN of these mice (although some were mildly directionally-modulated, Valerio and Taube (2016)). As such, there is good evidence that the HD signal is dependent on, and therefore likely generated by, vestibular signals from the inner ear.

Neuroanatomical studies in the rat have discovered multiple plausible routes by which vestibular information may reach HD nuclei from the inner ear. Although early evidence existed for a direct projection from the medial vestibular nuclei (MVN) to the DTG (Liu et al., 1984), further work using both anterograde and retrograde tracing techniques did not replicate these results (Hayakawa and Zyo, 1985; Biazoli Jr et al., 2006).

Vestibular input into the HD circuit appears to arise predominantly from projections from the supragenual nucleus to both the contralateral DTN and ipsilateral LMN (Biazoli Jr et al., 2006) and nucleus prepositus hypoglossi (NPH) projections to the ipsilateral DTN (Brown et al., 2005). There is no evidence that the NPH projects to LMN (Shibata, 1987). These tracing data together provide evidence that vestibular information about the movement of the rat's head may reach the HD circuit via multiple routes, which may be integrated into a representation of heading direction.

Accordingly, lesions of vestibular nuclei give further evidence to the hypothesis that intact vestibular processing is required for the generation of the HD signal. Bilateral ablations of the supragenual nuclei abolish the HD signal in the ADN in rats, whereas HD cells was present (although impaired, with unstable PFDs) following unilateral lesions of the supragenual nucleus (Clark et al., 2012a). The NPH also appears to provide an important input to the tegmento-mammillary circuit: complete bilateral lesions of NPH abolished the directional signal in ADN (Butler and Taube, 2015), and unilateral optogenetic inactivation of the NPH $\rightarrow$ DTG projection reduced the stability of ADN HD cells, and caused the PFDs of HD cells to drift more quickly (Butler et al., 2017).

A good review of vestibular influences on the HD signal can be found in Clark and Taube (2012). Overall, the projection of vestibular information into the DTG-LMN circuit appears to be necessary for the stable generation of the HD signal. In principle, this could occur through the integration of an angular head velocity signal from the vestibular system into a representation of angular direction, implemented within the recurrent connections between the DTG and LMN.

1.4.4.2 Propagation of the HD signal to the thalamus

Data from vestibular intervention studies lead to the working hypothesis that the HD signal is generated between the DTG and LMN from the integration of angular velocity information projected into these two areas. After the generation of the HD signal, it must be propagated throughout the network. A plausible substrate for this is the substantial projection from LMN into the ADN in the thalamus (Hayakawa and Zyo, 1989; Shibata, 1992).

Supporting this idea, bilateral electrolytic lesions directed toward the LMN ablated the HD signal within the ADN ((Blair et al., 1998, 1999)). In one of these experiments, HD cells characterised pre-lesion lost their directional firing post-lesion (but maintained some rhythmic bursting properties). In contrast, control lesions directed outside of the LMN, and unilateral lesions of the LMN, did not abolish the HD signal post-lesion (although there was a mild impairment in directional information). Similarly, complete bilateral lesions of the DTN entirely abolishes the HD code within the anterior thalamus, and incomplete lesions significantly reduced the incidence of ATN HD cells compared to non-lesioned controls ((Bassett et al., 2007)).

Moreover, analysis of synaptic properties in *ex vivo* preparations containing the mammillothalamic tract have shown that the projection from LMN to ADN exhibits qualities of a driver pathway, whereas afferents into ADN from cortex display features of a modulating pathway (Petrof and Sherman, 2009). This is consistent with the idea that the HD signal is propagated forwards from the DTN-LMN circuit to the ADN, which extends both ipsi- and contralaterally.

ADN HD cells may retain an intrinsic architecture even when uncoupled from LMN input. If the attractor architecture of the ADN HD system is retained, bursts are seen from the cells whenever the hill of activity invokes the cell. Ordinarily, the hill of activity moves as the animal turns, and so bursts are seen from each cell when the animal faces near its PFD. However following lesions, the hill of activity will move independent of the direction of the animal, and so bursts will occur seemingly at random. Following LMN lesions, some ADN HD cells still show bursts of spikes and maintain consistent relationships in crosscorrelations of their spike times during these bursts ((Blair et al., 1999)), as predicted by the ADN attractor model. These 'bursty' cells have been observed in a number of further studies across multiple species (chinchillas: Muir et al. (2009), mice: Yoder and Taube (2009)). However this finding is inconsistent, with some authors finding no bursty activity following vestibular inactivation (Stackman et al., 2002) or DTN/LMN lesion ((Bassett et al., 2007)), and others observing that HD cells recorded before vestibular lesions did not turn into bursty cells post-lesion (Stackman and Taube, 1997).

Whether or not an attractor architecture exists intrinsic to the anterior thalamus, it is evident that directional firing of ADN HD cells is dependent on an intact tegmento-mammillary

HD circuit. Consistent with this, lesions directed towards the PoS or RSC do not abolish HD cells in the ADN (Goodridge and Taube, 1997; Clark et al., 2010). As such, it appears that the HD signal is likely to be propagated into the anterior thalamus from the LMN, and it is plausible that the signal is further propagated from the ADN to cortical HD areas (see Section 1.4.4.4). The LMN also receives an important backprojection from the PoS (van Groen and Wyss, 1990c), which is believed to help bootstrap the HD signal after being anchored to the external world using input from allothetic modalities, so as to remain coherent between areas (Yoder et al., 2015).

1.4.4.3 The HD signal in other thalamic areas

Although the ADN is the best studied of the thalamic HD nuclei, it is important to note that other nuclei are well seated to receive and propogate directional and other spatial information throughout the circuit. The AVN and AMN similarly receive inputs from the mammillary bodies (the medial mammillary nuclei, MMN, Seki and Zyo (1984)) via the same mammillothalamic tract as carries the LMN→ADN projection (Dillingham et al., 2015). The MMN are nuclei containing theta cells (Vann and Aggleton, 2004), consistent with the greater theta modulation of neurons in AVN/AMN compared with the ADN. Both the AVN and AMN are reciprocally connected with cortical HD areas, including the RSC, and the AVN reciprocally projects to PoS (Jankowski et al., 2013). Similarly, the LDN is reciprocally connected to both PoS and RSC (van Groen and Wyss, 1990c,b, 1992; Van Groen and Wyss, 2003), and receives a bilateral projection from DTG (Ryszka and Heger, 1979).

The anatomical connections of the NRe, another thalamic HD area, strongly implicate its role in spatial learning. The NRe provides a major projection into hippocampal CA fields (Su and Bentivoglio, 1990), and viral tracing work has shown the NRe disynaptically links the HPC to the medial prefrontal cortices (Prasad and Chudasama, 2013). The NRe is further well connected with numerous areas of the HD circuit: it also receives projections from the LMN, receives input from cortical HD areas (PoS and RSC), and projects to ADN. In spite of being centrally situated within the network, the functional role of the NRe in the generation and maintenance of the HD signal remains unknown.

However, current evidence points towards the ADN as the critical thalamic relay for the HD signal, given its unique projections from bilateral LMN (that AVN/AMN do nor receive), and that it is necessary for the maintenance of the HD signal downstream in cortical areas (see Section 1.4.4.4). As such, there is good evidence that the ADN sits between the LMN and cortical HD areas such as the PoS and RSC, in the HD system hierarchy, showing how the HD signal propagates through the mammalian brain. This canonical HD circuit is shown in Figure

1.9A, with a slightly more complete version (including some of the connections of other anterior thalamic nuclei) in Figure 1.9B.

1.4.4.4 HD activity from the thalamus to the cortex

The LMN provides projections to multiple nuclei in the thalamus, including the anterior thalamic nuclei and the laterodorsal thalamus, which appears to convey HD information. Similarly, the ADN appears to propagate the HD signal into cortical HD areas such as the PoS and RSC, to which it is reciprocally connected. Supporting this, lesions of the anterior thalamus abolishes the HD cells in the PoS, whereas HD cells can still be recorded in the ADN following PoS lesions (Goodridge and Taube, 1997). This is consistent with tracing showing strong connections between the PoS and ADN (van Groen and Wyss, 1990c), and RSC and ADN (van Groen and Wyss, 1990b, 1992; Van Groen and Wyss, 2003). Similarly, lesions in other downstream cortical areas such as mEC do not ablate the HD signal in the ADN (Clark and Taube, 2011).

ADN lesions do ablate HD cell activity in the PrCM, and greatly reduce the proportion of HD cells seen in the dorsal striatum (Mehlman et al., 2019b), indicating that the HD signal is largely propagated from the limbic thalamus into these extra-limbic areas. However, AHV cells in both areas were still present following ADN lesions.

Joint lesions of the PrCM and dorsal striatum, however, did not alter ADN HD cells in any assessed metric, including peak firing rate, encounter rate, and landmark anchoring to a prominent visual cue (Mehlman et al., 2019b). As such, the limbic HD circuit does not appear to receive self-motion information from AHV or HD cells in these regions, nor landmark information about the surrounding area. These findings are consistent with retrograde tracing experiments demonstrating significant projections from the ADN (and other anterior thalamic nuclei), mEC and LMN into the dorsal striatum, and projections from the RSC into both the dorsal striatum and PrCM (Mehlman et al., 2019a).

Although there is evidence that the HD signal in the anterior thalamus is required for HD cells in the PoS and RSc to maintain their directionality, bilateral lesions of the LDN do not abolish HD cells recorded in the PoS (Golob et al., 1998). Following LDN lesions, HD cells continued to fire with a unimodal PFD and similar peak firing rates, and successfully landmark anchored to 90° rotations of a cue card. As such, it appears that the HD signal propagates into cortex via the ADN, whereas other thalamic nuclei may not be necessary for the maintenance of the cortical HD signal.

1.4.4.5 Outputs of the HD system

The PoS sends large projections to the mEC (Preston-Ferrer et al., 2016), and the RSC is reciprocally connected with the mEC (Wyss and Van Groen, 1992; Jones and Witter, 2007; Agster and Burwell, 2009), providing candidate routes for the HD signal to reach directional and spatial representations in the area. Large excitotoxic lesions or inactivation of the ADN with lidocaine impaired the HD signal in mEC, with significantly fewer neurons being classified as HD cells post-intervention (Winter et al., 2015). However, a small population of directionally-modulated neurons remained, although these displayed significantly poorer directionality (assessed by mean vector length) than HD cells recorded in sham-lesion or non-inactivated animals.

Similarly, HD cells provide an important input to generate the spatial selectivity of grid cells. Inactivation or lesion of ADN disrupted the grid signal in mEC, with fewer grid cells found following intervention (Winter et al., 2015). mEC HD cells maintain a stable representation of direction even when the grid cell map fragments due to the environmental configuration (Whitlock and Derdikman, 2012), and unlike grid cells maintain their spatial precision in the absence of theta oscillations following medial septal inactivation (Koenig et al., 2011; Brandon et al., 2011, 2013). That the PoS (and PreS) HD cells project into the grid system of the mEC is further supported by the observation that most cells projecting into mEC originate within PoS layer III, where the highest density of HD cells are found (Preston-Ferrer et al., 2016; Huang et al., 2017). Juxtacellular labelling of functionally characterised layer III PoS HD cells demonstrated that these cells project most strongly into layer III of mEC, where neurons display strong directional correlates (Tukker et al., 2015; Preston-Ferrer et al., 2016). However, *ex vivo* assessments of connectivity indicate that all layers of mEC may receive some PoS, PreS and ParaS input via monosynaptic connections (Canto et al., 2012).

Together these findings indicate that the HD system may provide a direct and generative input into the mEC grid and HD systems, and is consistent with models that integrate HD, border, and speed information to form the grid cell lattice (Giocomo et al., 2011; Zilli, 2012).

The mEC also constitutes a major input to the hippocampus via the perforant pathway, and receives projections from hippocampal CA1 field and subiculum (for review, see van Strien et al. (2009)). Accordingly, excitotoxic lesions using ibotenic acid directed towards the hippocampus did not disrupt the HD cell activity recorded in the PoS or ATN (Golob and Taube, 1997). In all animals, the CA1 field of the hippocampus (from which major hippocampal outputs arise) was completely lesioned, indicating that the HD signal is generated and maintained external to the hippocampal place cell circuit.

Interestingly, lesions of areas of the HD circuit impairs the place selectivity of place cells (Calton et al., 2003). Similarly, reversible inactivation of the LDN using tetracaine impaired

the location specificity of the majority of hippocampal place cells on a radial maze (Mizumori et al., 1994), with the authors suggesting that the area may be involved in the binding of visual information into the directional sense in an experience-dependent fashion (see Section 2.6).

Place cells ordinarily can utilise a directional input to distinguish visually similar compartments: place cells repeat their firing fields less often across compartments oriented at different angles (Grieves et al., 2016) than across parallel compartments (Spiers et al., 2015). Lesions of the HD system increased place cell repetition across multiple differentially-oriented compartments (Harland et al., 2017), indicating that the HD system may be involved in propagating directional information through to the hippocampus. One candidate route for this is through the generation of BVCs, whereby place field repetition could result from repeating local geometry. In such a case, BVCs can provide a discriminating input to place cells in compartments that are aligned in different orientations (Grieves et al., 2018).

1.4.5 Landmark anchoring of HD cells

As discussed above, the HD signal is generated from vestibular inputs of the inner ear that code idiothetic information about the animal's head turns. However, any neural basis of orientation must be able to integrate sensory information from the external world (allothetic information) into its representation, if it is to be used for navigation in an allothetically rich world. In this vein, spatial representations should be consistent between successive exposure to environments – whether between days in the real world, or between trials within an experiment. As would be expected, HD cells maintain a consistent PFD relative to a learned visual cue over successive trials and days (Berkowitz et al., 2015).

As such, these allothetic landmarks exert an orienting influence over the HD system. HD cells 'landmark anchor' to the allothetic environment, and thus a given HD cell will maintain a constant PFD relative to the external world when recorded between trials. For example, if a HD cell is recorded from an animal in a circular arena with a single cue card, as shown in Figure 1.10, it will display a PFD that subtends some angle in the environment (in this case, approximately 30°). If the animal is removed from the cylinder, disoriented, and replaced in the cylinder – which has been rotated by some angle – the same HD cell will be seen to rotate its PFD by a similar angle. Here, the black cue card on the inside wall was rotated by 180° between trials 1 and 2, and the HD cell has rotated its tuning curve by a similar angle.

In this way, animals are integrating information about the external world into a representation of direction, providing a means for the HD system to correct any error accumulated due to reliance on path integration (Page and Jeffery, 2018). The following sections will review the sorts of sensory information to which HD cells landmark anchor, before discussing in detail

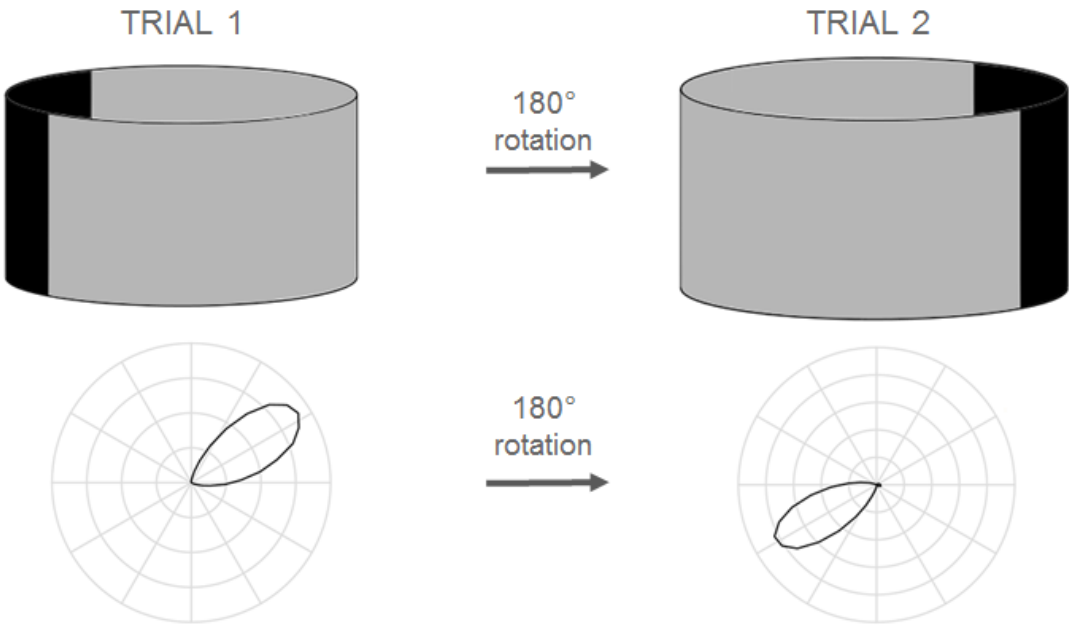

Figure 1.10: An HD cell recorded over two successive trials, between which a prominent landmark (here a black cue card attached to the inside wall) is rotated, will rotate its tuning curve to follow the cue. This process is landmark anchoring, and indicates the cell it using the visual scene to recalibrate its firing with the external world.

experimental and theoretical work on anchoring to visual landmarks.

1.4.5.1 Sensory hierarchy for landmark anchoring

Although numerous sensory modalities can provide anchoring input to HD cells, vision appears to exert the strongest influence over the rodent HD system (Goodridge et al., 1998). The strength that vision exerts over the HD system may be surprising given the low acuity of rodent vision (see Chapter 2).

Nonetheless, HD cells recorded in the dark, without access to distal landmark information provided by vision, appear to drift slowly over time at a rate of approximately 2.9 °/min (Goodridge et al., 1998). This is in spite of other possible allothetic influences such as sound, texture, smell and geometry. Moreover, in cases of conflicting inputs from differing modalities, the HD system sometimes appears to weight input from visual landmarks similarly to geometry (Clark et al., 2012b), and stronger than internal path integrative cues (Knight et al., 2011, 2014).

Of note, Goodridge et al. (1998) recorded PoS and ATN HD cells during rotations of visual, auditory, or olfactory landmarks. A peppermint-scented cotton-bud on the wall of the arena provided a weak orienting olfactory landmark to the HD cells, with rotations of the scented cotton correlating with shifts of HD cell PFDs with an angular deviation from the expected shift of $55 \pm 14°$, indicating that the animal can utilise odour information to orient itself in an

environment. The shifts following olfactory landmark rotations were significantly different from chance, although stimulus control was weaker in subsequent trials with shifts of the olfactory landmark. Similarly, rotating the entire apparatus (walls and floor) whilst the animal was blindfolded – which would amount to a rotation of any olfactory and tactile cues in the arena – led to shifts of the HD cell tuning curves, although the shift was smaller than would be expected, with a mean deviation of $47 \pm 12°$ (Goodridge et al., 1998). Although more error prone than PFD shifts following visual landmark rotations (cf Taube et al. (1990b)), the Rayleigh vector of the shifts was significantly different from random.

However, the authors found that a distal auditory cue, provided by a 1 Hz clicker or white noise burst, did not provide an anchoring stimulus to HD cells in the PoS or ATN. Accordingly, following rotations of the sound source, HD cell PFDs shifted with an average deviation of $112 \pm 8°$, an angle not significantly different from random (Goodridge et al., 1998).

Together, the data currently suggest that HD cells can integrate information from a variety of allothetic sources, although the influence from tactile and olfactory cues may only be weak. The observed underrotations may be due to conflict from a maintained idiothetic sense of direction or other allothetic cues, and so input from olfaction and touch may be weighted less strongly than this information.

Rotations of HD cells are frequently accompanied by concomitant rotations in other spatial cells. HD cells and grid cells in mEC rotate coherently (Sargolini et al., 2006), and place cells landmark anchor to non-ambiguous rotations of prominent visual cues (Cressant et al., 1997; Yoganarasimha and Knierim, 2005).

Vision exerts the strongest influence over the HD system – which might be explained as it is a more distal sense than olfaction or touch, and cue control in HD cells appears to be stronger for more distal landmarks (see Section 1.4.6).

1.4.6 Visual landmark anchoring

Cells anchor to a large variety of visual scenes, as has been demonstrated over the course of years of research. For example, HD cells have been observed to landmark anchor to white cue cards on a grey wall (the typical setup of Jeffrey Taube's lab: (Taube et al., 1990b)), a white or grey cue-card on a black wall of a triangular arena (Knight et al., 2011), a white torch-light shined in a spot on a translucent grey wall (Knight et al., 2014), and various patterned cues (Lozano et al., 2017).

Landmark anchoring in HD cells has been observed directly in many of the areas from which they have been recorded (PoS: Taube et al. (1990b), RSC: Lozano et al. (2017), LMN: Stackman and Taube (1998), ATN: Goodridge and Taube (1995)).

In order to provide useful information, a landmark should provide consistent directional information. This leads to the supposition that distal landmarks provide more orienting information than proximal landmarks – if the landmark is further away, there is less 'parallax error' caused by the landmark shifting its relative position in the visual field as the animal explores.

Accordingly, HD cells prefer to use distal landmarks to anchor their representation of orientation, as has been assessed by a number of cue conflict studies (this preference is less pronounced for place cells). Similarly, a number of models have been developed to explain how distal landmarks may be preferentially selected by the system for anchoring (Jeffery et al., 2016; Jacob et al., 2017).

In cases of allothetic cue conflict, introduced by rotating two visual cues in opposite directions, HD cells are likely to landmark anchor to a distal cue, with their PFDs shifting coherently to follow translations of this cue. Few cells rotated to follow the shift of a proximal cue, in the opposite direction (Yoganarasimha et al., 2006). For example, rotating a cue distal to an This trend was consistent across multiple sessions recorded with HD cells, and all HD cells co-recorded within a session were seen to exert the same behaviour. This coherent behaviour was not observed in CA1 place cells, which exhibited heterogeneous behaviour in a similar visual cue conflict paradigm (Knierim, 2002; Yoganarasimha et al., 2006), and is consistent with the attractor architecture model of HD cells (Section 1.4.4).

The HD system quickly learns associations between visual landmarks and directions, such that an HD cell will anchor to landmarks within the first few moments an animal is exposed to the environment. This will frequently happen even when the cue is in conflict with the animal's idiothetically maintained sense of direction: the cue will be used to 'reset' the directional firing of the HD system. Goodridge and Taube (1995) allowed rats to explore an environment with a large visual cue, which was subsequently taken away. The animal would then have to maintain its sense of direction using solely idiothetic information. However, reintroducing the cue after a period of time, in conflict with the idiothetic estimate of direction, caused HD cells to shift their PFDs to align with the original orientation relative to the cue. This demonstrates an ability of the HD system to use visual cues to reorient, even when these cues are in conflict with an internally-updated sense of direction (Taube and Burton, 1995). Similarly, HD cells rotated their firing fields to follow rotations of a T-maze, even when the animal was not disoriented, indicating that the HD system was more influenced by allothetic (including visual) components that defined the local reference frame of the T-maze, than by an internal sense of direction Dudchenko and Zinyuk (2005). The authors also recorded HD cells as animals traversed between multiple rooms in a four-compartment arena; the HD cells maintained a consistent firing direction when the animal walked into a novel room, but in a

familiar compartment (that the animal had experienced before, and in which the HD system had formed an association with the landmarks) HD cells reoriented their PFDs relative to the original orientation they had learned (Dudchenko and Zinyuk, 2005). Over time (as the animal explored), the HD cells sometimes converged to a single representation, which was argued to show an increased weighting of self-motion information over time. However, this may be an example of weighted cue integration converging on a single stable representation.

Taken together, the results demonstrate a strong influence of visual scenes on HD cell directional firing – frequently weighted more strongly than inputs of other modalities. Knight et al. (2014) performed a similar experiment to Goodridge and Taube (1995), and found that HD cells followed a shifting visual landmark when it conflicted with the idiothetic representation of direction by up to 120°; conflicts greater than this angle caused the HD cells to ignore the cue, and weight the idiothetic estimate of direction more heavily.

As such, the system can also quickly learn to ignore a landmark it realises is unstable. This is more likely if the animal is aware the landmark is moving repeatedly, and conflicts more with the animal's idiothetic sense of direction. As such, it can be argued that HD cells perform a weighted-cue integration, so as to optimally combine idiothetic and allothetic information into a single representation of direction (Knight et al., 2014; Page et al., 2014). This would explain the phenomenon seen in some paradigms of 'under-rotation', in which some HD cells rotate their PFDs slightly less than the rotation of the cue card (Taube et al., 1990b; Knight et al., 2011); the weak influence of a remaining idiothetic sense of direction could cause a small deviation in the PFD shift.

Interestingly, learning to associate a visual landmark with a direction appears to be dependent on NMDA receptor activity. Systemic injection of an NMDA antagonist reduced peak firing rates of ADN HD cells (Housh et al., 2014; Berkowitz et al., 2015), but cells were still controlled by a salient visual landmark in an environment. However, if recorded over multiple days, HD cells recorded on the day following NMDA antagonist infusion displayed different PFDs relative to the PFD during the drug administration (Berkowitz et al., 2015). This indicates that the system failed to learn a representation in the visual environment, and that NMDA transmission is necessary for the plasticity needed for the HD system to associate a cue with a direction.

Although these authors recorded from the ADN, visual information appears to be integrated into the HD representation in the cortical HD areas, and backpropagated through the remainder of the system, presumably via the recurrent connections through the network, reviewed above. Lesions of the PoS abolish landmark anchoring in HD cells recorded from both the ADN (Goodridge and Taube, 1997) and LMN (Yoder et al., 2015), such that the HD cells no

longer rotate their tuning curves to follow rotational transformations of a prominent visual cue. ADN tuning curves were wider following PoS lesions (Goodridge and Taube, 1997), indicating that the landmark information provides a stabilising input that helps the HD system to maintain a precise representation of orientation while an animal navigates.

Another area involved in the integration of landmarks into the HD system appears to be the RSC: bilateral RSC lesions similarly impair landmark anchoring in ADN HD cells (Clark et al., 2010), although the deficit does not appear to be as severe as that following PoS lesions. Although taken together, there is good evidence that these cortical areas route landmark information throughout the HD system, it is unclear what the relative contribution of the PoS and RSC are. Moreover, both of these areas are well suited to receive visual information from a plethora of visual brain areas; it is unknown through which visual pathway landmark information reaches HD cells. Some candidate routes are discussed in Yoder et al. (2011), and in Section 2.6.

1.4.7 Where does landmark information come from?

This thesis concerns itself with the phenomenon of visual landmark anchoring of the HD system. In particular, although the HD system is known to anchor to a variety of (experimenter defined) landmarks – frequently cue cards on walls – it is still unknown in what form landmark information is presented to the HD system, how it is integrated into a pre-existing representation of direction, and the role that the visual system (and its component areas) play in the identification, extraction, and processing of landmarks.

In this thesis, I wish to address the question of whether the cortical visual pathway (reviewed in Chapter 2), traditionally associated with high-acuity vision, is necessary for a visual scene to exert cue control over the postsubicular HD system.

Chapter 2

Introduction to Vision

> Was der Fall ist, die Tatsache, ist das Bestehen von Sachverhalten.
>
> What is the case, the fact, is the existence of atomic facts.
>
> TLP 2; Wittgenstein (1922)

2.1 Introduction

Rodent vision is a richly studied functional system of the brain. Much early work in visual neuroscience, and the corresponding models of the visual brain that emerged from this work, used cats and non-human primates as animal models. Although much of what has been learned can be applied to rodent research, there are important differences in the structure and function of the visual system between rodents and higher mammals: for example, rodents lack a retinal fovea, contributing to a lower spatial acuity of the retina, and have a poorly developed X-cell system (Sefton et al., 2015).

Furthermore, although numerous studies have attempted to delineate visual cortical areas of different rodent species, it remains unclear whether differing rodent species possess the same visual processing areas of the brain (Laramée and Boire, 2015), and it may be argued that given the genetic and ecological diversity of rodents, research in one species may not be applied uncritically to another (Krubitzer et al., 2011). Therefore, because of these ethological differences, this chapter will exclusively review literature of the rodent visual system, focusing predominantly on the rat.

Visual pathways in mammals, including rats, are to some extent parallelised: the retina projects to multiple unique sites through the brain, each with unique connectivity and (presumably) function. Many of these pathways subtend simple behaviours, whereas others underlie

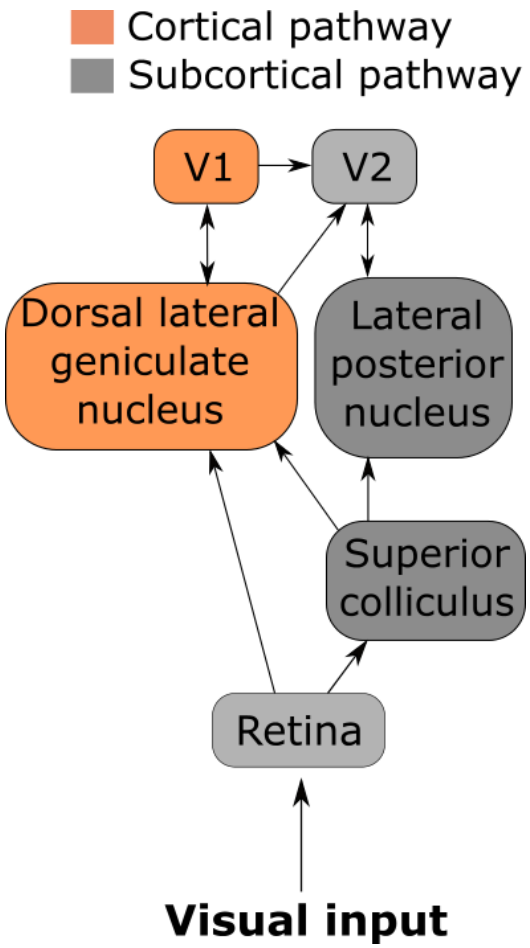

Figure 2.1: Simplified schematic of the cortical (geniculostriate) and subcortical (colliculopulvinar) pathways of the rodent visual system.

more complex actions and functions; this is often reflected in the physiology and electrophysiology of the areas. For example, some axons in the optic nerve, projecting out of the retina, terminate in the contralateral pretectal area and subtend the pupillary light reflexes – the contraction of the pupil in response to bright light (Hall and Chilcott, 2018).

Although the simplified model specifies that these pathways operate largely in parallel, with little overlap or interaction, in reality there are numerous projections between the brain nuclei involved in each pathway. This reflects the complexity of the visual system as a whole, and should be borne in mind when considering the physiology of the overall visual system. A simplified summary of the projections to be discussed in this chapter is shown in Figure 2.1.

2.2 The rodent retina and its fugal fibers

The electrophysiological characteristics of RGCs in the rodent are well described, but largely beyond our concern. They target a large number of visual areas within the rodent brain (reviewed in detail in Sefton et al. (2015)); of note, two large, organised projections target

the dLGN (Section 2.3) and the SC (Section 2.4). RGCs (and neurons downstream in the visual system) have restricted receptive fields within the animal's visual field (that is, responses can be evoked only from light stimulation coming from a particular region of the visual field), which frequently display characteristic centre-surround organisation (Brown and Rojas, 1965; Partridge and Brown, 1970). This organisation is such that a stimulus presented in the centre has the opposite effect on the cell to the same stimulus presented in the surrounding portion of the visual field; if a light presented in the centre of an RGC's receptive field elicits an increase in the RGC's firing rate, shining a light in the receptive field surround will decrease the cell's firing rate. This sort of cell is referred to as an ON-cell, as increases in luminance on the receptive field centre cause an increase in firing rate. Cells that decrease their firing rate to a light presented at the centre of their receptive field (and therefore increase their firing rate when the light is presented on the antagonistic surround) are called OFF-cells, and therefore would be excited by a decrease in receptive field centre luminance (i.e. darker than the surround). More complex variants of this classification have been described (Brown and Rojas, 1965; Partridge and Brown, 1970; Sagdullaev and McCall, 2005; Heine and Passaglia, 2011).

In general, rodent RGCs have quite large receptive fields, with an average centre size of 7° and surround size of 12° (Brown and Rojas, 1965; Partridge and Brown, 1970; Heine and Passaglia, 2011); this corresponds with the observed extremely low spatial acuity of RGCs, which appears to have a limit of 0.2 cycles/° (cpd, Powers and Green (1978); Heine and Passaglia (2011)), and the generally accepted low acuity of the rodent assessed through visual behavioural experiments (Dean, 1981b).

The temporal dynamics of neural spiking during light stimulation allowed classification of rat RGCs into 'brisk' and 'sluggish' cells (short versus high latency between stimulus and cell responses, respectively) (Heine and Passaglia, 2011). As a population, brisk RGCs on average displayed mild preferences for the orientation of sinusoidal gratings presented on their receptive fields, although some variation between units was seen and not all showed clear orientation preferences (Girman and Lund, 2010; Heine and Passaglia, 2011). This is similar to orientation biases seen in RGCs from other species (such as cat, Levick and Thibos (1982)), and no evidence was found for a topography of orientation preferences over visual space. However it is likely that some early processing is occuring to extract visual features (e.g. orientation of edges) at the retinal level, which may aid extraction of landmark information about the visual scene (e.g. the locations of corners in an arena). Although early work in rodents such as squirrels suggested that these direction-sensitive RGCs targeted superior colliculus, and did not project to dLGN (Michael, 1972; Semm, 1978) – consistent with the finding that the dLGN in general exhibits weaker orientation and direction encoding than other parts of the visual system, such

as visual cortex (Scholl et al., 2013; Zhao et al., 2013) – it is now known that a direction- or orientation-selective population of RGCs do also project into dLGN (Piscopo et al., 2013; Ellis et al., 2016).

However, visual environments typically used in navigation experiments typically have large cue cards that subtend large angles of visual space; the low spatial frequencies of rodent RGCs are well within the acuity of the retina as determined electrophysiologically. As HD experiments demonstrate the integration of visual information into representations of heading direction (see Chapter 1), it is evident that the retina is able to process pertinent information from these visual scenes.

2.3 Cortical pathway

One significant visual pathway present in mammals is the geniculostriate pathway: a projection from retina, through the dorsal lateral geniculate nucleus (dLGN), into the primary visual cortex (V1; also known as striate cortex or Oc1, and corresponds to Brodmann area 17). As, in this thesis, interventions will be directed towards the dLGN, particular time will be spent reviewing its connectivity.

2.3.1 dLGN

2.3.1.1 Afferents

In rats, the retinogeniculate projection is smaller than in primates, with only an estimated $25 - 50\%$ of RGCs projecting to dLGN (Dreher et al., 1985; Linden and Perry, 1983; Martin, 1986). As in other mammals, the rat dLGN receives projections from RGCs whose receptive fields lie in the contralateral visual field, and which cross hemispheres at the optic chiasm. In the rat, this means that the majority of innervation of the dLGN is provided from the contralateral eye, as there is only a small binocular angle of visual field. However, there is a distinct region of dLGN that is recipient of axons from the ipsilateral eye, corresponding to the most nasal portion of visual field in the ipsilateral eye (Reese and Cowey, 1983; Reese, 1988).

There is a general tendency in the mammalian visual system for RGC terminals in dLGN to preserve a retinotopy via 'lines of projection' through the nucleus (Bishop et al., 1962). As a rule, RGC axons from the ipsilateral and contralateral eye terminate in distinct laminae (visible in Nissl stains of brain slices), with a point in the visual field being represented by all neurons along the line of projection drawn orthogonally through the laminar planes. As such, RGCs from both eyes with receptive fields similar in position are brought into alignment.

In the rat, some electrophysiological attempts of finding retinotopy in the dLGN failed to

correlate receptive field position of recorded neurons with electrode location in the nucleus (Montero and Guillery, 1968). However, recordings were frequently made from albino rats, which possess genetic mutations known to cause significant changes across the visual system (Reese, 1988).

Nissl and myelin staining of the dLGN in the hooded rat also failed to show clear laminar organisation as is present in higher species, although there is a clear segregation of inputs from each eye (Reese, 1988). Evidence has since acculumated that the rat dLGN contains 'hidden laminae' that, in spite of being invisible to standard cytoarchitectural analysis, underlie a similar retinotopy to that seen in the cat and primate (Reese, 1988). Localised retinal lesions in the hooded rat produced anterograde degeneration in restricted areas of the dLGN, that was organised topographically (Reese and Cowey, 1983). Nearby points on the visual field were apposite within the dLGN, although clear laminae were not visible.

Furthermore, neurons were recorded extracellularly, in anaesthetised hooded rats, in regions of dLGN known to receive input from the contralateral or ipsilateral retina (Reese and Jeffery, 1983). When recorded in this way, the projection from each eye was shown to be individually retinotopic, and organised such that the superior/inferior axis of visual field is distributed across the anteroposterior axis of dLGN, and the mediolateral axis in the nucleus mapped the nasal-temporal axis of visual field. 'Lines of projection' of the binocular visual field extended rostroventrally, so were oriented obliquely through the nucleus (Reese, 1988).

The rat dLGN has been argued to be divisible into two broad regions: an outer 'shell', occupying the posterior and dorsolateral edges of the nucleus, and an inner 'core' that lies anteromedial inside dLGN (Reese, 1988). It should be noted that the ispilateral retinal projection into dLGN is restricted to a subregion within the anterior and medial portion of the dLGN, and therefore lies within the inner core of the dLGN.

The dLGN shell appears to receive distinct projections compared with the core: direction-sensitive RGCs project exclusively into the dLGN shell (Cruz-Martín et al., 2014), and receives strong inputs from the superior colliculus (Grubb and Thompson, 2004). These tecto-geniculate projections appear to be 'driver-like', rather than modulatory, leading to the proposal that the dLGN shell is a location of convergence of information about stimulus motion and orienting movements (Bickford et al., 2015).

Interestingly, the shell and core have different layer-specific projection targets within rodent V1: the shell projects more heavily to layer I, whereas the core projects more stronger to deeper layers such as layer IV (Cruz-Martín et al., 2014). Coupled with the finding that dLGN cells projecting into V1 layer I are more strongly modulated by grating orientation and direction than those projecting to layer IV (Cruz-Martín et al., 2014; Kondo and Ohki, 2015), there

LGN Afferents	
Retina	Reese and Jeffery (1983)
Superior colliculus	Grubb and Thompson (2004); Bickford et al. (2015)
V1 (layer VI)	Nauta and Bucher (1954)
Reticular nucleus of thalamus	Coleman and Mitrofanis (1996)
Parabigeminal nucleus	Sefton et al. (2015)
Postrhinal cortex	Tomás Pereira et al. (2016)
LGN Efferents	
V1 (layer IV)	Ribak and Peters (1975)
V1 (layers I/VI)	Peters and Saldanha (1976); Cruz-Martín et al. (2014)
Reticular nucleus of thalamus	Coleman and Mitrofanis (1996)
Higher visual areas	Hughes (1977)
Postrhinal cortex	Agster et al. (2016)

Table 2.1: Summary of some afferent and efferent projections to and from dorsal lateral geniculate nucleus (dLGN).

is evidence for parallel routes of information to flow through dLGN into the visual cortices (Bickford et al., 2015).

Besides visual influences from the retina and superior colliculus, the dLGN also receives information from layer VI of V1 (Nauta and Bucher, 1954), which are likely to be modulatory in nature (Petrof and Sherman, 2013) and execute gain control on the main efferent neurons in the dLGN (Olsen et al., 2012). This provides a plausible route by which contextual information can help to sharpen dLGN neuron stimulus selectivity and to provide heuristics for the appropriate early processing of sensory inputs into the correct perceptual categories (argued to be a form of 'graceful degradation', and discussed in Weyand (2016)). Therefore, it appears the dLGN can perform a large set of visual processing functions, and therefore may be considered more than a 'simple' first-order relay.

The dLGN also receives convergent projections from a large number of other sources, including a number of nuclei in the brainstem and a substantial inhibitory projection from the thalamic reticular nucleus. These will not be discussed here, but are reviewed in Monavarfeshani et al. (2017) and are summarised in Table 2.1.

2.3.1.2 Electrophysiological characteristics of the dLGN

Electrophysiology in the rodent dLGN has demonstrated similar visual response characteristics to those seen in the retina. ON- and OFF-cells were both seen, alongside cells which positively coded both increases and decreases of luminance within their receptive field centres (ON-OFF cells, Fukuda et al. (1979)). Units recorded from the dLGN have been shown to display both linear and non-linear spatial summation over their receptive fields, and demonstrated similarly low spatial acuities as RGCs (with a spatial frequency preference of 0 05-0.09 cpd, Lennie and Perry (1981)).

There is evidence of a population of cells in dLGN that show preferences to particular orientations of gratings, and to the direction of motion of gratings (Piscopo et al., 2013; Scholl et al., 2013; Zhao et al., 2013; Tang et al., 2016), which appears not to be inherited from visual cortex, but propagates to it (Scholl et al., 2013). Some cells have been shown to negatively code for contrast, displaying maximal firing rate to a uniform grey full field, and a lower firing rate when high contrast objects (black/white circles) are visible on the field (Piscopo et al., 2013). Rodent recordings have in general unveiled a larger diversity in response properties of dLGN neurons than has been seen in other species (Usrey and Alitto, 2015). That a diverse set of visual features is encoded in the neuron populations in dLGN supports the notion that information relevant to the visual content of space could be extracted in the region.

Further implicating the role of the dLGN in spatial processing is the recent discovery of place-like cells within dLGN (Hok et al., 2018). These will be discussed in more detail in Section 2.6.

2.3.1.3 Efferents

In contrast to the ventral portion of the LGN (which does not project to visual cortex), the predominant projection from dLGN is into layer IV of primary visual cortex (V1) via the optic radiation (Ribak and Peters, 1975; Peters and Feldman, 1976), while another projection terminates in V1 layer I (Cruz-Martín et al., 2014; Ji et al., 2015). A small projection into layer VI has also been reported (Peters and Saldanha, 1976), but is not substantiated by recent work. The geniculo-striate projection preserves the retinotopy within dLGN (LeVere, 1978). However, multiple projections from the dLGN into areas adjacent to V1 (the medial and lateral extrastriate cortices) have also been found – indicating that there may also be direct visual thalamic input into higher visual areas (Hughes (1977), Agster et al. (2016), see Section 2.5). The only other notable projection from dLGN in the rodent is a substantial projection to the ipsilateral thalamic reticular nucleus, likely from collaterals of relay cell axons projecting to V1 (Kerschensteiner and Guido, 2017; Monavarfeshani et al., 2017).

That the efferent projections from the dLGN are (in a sense) simpler than those of other visual areas of the rodent brain attests to the singularity of function of the rodent dLGN (Monavarfeshani et al., 2017), and has led to the traditional classification of the dLGN as a first-order relay nucleus with the sole function of projecting visual information forwards to the visual cortex (Sherman, 2007). However, a single neuron in dLGN is known to extensively receive from and project throughout the rodent visual thalamus, indicating a large degree of convergence of visual information into the nucleus (Morgan and Lichtman, 2019).

A number of excellent, recent reviews on the anatomy, function, and connectivity of the

LGN have recently been written: Usrey and Alitto (2015); Weyand (2016); Kerschensteiner and Guido (2017), and Monavarfeshani et al. (2017).

2.3.2 V1

Axons leaving dLGN project via the optic radiation along the superficial layers of the subcortical white matter into V1 (Woodward and Coull, 1984; Woodward et al., 1990). The retinotopy in mice is such that the medial V1 represents temporal visual space (the nasal retina), and anterior cortex represents the inferior visual field (superior retina, Schuett et al. (2002)).

Besides the projection from dLGN, V1 receives a number of projections from other cortical areas – including feedback projections from higher visual areas as a top-down processing signal (broadly from both from V2M and V2L, Coogan and Burkhalter (1993); Berezovskii et al. (2011)), and a motor efference signal presumed to signal a prediction of optic flow from M2 (Leinweber et al., 2017).

Interestingly, the projections from dLGN to V1 are patchy, and have been shown to align with areas of V1 that contain neurons with higher spatial acuity; neurons in areas outside of the patchy dLGN afferents show higher temporal acuity (Ji et al., 2015). This is consistent with the finding that direction-sensitive RGCs are projecting to layer I of V1 (Cruz-Martín et al., 2014), and may indicate different routes of information flow into different cortical streams.

One significant set of outputs from V1 is into the flanking extrastriate areas immediately medial and lateral to it (Olavarria and Montero (1981), see Section 2.5). This propagates visual information into higher-level representations, that plausibly could include the detection and extraction of landmarks from a visual scene. However, there are also direct projections from V1 into cortical HD areas: including the RSC (van Groen and Wyss, 1990b, 1992; Van Groen and Wyss, 2003) and PoS (van Groen and Wyss, 1990c), and to other areas in which HD cells have been identified, such as the dorsomedial striatum (Khibnik et al., 2014) and S1 (specifically the region containing somatosensory representations of the animal's head, Olavarria and Montero (1984)). These projections could convey a landmark signal directly into the HD system.

Within the visual system, V1 provides an important large feedback projection from layer VI into the dLGN and its adjacent thalamic reticular nucleus (Erişir et al., 1997; Wang and Burkhalter, 2007). For a review of some of these cortico-thalamic projections, see Crabtree (2018). V1 also projects through into higher visual areas in the flanking extrastriate cortex, here collectively referred to as V2. As such, visual information is propagated into further specialised regions that may subtend other visual behaviours (see Section 2.5).

2.4 Subcortical pathway

The majority of RGCs in the rodent retina project through a subcortical visual pathway involving the superior colliculus. Historically, this general area has been referred to as the optic tectum, and is well conserved across multiple species (Vanegas, 1984), indicating its evolutionary age. Ethologically, the observations that some areas in this pathway are conserved across diverse taxa (Northcutt, 2002), and that visual orienting and navigating behaviours are likely to be evolutionarily early (Nilsson, 2009), further indicates it may play a role in the processing of various types of visual information and may subtend numerous visual behaviours including in the integration of vision into representations of orientation.

Here, we briefly review the anatomy of the subcortical visual pathway, and discuss some behaviour known to involve these visual areas.

2.4.1 Superior colliculus

2.4.1.1 Connectivity

At least 70% of RGCs from the rodent retina project via the optic tract into the superior colliculi (SC, Hofbauer and Dräger (1985)), with some estimates as high as 90% (Ellis et al., 2016). Interestingly, a large proportion (80%) of the RGCs that project into the dLGN send branched axons that also project into the SC (Ellis et al., 2016). Grossly, the SC are easily identified as a pair of hillocks jutting out of the dorsal surface of the midbrain (mesencephalon), and can histologically be separated into seven separate layers of alternating neuropile and myelinated fibres (Lund, 1972; LeVere, 1978). It is typical to divide these layers into two groups: the superficial layers (sSC, comprised of the zonal, superficial grey, optical, and (part of the) intermediate grey layers) and deep layers (the intermediate grey, white, deep grey, and deep white layers). This classification broadly corresponds to fundamental anatomical and functional differences between the layers: superficial layers are more strongly connected with visual areas of the rat, both receiving and projecting across the visual system (see Lund (1972) and LeVere (1978) for review), whereas deeper layers receive inputs from additional modalities such as the auditory and somatosensory systems, and provide efferents to motor and brainstem systems (for head and eye movements, see Sparks and Hartwich-Young (1989) for review).

The vast majority of retinal afferents arise from the contralateral retina, having crossed at the optic striatum (LeVere, 1978), and terminate in the superficial layers of the SC. There is a retinotopy to the projection into the sSC, as has been quantified electrophysiologically (Siminoff et al., 1966). The temporal visual field (represented in the nasal retinal quadrants) projects into the posterior portions of the sSC, whereas the nasal field (temporal quadrants) project

anteriorly. Similarly, the ventral-dorsal axis of the retina projects along a medio-lateral axis in the sSC, with the upper (dorsal) quadrants projecting more laterally (Siminoff et al., 1966; Lund, 1972; LeVere, 1978; Ito and Feldheim, 2018). A small ipsilateral projection into sSC has been shown to originate from the lower temporal retinal quadrant (Lund et al., 1980; May, 2006; Kim et al., 2010; Ito and Feldheim, 2018).

The visual cortex also sends substantial projections into the sSC, which arise from both primary and extrastriate visual areas (Nauta and Bucher, 1954; May, 2006). The projection in rat arises from ipsilateral visual cortex, and terminates only in the sSC (Lund, 1969, 1972; LeVere, 1978). Restricted lesions of V1 lead to localised degeneration in SC, indicating a topographic map like that from the retina. This map is organised such that neurons in V1 project to the region of sSC encoding the same part of the visual field (Lund, 1972). Multiple areas of rat extrastriate visual cortices also project into the SC, showing similar topography of projection as that from striate cortex (Olavarria and Van Sluyters, 1982).

One major output of the superficial layers of SC is into the lateral posterior nucleus of the thalamus (Tohmi et al., 2014). Although not considered here, one of the largest outputs of superficial layers of sSC project into the deeper layers of SC, which in turn projects to brainstem and posterior thalamic areas to drive saccadic and head movements (LeVere, 1978).

The superficial SC also sends an important projection into dLGN (Grubb and Thompson, 2004; May, 2006), such that processing in the subcortical visual pathway can modulate activity in the geniculostriate pathway. Indeed, although this projection is quite small compared to the SC's other outputs, the SC appears to perform gain modulation in dLGN, such that optogenetically inactivating SC reduces neural responses to visual stimuli in V1, an effect not mediated by its projections to the lateral posterior thalamus (Ahmadlou et al., 2018). These projections appear to convey information about larger or rapidly moving stimuli (Gale and Murphy, 2014), and provides a route by which the sSC can indirectly modulate visual responses in V1. The sSC also projects into the ventral portion of the LGN (LeVere, 1978). As such, the sSC projects into a large variety of other visual areas in the rodent brain.

Through these connections, the sSC could provide input throughout that subtends visual behaviours (including those that are observed following ablations of striate cortex) that may include the processing of landmarks in the visual scene for attention and orientation.

2.4.1.2 Electrophysiology

Electrophysiologically, neurons in the mouse sSC have been well described. As in the dLGN, SC neurons encode information about a variety of visual features, including for the orientation (Girman and Lund, 2007; Wang et al., 2010) and direction (Humphrey, 1968; Girman and

Lund, 2007) of moving gratings, and frequently display optical stimulus sizes consistent with centre-surround organisation of receptive fields (Girman and Lund, 2007; Ahmadlou et al., 2017; De Franceschi and Solomon, 2018). Neurons in the SC display a large variety of preferences for spatial and temporal frequencies of gratings (Prévost et al., 2007; Wang et al., 2010), and show the classical centre-surround organisation of receptive fields (Girman and Lund, 2007; Wang et al., 2010). There is evidence that neurons projecting to different targets downstream of the sSC tend to encode different visual properties: for example, those projecting to dLGN have large receptive fields and are rarely directional, whereas those projecting to LPN have smaller fields and occasional directionality (Gale and Murphy, 2014).

There also appears to be a difference in the functional characteristics of RGCs projecting to SC compared with those projecting to dLGN: a higher proportion of SC-projecting RGCs show transient firing to visual stimulation (and tend to prefer smaller stimuli, with RGC populations including the direction-sensitive ON-OFF, transient-ON, and transient-OFF cells), whereas those projecting to dLGN tended to display sustained firing (sustained ON and sustained OFF RGCs, Wang et al. (2010); Ellis et al. (2016)). This finding could explain functional differences between electrophysiological characteristics of neurons in the SC and dLGN, and may underlie how different visual pathways process and extract information about the visual scene.

Of note, differences in spatial frequency coding between the cortical and subcortical visual pathways may in part subtend the differences between the functional roles these pathways have. It is unknown whether landmark information is derived predominantly from low- or high-spatial frequency content in a visual scene, although in principle low-spatial frequency information would carry coarse global information that could be used to quickly recognise a scene and presumably orient oneself in space (Kauffmann et al., 2014; Musel et al., 2014; Berman et al., 2017; Dima et al., 2018).

2.4.2 Lateral posterior thalamus

The lateral posterior nucleus of the thalamus (LPN) is a high-order thalamic nucleus (Sherman, 2007) that integrates information from a large number of cortical and subcortical areas (Takahashi, 1985; Kamishina et al., 2009). In higher mammals, the homologue of the lateral posterior thalamus has grown in size, in correspondence with the growth of higher visual cortical areas, leading to a cluster of thalamic nuclei referred to as the pulvinar complex in cats, non-human primates and humans (Felleman, 2001; Zhou et al., 2017). Although much work has been undertaken to describe the function and significance of the pulvinar complex in higher species (for review, see Shipp (2003) and Smythies et al. (2014)), here we will consider only work pertaining to the rodent.

2.4.2.1 Connectivity

The LPN receives significant projections from the sSC and diverse regions of visual cortex (Tohmi et al., 2014; Zhou et al., 2017). A number of subdivisions of the LPN have been described (Takahashi, 1985). Afferent projections from sSC and visual cortex appear terminate in different areas, with the more posterior extent of LPN receiving input from the sSC (the tecto-recipient zone), and anterior LPN receiving from cortical areas 17, 18, and 18a (the cortico-recipient zone, Mason and Groos (1981); Takahashi (1985)). These adjacent, but separate, zones may suggest that the two retinotopic maps observed in the pulvinar complex of primates (Shipp, 2003) also exist in rodents. Accordingly, receptive field mapping of single neurons in the LPN did find evidence of a preserved retinotopy (Allen et al., 2016), although evidence of two independent maps was not reported. The retinotopy of the LPN was such that the contralateral nasal visual field was represented in the lateral LPN, and the temporal field more medially. It has since been shown that at least two retinotopic maps exist in the LPN, one within the tecto-recipient zone and one within the cortico-recipient zone (Bennett et al., 2019).

Consistent with the existence of two separate zones in LPN, single-unit recordings coupled with optogenetic inactivation of V1 drastically reduced visual responses of neurons in the cortico-recipient (anterior) zone, whilst only mildly affecting neural responses in the tecto-recipient (posterior) zone. Pharmacological inactivation of SC caused the opposite pattern: neural responses to visual stimuli were greatly reduced in the tecto-recipient zone, but not in the cortico-recipient zone (Bennett et al., 2019).

Various other regions of cortex also project into the LPN, which will not be reviewed in detail. Within the cortico-recipient zone, there is evidence that distinct higher visuals areas within areas 18 and 18a project to distinct subregions of the LPN (Tohmi et al., 2014). Also of note, Mason and Groos (1981) observed some projections from area 36 into the tecto-recipient zone, which may correspond to the peri/postrhinal cortices of the rat (Burwell et al., 1995). These parahippocampal areas have been implicated in the processing of visual environmental landmarks (Peck and Taube, 2017), and in memories of contexts, objects, and places (Eacott and Gaffan, 2005).

The LPN also sends projections to V1, and back to the extrastriate areas it receives from (Kamishina et al., 2009), with different extrastriate areas receiving input from distinct subregions of LPN (Tohmi et al., 2014). This input appears to be significant (and driver-like), such that optogenetic activation *ex vivo* of LPN neurons projecting to extrastriate cortices reliably evoked action potentials in extrastriate neurons to which they synapsed (Zhou et al., 2018). Action potentials were more often evoked in extrastriate neurons projecting to the striatum or V1 than those projecting to the SC, and implicates the LPN in higher visual processing and

function.

Within the rostral LPN, a number of spatial and associational cortical areas are reciprocally connected to the LPN. These include some areas that are known to contain HD cells, including the granular and dysgranular retrosplenial cortices, posterior parietal cortex (an area containing HD cells and other egocentric representations of space, see Section 1.4.1.2.4 and Whitlock et al. (2008)) and V2M (Kamishina et al., 2009). Parts of the LPN also project into the dorsocentral striatum, and the dorsolateral and dorsomedial striatum (Kamishina et al. (2008), where HD cells have been reported, Mehlman et al. (2019b)). As such, it is plausible that the LPN is a route by which highly processed visual information reaches the HD system.

2.4.2.2 Electrophysiology

Little work has been performed to characterise the visual response properties of LPN neurons until recently. Similar to in other visual areas, a variety of response profiles were observed; approximately half of all recorded neurons showed visually-evoked responses (247/526, Allen et al. (2016)). Although it is possible the authors likely also recorded from sites adjacent to LPN, they found no anatomical segregation between visual and non-visual cells. Rather, it is likely that these cells were not responsive to the stimuli tested, and may respond to moving or orientation stimuli, or they may integrate information from multiple sensory modalities. In accordance with this, there is evidence that a population of cells in LPN are sensitive to a conjunctive of light and nociception (Noseda et al., 2010). That the LPN may integrate and bind information from multiple sensory sources is consistent with its plausible role in extracting and processing information for spatial orientation, for which representations are frequently abstract and multimodal.

Of visually-responsive cells, most displayed transient activity following the onset or offset of a stimulus, with most cells sensitive to both (Allen et al., 2016). A subset displayed sustained responses to visual stimuli, and a small number exhibited a delayed response to stimulus presentation. Most ON-cells displayed large receptive fields, with little detected surround-inhibition. Indeed, the receptive field size of LPN cells tended to be larger than those seen in the mouse dLGN (Grubb and Thompson, 2003).

Recent work has characterised the neural response in LPN to a number of varied visual stimuli (Bennett et al., 2019). Consistent with the low number of visual neurons seen in Allen et al. (2016), a smaller proportion of neurons responded to sparse noise stimuli than other types of stimulus tested. There were differences in visual responses between anatomical subregions of the LPN: neurons in the posterior portion of LPN (that receives input primarily from sSC) responded more strongly to moving gratings and looming stimuli, consistent with electro-

physiology in the sSC. Similarly, posterior LPN neurons had larger receptive field sizes than neurons in the other (anterior or antero-medial) subregions. However, posterior LPN neurons still responded more strongly to small (5°) stimuli than other neurons.

Coupled with the connectivity of the LPN into HD areas and regions implicated in spatial processing, it remains plausible that the subregions of LPN contribute to different visual functions, one of which may be processing of visual landmarks.

2.5 Higher visual areas

Similar to primates and other animals, rodents possess a number of higher visual areas that appear to be (at least in part) specialised for certain visual functions. These areas encode higher-order visual representations that may be important in performing complex visual tasks (Huberman and Niell, 2011). These areas in cats and primates are known to contain codes for object recognition, depth perception, and motion, with evidence existing separate 'streams' of information processing: a dorsal stream that processes object location and spatial vision, and a ventral stream that processes object identity (the 'where' and 'what' pathways, respectively, Mishkin et al. (1983); Ungerleider and Haxby (1994)). Therefore it may be within these areas that many representations relevant to spatial orientation and localisation are extracted and presented to spatial systems.

Early categorisation of the rat extrastriate cortex by some authors described a single higher visual area V2, lying laterally to V1 (Wagor et al., 1980; Kaas et al., 1989; Malach, 1989), a view which was later recapitulated by Rosa and Krubitzer (1999). However, the extrastriate areas were more frequently delineated into two areas of higher visual cortex lying either side of V1, based on asymmetric anatomical connectivity Coogan and Burkhalter (1993): V2L (which lies lateral to V1 and corresponds to cytoarchitectonic area 18a), and V2M (medial to V1, cytoarchitectonic area 18b[1]). It is well known that both V2L and V2M receive extensive projections from V1 bilaterally (Nauta and Bucher, 1954). It is evident that both V2M and V2L contain many smaller higher visual areas from both anatomical (Montero et al., 1973a; Olavarria and Van Sluyters, 1982; Olavarria and Montero, 1984; Montero, 1993) and electrophysiological (Montero et al., 1973b; Espinoza and Thomas, 1983; Espinoza, 1983) work in rats. A large number of areas have been described, with some authors cataloguing up to 11 distinct extrastriate areas in the rat (Olavarria and Montero, 1984). Some subdivisions of V2M and V2L are shown in Table 2.2, and, as in V1, these extrastriate areas are known to each contain a retinotopic map of visual space (Espinoza and Thomas, 1983; Montero, 1993; Schuett et al., 2002; Wang and Burkhalter, 2007). However, beyond their presumed role in visual processing

[1]Frequently referred to as area 18 in some older work (Krieg, 1946).

based on limited anatomical and electrophysiological work, little is known about the functional specialisation of many rodent extrastriate areas, although tracing work has indicated that these areas are likely to be hierarchically organised, showing that the lateromedial (LM) and anterolateral (AL) areas are likely to be early in the hierarchy (Coogan and Burkhalter, 1993) and receive the strongest projections from V1 into V2L (Wang and Burkhalter, 2007). Interestingly, there is (limited) evidence that V2L may contain place-specific neurons, although these are not well characterised (Burwell and Hafeman, 2003).

The differences in encoding between different extrastriate areas provides evidence for differences in function. It has been suggested that the mouse visual cortex contains separate 'streams' for processing object-related or visuospatial information (akin to the ventral and dorsal streams, respectively, in monkey, Mishkin et al. (1983); Kravitz et al. (2011)). Accordingly, visual areas AL, rostrolateral (RL), and anteromedial (AM) more strongly process motion information (are more direction-sensitive) than area LM. Parts of these areas also been labelled as the posterior parietal cortex (Kolb, 1990; Torrealba and Valdés, 2008; Marshel et al., 2011), and has been implicated in spatial navigation (Pinto-Hamuy et al., 2004) and contains HD cells in the rat (see Chapter 1). AL-projecting V1 neurons may also prefer stimuli with lower spatial frequencies and have higher sensitivity to differences in contrast, compared with neurons projecting to LM (Gao et al., 2010), although may not reflect differences in spatial and temporal frequency codes in AL and LM themselves (Marshel et al., 2011).

Consistent with the findings that areas LM and AL are major projection outputs from V1 (Wang and Burkhalter, 2007), quantitative anatomical methods coupled with electrophysiology have identified areas LM and AL as 'gateways' into the ventral and dorsal streams, respectively (Wang et al., 2011, 2012). Using network analysis the authors further classified 9 higher visual areas into two network 'modules' – one corresponding to the dorsal stream (AL, RL, AM, PM, and A) and one corresponding to the ventral stream (P, POR, LM, and LI, Wang et al. (2012)). Although this classification is not a simple case of lateral vs medial extrastriate cortex corresponding to ventral and dorsal streams, all areas within V2M have been assigned to the dorsal (visuospatial) stream (Wang et al., 2012).

Consistent with its role in visuospatial processing, area AL provides stronger input than LM to spatial areas such as posterior parietal cortex (a component of the dorsal visual stream) and mEC in the mouse (Wang et al., 2011). However, it is interesting to note that the dorsal stream overall sends less dense projections to spatial areas (mEC, PaS, CA1 and Sub) than the ventral stream, with the exception of the PrS (which was not distinguished from PoS), which receives mildly stronger inputs from the dorsal stream (Wang et al., 2012). Indeed, all of the 9 higher visual areas traced in this work send projection targets to some combination of these spatial

Acronym	Name	Visual area	Citation
AM	Anteromedial	**V2M**	Olavarria and Van Sluyters (1982) Espinoza and Thomas (1983) Olavarria and Montero (1984, 1989) Montero (1993) Schuett et al. (2002) Wang and Burkhalter (2007) Marshel et al. (2011)
PM	Posteromedial		Espinoza and Thomas (1983) Montero (1993) Wang and Burkhalter (2007) Marshel et al. (2011)
A	Anterior		Montero (1993) Sánchez et al. (1997)
		V2L	Olavarria and Montero (1984) Schuett et al. (2002) Wang and Burkhalter (2007) Marshel et al. (2011)
AL	Anterolateral		Montero et al. (1973a) Olavarria and Van Sluyters (1982) Espinoza and Thomas (1983) Olavarria and Montero (1984, 1989) Coogan and Burkhalter (1993) Montero (1993) Schuett et al. (2002) Wang and Burkhalter (2007) Marshel et al. (2011)
LM	Lateromedial		
LI	Laterointermediate		Espinoza and Thomas (1983) Olavarria and Montero (1984, 1989) Montero (1993) Wang and Burkhalter (2007) Marshel et al. (2011)
LL	Laterolateral		Olavarria and Van Sluyters (1982) Espinoza and Thomas (1983) Olavarria and Montero (1984, 1989) Montero (1993)
LLA	Laterolateral anterior		Olavarria and Montero (1984)
PL	Posterolateral		Olavarria and Van Sluyters (1982) Olavarria and Montero (1984, 1989) Montero (1993)
RL	Rostrolateral		Montero (1993) Coogan and Burkhalter (1993) Wang and Burkhalter (2007) Marshel et al. (2011)
P	Posterior		Olavarria and Van Sluyters (1982) Montero (1993) Wang and Burkhalter (2007) Marshel et al. (2011)
M	Medial		Olavarria and Montero (1984)
PAR	Pararhinal cortex		Olavarria and Montero (1984)
POR	Postrhinal cortex		Wang and Burkhalter (2007) Marshel et al. (2011)

Table 2.2: Table summarising the common cited higher visual areas of extrastriate cortex, along with their classification into V2M and V2L. Note that some authors disagree on classification (notably of the Anteior area), and not all authors classify all areas.

areas, and substantial connectivity between the streams was observed (see also McDonald and Mascagni (1996)).

The classification of ventral and dorsal streams is broadly consistent with behavioural deficits observed following lesions to higher visual and associated areas. Lesions of dorsal extrastriate area AM (posterior parietal cortex) impaired learning of a visuospatial task requiring rats to differentiate lights presented at different locations, but did not impair rats on a brightness discrimination task (that did not require a location-dependent response, Sánchez et al. (1997)). Similarly, lesions to this area in rats impaired memory on a Lashley-III maze in the absence of visual cues (Pinto-Hamuy et al., 2004), impaired learning in a visuosomatic task requiring approaching a stimulus depending on its brightness and roughness (Pinto-Hamuy et al., 1987), impaired navigating in a water maze to a platform located relative to a visual landmark (Kolb and Walkey, 1987), and thus is implicated in the integration of vision (and other modalities) into an allocentric representation of space (Save and Poucet, 2009).

Lesions in the downstream ventral stream areas produce deficits in pattern discrimination (Gallardo et al., 1979; Dean, 1981b; McDaniel et al., 1982), but largely spared performance in spatial tasks on a water maze (Tees, 1999). Interestingly, lesions directed towards higher visual areas seem to produce more severe deficits than control lesions in striate cortex (Dean, 1978; Gallardo et al., 1979; Dean, 1981a; Pinto-Hamuy et al., 2004), indicating that extra-geniculate (or geniculo-extrastriate) pathways may subtend some sparing in behaviour deficits (Dean, 1981a) or small areas of spared striate cortex may be sufficient to convey patterned information for learning (Lashley, 1939). Co-morbid lesions of SC with lesions of striate cortex impaired pattern discimination to a similar degree as large occipital cortex lesions (Dean, 1981a), indicating that visual behaviours believed to be associated with the ventral visual stream are at least partially subtended by projections from the subcortical visual pathway (via the SC and LPN) into extrastriate cortex.

The anatomical classification of higher visual areas within V2M as members of the dorsal stream, coupled with the spatial deficits following dorsal/medial extrastriate lesions, implicates the dorsal stream in the processing of visual information for the construction of spatial maps (Yoder et al., 2011). However, as the ventral stream also contains connections with spatial areas, landmark information may be propagated via this pathway. Of particular note, the postrhinal cortex, which receives substantially stronger inputs from the ventral stream Wang et al. (2011, 2012), has been proposed as a route by which landmark information may reach HD cells (Yoder et al., 2011). Alternatively, via their roles in processing objects and strong connections with the ventral stream, the lateral EC (Deshmukh and Knierim, 2011) and perirhinal cortex (Horne et al., 2010) have been proposed as routes by which external objects and landmarks may be

extracted from the visual scene for use by spatial areas (Yoder et al., 2011; Wang et al., 2012). However, it appears that the lateral entorhinal cortex may be involved in the use of local, but not global, cues when navigating (Kuruvilla and Ainge, 2017). Some of these will be discussed in Section 2.6 below.

2.6 Vision to navigation: Routes of landmark integration into the HD system

Visual pathways that provide plausible routes by which external landmark information may reach the HD system are numerous, with a plethora of anatomical and behavioural evidence discussed above implicating various visual areas in spatial processing. However, few studies have assessed the role of these differing visual systems on properties of spatial cells within the rodent brain.

There is evidence that landmark information is integrated into the HD system at the level of the cortical HD areas PoS and RSC. Lesions of the PoS disrupt landmark anchoring of HD cells upstream in the LMN (Yoder et al., 2015), and the PoS is known to send feedback projections to the LMN (van Groen and Wyss, 1990c; Huang et al., 2017) and to be reciprocally connected to ADN (van Groen and Wyss, 1990c). Similarly, lesions of the RSC moderately impair landmark anchoring of HD cells in the ADN, thus implicating these cortical areas as plausible sites of confluence of orientation and visual representations.

The reciprocal connections between PoS and RSC (van Groen and Wyss, 1990c,b, 1992) means it is unknown what the relative contribution of each is to landmark processing of the HD system. Electrophysiologically, the RSC contains landmark-sensitive directional cells – bi-directional cells (Jacob et al., 2017) – that have been proposed to be a basis for cue integration, through Hebbian associations between cues and directions, leading to bootstrapping of visual inputs with HD representations (Page and Jeffery, 2018). A separate model proposed distinct roles for PoS and RSC in processing landmarks: the PoS integrates landmarks from distal cues and feeds back to upstream HD areas; the RSC corrects for parallax errors in proximal cue control using place-by-direction cell sheets (Bicanski and Burgess, 2016). However, it remains unclear how the brain would construct dichotomic processing pathways for proximal and distal cues.

V1 is known to project directly to both PoS and RSC (van Groen and Wyss, 1990c; Wang et al., 2012). These projections provide a plausible direct route of entry of visual information into HD areas. Although no one has tested the effect of striate cortex lesions on HD cell landmark anchoring, place cells have been recorded following thermal lesions (using a soldering

iron) of V1 (Paz-Villagràn et al., 2002).

In this study, place cells were recorded whilst rats foraged in a cylinder with three distinct objects placed against the walls as anchoring cues. Place cells in V1 lesioned animals displayed significantly reduced spatial coherence relative to controls, while other cell characteristics (peak firing rate, field size, spatial information content) were unaffected. Rotations of the objects in intact animals resulted in appropriate rotations of the place fields to follow the objects. Successful place cell anchoring to this configuration of objects has also been reported previously, and in early-blind rats (Save et al., 1998). However, place cells in V1 lesioned animals did not anchor to the objects, with the field rotation following the object rotation in only 14/52 sessions (in all other sessions, the fields were stable relative to the distal room).

This paper indicates that processing in early visual cortical areas is important for landmark integration by spatial cells. However, it is important to note that the presence of anchoring to the distal room in lesioned animals could indicate poor control of conflicting landmarks, given that distal landmarks can sometimes control place cell firing (Lee et al. (2004); Yoganarasimha and Knierim (2005), but see Knierim and Rao (2003); Knierim and Hamilton (2011)). Nonetheless, this paper indicates an important role in the cortical geniculo-striate pathway in the processing of landmarks in a visual scene.

This landmark information could be propagated directly into spatial networks via projections into HD areas PoS and RSC, or it could be sent via higher visual areas (the dorsal or ventral streams). There also appear to be direct projections from V1 into mEC (Wang et al., 2012), although lesions of mEC did not impair landmark anchoring in HD cells (Clark et al., 2010) and so landmark information is unlikely to be routed into the HD system via the mEC (although a mild impairment in anchoring of place cells was seen following EC lesions, Van Cauter et al. (2008)). As discussed above, Wang et al. (2012) found that all 9 areas tested in the extrastriate cortices sent projections into RSC and PoS, and therefore are plausible routes of integration. However, large lesions of the parietal cortex, which included substantial overlap with V2M (recall posterior parietal cortex is frequently considered to contain parts of V2M, and areas AM and A were likely entirely destroyed in these lesions) and V1 (although these lesions may not have been complete), did not impair landmark anchoring in HD cells (Calton et al., 2008) or place cells (Save et al., 2005).

It is unknown whether the more posterior areas of V2M (such as area PM) are required for landmark anchoring of spatial cells, or the contribution the geniculo-striate pathway makes to landmark anchoring of HD cells. However, some routes within the ventral stream have been assessed; in particular the postrhinal cortex (POR) was considered an area that may be involved in the recognition and processing of visual objects as landmarks, and is thought to contain

spatial cells (Burwell and Hafeman, 2003). As with other higher visual areas, the POR sends projections into a number of (para)hippocampal areas, including CA1, PreS (possibly PoS), Pas, RSC and mEC (Furtak et al., 2007; Wang et al., 2012), along with projections into perirhinal cortex, and other higher visual areas (including reciprocal projections with visuospatial areas in the dorsal pathway). Alongside its strong input from various cortical visual areas (Burwell and Amaral, 1998; Furtak et al., 2007), it also receives projections from many of these spatial areas, including from CA1, PreS (PoS), PaS and EC (Furtak et al., 2007), and visual afferents from the LPN (Tomás Pereira et al., 2016). The POR may also receive a very small projection from LGN (Tomás Pereira et al., 2016), but sends a significant efferent projection to it (Agster et al., 2016).

These connections suggest the POR sits in a privileged position to receive and process visuospatial information, which may be integrated within spatial circuits. The contribution of the POR to landmark anchoring of HD cells was tested directly in a recent lesion study in hooded rats (Peck and Taube, 2017). HD cells were recorded from the ADN following bilateral excitotoxic lesions of the POR, in a standard cue rotation paradigm in a cylinder. HD cells in lesioned animals still shifted in register with rotations of a single cue card, and there was no significant difference in the amount of PFD shift following cue rotations between the lesioned and control groups. This provides direct evidence that an intact POR is not necessary for the integration of landmark information into the HD system. The role of other ventral stream visual areas have not been directly tested.

Other plausible routes exist which could provide small visual inputs to areas containing spatial cells. A sparse direct projection has been observed from retinal ganglion cells to ADN and AVN in the rat (Itaya et al., 1981), both HD cell areas. This projection appears to be conserved across species, and has been observed in macaque monkey (Itaya et al., 1986) and tree shrew (Conrad and Stumpf, 1975). The functional role of these projections is untested, and so their contribution to HD cell firing is unknown. However, these projections may be non-image forming (Martinet et al., 1992), and so may not process explicit landmark information in a manner that would be of use to the HD circuit. Non-image forming processing instead may only subtend non-visual photic responses (Güler et al., 2008), such as the pupillary light reflex and circadian rhythms in mice. In general, these projections are poorly-characterised and seem unlikely to provide a substantial landmark input into the spatial systems, although may convey contextual information about light intensity to the HD system.

2.6.1 Geniculate versus extrageniculate pathways

As discussed above, lesion studies focussing on higher visual areas (posterior parietal cortex and POR) have failed to show any necessity of these areas for intact visual landmark processing by HD cells. These extrastriate areas receive substantial input from both visual pathways, and a number of extrastriate areas have not yet been assessed. The areas directly tested for their influence on the HD system thus far have therefore been higher visual areas, with presumed specialised function. As these areas integrate information broadly across the visual system, the representations coded by them likely derive their response profiles from both striate and subcortical inputs (Zhou et al., 2018).

As such, it remains to be seen what the relative contribution of the geniculate pathway is to landmark processing in the rodent brain, and we propose interfering early in these pathways to assess this. That V1 lesions disrupt cue control of place cells is consistent with a role for the geniculostriate pathway in landmark processing. However, it remains possible that the subcortical collicular pathway is involved in this process, as information can reach V1 from this pathway: the sSC projects into dLGN and the LPN projects into V1, possibly providing an important input that is integrated into these areas. Furthermore, the SC as the optic tectum is an evolutionarily ancient structure within the brain, having homologue areas in numerous species across many taxa; as HD cells are also found in a great variety of species, it is reasonable to suspect the underlying structures that convern their function are ancient.

However, a recent thesis (Rodriguez, 2017) presented data from free-foraging rats in which HD cells were recorded following infusion of muscimol (or saline) into the SC. HD cells successfully anchored to a visual landmark (white cue card) in both control and muscimol conditions: the shift of HD cell PFDs was close to the rotation angle of the landmark, and was significantly different from uniform. However, there was some evidence of an increased angular dispersion of PFD shifts following cue rotation, indicating that some error was introduced into the HD system, which could less reliably and precisely anchor to the cue card.

However, no histology is presented in this work, and so it is unclear how accurately the SC was targeted and the spread of the muscimol is unknown. Moreover, as the landmark consisted of a single cue card on the inside wall of the arena, it provides additional orienting information to the rat (e.g. in the form of a tactile landmark at its edges) that could plausibly be used by the HD system in the absence of vision (the rotated floor in Goodridge et al. (1998) could cause HD cell PFD shifts due to tactile inhomogeneities). Nonetheless the finding is consistent with the observation that the POR is not necessary for landmark anchoring of HD cells (Peck and Taube, 2017), as this area is predominantly driven by subcortical collicular input (Bickford

et al., 2015).

As such, it is still unclear what contribution the cortical or subcortical visual pathways make to landmark processing in the rodent. If the SC is not necessary for landmark anchoring, this implicates the cortical pathway in landmark processing and extraction. This thesis aims to address two questions: (1) whether orienting information can be derived from a low-spatial frequency scene, plausibly provided from visual areas with with low-acuity representations, and (2) the contribution to landmark processing by this system by the lateral geniculate nucleus, the key relay of the cortical visual pathway. We will present HD cells recorded from the PoS of the rat during free foraging in a cylinder. In the first experiment, we will use a landmark anchoring paradigm designed to test cue control exerted by a broad contrast gradient subtending the entire visual panorama, to assess whether HD cells can integrate low spatial-frequency information. In the second experiment, we chemically ablate the dorsal LGN and test for detection and discrimination of cue cards in a two-cue paradigm published previously (Lozano et al., 2017). Together, these experiments aim to provide insight into how landmark information is extracted from a visual scene and propagated into the HD system.

Chapter 3

General Methods

Das logische Bild der Tatsachen ist der Gedanke.

The logical picture of facts is the thought.

TLP 3; Ludwig Wittgenstein

3.1 Animals

All experiments used male Lister-Hooded rats (Charles River). Experiments were performed under the jurisdiction of the Animal (Scientific Procedures) Act (1986) and the European Communities Council Directive of 24 Nov 1986 (86/609/EEC). Animals were group housed prior to surgery on a simulated 11 h:11 h day:night cycle, with 1 h of simulated dawn/dusk each day. Following surgery, animals were singly-housed on the same simulated day:night cycle.

3.2 Surgery

Animals underwent sterile surgery involving intracranial injections (of NMDA or saline) into the lateral geniculate nucleus and/or the implant of a 16-channel poorlady microdrive (Axona Ltd., St Albans, UK) directed towards the postsubiculum.

Animals were induced under isoflurane (Piramal Healthcare UK Ltd., 3 %-5 % in 3 L oxygen), and maintained under isoflurane (1.5 %-4 % in 2−3 L oxygen). During induction, animals were shaved, given appropriate analgesia (1 mL kg^{-1} of carprofen 0.5 % given subcutaneously), and placed into a stereotaxic frame. The surgical site was disinfected with antiseptic (povidine-iodine, WHO, 2009). A midsagittal incision was made along the dorsal surface of the head, and the skin and fascia were clamped to the side using haemostatic forceps to expose the dorsal skull surface.

A craniotomy was drilled in the skull using a 2.3 mm trephine drill above the coordinates for injection or implantation. In the case of implantation, additional 1.2 mm burr holes were drilled, into which skull screws were attached to the skull. One screw contralateral to the implanted hemisphere was brought in contact with the brain cortex and served as the local ground during recordings. Anteroposterior (AP) and mediolateral (ML) coordinates for injections and implantation are given relative to bregma, whereas dorsoventral (DV) coordinates are given relative to brain surface.

Injections were made through a 0.66 mm diameter glass pipette. The pipette was lowered to the coordinate, and the appropriate volume was pumped through the pipette. Following injections, the pipette was ordinarily left in the brain for 5 minutes to allow for diffusion of the injected liquid. Where possible, injections were made through the meninges so as to minimise damage to the cortex; in these cases, 0.1 mm was added to the DV coordinate to account for the additional thickness of the meninges.

For implantations, the microdrive was attached to a custom-built mount and positioned straight relative to the stereotaxic frame. The meninges were removed inside the craniotomy and the drive was lowered through the tissue to the relevant coordinate. The microdrive was held in place using dental cement. The tetrodes were protected from the cement by an outer cannula lowered over them to touch the surface of the brain. Immediately at the end of surgery, the microdrive was turned $\frac{1}{4}$ anti-clockwise to ensure the screw mechanism on the microdrive was functional.

Following surgery, animals were placed in a heated recovery box and monitored closely until awake. After the animal was awake, it was returned to its cage and monitored for the following 5 days. Animals were given post-operative analgesic for 3 days (approximately 3 drops of $10\,\mathrm{mg\,mL^{-1}}$ meloxicam given in condensed milk or high-protein wet-mash). Animals were allowed at least 7 days of recovery before beginning experimental procedures.

3.3 Single-unit recording

3.3.1 Microdrive preparation

Neural recordings were performed using 16-channel microdrives (Axona Ltd., St Albans, UK) containing moveable microelectrodes that were wired by the experimenter. A drive consisted of a precision screw held under spring tension, and a 21 gauge cannula cemented to the screw chassis to house the electrodes (Figure 3.1). Electrodes were made of 25 µm diameter 90:10 platinum-iridium alloy (California Fine Wire Co., CA), and were wound into bundles of 4, forming a single 'tetrode'. Four tetrodes were then threaded through the inner cannula, and

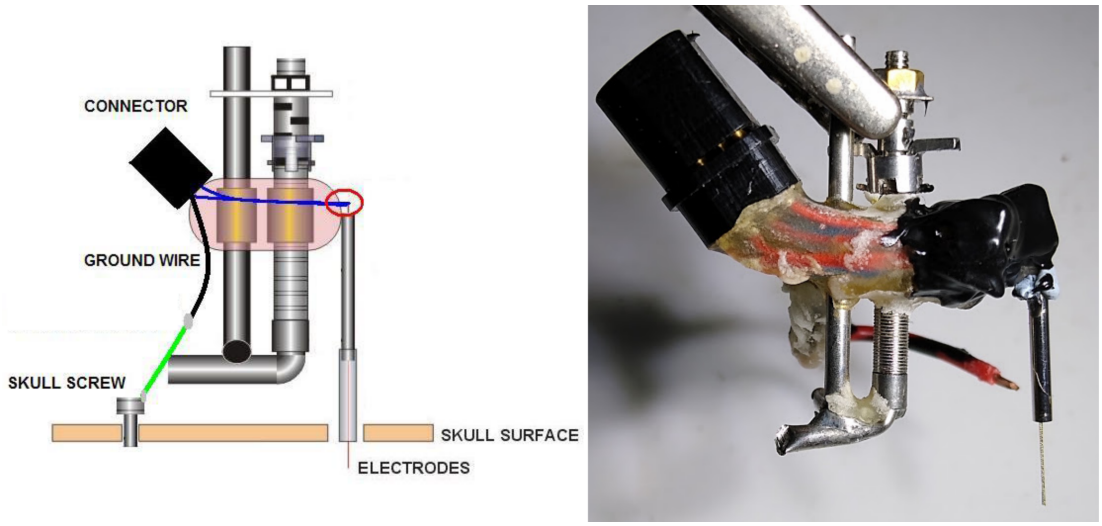

Figure 3.1: Left: schematic of the implanted microdrives, as it would appear when positioned above a rat's skull. The tetrodes extend through the skull into the brain. The screw mechanism on the chassis allows the tetrodes to be advanced deeper into brain tissue. Schematic taken from Axona Ltd. (`www.anoxa.com`, St Albans, UK). Right: photograph of a microdrive loaded with 4 tetrodes.

wrapped around exposed wires. The connection between electrodes and wires was improved using silver paint, and were protected by coating the exposed wires with nail varnish or a rubber coating (PlastiDip UK Ltd., Hampshire, UK).

3.3.2 Data acquisition and tracking

Single units were recorded using an Axona recording setup (Axona Ltd., St Albans, UK). A headstage amplifier plugged into the animal's microdrive was tethered to a pre-amplifier and system unit via a low-noise flexible cable. A camera mounted above the environment recorded an animal's position and heading direction by tracking two LEDs mounted on the headstage at 50 Hz.

The headstage performed unity-gain buffered amplification, and further amplification was performed within the pre-amplifier followed by differential referencing and analog-to-digital conversion. The system unit subsequently filtered the digital signal, synchronised the neural recording data with tracking data from the camera, and passed the information to computer software via a USB connection (DacqUSB, Axona Ltd., St. Albans, UK). A schematic of the recording equipment is displayed within Figure 1.2.

Single unit activity was recorded following high-pass filtering at 48 kHz. For a recording session, the experimenter manually assessed the electrode signals for spiking activity, and set the digital gain of each channel and the spike-trigger threshold voltage. Any deflection greater than the threshold triggered storage of the voltage amplitudes on all electrodes in the tetrode for 200 µs pre-trigger and 800 µs post-trigger for offline analysis (see Section 3.5). The ex-

perimenter additionally set the reference channel (ideally with low spiking activity) for each tetrode, providing a differential ground from which raw recordings were subtracted within the pre-amplifier.

Local field potential recordings were made by storing low-pass filtered data from one or two channels at either 250 Hz or 4800 Hz.

3.3.3 General screening protocol

Animals were screened for directionally modulated units in a separate room from the main recording room. This room measured 3.3 m-by-2.8 m, and contained a rectangular screening box of either 1 m-by-1 m or 1.2 m-by-0.6 m. The box contained one prominent cue card attached to the wall, and was in full view of numerous distal cues in the room (including a cue card attached to the wall of the room, shelving, and the experimenter; see Figure 3.2), providing a rich distal scene.

Animals were screened for a minimum of 10 min in the screening box for a minimum of 1 trial, while the experimenter adjusted the recording gains, thresholds and reference channels to isolate any potential units. Following a screening trial, the clusterspace was manually visualised in Tint (Axona Ltd., St Albans, UK) to check for directionally modulated units. If present, further screening sessions were conducted to assess stability of the clusterspace and unit activity, and in which the recording parameters were adjusted until the directional unit was well isolated. Following screening, the animal was entered into a recording session.

If no directional units were found, the tetrodes in the microdrive were advanced by 50 µm-200 µm and the animal was screened again a minimum of 4 h later.

3.3.4 General recording protocol

The recording room measured 4.4 m-by-3.3 m, and contained a black curtain suspended from ceiling to floor that enclosed a circular area of diameter 2.5 m. A schematic of the room is shown in Figure 3.2. Details of the recording environments are given in the respective results chapters.

All environments were placed in the centre of the curtained enclosure, and recordings were performed with the curtains closed so as to limit distal visual cues. During recordings, a speaker mounted to the ceiling played white noise to mask auditory cues that could provide distal landmark control over the HD system.

Arenas were placed on black vinyl flooring, underneath which aluminium foil was connected to the ground of the pre-amplifier to providing a grounding plane and reduce electrical noise. Before each trial within a session, the apparatus (walls and cue cards) and floor were wiped

down with an ethanol/chlorhexidine spray, and the animal was disoriented by the experimenter prior to placement in the arena.

The visual scene within the arena used was rotated a true random multiple of 45° between trials to assess for landmark control over the HD system. Depending on the arena used, only the visual scene was rotated, and the physical cylinder was kept stationary (Chapter 4), or the cylinder and cue card were rotated together (Chapter 5). Rotations were determined in advance of the recording session using custom MATLAB code (MATLAB 2015a, Mathworks, Natick, MA) that generated numbers using the API of an online true random number service `random.org`. In cases where the website was unavailable, then rotations were generated using pseudorandom integers produced by MATLAB's inbuilt `randi()` function.

Following the recording session, where possible, a post-recording session was run, so as to check whether cell clusters were still visible. Following recording, the cell was either kept or tetrodes were advanced 50 µm-200 µm, and the animal was recorded from on a following day; the post-recording session guided the experimenter's decision to lower or not lower the tetrodes.

3.4 Histology

3.4.1 Culling and brain extraction

At the end of the experiment, rats were lightly anaesthetised with isoflurane 3-5% and killed using an overdose of intraperitoneal pentobarbitone (Pentoject, pentobarbitone sodium 20% w/v). Following cessation of breathing, rats were exsanguinated by perfusion through the heart with 0.9 % saline, followed by perfusion with 10 % neutral buffered formalin to fix the nervous tissue.

The brain was subsequently extracted from the skull and left for a minimum of 24 h in 10 % neutral buffered formalin to continue fixation.

3.4.2 Histological preparation

Before sectioning, brains were transferred to a solution of 30 % w/v sucrose in phosphate-buffered saline to dehydrate. Brains were ordinarily kept in this solution for a minimum of 48 h, and were judged to be sufficiently dehydrated when they had sunk to the bottom of the solution.

To section, brains were frozen to approximately −20 °C in a cryostat (Leica CM1850, Leica Camera AG, Wetzlar, Germany) and mounted onto a microtome. Brains were sliced into coronal sections of between 30 µm-50 µm thickness, and mounted onto slides for staining.

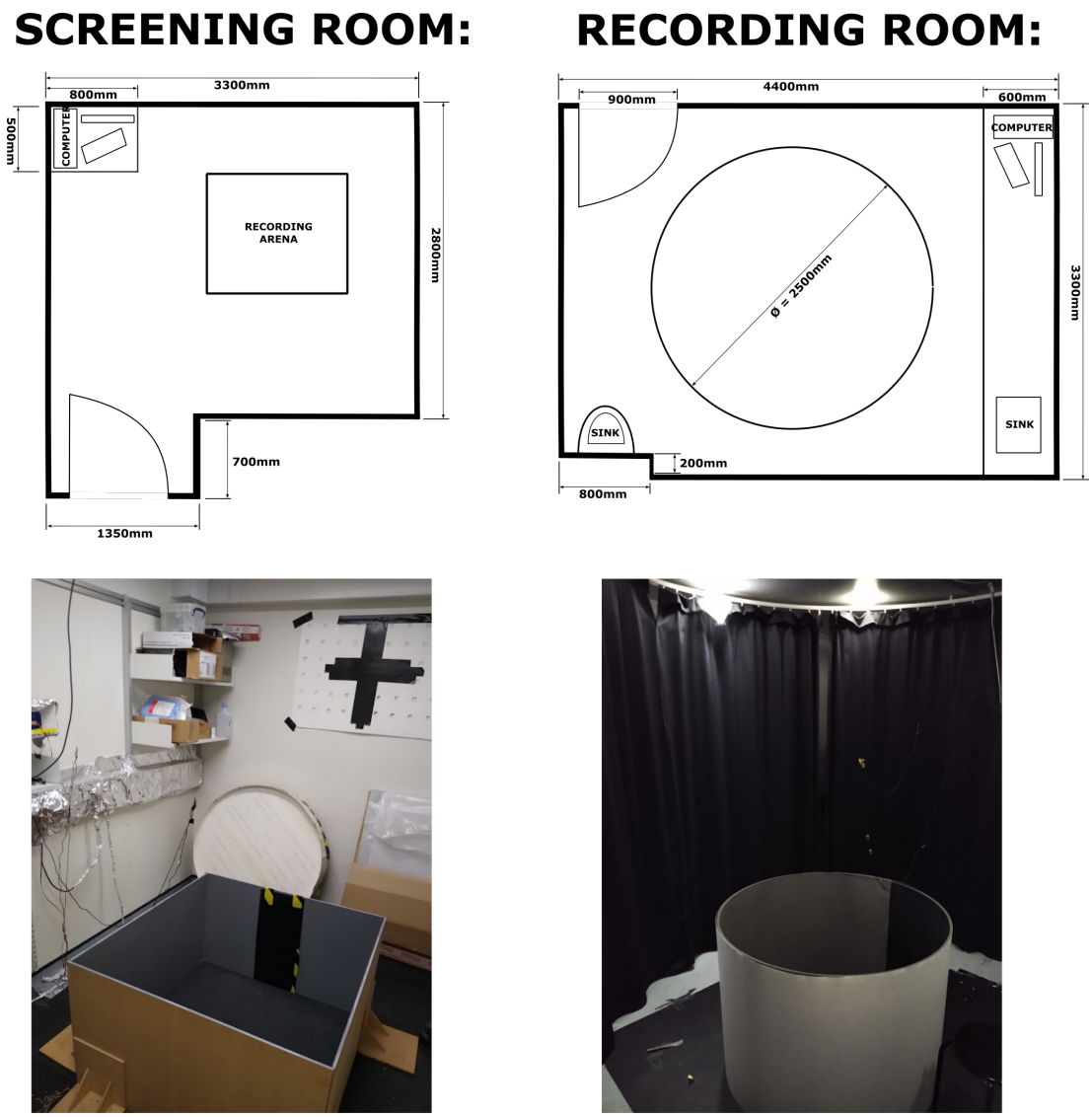

Figure 3.2: Top-down schematics of screening and recording rooms, alongside photographs of the recording apparatuses in each room.

3.4.3 Staining

Slides were Nissl-stained using cresyl violet to visualise neurons in the brain by colouring the ribosomal RNA on rough endoplasmic reticula of cells. Following immersion in cresyl violet solution, slides were washed in distilled water, dehydrated in increasing concentrations of ethanol, cleared in Histo-Clear (National Diagnostics, Nottingham, UK), and coverslipped with DPX (Sigma-Aldritch, Dorset, UK).

3.4.4 Imaging and analysis

Slices were imaged under bright-field illumination, using a Leica (DMi8) microscope (Leica Camera AG, Wetzlar, Germany). Imaged slices were manually aligned to the closest reference plate in the atlas (Paxinos and Watson, 2007). Tetrodes were confirmed visually to have penetrated the postsubiculum, and an estimate of the final dorsal-ventral coordinate was extracted from the deepest visible point of the electrode track.

Lesion extent was assessed manually by the experimenter. For each coronal plate in the atlas, a polygon was drawn in each hemisphere around the region containing no/few identifiable cell bodies. Similarly, a polygon was drawn around the estimated boundary of the dLGN. Although the boundaries of the dLGN are easy to identify in Nissl-stained material (Evangelio et al., 2018), these criteria are frequently based on neuron cell density. As NMDA lesions kill cell bodies in the affected area, we noticed a difficulty in using the architecture of the neuropil to define the medial and ventral boundaries of the dLGN. As such, where possible we estimated the boundaries of the dLGN using nearby landmarks – including the shape of the thalamic border, the hippocampus, and visible white matter tracts.

3.5 Analysis of neural recordings

3.5.1 Single unit isolation

Spike data from recordings were clustered offline to isolate single units for further analysis. All trials in a recording session (excluding screening trials, which were analysed separately) were concatenated and loaded together into a graphical interface for clustering (Tint, Axona Ltd., St. Albans, UK). Concatenating and clustering trials together reduced the chance of experimenter bias by preventing the experimenter from "searching" for cells that were present in previous trials.

Individual neurons will generate distinct waveforms when firing. The shape of the action potential waveform will depend on a number of properties, which include the type of neuron

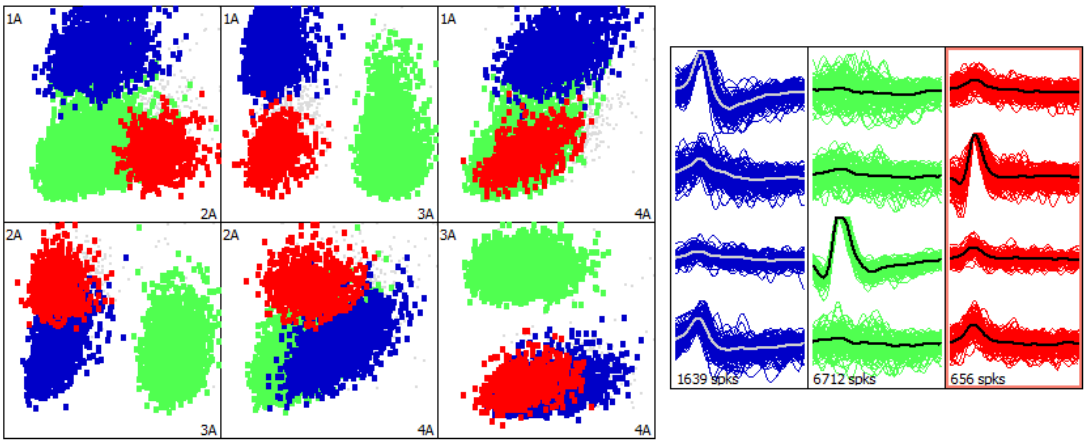

Figure 3.3: Example clusterspace recorded from an animal by the author (R880_20171220_Tr8_T4). Here, three cells have been isolated using the automated clustering algorithm KlustaKwik, implemented in Tint (Axona Ltd., St Albans, UK). Each point on the scatter plots represents a feature of one spike: here, the amplitude of the waveforms of all spikes on each electrode have been plotted in all combinations, creating 6 2-D representations through a 4-D clusterspace. The colour of each point represents the cluster to which the spike has been assigned (grey points are unassigned spikes); average waveforms of each electrode for each cluster are plotted on the right. Here, we can see each cluster is well isolated in the clusterspace, corresponding to qualitatively different waveforms on each electrode.

(such as pyramidal cells versus interneurons, Viskontas et al. (2007)) and position of the electrode relative to the cell. For tetrode recordings, the use of multiple electrodes enables the identification and separation of multiple cells recorded simultaneously using variations in amplitude: whereas one cell may show highest amplitude spikes recorded on one electrode, another cell (due to it being positioned differently) may display highest amplitude spikes on a different electrode (an example clusterspace is shown in Figure 3.3). As such, if metrics for waveform shape and/or amplitude are extracted and plotted in multi-dimensional space, a set of cells recorded on one tetrode will each occupy a unique position within that 'cluster-space'.

Spike data underwent automated clustering according to a variant on the expectation-maximisation algorithm (Klusta-kwik, Harris et al. (2000)) over the feature space defined as including the first waveform principal components and spike amplitude on each electrode (a 12-16 dimensional cluster-space).

3.5.2 Cluster quality analysis

Putative cell clusters were assessed for cluster quality over a session. A cluster was considered to be well isolated if it was physically separated in the featurespace from all spikes not placed within the cluster ('noise spikes'). This was assessed using two metrics: the L-ratio and the isolation distance (Schmitzer-Torbert et al., 2005). Consider that each spike x_i can be represented as an n-dimensional vector of values pointing to its location in the featurespace. For a cluster C, the Mahalanobis distance for a given spike can be calculated using the formula:

$$D^2_{i,C} = (x_i - \mu_C)^\intercal \, \Sigma_C^{-1} \, (x_i - \mu_C) \tag{3.1}$$

where x_i notates the n-dimensional values for spike i, μ_C denotes the mean n-d values of cluster C, and Σ_C denotes the covariance matrix of spikes in cluster C. Intuitively, one can think of the Mahalanobis distance as an extension of the n-dimensional Euclidean distance ($d^2 = \sum_{j=1}^{n}(p_j - q_j)^2$) wherein the dimensions (notated by j here) are not orthogonal (can covary).

With each spike assigned a Mahalanobis distance from the centre of cluster C, the isolation distance uses this to assess how near the noise spikes ($i \notin C$) are to spikes in the cluster. Formally, if there are n_C spikes inside cluster C, the isolation distance is defined as the Mahalanobis distance of the n_Cth closest noise spike, $D^2_{n_C}$. As such, the larger the isolation distance, the better isolated the cluster is from noise.

Alternatively, the L-ratio is defined using the quantity L for cluster C:

$$L(C) = \sum_{i \notin C} 1 - CDF_{\chi^2_{df}}(D^2_{i,C}) \tag{3.2}$$

where $CDF_{\chi^2_{df}}$ denotes the cumulative distribution function of the χ^2 distribution with 8 degrees of freedom. Because the quantity L will grow with the size of the cluster, a normalised quantity, the L-ratio, was derived that takes this into account:

$$L_{ratio}(C) = \frac{L(C)}{n_C} \tag{3.3}$$

For this metric, smaller L-ratio values denote better isolated clusters.

3.5.3 HD cell identification

Following clustering, each unit was analysed in MATLAB (Mathworks Ltd., Natick, MA) using custom-written functions alongside the CircStat package (Berens, 2009). For each cell, a circular histogram of firing rate was constructed using the head position of the animal at each timestamp the unit fired a spike. Position samples were binned into 60 bins of 6° width, and the trial-averaged firing rate in each bin (FR_θ) was calculated as the number of spikes in each bin ($spike_\theta$) divided by the total dwell time spent by the animal facing that direction ($time_\theta$):

$$FR_\theta = \frac{\sum spike_\theta}{\sum time_\theta} \tag{3.4}$$

The resulting circular histogram was smoothed using a boxcar kernel of 5 bins wide to yield the directional tuning curve for that unit, on which subsequent analysis was performed.

A cell was classified as a HD cell if its tuning curve met all of four criteria: (1) the peak firing rate on the circular histogram was greater than 1 Hz; (2) the length of the Rayleigh vector was greater than 0.3 (see Section 3.6.2.2); (3) the length of the Rayleigh vector was greater than the 99th percentile of a shuffled distribution for that cell and trial; (4) fewer than 1% of spikes contaminated a refractory period of 2 ms duration.

For the two-cue experiment, a cell had to pass all criteria in trials 1 and 2 (the baseline trials) to be classified as a HD cell; in the gradient experiment the cell had to pass all criteria in the first and last baseline trials to be classified as a HD cell.

3.5.4 Cell spiking properties

Intrinsic spiking properties of all recorded units were assessed. These are described below.

3.5.4.1 Refractory period and burst spiking in the autocorrelogram

For each cell, spike trains for all trials in the recording session were autocorrelated to produce a single autocorrelogram for each cell. As concatenating the spike trains for each trial would introduce noise into the autocorrelogram due to discontinuities in the trains between trials (i.e. the last spike of the previous trial and the first spike of the next trial are not adjacent in time), autocorrelation spike histograms were computed for each trial and summed, before being normalised to generate an autocorrelogram of spike probability for an entire session.

Following the creation of the autocorrelogram, we extracted the number and percentage of spikes that were contained within the putative refractory period of neurons (defined as 2 ms here).

3.5.4.2 Theta modulation

Some cells in the subicular cortices have been shown to be theta-modulated (Cacucci et al., 2004; Kornienko et al., 2018). We assessed for both theta-modulation (Tsanov et al., 2011a) and theta-skipping (Jeffery et al., 1995; Brandon et al., 2013) modulation in each cell's autocorrelogram by fitting the following mixture of cosine exponential curves to the spike probability bounded between [−400 ms,400 ms]:

$$\left(a_1(\cos(\omega x)+1)+a_2(cos\left(\frac{1}{2}\omega x\right)+1)+b\right)e^{\frac{-|x|}{\tau_1}}+ce^{\frac{-x^2}{\tau_2^2}} \tag{3.5}$$

where the parameters a_1, a_2, b, c, ω, τ_1 and τ_2 were fit to the curve using a nonlinear least squares method in MATLAB's `fit` function.

For each cell, a theta index value will be extracted from the autocorrelation fit, defined as $\frac{a_1}{b}$ as derived from the fit results. This provides a metric estimating the oscillatory component of spiking as a ratio of the total spiking probability in the autocorrelation.

3.5.5 HD cell tuning characteristics

A number of metrics were used to assess the characteristics of the tuning curves of the HD cells. These were the peak firing rate, the mean firing rate, the mean resultant vector length, and tuning width, and the drift rate.

The peak firing rate was defined as the firing rate of the maximal bin of the smoothed tuning curve. The mean firing rate was defined as the trial-averaged firing rate (number of spikes/length of trial) ignoring directional sampling.

The tuning width was calculated as twice the circular standard deviation of the tuning curve, given by the output of the `circ_std` function from the CircStat toolbox (Berens, 2009). This was related to the Rayleigh vector length, a value used to assess the degree of directionality encoded in a given HD cell's firing (explained in Section 3.6.2.2). To assess whether HD cells maintained a consistent PFD throughout a trial, we used two methods for each trial: (1) we computed an estimate of the linear drift of the HD cell's firing (see below), and (2) we computed the angle between PFDs of tuning curves constructed from cell spiking during the first and second halves of trials. We considered that a cell that drifted more would show a greater change in its PFD between the first and second trial halves.

3.5.5.1 Directional information content

We also calculated the directional information content (DIC) of the putative HD cell's spike train. This is an adapted form of the spatial information measure presented by Skaggs et al. (1993), applied to the direction the animal is facing, rather than the spatial location of the animal. This metric provides a measure of how much information is contained in the neuron's tuning curve about the direction the animal is facing, and so a large directional information content provides evidence that the neuron encodes a precise representation of spatial orientation.

DIC, measured in bits/spike, is calculated as follows:

$$DIC = \int_{\theta} \frac{\lambda(\theta)}{\lambda} \log_2 \frac{\lambda(\theta)}{\lambda} p(\theta)\, \mathrm{d}\theta \tag{3.6}$$

where $\lambda(\theta)$ denotes the firing rate of the cell when the rat faces direction θ, λ is the mean firing rate of the cell, and $p(\theta)$ is the probability the animal faced direction θ during the trial. Information theoretically, the equation is related to the mutual information of the two distributions of firing rate and directional sampling, providing an estimate of the amount of information captured conveyed by the animal's direction about the cell's firing rate.

3.5.5.2 Drift rate

An estimate of the average drift rate was computed for each trial by fitting a circular linear regression over the head direction of the animal at the time of each spike. We considered that, if we consider the PFD of an HD cell to drift linearly over a trial, the head direction at each spike could be represented as a function of the initial PFD at the begining of the trial, the drift rate of the HD cell, and the time at which the spike occurred, akin to a first-order differential equation $x(t) = x(0) + t\frac{d}{dt}x$.

Therefore, for a number of putative drift rates ω, the head direction at each spike $phi(t)$ was transformed to a new set of head directions:

$$\hat{\phi}(t) = \phi(t) - \omega t \tag{3.7}$$

where t is the time at which the spike $\phi(t)$ occurred. If ω well approximates the drift rate of the attractor, this will transform all spike angles to similar values: it will decrease the circular variance of the set of transformed angles, and increase the Rayleigh vector of the transformed angles.

As such, we computed the Rayleigh vector following this linear transformation, and found the value of ω that maximises the Rayleigh vector length of the set of transformed angles:

$$\arg\max_{\omega} \|\vec{R}(\hat{\Phi})\| \tag{3.8}$$

where $\vec{R}$ denotes the Rayleigh vector of the set of transformed angles $\hat{\Phi}$. This value is taken as the trial drift rate for that cell.

As it has been proposed that attractor drift occurs primarily as error accumulation during

head turns, it may be expected that in trials where the animal turns its head more frequently then the HD cell's tuning curves will drift more over the course of the trial. Similarly, a cell which drifted equally in both directions (e.g. clockwise in the first half and anticlockwise in the second half of a trial) may overall appear to not drift at all according to a linear regression.

However, a linear regression was nonetheless chosen to characterise drift. This is because the linear coefficient ω was easily interpretable, providing a single-order value denoting the rate of change of the cell PFD. The distributions of this value could then be compared between groups.

3.5.6 Landmark anchoring

In order to assess the extent of visual control over the HD system, analyses were performed to assess the precision with which recorded cells anchored to the visual scene following rotations of the environment. Two methods were used to perform this analysis.

3.5.6.1 Clustering analysis

In order to adequately represent the shifts of HD cell tuning curves over the course of a session, it was important to develop a method to normalise all recorded HD cells so as to have comparable PFDs, as the PFDs of two corecorded HD cells could together subtend any angle. An outline of this procedure is described below, and schematised in Figure 3.4.

To correct for this, the PFDs of HD cells in each trial were expressed relative to one of the cues in the arena. This transformed the PFDs from the global camera frame of reference into a local reference frame defined by the visual scene of the environment.

Subsequently, one trial was selected from each session to be the 'baseline' trial, and for each cell the PFD in the baseline trial was subtracted from the PFDs of all trials, providing a normalised PFD. The baseline trial selected was the same for all corecorded HD cells in a single session. In the case of perfect landmark anchoring (that is, consistent angles subtended relative to the cue cards) this would transform all PFDs of all cells in all trials to 0, whereas any deviation from 0 would provide a measure of error in the anchoring of that cell.

The baseline trial was then excluded (so as to remove artefactual zeros from the population dataset), and the normalised PFDs of all HD cells were averaged to provide a population estimate of the total error in landmark anchoring for each trial. These were then analysed using circular population statistics (see Section 3.6.2).

The baseline trial was selected so as to maximise clustering around 0. This was assessed by finding the datapoint that maximised the measure:

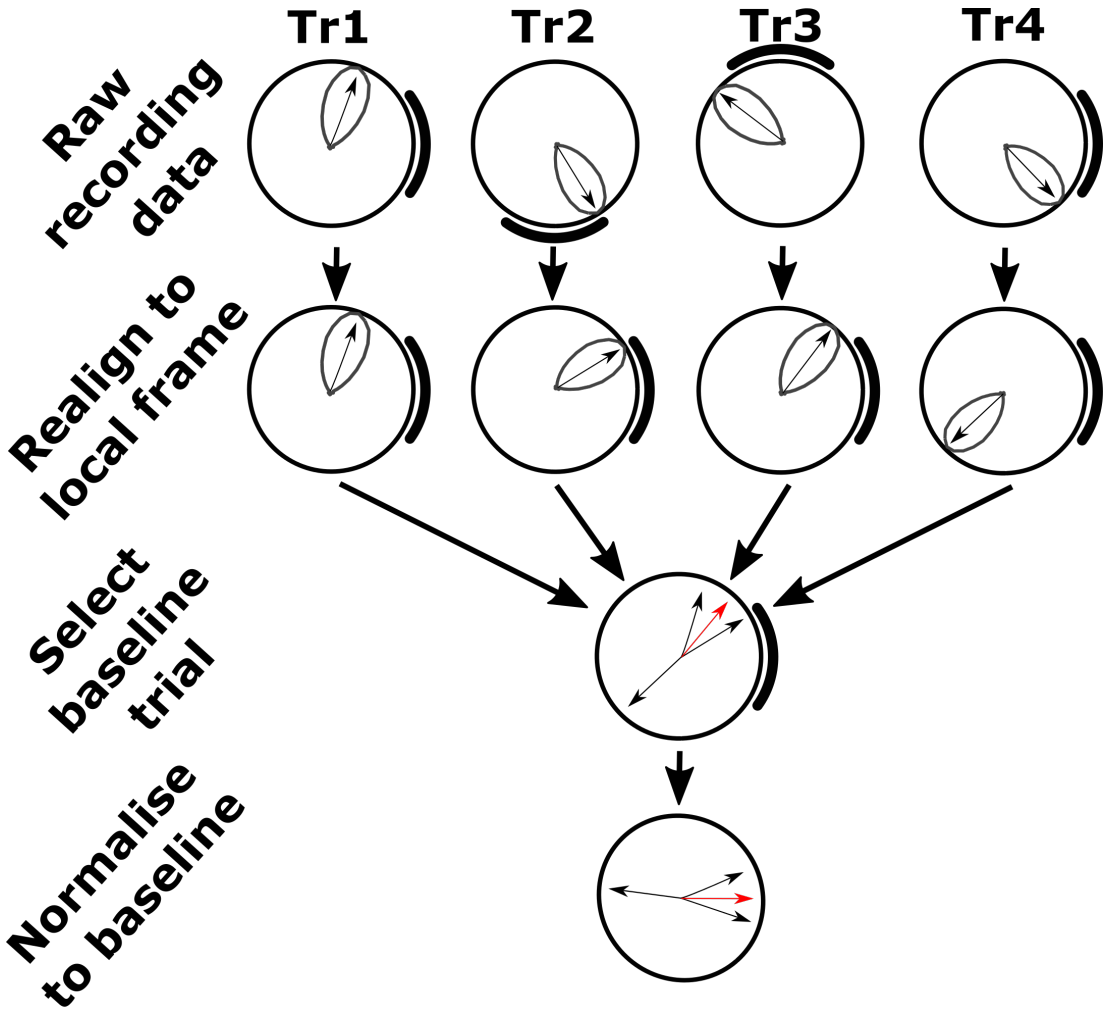

Figure 3.4: A schematic of the method used to normalise the directions of PFDs across a session, applied to four trials of fake data. Firstly, the PFDs (arrows) of the tuning curves (grey) are aligned relative to the local cue card. Then, a baseline trial (highlighted in red) is selected that maxmimises the summed cosine metric discribed in the main text. This value is subtracted from the PFDs of all trials to express them relative to this trial. Successful and consistent anchoring over a session would result in all PFDs being normalised to near 0°. The baseline trial (red arrow) is removed before analysis or statistics are applied.

$$\arg\max_{tr \in Sess} \sum_{j=1}^{cells} \sum_{i=1}^{n} \cos(\theta_{j,i} - \theta_{j,tr}) \tag{3.9}$$

where n is the number of trials in the session, indexed by i, $theta_{j,tr}$ is the normalised PFD of cell j in the putative baseline trial tr, selected from the set of all possible trials. This metric searches for the trial with a normalised PFD that is on average closest to all other normalised PFDs in the session. As multiple HD cells could be recorded in a session, this metric was also summed over all cells (index j), so that the same baseline trial was used for all cells in one session.

The use of this metric provides a generous definition of landmark anchoring, as it will identify the trial most consistent with the representation of direction in the rest of the session. This avoids difficulties that arise due to experimenter-defined baseline trials, such as the first trial or the $(n-1)$ trial; a cell may shift its PFD in trial 2 and remain consistent for the rest of the session, or may only change its PFD in one trial from the session, leading to underestimates of anchoring success if these definitions of 'baseline' are used.

3.5.6.2 Descriptive statistics

Following the extraction of the normalised PFD shifts for each session, the data were concatenated across animals and tested against a number of hypotheses.

To test for successful landmark anchoring to the visual scenes, the set of all PFD shifts in all animals was tested for deviations from uniformity using Rayleigh and V tests (see Section 3.6.2). These will detect unimodal deviations from uniformity, indicating that the PFD shifts did not occur uniformly, but were non-randomly clustered.

To test whether landmark anchoring was similar between multiple groups (of animals or conditions), the distributions of PFD shifts were compared using a Kuiper test, to compare the circular cumulative distributions.

3.5.6.3 Testing over multiple animals

As individual animals may contribute different numbers of trials into the above analysis, a further metric was designed to correct for this and enable animal-wise statistics. We utilised the anchoring metric above (Section 3.5.6.1), as it provides a numerical estimate of the cue control exerted over the recorded HD cells.

As such, we took the normalised PFD shifts, and concatenated these over all trials recorded in each animal and cue condition (providing a vector of normalised shifts ϕ). As these had been

normalised using the cosine metric above, these could be combined for a single animal and cue condition. We then calculated the average cosine transform over all (n) of these shifts:

$$\frac{\sum_{i=1}^{n} \cos(\phi_i)}{n} \tag{3.10}$$

Values close to 1 indicate very good anchoring over all recorded trials. This provides a single number per animal per cue condition, which can be compared using linear statistics and correlated with lesion extent.

3.5.7 Coherence of HD cells

The population of HD cells is classically modelled with a 1-D attractor architecture. As such, co-recorded HD cells should shift coherently between trials, subtending a constant angle between their PFDs.

To test whether HD cells behave coherently, we extracted the angle between PFDs of co-recorded HD cell pairs in each trial. If cells maintained a coherent representation of direction over a session, these angles should be similar over all trials in which the HD cells were recorded. As such, for each HD cell pair, we compute the Rayleigh vector (see Section 3.6.2.2) of this set of angle differences. A high (near 1) Rayleigh vector length would indicate that the cells shifted coherently, whereas lower values (near 0) would provide evidence that the HD cells were not maintaining a consistent relationship through a session.

To statistically assess whether HD cells were more coherent than chance, we compared the distribution of Rayleigh vectors generated from all co-recorded HD cell pairs to a shuffle distribution generated by performing the analysis above on all pairs of HD cells recorded in different sessions. As the rotations of the visual scene were randomly generated, and differed between sessions, HD cells recorded in different sessions should possess uncorrelated PFD shifts. As such, comparing this distribution to that of co-recorded PFD shifts enabled us to assess whether the set of co-recorded HD cells behaved more coherently than chance.

3.5.8 Foraging behavioural analysis

To ensure that results from the comparison of single-unit recordings between groups were not due to differences in the behaviours of the animals between conditions, a number of metrics were extracted from the animal's foraging behaviour during the trials for control analyses.

3.5.8.1 Thigmotaxis

Animals frequently display stereotyped exploratory behaviours. One example of such stereotypy is the tendency for animals to remain close to vertical walls (thigmotaxis, Lamprea et al. (2008)), especially within novel environments. This behaviour has been used as a metric of anxiety (Simon et al., 1994), and may represent a form of 'agoraphobia'.

As it is possible that animals in different conditions may explore the environment differently, we attempt to show that there are no differences in thigmotaxic behaviours between groups. In order to show this, we extracted for each trial the percentage of time the animal spent in the central- and peripheral-halves of the arena.

3.5.8.2 Distance and speed

It is believed that the drifting of an unstable ring attractor is associated with angular head turns; a discrepancy in the gain of each turn between directions would result in an activity packet slowly drifting as an animal explores (Tocker et al., 2018). This drift could also be caused due to a substantial bias in the direction an animal turns while exploring, due to stereotyped exploratory behaviour. If error accumulation occurs systematically in a manner related to head turns (e.g. due to a mis-set AHV gain), then an animal that turns more in one direction than another will cause error to accumulate more in that direction. Supporting this, there is evidence that attractor drift is higher when an animal is moving than stationary (Butler et al., 2017).

This leads to the possibility that differences in HD cells between groups are caused by differences in the angular head velocity profiles of the animals when exploring. Therefore, it is important to characterise animal movement. In particular, we calculate the total path distance and angular distance travelled by an animal in each trial and each session, along with the median linear and angular speed of the animal in each trial and session. When extracting speed profiles for each trial, the instantaneous speed estimate derived from successive position samples was smoothed using a 5-bin boxcar, to minimise aberrant tracking artefacts.

3.6 Statistics

3.6.1 Linear statistics

In general, statistical comparisons will be made using appropriate non-parametric tests, unless there is evidence for an assumption of normality to hold. When comparing across multiple groups or factors, appropriate 1- or n-way ANOVAs will be used, accompanied by corrections for multiple comparisons (Tukey-Kramer).

3.6.2 Circular statistics

As HD cells encode directions on an azimuth plane, statistical descriptions and comparisons frequently make use of circular statistics.

As these are often unfamiliar, a number of common ideas and tests, that are to be used in this thesis, will be briefly reviewed here. All circular calculations are performed in MATLAB (2015a, Mathworks Ltd. Natick, MA), using the CircStat 2012 package (Berens, 2009) unless otherwise stated.

3.6.2.1 Resultant vector

As linear definitions of the sample mean will not work for circular data, the mean direction of data distributed on a circle is characterised differently. If circular data takes the form of a series of observed angles θ_i, each datapoint may be transformed onto the unit circle by converting from polar coordinates $(1, \theta_i)$ to Cartesian coordinates $(\cos\theta_i, \sin\theta_i)$. Accordingly, each datapoint defines a unit vector $\hat{r_i}$ from the origin O to the datapoint.

For a series of n observed angles $\theta_1, \theta_2, \theta_3, ...\theta_n$, we represent each data point as a unit vector (with length 1) extending from the origin at angle θ_i. The resultant vector R is the vector sum of each unit vector,

$$\vec{R} = \sum_{j=1}^{n} \hat{r_j} = (C, S) = (\sum_{j=1}^{n} \cos\theta_j, \sum_{j=1}^{n} \sin\theta_i) \tag{3.11}$$

The length of the resultant vector $\vec{R}$ can be expressed as its norm:

$$R = \|\vec{R}\| = \sqrt{C^2 + S^2} \tag{3.12}$$

As any vector $\hat{p}$ subtending angle θ from the origin can therefore be expressed as a scalar multiple of a complex number,

$$\hat{p} = \|p\| \cdot \mathrm{e}^{\mathrm{i}\theta} \tag{3.13}$$

and remembering that the magnitude of each unit vector is unity, the sum of n unit vectors $\hat{r_i}$ can be expressed as the complex sum

$$\sum_{j=1}^{n} \hat{r_j} = \sum_{j=1}^{n} \|r_j\| \mathrm{e}^{\mathrm{i}\theta_j} \tag{3.14}$$

This fact allows the resultant vector to be rescaled to $[0, 1]$ by division by n, producing a normalised vector that can be compared to test distributions (see Section 3.6.2.2 below).

3.6.2.2 Rayleigh vector

HD cells are traditionally classified using the modulus of the resultant Rayleigh vector of the tuning curve. The Rayleigh (R) vector can be conceptualised as a weighted vector sum around the circle; in the case of a HD tuning curve this sum is over binned firing rates around the azimuth plane. The angle of this vector then indicates the preferred direction of the cell, whilst the modulus (absolute value) of the vector indicates the strength of directional modulation.

Formally, the Rayleigh vector is the normalised complex sum expressed by

$$\vec{R} = \frac{\pi}{n \cdot \sin\left(\frac{\pi}{n}\right)} \cdot \frac{\sum_{j=1}^{n} r_{\theta_j} \mathrm{e}^{\mathrm{i}\theta_j}}{\sum_{j=1}^{n} r_{\theta_j}} \tag{3.15}$$

where n is the total number of bins to be summed over and r_{θ_j} is the firing rate in bin θ_j.

Intuitively, this can be understood by appeal to the equivalence $\mathrm{i}\sin x + \cos x = \mathrm{e}^{\mathrm{i}x}$. If the firing rate in each bin, r_{θ_j}, can be understood as a scalar multiple of the vector expressed as the sum of $r \cdot (\sin\theta_j + \cos\theta_j)$, then its sum over all bins is $\sum_{j=1}^{n} r \cdot (\sin\theta_j + \cos\theta_j) = \sum_{j=1}^{n} r_{\theta_j} \cdot \mathrm{e}^{\mathrm{i}\theta_j}$.

The constant $\frac{\pi}{n \cdot \sin\frac{\pi}{n}}$ specifies a correction factor for the bias introduced in the estimation of R due to the use of binned data.

The modulus of the Rayleigh vector can be z-transformed and tested for significance; functions for this are provided in the MATLAB package CircStat (Berens, 2009). Importantly, the Rayleigh test assumes that any deviations from uniformity are unimodal (for example, a von Mises distribution), and the test will not necessarily detect deviations from uniformity that have multiple peaks. In particular, diametrically bidirectional (axial) data will show low R vector lengths. However, as HD cells are traditionally considered to exhibit unimodal directional tuning, the Rayleigh remains a common method for classification of HD cells.

3.6.2.3 Circular moments: mean and standard deviation

The mean direction of a sample of circular data is characterised as the direction of the resultant vector or Rayleigh vector $\vec{R}$, and is denoted $\bar{\theta}_0$. It is calculated as the 4-quadrant-specific inverse tangent of the vector,

$$\bar{\theta}_0 = \mathrm{atan2}(S/C) \tag{3.16}$$

where

$$\text{atan2}(S/C) = \begin{cases} \arctan(S/C) & : C > 0 \\ \arctan(S/C) + \pi & : C < 0 \text{ and } S \geq 0 \\ \arctan(S/C) - \pi & : C < 0 \text{ and } S < 0 \\ +\frac{\pi}{2} & : C = 0 \text{ and } S > 0 \\ -\frac{\pi}{2} & : C = 0 \text{ and } S < 0 \\ \text{undefined} & : C = 0 \text{ and } S = 0. \end{cases}$$

Similarly, circular measures of dispersion have been developed that are analogous to the linear standard deviation of the mean. These tend to revolve around recognising that, as R is a measure of the concentration of the dataset, $V = 2(1 - R)$ is an expression for the dispersion in the dataset, or circular variance.

This led to the proposal of a definition for circular angular deviation that will be used here:

$$s = \sqrt{2(1 - R)} \tag{3.17}$$

Although other definitions have been proposed and are discussed in (Zar, 2010), this relation will be used for all reports of circular standard deviations in this thesis.

3.6.2.4 Tests for non-uniformity

Various test statistics have been designed to detect non-uniformity of a distribution of sample datapoints around a circle, some of which use the above-described descriptive statistics. These will not be discussed here in detail, but will be briefly listed alongside any significant assumptions made.

The Rayleigh test derives a test statistic from the Rayleigh vector length, to test for unimodal deviations from uniformity. Its null hypothesis states that the data are drawn from a uniform circular distribution, and tests for significant deviations from uniformity in any single direction; a significant Rayleigh vector indicates substantial concentration of datapoints around a particular direction on the circle.

The Rayleigh test makes the assumption that any deviation from uniformity is unimodal, and therefore is not appropriate for bi- or multi-modal distributions. Of particular note, 'perfectly' bimodal distributions will display non-significant Rayleigh vector lengths. An example of this is an axial dataset, plotted from $[0, 2\pi)$ such that each datapoint is displayed twice: θ and $(\theta + \pi)$, which in these cases will trivially have Rayleigh vector $R = 0$.

A variant on the Rayleigh test is the V test, which looks for unimodal deviations from

uniformity towards a specified test direction, θ. Like the Rayleigh test, the V test assumes any deviation from uniformity is unimodal, and provides a more sensitive and powerful test for deviations from uniformity when there is an *a priori* expected direction towards which data should be clustered. The test statistic is computed as

$$V = nR\cos(\bar{\theta}_0 - \hat{\theta}) \tag{3.18}$$

A number of non-parametric tests exist to test for deviations from uniformity without the underlying assumption of unimodality. Common examples of these are the Rao spacing test, which detects deviations from the expected distance between ordered samples if the data were drawn from a uniform distribution, and the omnibus test, which looks for clustering of data-points on one half of the circle.

3.6.2.5 Kuiper test

The Kuiper test is a non-parametric test designed to detect differences in cumulative distributions around the circle; it is an analogue to the Kolmogorov–Smirnov (KS) test for linear data.

Whereas the KS test searches for the greatest absolute distance between the two cumulative distributions of interest, the Kuiper test looks for the greatest positive and negative distances between the distributions; the sum of which defines the test statistic. This difference ensures the statistic is invariant under cyclical transformations of the cumulative distribution graph, and therefore makes it appropriate for testing differences between circular distributions (Kuiper, 1960).

Chapter 4

Head Direction Cell Anchoring to Visual Panoramas

> Der Gedanke ist der sinvolle Satz.
>
> The thought is the significant proposition.
>
> TLP 4; Ludwig Wittgenstein

4.1 Introduction

To maintain a sense of direction when exploring an environment, animals must integrate allothetic information about the external world with representations of direction generated from self-motion cues. This information is often considered to be in the form of landmarks: points in the visual scene with specific, object-like features that can be associated with an allocentric direction. Do representations of direction require point-like landmark features in the visual scene? Spatial orienting can, in principle, use visual information with low spatial resolution (Wystrach et al., 2016). In the absence of object-like landmarks, can representations of direction integrate visual information from the entirety of the visual panorama?

In the rodent brain, head direction (HD) cells (Taube et al., 1990a,b) form a representation of orientation, with a given HD cell firing action potentials only when the animal's head is facing a specific direction in an environment: the cell's preferred firing direction (PFD). HD cells are found distributed across a number of regions of the brain. These include the dorsal tegmental nucleus (Sharp et al., 2001b) and lateral mammillary bodies (Stackman and Taube, 1998) – which are believed to generate the HD signal by integrating vestibular information about angular turns (Sharp et al., 2001a; Bassett et al., 2007) – anterior thalamus (Taube,

1995a), retrosplenial cortex (Chen et al., 1994b), and postsubiculum (Taube et al., 1990a).

HD cells integrate information about visual landmarks in the environment by using these to reorient their PFD in space following disorientation (Dudchenko et al., 1997; Knight et al., 2011). This process is referred to as 'landmark anchoring', and ensures that the representation of heading direction in the HD system remains aligned with distal cues in the external world (Yoganarasimha et al., 2006). As such, between trials the direction represented by a given HD cell will be consistent in the landmark-based reference frame, and an HD cell will rotate its PFD to follow any rotational transformations of the visual landmarks between trials (Taube et al., 1990b). Indeed, vision exerts stronger cue control over HD cells than many other sources of allothetic information (Goodridge et al., 1998). Knight et al. (2014) rotated a visual cue provided by a light shone on an arena wall, following a period of darkness during which the animal remained in the arena, and demonstrated that rotations of the visual cue up to 120° influenced the PFDs of PoS HD cells. Beyond this, rotations of the visual cue were correlated with progressively smaller shifts of the PFDs, indicating the cells were weighting idiothetic (self-motion) information more strongly as the cue was more clearly less stable.

A variety of visual cues have been demonstrated to exert cue control over HD cells (Lozano et al., 2017). Traditionally, the visual scene contains one or more solid cue cards, attached to the inside wall of the environment the animal explores (Taube et al., 1990b; Lozano et al., 2017). The use of (high contrast) cue cards, different in luminance to the surrounding wall, creates a visual scene with clear 'point' landmarks – areas on the wall where the contrast and luminance changed suddenly from, for example, black to grey. These could provide visual features – such as in the form of edges – to which HD cells could anchor (Knierim and Hamilton, 2011), and thus provide visual objects to which the HD system can anchor.

Do HD cells require landmarks consisting of point-like objects in the visual panorama for landmark-anchoring to occur? To date, no work has tested directly whether HD cells can landmark anchor to visual panoramas that do not contain discontinuous changes of luminance. Rodent navigating behaviour is consistent with view-based approaches, whereby rats minimise differences between a learned view and the entire visual panorama (Cheung et al., 2008). Similarly, low resolution information about the visual scene is thought to be optimal for spatial orientation (Wystrach et al., 2016), perhaps through view-matching the current visual input with a remembered viewpoint (Zeil, 2012). Can the representation of orientation provided by the HD cells anchor to visual scenes containing only low spatial frequency information, thus integrating visual information from the entire panorama?

Here, we record HD cells in freely moving rats in a landmark anchoring paradigm, while rats foraged inside a transparent Perspex cylinder. Around the outside of the cylinder were

wrapped large visual panoramas, which could be rotated independently from the cylinder walls and floor.

A number of panoramas were used, shown in Figure 4.1A. One displayed a large solid black segment and a large grey segment, each subtending 180° of arc. The two segments were designed to emulate a cue card edge – for example, a black cue card held against a grey wall. The other panoramas displayed continuous luminance gradients shifts continuously from black to grey to black. This contained no discontinuities or 'edges', and as such could be considered a single low spatial-frequency grating subtending the entire 360° of arc.

We used these to test whether HD cells were able to anchor to low spatial-frequency visual scenes, with no edges or discontinuities that might constitute 'visual features' as are commonly used in landmarks. If HD cells rotated their tuning curves to follow rotations of the visual gradient, this would indicate that the cells can integrate information from a large region of the visual panorama, when discrete landmarks were not available. Failure of HD cells to rotate their tuning curves to follow the panorama would indicate that the cells require discrete, object-like landmarks to landmark-anchor. Any anchoring that is observed may be more error-prone, in which case we would predict a greater discrepancy between the rotation of the visual panorama and of the HD tuning curve. This would indicate that, although visual information about the entire panorama reached the HD system, this information was less directionally precise in the absence of discrete landmarks. In this way, whether HD cells are able to use visual information from these sorts of panoramas to reset their firing directions could shed light on what sort of information can be integrated into the HD signal, and ultimately on how vision and spatial representations interact.

4.2 Materials and methods

4.2.1 Animals

4 adult male Lister Hooded rats were used in the experiment. Animals were housed individually following surgery in a room maintained with a 12:12 hour day:night cycle, including 1 hour simulated dawn/dusk. Animals were fed a lightly food-restricted diet so as to maintain a minimum of 90 % estimated free-feeding weight, and had *ad libitum* access to water. All procedures were performed in compliance with the regulations outlined by the UK Animals (Scientific Procedures) Act (1986) and the European Communities Council Directive of 24 Nov 1986 (86/609/EEC), and under protocols outlined in a UK Project License.

AP	ML	DV
-7.5 mm	±3.4 mm	-2.0 mm

Table 4.1: Implantation co-ordinates of tetrodes, targeted at the postsubiculum.

4.2.2 Surgery

Animals underwent unilateral implantation of 16-channel 'poorlady'-style microdrives (Axona Ltd, St. Albans, UK) into the postsubiculum (see Table 4.1), as described in Chapter 3.

Post-operatively, animals were placed in a heated recovery box and closely monitored. They were provided with post-operative analgesia (meloxicam) for 3 days after surgery and were allowed 7 days of recovery before recording sessions began.

4.2.3 Recording procedure

Single units were recorded using an Axona multichannel recording system (Axona Ltd., St Albans, UK). Animals were tracked using 2 LEDs (one large, one small) attached to the head-stage placed on the animal's head during recordings. This allowed for accurate reconstruction of head direction alongside position of the animal.

4.2.3.1 Screening recordings

Initially, animals were recorded in a separate room from the experimental room to assess whether any head direction cells could be isolated within the clusterspace. The screening apparatus consisted of either a 1×1m or 0.6×1.2m rectangular box, which contained one large prominent cue card on the wall. Distal cues (such as cue cards on the walls of the room and the experimenter) were available to the animal so that it would have a cue-rich and unambiguous environment in which to anchor its spatial representations.

If a head direction cell was identified following inspection of the clusterspace, the animal was moved to the experimental room and recorded in the Perspex cylinder. Following the session, a post-screening recording was performed to assess the stability of the clusterspace.

4.2.3.2 Session apparatus

After a cell was identified, the animal was carried into a separate recording room for the experiment. Here, recordings were made while the animal freely foraged inside a large, clear Perspex cylinder (1 m diameter and 0.75 m height). Around the outside of the cylinder, a large (3.2 m by 0.75 m) matte-printed paper poster (Captain Cyan, London, UK) was wrapped and secured with Velcro fastenings. This creates a complete visual panorama from the perspective of the animal inside the cylinder. Importantly, due to its placement outside of the cylinder,

the animal cannot touch the card that subtends the panorama, and this can then be rotated independently of the apparatus itself (both the cylinder and floor). As such, rotations of the card entail *only* rotations of the visual content of the panorama, and will be decoupled from plausible olfactory or tactile landmarks inside the cylinder.

A number of different visual panoramas were used, designed to assess the capacity of the HD system to anchor to low-spatial frequency visual scenes. Schematics of these are shown in Figure 4.1A. One 'control' card was used, alongside two 'gradient' cards. The low-frequency gradients consisted of a single, continuous and gradually changing luminance gradient from black to grey to black, subtending 360° of arc. The luminance change shifted from black (RGB $[0, 0, 0]$) to middle-grey (RGB $[140, 140, 140]$), and the transition between these extremes followed a cosine function around the circle, such that the rate of change of the RGB value was zero (the stationary points) at the centres of the black and grey extremes, and greatest (the inflection points) midway between black and grey.

Two gradient cards were used. These had identical visual scenes generated as described above, but were offset relative to the edge of the poster by 90°. The purpose of this was to isolate any anchoring effects due to the seam created when the poster was wrapped around the cylinder. In a given session, both gradient panoramas were used (see below), and – as the seam was located in a different place on each panorama – if the system was using this discontinuity to anchor, we would observe changes in HD cell PFDs when the gradient panoramas were swapped.

The control card was designed to emulate more closely traditional cue cards from landmark anchoring experiments. This panorama consisted of a single block of black (RGB $[0, 0, 0]$) abruptly changing to a solid block of middle-grey (RGB $[140, 140, 140]$), each subtending 180° of arc. This would be similar to the visual scene created by mounting a 180° black cue card onto the inside wall of a grey cylinder. It was chosen for the discontinuous edges to be separated by 180°, so as to align with the inflection points of the cosine gradient, which are also spaced 180° apart.

Cosine functions are frequently used to generate gratings in visual experiments (e.g., De Franceschi and Solomon (2018)) and provide the basis for Fourier decompositions of a visual scene into frequency space (Westheimer, 2001). The cosine curve has an always continuous derivative, and therefore was selected to minimise any perceptual discontinuities at the stationary points, where the colour gradient changed direction[1].

[1]To compare, a linearly changing gradient from black to grey, which then linearly shifts back from grey to black, would appear to humans to have edges at the point where the gradient 'changes direction' – in this case at the extreme values of black and grey. Although there is some evidence rats are not subject to the same visual illusions as humans – they do not generalise learned shape discriminations to illusory contours of Kanizsa shapes, and may instead attend to luminance differences in the lower hemifield (Minini and Jeffery, 2006) – it is unknown whether rats may be subject to other sorts of perceptual illusions and therefore the gradients were generated to minimise this possibility.

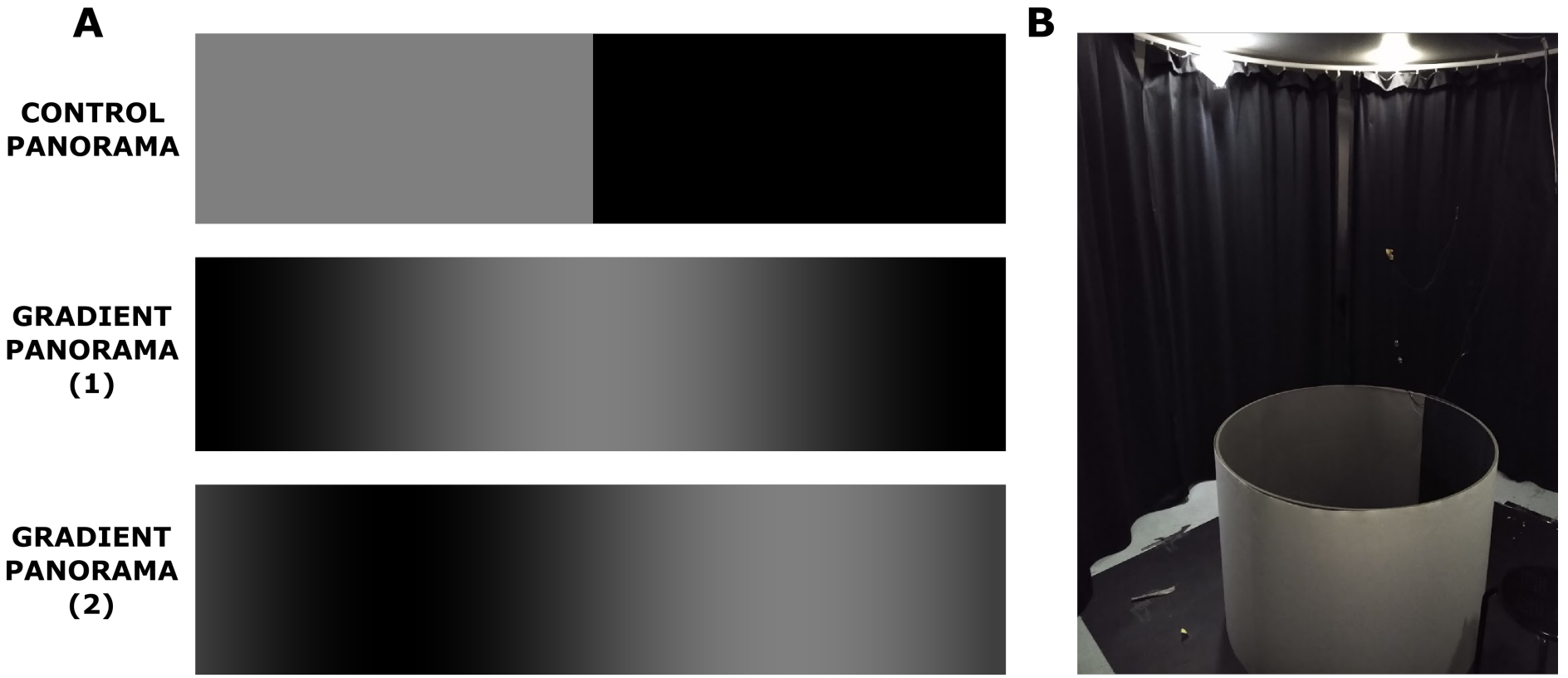

Figure 4.1: A: Schematic of the three panoramas used in the experiment: a control panorama that changes suddenly from grey to back; a gradient that shifts gradually from grey to black to grey; a similar gradient, but with the seam shifted by 90°. B: Photograph of the Perspex cylinder inside the curtained recording room, with the control gradient wrapped around the outside of the cylinder.

4.2.3.3 Session recording

If a recording session was to be performed, rats were carried to a separate room for recording in an opaque box. Recording sessions consisted of 9 trials, with (in general) the following structure: trials 1-4 using the control panorama, trials 5-8 using the gradient panoramas, and trial 9 using the control panorama (see Figure 4.2). Between each trial, the animal was placed in an opaque holding box, and the walls and floor of the cylinder were cleaned with ethanol, in order to scramble any olfactory cues present. Before each trial, the animal was disoriented by the experimenter, by being carried in circles around the room inside the holding box. Trials 1 and 9 constituted 'baseline' trials, in which the panorama was unrotated (definitionally at 0°). In all other trials, the panorama was rotated relative to baseline at a random multiple of 45°, selected at random. Within the four trials using gradient panoramas, the first two trials used one of the two panoramas (gradients 1 and 2, as per Figure 4.2), and the next two trials used the other panorama. The order in which the gradient panoramas were used in any given session was also randomly assigned. As such, assessing the extent to which HD cell PFDs shifted between trials 6 and 7 would test the contribution of the poster seam to cue control over the HD cells.

The rotation angles of the panoramas was kept consistent across all panoramas used. That is, for example, if the centre of the black 'cue card' was defined as 0° for the control panorama, this was also true for both of the gradient panoramas. This enabled us to assess whether the directionality encoded by HD cells was transferred in a consistent fashion between gradient and control panoramas (between trials 4 and 5).

In one animal (R974), the order of exposure to control and gradient panoramas was also randomised. As only one session was recorded from this animal, this resulted in the animal being exposed initially to the gradient panoramas (trials 1-4), subsequently to the control panorama (trials 5-8), and to the gradient panorama again (trial 9).

Following a recording session, where possible, the HD cell was re-recorded in the screening room before the animal was replaced in its home cage.

4.2.4 Cell isolation and analysis

Putative cell clusters were isolated as described in Chapter 3. Final clusters were saved and imported into MATLAB 2015a (Mathworks Ltd., Natick, MA) for further analysis. Custom analysis functions were written, which made use of the CircStat package for circular statistics (Berens, 2009).

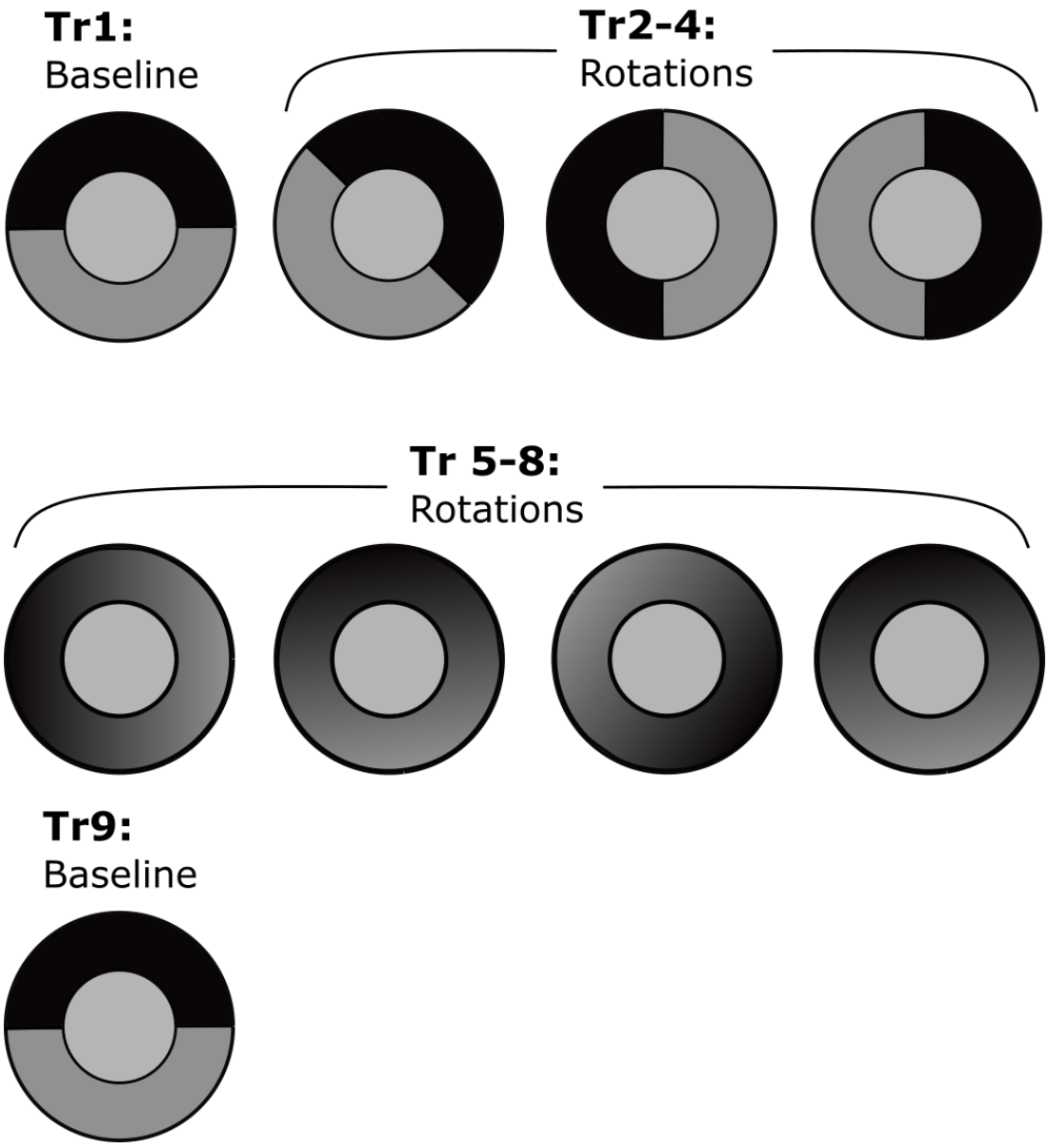

Figure 4.2: Representation of design of a given recording session. Trial 1 consistutes a baseline trial, here using the control panorama. Trials 2-4 consist of rotation trials using the control panorama. Trials 5-8 consist of rotation trials using the gradient panorama. Trial 9 is a second baseline trial using the same panorama as in Trial 1.

4.2.4.1 HD cell classification

Putative neurons were classified as HD cells if they exhibited a peak firing rate of >1 Hz, refractory period violations of $< 1\%$, and a Rayleigh vector length, R, satisfying both $R > 0.3$ and $R > P_{99\%}$ of a shuffle distribution calculated from repeatedly time-shifting the spike train relative to the animal's position and recalculating the R vector of the tuning curve using this new dataset ($n = 10000$ shuffles per cell). These criteria had to be met for the baseline trial 1 of the recording session for the cell to be included in the rotational analyses.

4.2.4.2 Firing properties of HD cells

For each recorded HD cell, numerous properties were extracted from its tuning curve and spike timeseries to assess the cell's firing characteristic.

This comprised the peak firing rate of the smoothed HD cell tuning curve, the mean firing rate of the cell in each trial, the tuning width of the curve (circular standard deviation, estimated as $-2\log(|R|)$), and the directional information content of the HD cell spike train.

4.2.4.3 Rotation analysis of HD cells

In order to assess whether the population of HD cells successfully landmark anchored to the local reference frame of the two-cue cylinder, the recorded activity of the cells had to be normalised both across cells (which had different PFDs) and across trials in a session (which had different rotation angles). Each cell PFD was initially normalised into the local reference frame of the cylinder by subtracting the rotation angle of the panorama.

Following this, an estimate of each cell's preferred direction of the session was derived by selecting the trial around which PFDs from all other trials clustered most closely across the session. The PFDs of all cells in this trial were subtracted from the PFDS of all other trials, which – if the cells shifted non-randomly – would have the effect to shift the majority of PFD values across all cells to near zero. This normalised trial was then removed, as it is definitionally set at 0°. The normalised PFDs were averaged across all cells recorded in each trial, to provide a single estimate of how much the attractor shifted between trials.

In order to select the trial, we used the following metric:

$$\underset{tr \in Sess}{\arg\max} \sum_{i=1}^{n} \cos(\theta_i - \theta_{tr})$$

where θ_i is the HD cell PFDs in trial i, and n is the number of trials in the session. The effect of this is to select the trial tr with HD cell PFDs θ_{tr} that are near the HD cell PFDs in all other trials. This provides an interpretation of the representation of direction encoded in

the local reference frame by the HD cell population across the whole session.

4.2.5 Histology

At the end of the experiment, rats were killed with an overdose of pentobarbitone and perfused transcardially with 0.9 % saline, followed by 10 % neutral-buffered formalin. The brains were extracted, kept in a formalin solution for a minimum of 24 h, and subsequently transferred to 30 % sucrose by weight in phosphate-buffered saline for dehydration. Brains were then frozen to $-21\,^{\circ}$C and sectioned into 30 µm-50 µm coronal slices. Slices were Nissl stained with cresyl violet for assessment of electrode placement.

4.2.6 Nomenclature

Individual rats, when discussed, will be referred to using the internal reference code given to rats within the animal facility they were housed in. This takes the form of the letter R followed by a designation number; for example: 'R909'.

4.3 Results

53 HD cells were recorded from a total of 245 putative units in 4 animals, over 14 sessions. This corresponded to 117 trials, consisting of 69 control panorama trials and 57 gradient panorama trials. Overall, 21.6% of recorded PoS cells were classified as HD cells.

4.3.1 Histology

4.3.2 HD cell characteristics

Intrinsic firing characteristics of the recorded HD cells were compared between trials with the control and gradient visual panoramas. For this, we averaged the metrics discussed below over control and gradient trials, and tested the distributions of these means over all cells.

The median peak firing rate of all recorded HD cells during control trials was 3.43 Hz, and was 3.13 Hz during gradient trials, which did not differ between control and gradient sessions ($z = 0.79$, $p > 0.78$, Wilcoxon ranksum test, $n = 53$ cells), indicating that cells behaved broadly similarly during gradient trials as control trials (see Figure 4.3).

We hypothesised that if HD cells received less precise landmark information during gradient trials, this may be reflected by a decrease in the observed directionality of cells during these trials. To test this, we compared the tuning widths (related to the R vector) of HD cells during gradient versus control trials. However, we saw no difference in tuning widths of HD

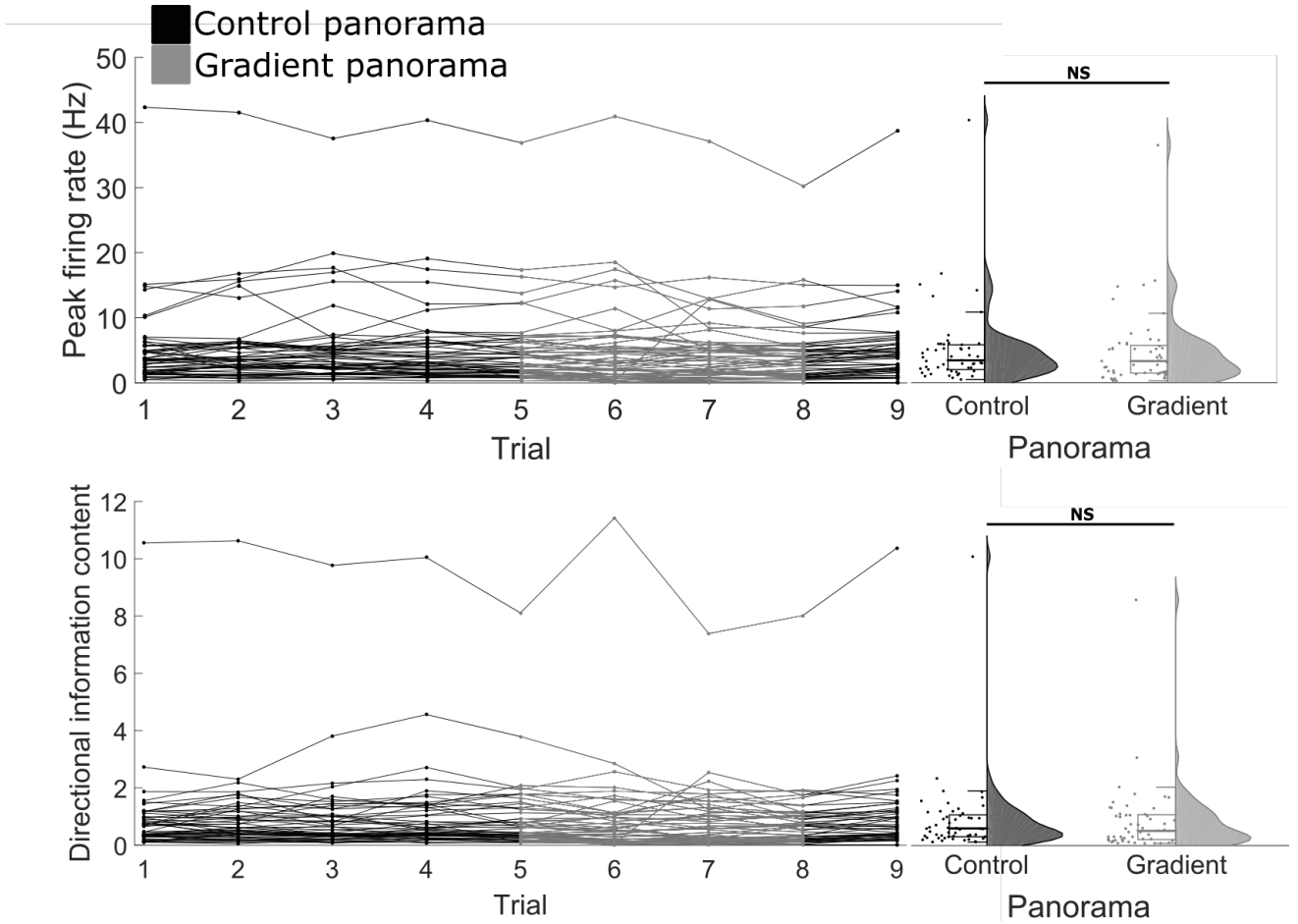

Figure 4.3: Comparison of peak firing rates (PFR) and directional information content (DIC) of HD cells. Left: plots of PFR and DIC for all HD cells in each trial in a session. Right: mean PFR and mean DIC over all control trials and gradient trials, for each HD cell. NS: not significant.

cells between control and gradient trials (median control tuning width: 125°, median gradient tuning width: 127°, $t = -0.74$, $df = 47$, $p > 0.4$, t-test). This is displayed in Figure 4.4, and indicated that HD cells were no less directional in the gradient trials, but maintained a similar precision in their encoding of direction.

Consistent with this, we saw no difference in the average directional information content of HD cell tuning curves between control and gradient trials (median control DIC: 0.612, median gradient DIC: 0.524, $t = 1.40$, $df = 52$, $p > 0.10$, t-test, see Figure 4.3).

4.3.3 Landmark anchoring to the visual panorama

The degree of cue control exerted by visual panoramas over the HD system was assessed. Grouped together over all animals, there was evidence that HD cells landmark anchored to both the control panorama and the gradient panoramas, with the set of normalised shifts over all trials possessing significant deviation towards the predicted angle of 0° (control: $R = 0.64$, $V = 35.7$, $p_V < 10^{-11}$, $n = 56$ trial shifts; gradient: $R = 0.52$, $V = 21.5$, $p_V < 10^{-5}$, $n = 42$ trial shifts). This indicates that, following rotations of the panorama, HD cells tended to rotate their representation of direction a similar angle, and therefore may be able to integrate visual information from panoramas with and without discontinuities in luminance. Because the visual panoramas were mounted on the outside wall of a clear cylinder, and the cylinder/floor itself did not rotate between trials, the only changing features of the environment between trials are the visual contents of the panorama. Thus, both control visual panoramas and low-spatial frequency gradients were able to exert significant cue control over the HD system.

Of note, landmark anchoring of HD cells to the tested cues sometimes varied between animals – with HD cells in some animals failing to be controlled by the visual panoramas – leading to difficulties in grouping data together across animals. Two general trends emerged: HD cells in one set of two animals (R908 and R931) displayed good cue control, and little evidence of anchoring to the distal room, as in these cases the Rayleigh vector lengths show that the PFD shifts more closely followed the rotations of the visual panorama than the distal room. In the other two animals (R909 and R974), HD cell PFDs did not shift to follow rotations of the panorama as consistently as in the other animals, resulting in lower Rayleigh vector lengths for these shifts. This seems likely due to the HD cells from these animals anchoring to a distal representation of the room, as in this reference frame we see the recorded cells displaying consistent PFDs for these two animals (see next section and Table 4.2). The distributions of HD cell PFD shifts for control and gradient panorama rotations and relative to the distal room, for individual animals, are shown in Figure 4.5.

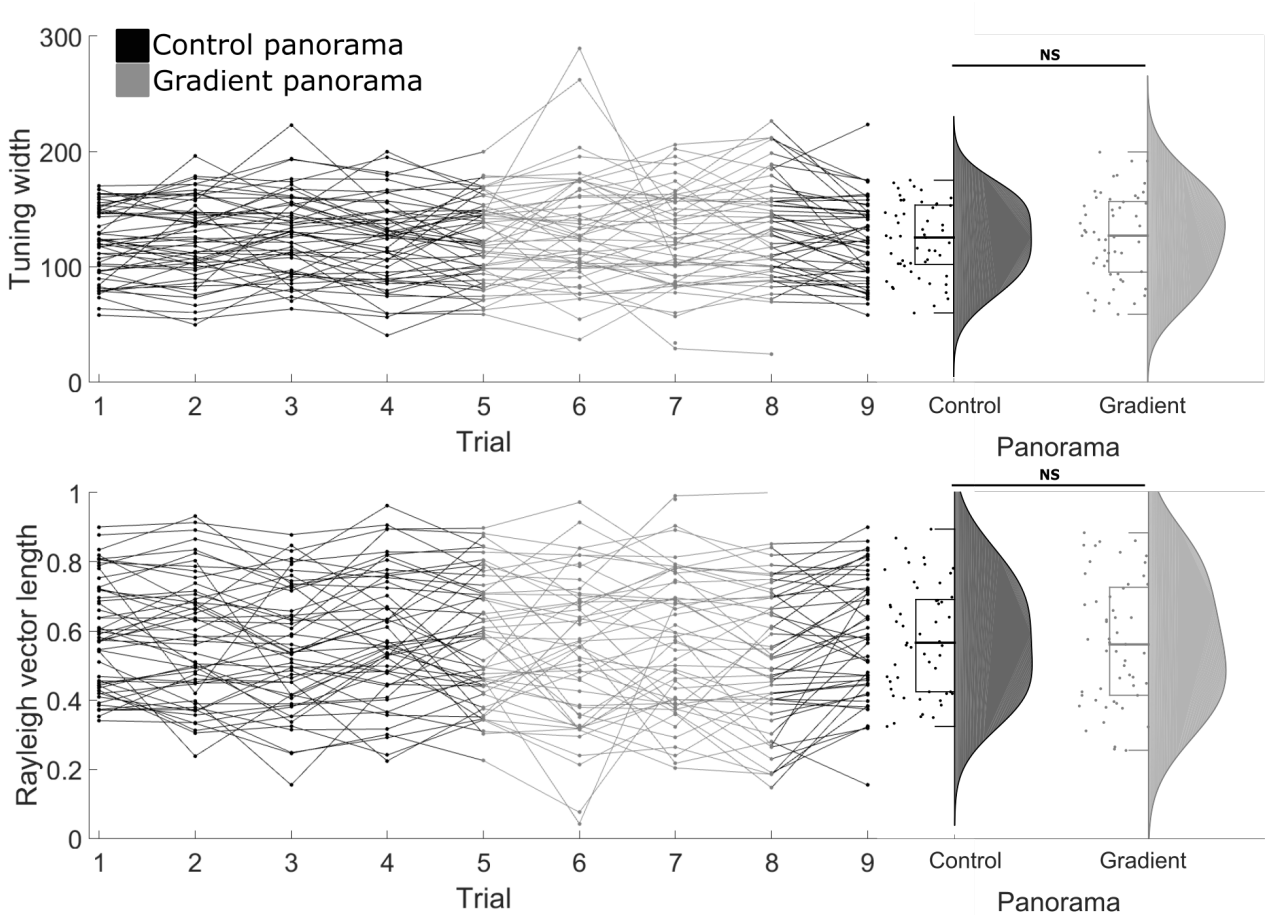

Figure 4.4: Comparison of tuning widths and R vector lengths of HD cells. Left: plots of tuning width and R vector length for all HD cells in each trial in a session. Right: mean R vector and mean tuning width over all control and gradient trials, for each HD cell. NS: not significant.

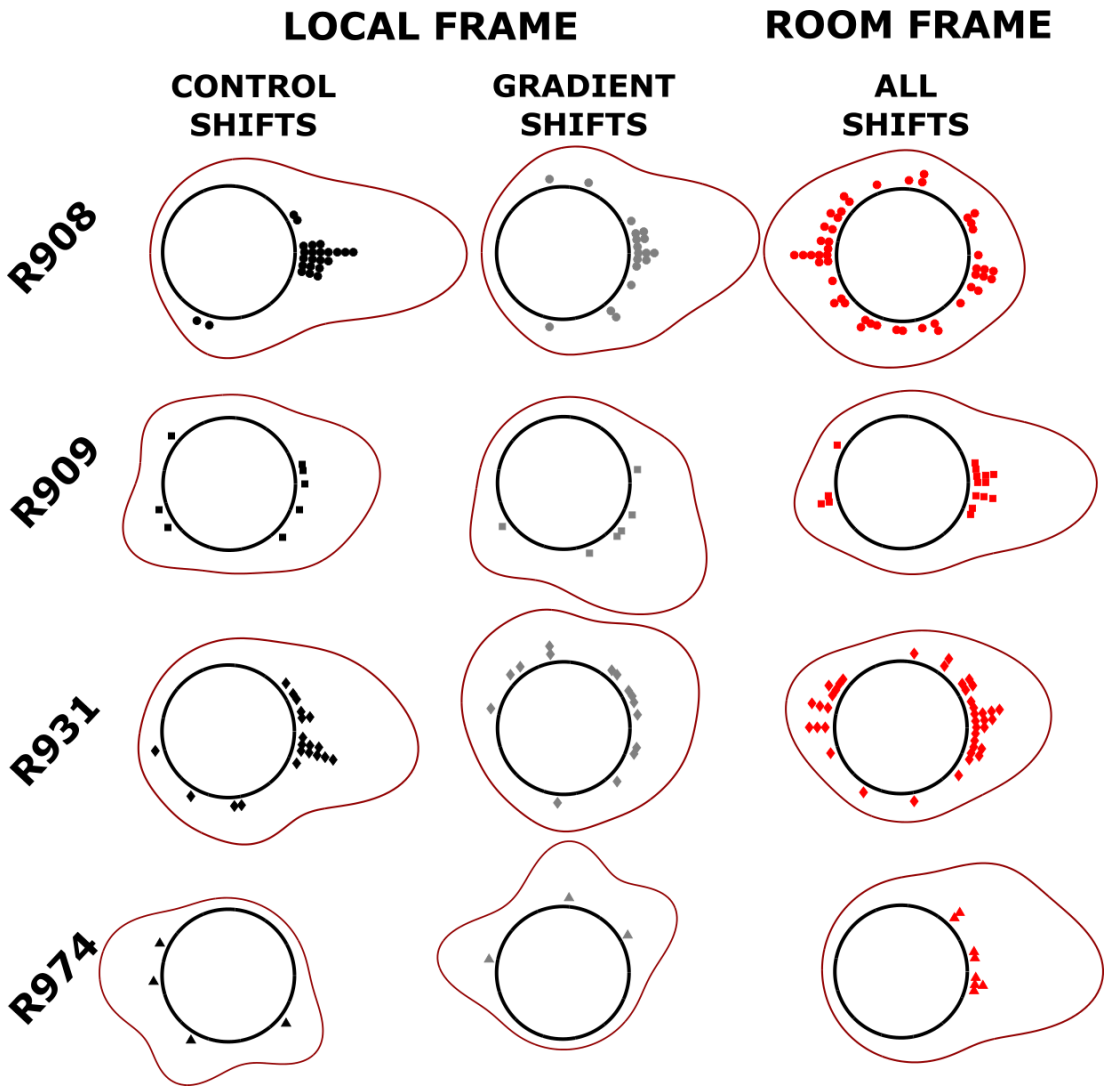

Figure 4.5: Distributions of PFD shifts across trials for each individual animal, plotted for all shifts of control panoramas (left column), gradient panoramas (middle column) and relative to the distal room (right column). Two animals (R909 and R974) show greater anchoring to the distal room than to the control cue card shifts.

	R_{vis}	p_{vis}	R_{room}	p_{room}	n
R908	0.831	1.5×10^{-15}	0.160	0.293	48
R909	0.459	0.050	0.500	0.016	16
R931	0.540	1.8×10^{-5}	0.315	0.018	40
R974	0.243	0.677	0.925	1.7×10^{-4}	8

Table 4.2: Summary statistics of PFD shifts between trials for each animal. Here, data from gradient and control trials were grouped together. Subscript *vis* indicates statistics calculated on PFD shifts relative to rotations of the visual panorama; *room* indicates statistics of PFD shifts relative to the distal room. R_{room} therefore indicates the Rayleigh vector length of PFD shifts in the distal room reference frame; p_{room} is the p-value associated with this vector length. R_{vis} and p_{vis} are defined analogously. Two animals (R908 and R931) show higher R vector lengths in the reference frame of the panorama than of the distal room; the other two animals (R909 and R974) show the opposite trend.

4.3.4 Landmark anchoring to the distal room

HD cells will anchor preferentially to more distal (versus proximal) cues if available (Zugaro et al., 2001), because these cues can provide more stable allothetic directional information into the navigation network (Page and Jeffery, 2018). If rats learnt the orientation of the distal room, outside of the enclosing curtain, HD cells would ignore the rotation of the proximal cylinder and remain stable in relation to the reference frame observed by the camera.

To test whether either HD cells in general landmark-anchored to the distal room configuration, the normalised PFD shifts of recorded HD cells were correlated against the distal (camera) reference frame instead of the visual scene of the cylinder. When data from all animals were grouped together, the Rayleigh vector of PFD shifts was marginally significant ($R = 0.18$, $p = 0.026$, $n = 112$ trial shifts). Visual inspection of the distributions shows a density around 0°, and plotting the PFD shifts relative to the distal room individually over all four animals shows that some animals anchored to the distal scene (see Figure 4.5).

Comparing these to the R-vectors derived above in the local reference frame of the visual panorama, we can see that for two animals the PFD shifts overall were more likely to anchor to the distal room than the panorama (R909: $R_{room} = 0.500, p_R < 0.05$; R974: $R_{room} = 0.925, p_R < 10^{-3}$) and for two animals the PFD shifts anchored more strongly to the panorama than the room (R908: $R_{vis} = 0.831$, $p < 10^{-14}$; R931: $R_{vis} = 0.540$, $p < 10^{-4}$).

As there was evidence that these animals learned a distal representation of the room, they were not included in the analyses below; we only included the data from the two animals that appeared to use the local reference frame.

4.3.5 Anchoring to control vs gradient panoramas

Of the two animals in whom we achieved cue control using the panoramas, HD cells anchored to both the control panorama and the continuous gradient significantly more accurately than

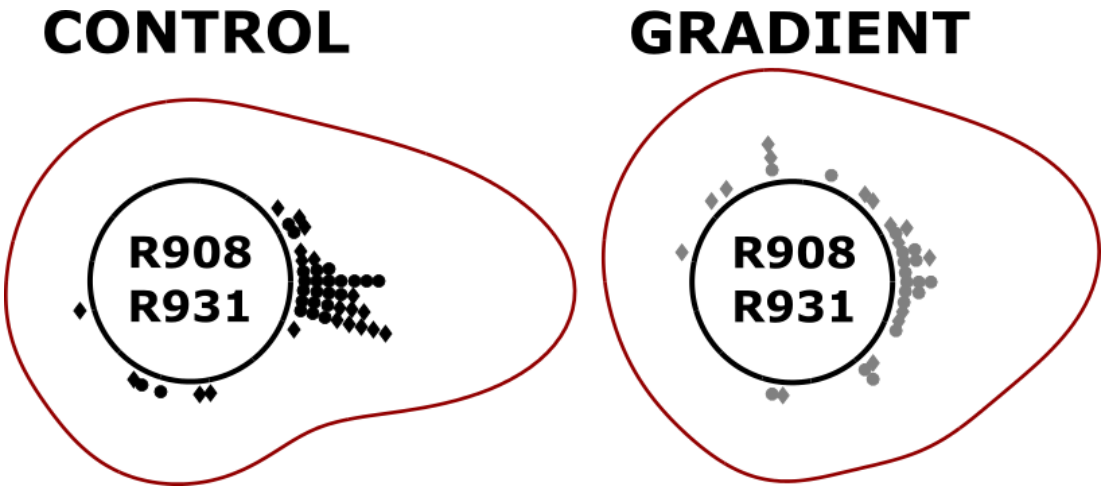

Figure 4.6: Anchoring to control (left) and gradient (right) panorama shifts in the two animals which exhibited good cue control in the gradient condition.

chance over all trials (control panorama: $V_0 = 35.0$, $p < 10^{-13}$, $n = 44$ trials; gradient panorama: $V_0 = 18.6$, $p < 10^{-5}$, $n = 33$ trials). However, analysis of the cumulative distribution functions of the two conditions highlighted that the two distributions of PFD shifts were significantly different from each other (Kuiper test: $k = 594$, $p < 0.05$, Figure 4.6). This provides evidence that, although the continuous gradient can provide visual anchoring information used by the HD system to reset its orientation, this process is significantly less precise than when the system has a visual scene with distinct edges available to it.

This was consistent with the observation that, over all trials, the Rayleigh vector of PFD shifts was greater during control trials than gradient trials (control: $R = 0.802$; gradient: $R = 0.586$). This corresponded to a greater circular standard deviation estimate of the PFD shifts following rotations of the gradient panorama than the control panorama (control: $s = 0.665$; gradient: $s = 1.034$). This trend was consistent across both animals recorded during the session (R908: control $R = 0.878$, gradient $R = 0.714$; R931: control $R = 0.771$, gradient $R = 0.440$).

Overall these findings imply that, although HD cells can anchor to visual scenes consisting of a single continuous contrast gradient, this gradient provides less precise orienting information to the HD system than more 'traditional' cues with clear sudden changes in contrast.

To test that the cells were not anchoring to the seam of the gradient panorama (where it was wrapped around onto itself), we analysed the PFD shifts between trials 6 and 7 for rats R908 and R931. This corresponds to when the two gradient panoramas in Figure 4.1A were switched. As these two panoramas have a seam in different places, we tested if PFD shifts between these trials clustered around 0°, which would indicate that the cells maintained a consistent representation of direction between the two panoramas. We saw a significant deviation towards 0° in the set of all shifts ($R = 0.57$, $V = 5.58$, $p_V < 0.01$, Figure 4.7). We took this as evidence that the

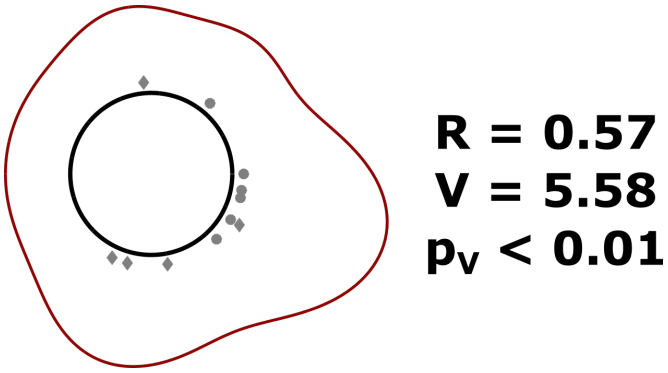

Figure 4.7: PFD shifts between trials 6 and 7, when the gradient panoramas were swapped (see Figure 4.1). There is a significant deviation towards 0°, as evident from the V test, indicating a consistent representation of direction between the two gradient panoramas.

representation of direction was consistent between the panoramas, and therefore was likely to be using the gradient content of the panorama rather than the seam to orient.

4.3.6 Cluster quality

To test whether the poorer anchoring observed in gradient trials was due to cell isolation becoming poorer over the course of a trial (which could introduce noise into the estimation of the PFD), we ran a number of analyses.

To assess whether the cell properties changed over the course of a session, we compared some characteristics between Trials 1 and 9 (the two baseline trials). A paired t-test showed no significant difference in the peak firing rate of HD cells between trials 1 and 9 ($z = -0.707$, $df = 52$, $p > 0.4$, see Figure 4.8), and no significant difference in the Rayleigh vector length of HD cells between trials 1 and 9 ($z = -0.210$, $df = 49$, $p > 0.5$, see Figure 4.8). This indicates that the HD cell clusters remained over the course of the session – with similar directionality and spike counts – and did not drift between trials 1 and 9.

4.3.7 Movement correlates

To assess animal movement, we analysed behavioural correlates over the course of each session. We extracted the linear distance and angular distance travelled in each trial,and performed a one-way ANOVA to assess whether there was any significant difference in distances travelled across trials.

As might be expected, the ANOVA showed a statistically significant difference between linear ($F(8, 117) = 18.14$, $p < 10^{-16}$) and angular ($F(8, 117) = 5.94$, $p < 10^{-5}$) distances travelled over trials. A Bartlett test showed that there was no evidence of heteroscedasticity between trials in the distributions of linear distance ($\chi^2_8 = 7.73$, $p > 0.4$) or angular distance ($\chi^2_8 = 4.87$, $p > 0.5$) travelled. Post-hoc tests (Tukey-Kramer) showed that, in general, both

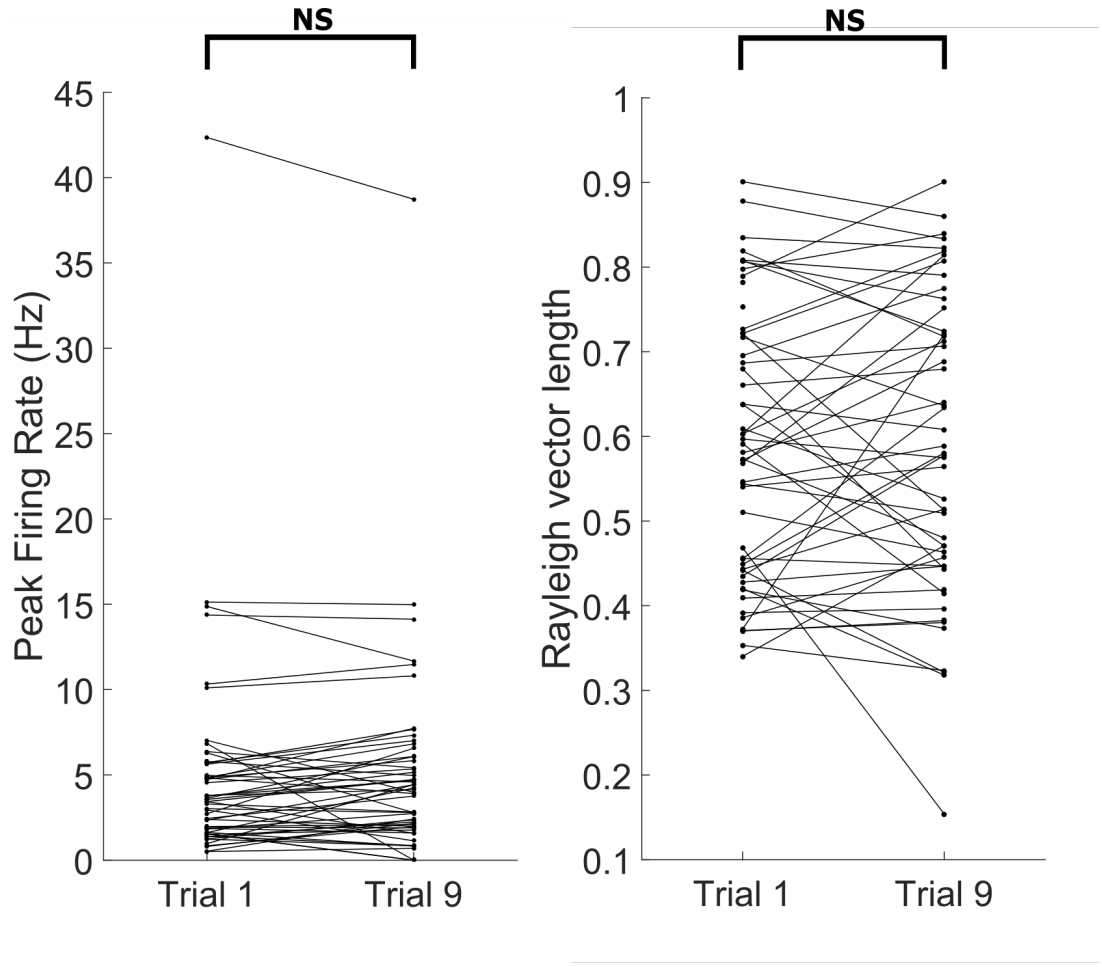

Figure 4.8: Paired distributions of HD cell peak firing rates and Rayleigh vector lengths between trials 1 and 9.

linear and angular distances travelled per trial gradually decreased over the course of the trial. Figure 4.9 shows the distributions of linear and angular distances travelled per trial for each session, showing that in general the animal travelled less of the course of a session.

4.4 Discussion

In this chapter, we recorded HD cells from the PoS of freely moving rats in a novel landmark control apparatus, in which the visual panorama was mounted on the outside of a transparent Perspex cylinder. A large body of literature has demonstrated the importance of visual landmarks in controlling the HD signal. Extending previous work attempting to characterise the visual features constituting landmarks, we designed visual panoramas without any discontinuities of the kind that would typically characterise traditional landmarks (such as cue cards with edges). These panoramas consisted of single gradients fading from grey to black to grey. Rotating these between trials allowed us to assess whether HD cells could anchor to visual scenes without edges, in which only low spatial frequency information is available. Rat visually-guided navigation is consistent with a view-based navigation, in which the rat attempts to minimise differences between its current view and a remembered reference image (Cheung et al., 2008), and computational approaches have argued that low spatial resolution visual information is optimal for robust spatial orienting (Wystrach et al., 2016). As such, we might expect good cue control by these large gradient panoramas over HD cells, if these integrate the low spatial-frequency visual view to orient.

The main finding of this chapter was that the visual panoramas tested could exert cue control over HD cells, as evidenced by HD cells maintaining a consistent firing direction over trials in the local reference frame subtended by the panorama. However, this cue control was remarkably less consistent between animals than is often seen in other cue control experiments, with HD cells from 2 of 4 animals showing evidence of anchoring to the distal reference frame of the room. This is evident from the R vector length of all PFD shifts to control panorama rotations ($R = 0.64$); this value is lower than that reported previously in a two-cue paradigm containing two highly discriminable cue cards attached to the inside wall ($R = 0.73$, Lozano et al. (2017)). Possible reasons for this are discussed below.

The rotations of the visual panorama would not correlate with shifts in cues of tactile, olfactory, and/or other modalities that could exert control over the HD cells. This is different from what would be observed in traditional cue control studies (Taube et al., 1990b; Lozano et al., 2017), in which cue cards are frequently mounted on the inside edge of the wall of the environment, and therefore could provide tactile or olfactory landmarks. For example, the edge

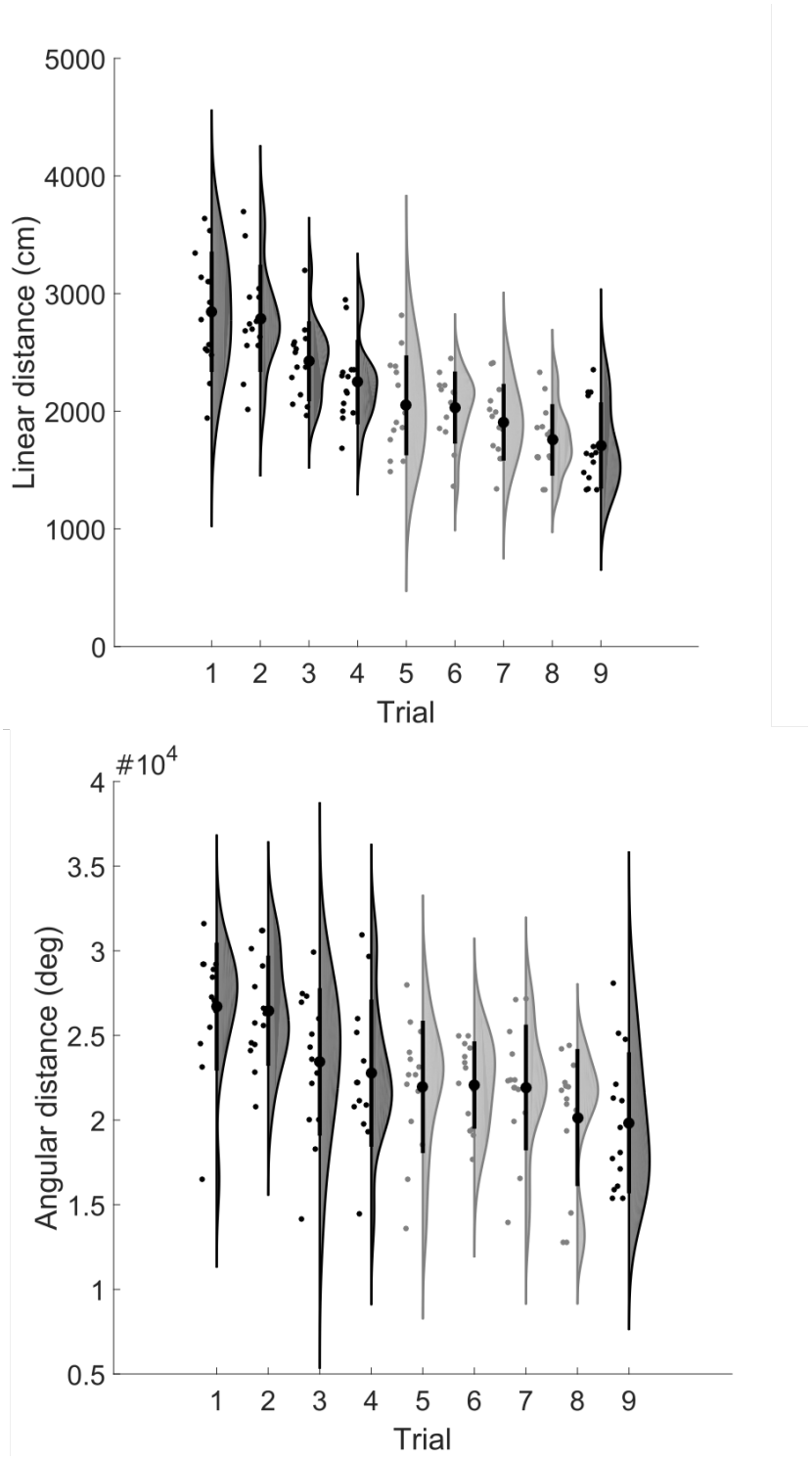

Figure 4.9: Summary movement characteristics over sessions. Top: linear distance travelled by the animal in each trial over all sessions. Bottom: angular distance travelled by the animal in each trial over all sessions.

of a polypropylene cue card, against a painted MDF arena wall, could provide directional tactile information and therefore could be used as a landmark by the HD system.

In our setup, as the panorama rotated, only the visual scene shifts. In animals where we observed significant correlations between the shifts observed in the HD representation and the rotations of the visual panorama, we consider this good evidence of visual cue control over the animal's sense of direction. We considered the PoS as an appropriate candidate structure from which to record HD cells, given the region receives extensive projections from primary and secondary visual cortices (van Groen and Wyss, 1990c; Wang et al., 2012), and has been implicated in landmark integration in the HD system (Yoder et al., 2015).

However, cue control was difficult to achieve in this setup, with only 2 of 4 animals showing any evidence of landmark anchoring to the control panorama. Three of these animals were recorded contemporaneously, suggesting that this was not due to changes in the recording setup or experimenter ability over time. One possibility we consider is that, without consistent olfactory and/or tactile cues rotating with the visual panorama, we induced a conflict between these local cue modalities. Indeed, olfactory cues co-incident with visual cues are known to potentiate learning of the visual landmarks in a spatial task (Lavenex and Schenk, 1997), although this effect may be more marked in juvenile than adult rats (Rossier and Schenk, 2003). The age of our rats at time of implant was estimated by weight curve to be between 4-6 months (Clemens et al., 2014), an age at which Rossier and Schenk (2003) noted that the transitory presence of an olfactory cue did improve spatial learning of a visual landmark, including following removal of the olfactory cue. As such, removal of the association between local olfaction and the visual panorama may worsen the integration of this visual information into neural spatial representations.

However, in the two animals in which landmark anchoring to the control panorama was observed, this cue control was precise. The Rayleigh vector of PFD shifts was $R = 0.80$, which reached statistical significance – indicating that HD cells were shifting non-randomly after rotations of the panorama. The magnitude of this Rayleigh vector was similar to that reported after rotations of highly discriminable cue cards in a previously published landmark anchoring paradigm ($R = 0.73$, Lozano et al. (2017)). As such, when HD cells were anchored to the panorama, this visual information was integrated with the same accuracy as is observed in traditional paradigms with uncontrolled cues from olfactory and other modalities. As vision appears to exert the strongest control over the HD system (Goodridge et al., 1998), this is not surprising.

However, we also found that, in these animals, the change in the PFD effected by a rotation of the visual scene was more precise when that scene contained a discontinuous step in its

contrast/luminance than when the visual scene was a single continuously fading gradient. The discontinuity in the control panorama defines a precise 'edge' to a landmark, to which the system can align its firing. When the panorama did not contain such an edge, we observed significantly greater variance in the PFD shifts of HD cells, consistent with the interpretation that HD cells can less precisely align their tuning curves to an external visual world without edges. Accordingly, the Rayleigh vector of PFD shifts following rotations of the gradient panorama was smaller ($R = 0.59$). This was significant – indicating that the HD cells were still controlled by the visual scene – but was significantly smaller than the shifts to the control panorama.

Interestingly, this imprecision in landmark anchoring was not accompanied by an imprecision in the representation of head-direction encoded by HD cells in individual trials. We saw no difference in average directional information, tuning curve widths or Rayleigh vector lengths of HD cells between control and gradient trials using paired statistics. This indicates that, within a single trial, HD cells represented the world with similar precision, and encoded similar information about head-direction when the animal was surrounded by the control and gradient panoramas. As such, the worse landmark anchoring observed to the panorama could not be explained by a widening of HD cell tuning curves causing an increase in the error of PFD or current head-direction estimates. It is possible that the intrinsic attractor dynamics could maintain a precise and stable representation of direction throughout individual trials. Alternatively, as the floor and apparatus were cleaned with alcohol between trials, within a single trial an animal could use local landmarks, such as those provided by scent marking, to keep an anchored representation of direction.

The gradient panorama consisted of a large low spatial frequency grating. Within a small area (such as the size of a typical retinal ganglion cell receptive field), the change in contrast would be small, and would perhaps provide little directional information. This is the opposite for a sudden discontinuity as seen in the control panorama: at this point, high spatial frequencies exist and a large change in contrast occurs. This contrast change would be sudden and localised in visuotopic space, and therefore could provide greater directional information to a downstream spatial system. Nonetheless, low spatial frequency information can provide some landmark information into the HD system, although with greater error, although high spatial frequencies may add precision to this process.

Of note, it is possible to consider situations in which anchoring to a small, localised feature may not provide useful anchoring information. Object-like visual features (cue card edges, buildings) could be shared amongst a number of different and dissimilar visual scenes, leading to improper generalisation of a given sense of direction in a different setting. Alternatively, a system should ideally maintain a consistent representation of orientation under different lighting

conditions in the same environment, such as during daytime versus nighttime. Visual features – such as points with specific contrast changes (e.g. from grey to white) – could appear different with changes in ambient lighting, and thus the directional system may fail to recognise the visual scene. Integrating visual information from the entire panorama could plausibly minimise these errors when orienting in complex visual environments.

In order to understand how the transformation of visual space to directional landmark information, further work could probe the contribution of visual brain areas to landmark anchoring in HD cells. As landmark anchoring was present but impaired to the gradient panorama, we considered that much of the landmark information may be processed and presented to the HD system via the geniculo-striate visual pathway, which is traditionally considered to process higher-acuity vision. However, that some anchoring still exists to the gradient panorama may suggest the lower-acuity and evolutionarily older collicular visual pathway may subtend some landmark information to the HD system. In the subsequent chapter, we test whether landmark anchoring in HD cells is preserved following disruptions of the lateral geniculate nucleus.

Chapter 5

Head Direction Cells in Cortically Blind Animals

> Der Satz ist eine Wahrheitsfunktion der Elementarsätze.
> (Der Elementsatz ist eine Wahrheitsfunktion seiner selbst.)
> Propositions are truth-functions of elementary propositions.
> (An elemantary proposition is a truth-function of itself.)
>
> TLP 5; Wittgenstein (1922)

5.1 Introduction

Rodents are able to maintain a consistent sense of direction while navigating, aligned with salient landmarks in the environment. In rats, the head direction (HD) system provides a plausible neural substrate for this sense of direction, and is found in various nuclei across the limbic system (Taube et al., 1990a; Taube, 2007). These cells integrate allothetic information about the external environment, and are seen to 'anchor' to prominent visual cues, such that these cues establish the orientation of HD cell PFDs when an animal enters an environment (Taube et al., 1990b). A number of visual areas, grouped broadly into two pathways, exist in the rat brain that could plausibly process landmark information for use by the HD system. In this chapter, we wish to assess whether one pathway – the cortical visual pathway – is necessary for intact and precise landmark integration of the HD system.

HD cells are capable of using a variety of cue cards and cue configurations to set their PFD orientations. Rotations of a visual panorama containing two prominent and discriminable cue cards consistently caused rotations of PoS and retrosplenial HD cell PFDs, indicating that HD

cells can rapidly process and integrate visual information (Taube et al., 1990b; Lozano et al., 2017). We found that visual panoramas with no discrete landmarks can exert cue control over the HD system (Chapter 4), although this cue control is remarkably less precise. This indicates that the HD system can integrate visual information from the entire panorama to reorient its representation, but may benefit from discrete features that can provide more directional information.

In rodents, there is evidence that vision is integrated into the HD system in cortical HD areas, such as the postsubiculum (PoS), as lesions of this area worsen the precision of HD cell tuning curves in the anterior thalamus (Goodridge and Taube, 1997), and disrupt anchoring to visual landmarks of HD cells in the anterior thalamus (Goodridge and Taube, 1997) and mammillary bodies (Yoder et al., 2015). PoS lesions also disrupt landmark anchoring of place cells in CA1 (Calton et al., 2003), indicating the HD system may provide some landmark input to place cells. The retrosplenial cortex – another cortical area containing HD cells – is also a plausible candidate for the integration of visual and directional information, as this area contains a population of cells that encode information about local visual cue configurations (Jacob et al., 2017), and lesions of the retrosplenial cortex impair anchoring of anterior thalamic head direction cells (Clark et al., 2010), although to a lesser extent than lesions of the PoS.

In a a large number of diverse species, HD cells have been found and observed to integrate vision, including the fly (Seelig and Jayaraman, 2015). This is in spite of the large variation in brain structures between these species. This indicates that the representation of direction is well conserved across species, and it was necessary early in evolution for this representation to integrate visual information. It is possible that the similarities in these representations imply a homology in how visual information is processed and presented to the HD system.

Nonetheless, it is unknown how/where landmark information is extracted from the visual scene, and in what form this information is propagated into the HD system. Broadly, two visual pathways exist in the mammalian brain (Sefton et al., 2015): a 'cortical' pathway through dorsal lateral geniculate nucleus (dLGN) into primary visual cortex (V1) (Schuett et al., 2002), and a 'subcortical' pathway through the superior colliculus, lateroposterior thalamus, and into V1 and extrastriate visual cortex (V2) (Kamishina et al., 2009; Tohmi et al., 2014). The relative contribution of each of these pathways to landmark processing of HD cells is unknown.

Whereas the superior colliculus has a known homologue structure in birds (the optic tectum), the telencephalon is less easily compared: birds possess no laminated neocortical areas (although they still possess two visual pathways; for review, see Shimizu and Bowers (1999)). The superior colliculus therefore appears to be better conserved between species, and may therefore be expected to perform the sorts of visual processing required for spatial orienta-

tion. Indeed, the colliculus is known to play a role in visually-guided orienting in the rodent (Goodale and Murison, 1975; Mort et al., 1980) and so may already possess the visuospatial representations needed to present landmark information to the HD system.

However, anatomical studies have identified that both PoS and the retrosplenial cortex receive direct projections from the geniculostriate pathway via V1 (van Groen and Wyss, 1990c,b, 1992; Van Groen and Wyss, 2003), indicating a role to be played by the cortical visual system. Accordingly, lesions of V1 disrupt anchoring of hippocampal place cells to objects placed at the periphery of an environment (Paz-Villagràn et al., 2002). Because HD cells appear to convey information into the place cell system (Calton et al., 2003), it is supposed that these lesions also disrupted landmark anchoring of the HD system. However, this was not explicitly tested by Paz-Villagràn et al. (2002), and most recorded place cells maintained a representation that was consistent relative to the distal room following object rotation, indicating that place (and HD) cells may have had access to distal landmark information.

A third possibility is that visual landmark information is extracted and presented to the HD system from the higher visual areas in extrastriate cortex. Indeed, a large number of areas within V2 are known to project to PoS and retrosplenial cortex (notably the posteromedial, anteromedial and anterior areas, Wang et al. (2012)). Within V2, the anteromedial and posteromedial areas have also been observed to contain HD cells and landmark-direction cells (Chen et al., 1994a,b; Wilber et al., 2014). That these representations exist in higher visual areas strongly suggest that they may be involved in landmark processing in the rodent brain.

Some studies have addressed the contributions of higher visual areas to landmark processing of the HD system. Lesions of the postrhinal cortex, a visual area predominantly driven by collicular inputs in rodents (Beltramo and Scanziani, 2019), did not impair anchoring of thalamic HD cells to visual landmarks (Peck and Taube, 2017). Similarly, lesions of posterior parietal cortex (which contains several higher visual areas, Wilber et al. (2015)) did not impair landmark anchoring of HD cells (Calton et al., 2008), in spite of this area receiving significant projections from primary and secondary visual cortices (Miller and Vogt, 1984; Kolb and Walkey, 1987).

In light of the large number of candidate routes by which anatomical information could reach the HD system, and the lack of positive results from previous studies, we propose to approach the question from the opposite direction: instead of disrupting individual high-level visual areas in turn, impairing one of the two visual pathways could provide good evidence for which visual areas are likely (or unlikely) to perform the relevant computations for landmark processing. Does visual cue control over HD cells require visual processing by the cortical visual pathway? Can landmark information be conveyed to the HD system through only the subcortical pathway?

Here, we present HD cells recorded from animals following excitotoxic lesions of the dLGN, the first-order thalamic relay nucleus of the geniculostriate pathway (Sherman, 2007), in a standard cue control paradigm (Lozano et al., 2017). Lesions of this nucleus will impair visual processing throughout the cortical visual pathway. We hypothesise that the cortical pathway may contribute to landmark processing, and as such predict that, following disruption of this pathway, we should see impaired anchoring of HD cells to rotations of the visual cue.

To test this, we used cue control paradigm in which two cue cards were attached to the inside wall of a cylinder at 180° apart. The cues and cylinder were rotated between trials, to assess whether HD cells oriented their tuning curves in each trial to consistently follow the local reference frame of the cylinder. The use of two cues enabled us to assess whether animals could not only detect the presence of a cue card, but also discriminate the visual content of the cards. As such, we were able to decouple anchoring to tactile or olfactory components of the cue cards from anchoring to their visual content, as evidence of precise anchoring to visually identical cue cards would indicate the system was relying on non-visual modalities.

This enabled us to assess whether intact cortical visual processing is necessary for precise landmark integration into the PoS HD signal.

5.2 Materials and methods

5.2.1 Animals

12 adult male Lister Hooded rats (weight range 341 g−668 g at time of surgery) were used in the experiment. Animals were housed individually following surgery in a room maintained with a 12:12 hour day:night cycle, including 1 hour simulated dawn/dusk. Animals were fed a lightly food-restricted diet so as to maintain a minimum of 90 % free-feeding weight, and had *ad libitum* access to water. All procedures were performed in compliance with the regulations outlined by the UK Animals (Scientific Procedures) Act (1986) and the European Communities Council Directive of 24 Nov 1986 (86/609/EEC), and under protocols outlined in a UK Project License.

5.2.2 Surgery

Animals underwent bilateral excitotoxic lesions of the LGN followed by tetrode implantation in the PoS, as follows. Details of general surgical procedure are given in Section 3.2.

Animals were anaesthetised using isoflurane (Piramal Healthcare UK Ltd.), and mounted on a stereotaxic frame for precision targeting of the lesions and implant. Bilateral excitotoxic lesions of the LGN were performed using 0.09M *N*-methyl-D-aspartic acid, and sham lesions were performed in the control group using 0.9 %w/v saline. NMDA causes lesions by excessive

Stereotaxic coordinates (mm)		
AP	**ML**	**DV**
Lesion		
−3.7	±3.2	+4.8
−4.2	±3.2	+5.2
−4.8	±3.4	+5.0
−5.3	±3.4	+5.0
Implant		
−7.5	±3.4	+2.0

Table 5.1: Stereotaxis co-ordinates for injection targets and implant placement. AP and ML are specified relative to bregma; DV is specified relative to brain surface.

stimulation of glutamate receptors causing overexcitation of neurons, resulting in cell death (Choi, 1992). Excitotoxic lesions were chosen for this study as this method only kills excitatory neurons in the lesioned area, while sparing local glial cells and traversing axon fibres (Kirby et al., 2012). The concentration of NMDA used was similar to that used in other papers performing excitotoxic lesions in the rat thalamus (Clark et al., 2009), and co-ordinates were piloted in $n = 3$ animals before combined lesion/implant surgeries were performed.

In both groups 0.80 µL−1.00 µL was injected over 4 sites per hemisphere (see Table 5.1) using a 0.66 mm diameter glass pipette. Injections were made at a rate of $0.10\,\mu L\,min^{-1}$ at each site, and the pipette was left at the injection site for approximately 5 minutes following each infusion to allow for the substance to diffuse from the tip of the pipette.

Where possible, injections were made through intact dura mater, so as to minimise mechanical damage to the cortex overlying the LGN. When this was performed, +0.1 mm was added to each DV coordinate. This was not always possible due to damage to the meninges from the craniotomy.

In the same surgery, after injections were complete, animals were implanted with 16-channel 'poorlady' microdrives (Axona Ltd., St Albans, UK), targetted at the postsubiculum. The microdrives housed 4 tetrodes made by the experimenter. Each tetrode was made by winding 25 µm platinum-iridium alloy electrodes into bundles of four (meaning 16 electrodes in total were implanted). Following surgery, animals were closely monitored for a minimum of 3 hours for signs of hypothermia, and were given appropriate analgesia for 3 days. Diazepam ($2.5\,mg\,kg^{-1}$ given intraperitoneally) was administered at the end of surgery to some animals receiving dLGN lesions, so as to prophylactically reduce the probability of seizures due to the NMDA. Animals were allowed a minimum of one week after surgery for recovery.

5.2.3 Single-unit recordings

Single units were recorded using an Axona multichannel recording system (Axona Ltd., St Albans, UK).

5.2.3.1 Screening apparatus and recordings

Initially, animals were recorded in a separate room from the experimental room to assess whether any putative cells could be isolated within the clusterspace. The screening apparatus consisted of either a $1 \times 1 \times 0.5$m or $1.2 \times 0.6 \times 0.6$m (length $\times$ width $\times$ height) rectangular box, which contained one large prominent cue card on the wall. Distal cues (such as cue cards on the walls of the room and the experimenter) were available to the animal so that it would have a cue-rich and unambiguous environment in which to anchor its spatial representations. A photograph of the screening room is shown in Figure 3.2.

If a cell was identified following inspection of the clusterspace, and was seen to be a HD cell by visualisation of its tuning curve in Tint (Axona Ltd., St Albans, UK), the animal was moved to the experimental room and recorded in the two-cue cylinder. Following the session, a post-screening recording was frequently done to assess the stability of the clusterspace.

5.2.3.2 Session apparatus

A recording session consisted of 8 trials of 8 minutes each. Animals were recorded in a 80 cm diameter, 50 cm tall cylinder with grey walls and two large polypropylene cue cards attached to the inside walls. As such, the cues subtended a visual scene, but also provided plausible tactile and olfactory landmarks to the animal as they were mounted on the inside walls. The cue cards were 50 cm-by-50 cm in size and subtended approximately 70° of arc. The cue cards were attached using Velcro fastenings at opposite walls of the cylinder, at 180°separation. A photograph of the room in which session recorded occurred is shown in Figure 3.2, and a photograph of the apparatus is shown in Figure 5.1B.

We could assess whether HD cells landmark anchored to the cue cards by tested whether rotations of the cylinder and cue cards resulted in concomitant rotations of the HD cell tuning curves. The use of two cards enabled assessment of the ability of the animal to both detect and discriminate the cue cards, as when the cue cards appear identical to the animal the apparatus possesses 2-fold rotational symmetry (see Section 5.2.4).

5.2.3.3 Session recordings

Trials 1 and 2 were 'standard' trials, between which the cylinder was not rotated. The cylinder orientation in Trials 1 and 2 defined 0°. Trials $3-8$ were 'rotation' trials, in which the cylinder

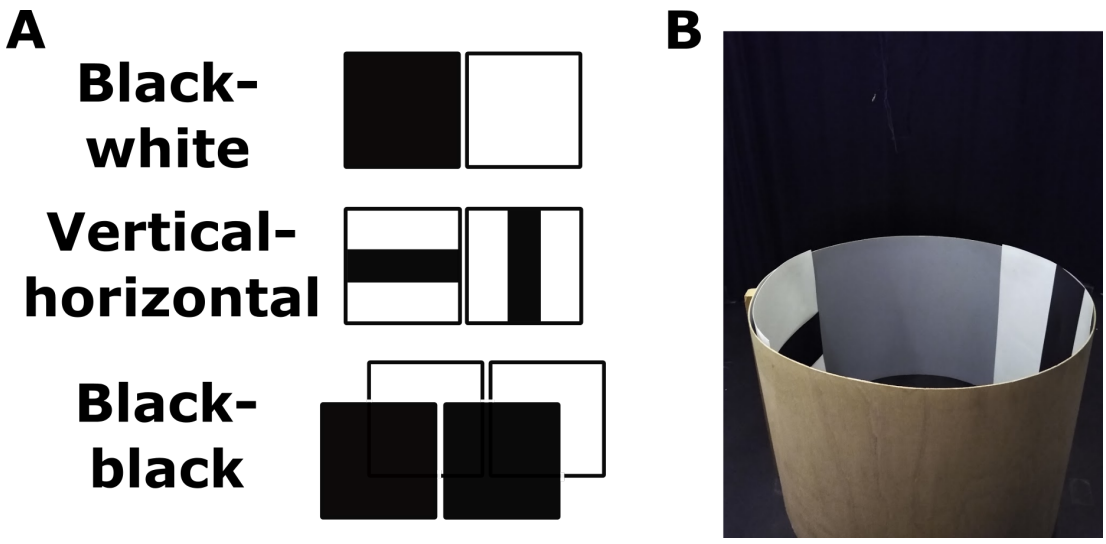

Figure 5.1: A: The cue card configurations used in this experiment. Note that, although the black-black condition is named as such for simplicity, it includes some sessions using white-white cue cards. B: Photograph of the apparatus used in this experiment, containing the vertical-horizontal cue cards.

and cue cards were rotated together, by a random multiple of 45° relative to baseline (that is, the possible rotations are 0°, 45°, 90°, 135°, 180°, −135°, −90° and −45°, with positive angles indicating anti-clockwise rotations). The rotation angle in each rotation trial was true-randomly selected using a custom-written MATLAB function interfacing with the API of an online true-random number generator (`https://www.random.org`).

One set of cue cards was used per session. Three configurations of cue cards were used, shown in Figure 5.1A: one black-white set of cards, one vertical-horizontal set, and one black-black or white-white set. The two visually identical sets (black-black and white-white) were grouped together for analysis (for simplicity, this will be referred to as the black-black cue condition). The first recording session for each animal used black-white cues, as this configuration was believed to exert the strongest cue control over the HD system (Lozano et al., 2017); in each following session, the cues to be used were pseudorandomly selected by the same custom MATLAB function described above, with all cue configurations aimed to be tested in each animal, where possible.

Following a recording, where possible, the cell was recorded in the screening room again, to assess cluster stability. Sometimes, the same cell could be recorded over multiple days. However, if the cluster seemed to be unstable or the cell had been recorded in every condition, the tetrodes were advanced deeper into the brain in order to sample from a new set of neurons.

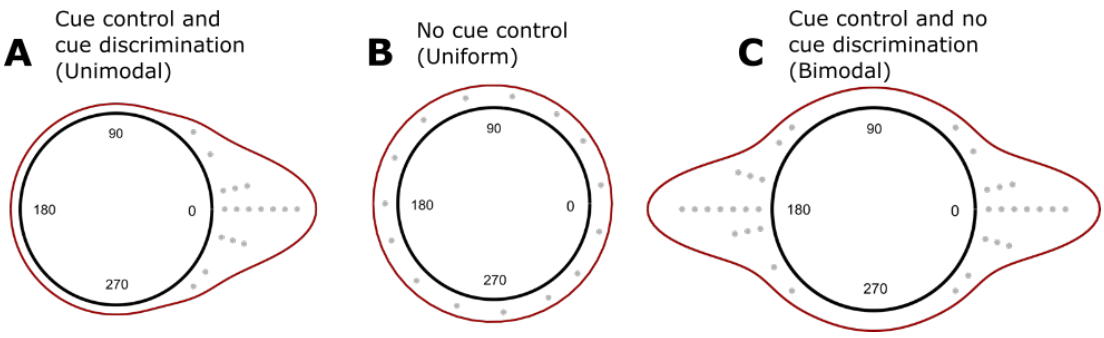

Figure 5.2: Schematics showing the characteristics of landmark anchoring data under different predictions. (A) If HD cells anchor to the cue configuration, then the distribution of PFD shifts should be centred around 0°. (B) If HD cells do not anchor to the cues, the distribution of PFD shifts should be uncorrelated with the cue rotations, and therefore appear as a uniform distribution. (C) If the HD cells anchored to the cues used, but could not differentiate the cues from each other, PFD shifts should be distributed bimodally about 0° and 180°

5.2.4 Landmark anchoring hypotheses

If the cells discriminated the two cues and anchored to them, the normalised PFD will be clustered around 0°on a circular histogram. Alternatively, a lack of anchoring of the system to the cues would result in PFDs shifting randomly relative to the rotation of the cylinder between trials, and therefore the distribution around the circle of normalised PFD shifts would be close to uniform.

Finally, if the system anchored to the cue cards, but could not discriminate the cards, then the distribution of PFD shifts would form a bimodal distribution clustered around 0°and 180°, representing the two-fold rotational symmetry of the environment. These possibilities are represented in Figure 5.2.

5.2.5 Cell isolation

Recorded spikes were clustered into putative neurons using the clustering software Tint (Axona Ltd., St Albans, UK). This software enabled semi-automated clustering of the featurespace using a variant on the CEM algorithm (KlustaKwik, Harris et al. (2000)), followed by manual refinement of clusters in the graphical interface. Clusters with non-neural waveforms and poor refractory periods in the spike autocorrelogram (numerous spikes at <2 ms) were excluded as electrical noise either while clustering or during analysis (see below). We also computed a number of quality metrics on the isolated clusters (see below).

5.2.6 Data analysis

Final clusters were saved and imported into MATLAB 2015a (Mathworks Ltd., Natick, MA) for further analysis. A package for performing circular statistics (CircStat, Berens (2009)) was

installed onto MATLAB.

5.2.6.1 HD cell classification

Putative neurons were classified as HD cells if they exhibited a peak firing rate of >1 Hz, and a Rayleigh vector length, R, satisfying both $R > 0.3$ and $R > P_{99\%}$ of a shuffle distribution. This shuffle was calculated by repeatedly time-shifting the spike train of the putative HD cell by a random time between 20 s and 20 s less than the duration of the trial (460 s). We then recomputed the tuning curve from each time-shifted spike-train, and associated R vector for this shifted data. Performing this 10000 times per cell generated a shuffled distribution of R vector lengths. These criteria had to be met for the baseline trials (trials 1 and 2) of the recording session for the cell to be included in the rotational analyses. Cells were excluded if their cluster contained substantial noise across the session, as assessed by the number of refractory period violations as a percentage of the total number of spikes in the session (cells with > 1% violations were excluded).

5.2.6.2 Cluster quality

Two cluster quality metrics were used to provide a quantitative measure of cell isolation quality. These are L-ratio and isolation distance (Schmitzer-Torbert et al., 2005), which were derived for each cluster. This allowed us to assess whether HD cells from Lesion animals tended to be poorly isolated compared with those from Sham animals, as this could explain some results discussed below. Detailed explanations of what these metrics are, and how these metrics were calculated, are given in Section 3.5.2.

5.2.6.3 Firing properties of HD cells

HD cell tuning curves were constructed and smoothed as described in Section 3.5.3. For each recorded HD cell, numerous properties were extracted from its tuning curve and spike timeseries to assess the cell's firing characteristics. These were: the neuron's peak firing rate (defined as the value of the bin with greatest firing rate in the smoothed tuning curve), PFD (the angle associated with the peak firing rate bin in the smoothed tuning curve), Rayleigh vector length (see Section 3.6.2.2), tuning width (the circular standard deviation of the tuning curve), and directional information content (see Section 3.5.5.1).

5.2.6.4 Rotation analysis of HD cells

In order to assess whether the population of HD cells successfully landmark anchored to the local reference frame of the two-cue cylinder, the PFDs of recorded cells had to be normalised

in two ways: across cells (so as different HD cells, with different PFDs, could be compared) and across trials in a session (so trials with different rotations could be compared). In doing this, we would achieve an estimate for each HD cell of the deviation from the expected amount its PFD would shift if it were following the cue card, between two trials: a PFD shift of 0° would indicate perfect landmark anchoring between two trials (no deviation between the rotation of the cue card and the rotation of the cylinder). It is important to note that this deviation is calculated using the PFD of a cell across two trials, so as to assess how the PFD shifted in response to the cylinder being rotated. As such, we needed to select a baseline trial to use in calculating this PFD shift for each cell. For all HD cells in a given session, we used the same trial as baseline (described below).

First, each cell PFD was normalised into the local reference frame of the cylinder. This was done by subtracting the current rotation of the cylinder from each cell's PFD, to express the PFD relative to the local visual cues.

Then, we selected the baseline trial in the session. As cells may shift their PFD in a single trial, but revert back in later trials (an 'instantaneous' orientation error), a estimate of each cell's preferred direction of the session was derived by selecting the trial around which PFDs of that cell in all other trials clustered most closely across the session. We selected the trial tr that maximised the following metric:

$$\arg\max_{tr \in Sess} \sum_{j=1}^{cells} \sum_{i=1}^{n} \cos(\theta_{j,i} - \theta_{j,tr}) \tag{5.1}$$

where $\theta_{j,i}$ is the PFD of cell j in trial i.

After this identified the baseline trial, PFDs of all cells in this trial were subtracted from the cell PFDs in all other trials. These are referred to as the PFD shifts. If HD cells subtended a consistent angle relative to the cue cards, this would normalise the majority of PFD shifts across all cells to near 0°. Any deviation from the expected angle relative to the cues would be reflected by greater PFD shifts after normalisation.

As HD cells are believed to rotate coherently (Yoganarasimha et al., 2006), we averaged the PFD shifts for each trial across all cells recorded in that trial. This provided a single value, per-trial, of the population estimate of heading direction, and as such all statistics assessing landmark anchoring are not performed per-cell.

5.2.6.5 Angle doubled rotation analysis

The above analyses were also performed on an angle-doubled dataset. This was to assess whether HD cells anchored bimodally to the two cues used, as might be expected if the cells could detect but not discriminate the cues (Section 5.2.4).

Here, before anchoring was assessed, all extracted PFDs from HD cells were doubled and wrapped $\mod 360°$. Shifts of the PFDs between trials was then calculated using the rotation analysis described above. As such, when assessing PFD shifts between trials, shifts of 180° will be transformed to 0°, while shifts of 0° will remain at 0°. As such, although uniform distributions of shifts will remain uniform following the angle-doubling procedure, bimodal distributions centred on 0° and 180° will be transformed to a unimodal distribution with a 0° peak. This would enable the use of circular statistics such as the Rayleigh vector and derived statistics to assess whether the PFD shifts after angle-doubling were non-random. A significant Rayleigh vector here (and a non-significant Rayleigh vector before angle doubling) provides good evidence for bimodal anchoring to the cue cards.

However, an important point to note is that, for unimodal (e.g. von Mises) distributions, angle-doubling will reduce the concentration parameter of the distribution (consider that angle doubling $[-1, 0, 1]$ degrees gives $[-2, 0, 2]$ degrees; the angles are now twice as far apart). As such, angle-doubling a unimodal distribution will reduce its Rayleigh vector length.

5.2.6.6 Anchoring metric summary for individual animals

As different animals may have contributed different numbers of sessions, we wished to obtain a single summary metric, A, for each animal, in each cue condition, so as to prevent biasing of the results. This also allowed for correlative assessment of landmark anchoring deficits with lesion extent.

For this, we used a similar metric as above: the summed cosine transform of all PFD shifts, normalised for the number of shifts recorded. That is, if n PFD shifts ϕ are recorded in a given condition, we defined

$$A = \frac{\sum_{i=1}^{n} \cos \phi_i}{n} \tag{5.2}$$

We performed this separately for each animal, for each cue condition. Values of A close to 1 indicate good anchoring to that cue configuration, whereas values closer to 0 or below indicate poorer anchoring.

5.2.6.7 Statistics

A number of statistical approaches were used to assess whether observed differences in cell characteristics or anchoring was significant between Lesion and Sham groups. When assessing HD cell characteristics (such as peak firing rate, R vector length, etc.), non-parametric linear statistics were usually used to assess differences in group medians.

Circular statistics used are described in more detail in Section 3.6.2. Briefly, these included the Rayleigh test (which assesses for unimodal deviations from uniformity of a circular distribution), the V test (which assesses for deviations in a circular distribution toward a predicted angle), and the Kuiper test (which assesses whether the circular cumulative distributions of two groups are significantly different).

Empirical cumulative distribution plots were frequently used to visualise distributions to be compared, as these can be overlayed and confidence intervals can be estimated. For linear distributions, Greenwood's formula was used to estimate the 95% confidence intervals at each point in the cumulative distribution. For circular distributions, a custom-written bootstrapping function was written to estimate the 95% confidence interval. Here, the distribution was randomly resampled (with replacement) 1000 times, generating 1000 new cumulative distributions. From these, the $50th$ and $950th$ values of the sorted cumulative distributions at each point define the $95th$ percentile confidence interval at that point. Using these plots, it is possible to visualise the overlap of multiple distributions.

Linear distributions are plotted as raincloud plots (Allen et al., 2019), using custom-written MATLAB functions. In these plots, all data points are scattered on one half of a plot, and a kernel density estimate of the distribution is plotted on the right. Superimposed over the scattered datapoints is a boxplot denoting the group median, lower and upper quartiles, and inner fences.

5.2.6.8 Co-rotation analysis

Populations of HD cells are modelled as a 1-dimensional ring attractor (Section 1.3.1.1), with the consequence that HD cells are generally observed to be coherent. This means that, if one recorded HD cell is observed to rotate its PFD following a rotational transformation of a cue card, any other HD cell recorded (and indeed any HD cell in the attractor population) will rotate its PFD by a similar angle. That HD cells rotate their PFDs as an ensemble has been observed previously (Yoganarasimha et al., 2006), and allows us to infer the orientation of the entire population of HD cells from the readout of a single cell's tuning curve.

However, frequently more than one HD cell may be recorded at once. This provides the opportunity to assess whether these co-recorded cells shift their PFDs coherently to follow

landmarks, following lesions of the dLGN. The coherence of the attractor network may depend on sensory input to some extent, and a subpopulation of HD cells have been shown to break traditional attractor dynamics in mice (Kornienko et al., 2018). To test whether HD cells were coherent in our recordings, we extracted the angle difference between PFDs of co-recorded HD cell pairs in all trials, and computed the Rayleigh vector length of this list of angles for each cell pair. If the cells shift coherently, the angle difference should be consistent, and correspondingly the R vector will be large. However, non-coherent cells will have less consistent PFD differences, and lower R vector lengths.

To assess whether the distributions of HD cell pair R vectors were larger than expected by chance, we compared these to a distribution of R vectors generated by the same process using HD cells pairs recorded in different sessions (and so rotations of their PFDs are expected to be uncorrelated). This generated a chance distribution of R vector lengths for uncorrelated PFD shifts. Distributions were compared using appropriate non-parametric statistics due to the non-normal properties of Rayleigh distributions.

A secondary analysis looked at how much the angle between PFDs changed across the course of a session. For each co-recorded HD cell pair, we extracted the relative angle subtended between the two PFDs in each trial. Across a session, for each pair, this results in eight relative angles. We subtracted the minimum relative angle across all trials from the maximum relative angle, giving an indication of how variable this relative angle was across the trial. We took the absolute value of this quantity, resulting in a set of values between $[0, 180]$. Values near 0 indicate the relative angle between the two PFDs was consistent across the whole session; larger values indicate less consistently oriented PFDs.

5.2.7 Histology

At the end of the experiment rats were killed with an overdose of pentobarbitone and perfused transcardially with 0.9 % saline, followed by 10 % neutral-buffered formalin. The brains were extracted kept in a formalin solution for a minimum of 24 h, and subsequently transferred to 30 % sucrose by weight in phosphate-buffered saline for dehydration. Brains were then frozen to approximately $-20\,^{\circ}$C and sectioned into 30 µm-50 µm coronal slices. Slices were Nissl stained with Cresyl violet for assessment of lesion extent and electrode placement.

Lesion extent was estimated for each animal by selecting one slice for each slide in the atlas between -3.48 mm to -5.40 mm, that was considered to best fit the atlas plate. This was assessed manually by reconstruction using the known distance between adjacent brain slices, and by reference to prominent landmarks: most frequently the thalamic border, the shapes of the hippocampal pyramidal layer, the medial and lateral habenular nuclei, the third

ventricle, and fasciculus retroflexus (Paxinos and Watson, 2007). We then traced a polygonal outline, in each hemisphere of each slice, of the lesion and dLGN in open-source histological analysis software (ImageJ, NIH; Schindelin et al. (2012)). The lesion extent was estimated by tracing the region of thalamus with no visible neuron nuclei (note this definition led to the inclusion of axonal tracts within the lesion extent, although these tracts should be undamaged by NMDA). The dLGN was delineated using either changes in cellular architecture where visible (Evangelio et al., 2018), or (as was frequently the case in lesioned animals, as NMDA disrupted cytoarchitecture) from the relative positioning of local landmarks such as the thalamic border and third ventricle.

This procedure was performed for all 20 slides in the atlas, which provided an estimate of the lesion shape over the entire AP axis of the dLGN. From here, the percentage of dLGN damaged was estimated from the intersection between the lesion and dLGN polygons.

5.2.8 Nomenclature

Individual rats, when discussed, will be referred to using the internal reference code given to rats within the institute's animal facility. This takes the form of the letter R followed by a designation number; for example: 'R721'.

5.3 Results

5.3.1 Histology

Lesion extent was estimated by analysis of Nissl-stained coronal slices taken through the extent of the dLGN. In all lesioned animals, a substantial ($> 50\%$) portion of the dLGN was destroyed following NMDA injection. As expected, the proportion of damaged dLGN was greater in lesioned animals than sham animals (see Figures 5.4 and 5.5 for representative slices through animals), although there was variation in lesion extent within the lesioned group. Figure 5.6 shows the estimated percentage in each animal of damaged dLGN across the 20 slices assessed along the AP axis, for the left and right hemispheres. In general, lesions extended well across the AP axis of the dLGN, but in some animals the lesion did not extend to the far anterior/posterior tips of the nucleus.

In general, lesion size and shape varied between animals, and the total estimated %-area of lesioned dLGN for each animal is summarised in Table 5.4 alongside summary metrics describing how well HD cells landmark anchored in each animal (described in Section 5.3.6).

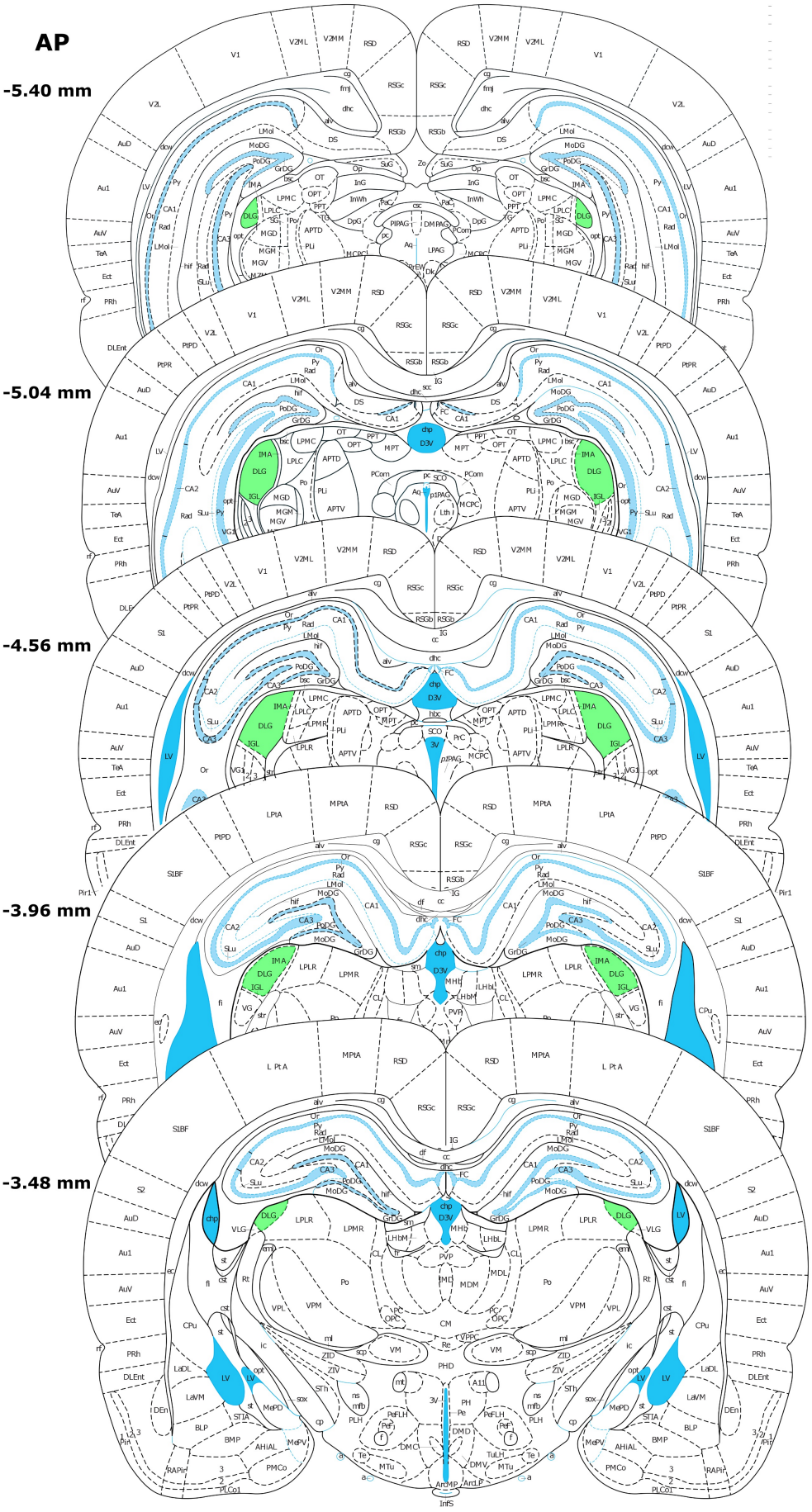

Figure 5.3: Schematic of the dLGN through the rat brain. The dLGN is highlighted in green, on five coronal slices spaced equally throughout its anteroposteror (AP) extent.

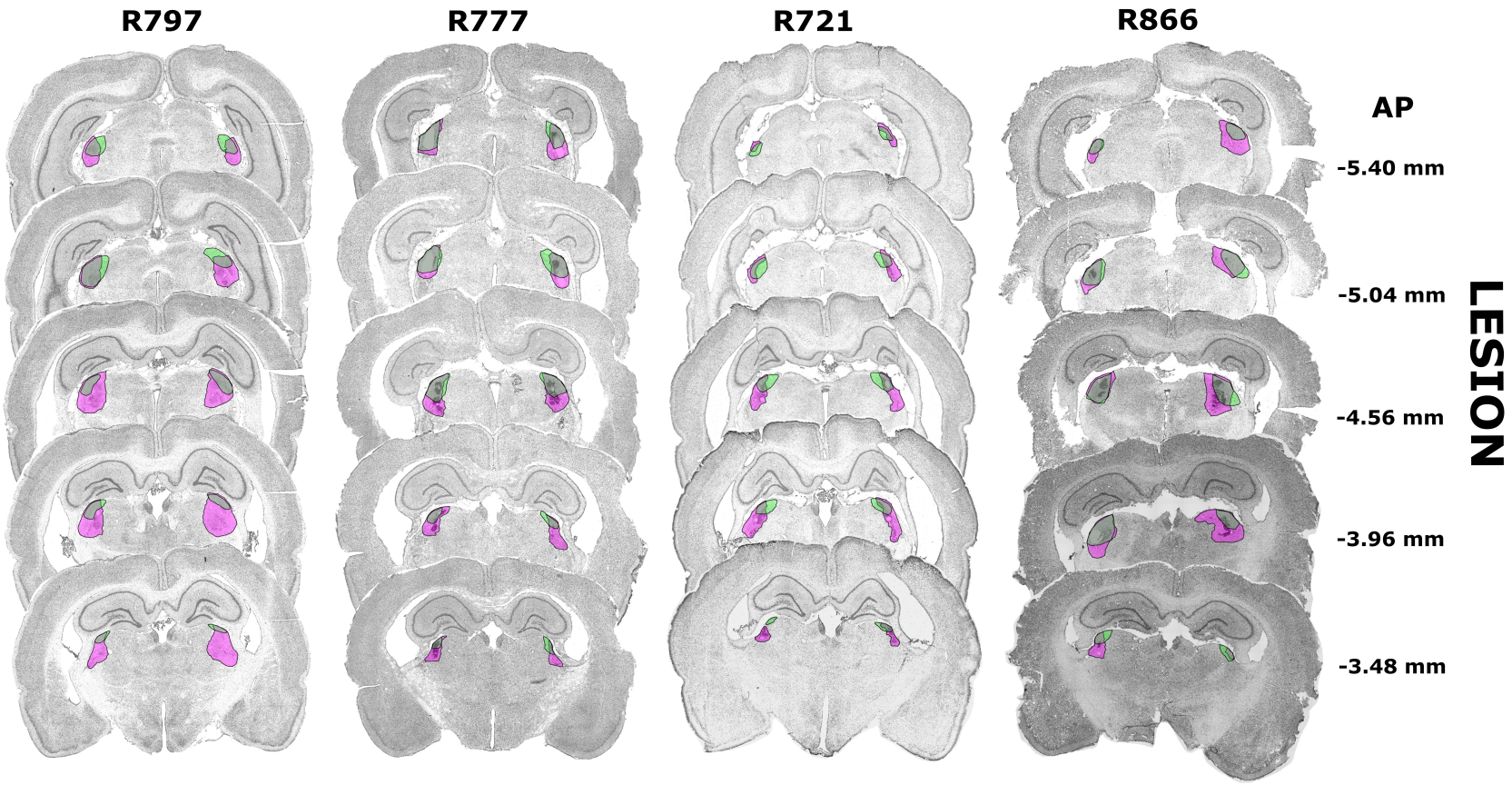

Figure 5.4: Histology images from lesioned animals taken at the same AP extent as in Figure 5.3. The estimated dLGN location is highlighted in green; the estimated lesion extent is highlighted in pink.

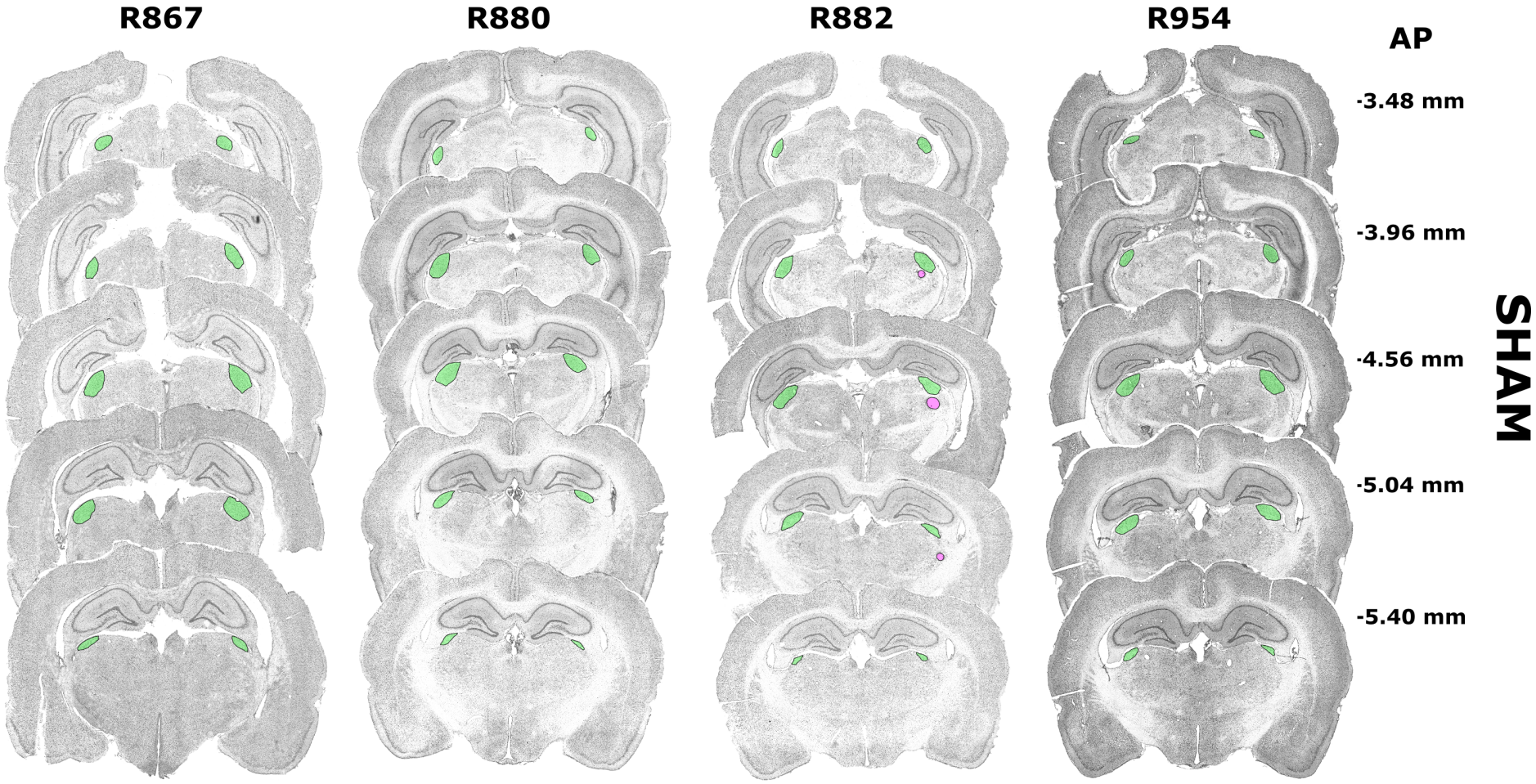

Figure 5.5: Histology images from sham animals taken at the same AP extent as in Figure 5.3. The estimated dLGN location is highlighted in green; the estimated lesion extent (where present) is highlighted in pink.

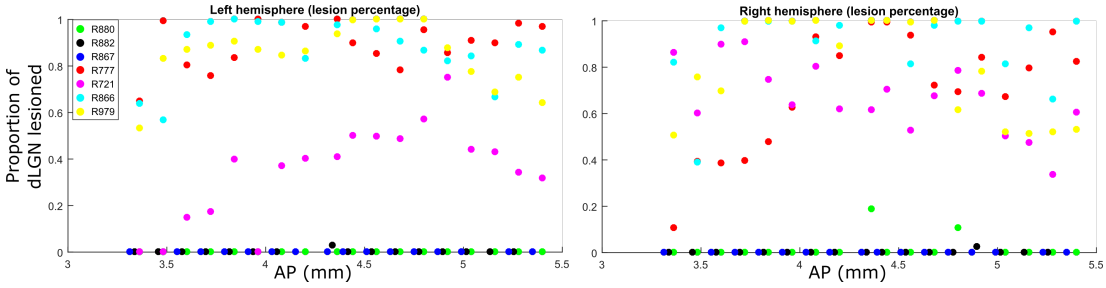

Figure 5.6: Proportion of dLGN lesioned at each AP co-ordinate in each rat.

Rat	Condition	HD cells	Total cells	Sessions
R721	Lesion	24	104	12
R777	Lesion	102	253	21
R866	Lesion	7	21	3
R968	Lesion	5	19	2
R979	Lesion	5	26	3
R1004	Lesion	8	28	2
R1005	Lesion	7	31	2
R867	Sham	35	186	14
R880	Sham	5	61	3
R882	Sham	46	167	11
R954	Sham	12	33	4
R1013	Sham	3	7	3

Table 5.2: Numbers of cells, HD cells, and sessions recorded from each animal.

5.3.2 HD cell characteristics

HD cells were successfully recorded from animals in both the lesion and the control group. 259 HD cells were recorded from a total of 938 putative units, from 12 rats (see Table 5.2). Of these, 158 HD cells were recorded from 7 lesioned animals, and 101 HD cells were recorded from 5 sham animals.

In total, 88 sessions were run over all animals; this comprised 52 sessions (416 trials) in Lesion animals, and 36 sessions (288 trials) in Sham animals.

Example HD cells from individual trials are displayed in Figure 5.7. These cells display the characteristic unimodal tuning curve of HD cells, with correspondingly large Rayleigh vector lengths. As such, it is evident that HD cells still exist following dLGN lesions. This is consistent with evidence that HD cells are believed to be generated from the integration of vestibular information, and are not dependent on consistent visual input (for instance, they are present in blindfolded rats, Goodridge et al. (1998)).

To assess whether we were less likely to record HD cells following dLGN lesions, we compared the encounter rate of HD cells within recording sessions in each all animal, for lesion and sham animals. Of total units, 22.3% were HD cells in Sham animals, whereas 32.8% were HD cells in Lesion animals. A two-tailed t-test of proportions showed that these were significantly different encounter rates for HD cells ($z = -3.59$, $n_{sham} = 454$, $n_{lesion} = 482$, $p < 0.001$), indicating

that we were slightly more likely to record HD cells in lesioned than sham animals. This could be due to variation in implant location, as many HD cells are located densely within Layer III of PoS and less densely in other layers (Preston-Ferrer et al., 2016).

Intrinsic firing characteristics of the recorded HD cells were compared between the Lesion and Sham groups. To assess whether HD cells uniformly represented all azimuthal directions, we tested the distribution of HD cell PFDs in trial 1 for deviations from uniformity. Figure 5.8 shows circular histograms of trial 1 PFDs of all recorded HD cells in the Lesion and Sham datasets, and shows the cumulative distributions of both datasets. There was no evidence of non-uniformity in the PFDs of HD cells recorded from either group (Lesion HD cells: $p > 0.5$, $m = 68$; Sham HD cells: $p > 0.5$, $m = 42$; Hodges-Ajne omnibus test[1]). The distribution of trial 1 PFDs did not differ between the lesion and sham groups ($p > 0.5$, $k = 2268$, Kuiper test). As such, lesioning the dLGN did not appear to introduce any bias into the directional code maintained by PoS HD cells, as there is no evidence that sham or lesion HD cells encoded azimuthal space non-uniformly.

5.3.2.1 Firing rates

The median peak firing rate of all recorded HD cells in the sham group was 3.42 Hz, and the median peak firing rate of HD cells in the lesioned group was 3.22 Hz. A non-parametric Wilcoxon ranksum test showed that there was no difference in the distributions of peak firing rates between the lesion and control groups ($z = 0.68$, $p = 0.496$), and this was visible as considerable overlap of the peak firing rate cumulative distribution plots (Figure 5.9A).

5.3.2.2 HD cell directionality

Interestingly, HD cells recorded from Lesion animals tended to show smaller mean Rayleigh vector lengths across sessions (median R vector in Lesion animals: $R = 0.567$, $n = 158$; Sham animals: $R = 0.709$, $n = 98$; $z = -3.96$, $p < 10^{-4}$, Wilcoxon ranksum test, see Figure 5.9C. To test whether this was due to the quality of cell isolation degrading over the course of a session, we also compared the Rayleigh vector length of HD cells in only trial 1, when the cell had most recently been identified and isolated. We still found a significant difference between Rayleigh vector lengths of HD cells recorded from lesioned and sham animals (trial 1 R vector in Lesion animals: 0.635; Sham animals: 0.739; $z = 2.65$, $p < 0.001$, Wilcoxon ranksum test). This indicates that there was a general reduction in the directionality of HD cells following LGN lesions, such that the representation of current heading direction may be less precise.

[1]NB: The Rao spacing test is not appropriate here, as these data are binned. The Rao test assumes that the average spacing for sorted continuous data drawn from a uniform distribution is 360/n, where n is the number of samples. In binned data, this is not true: spacing is 0, or a multiple of the size of the bin, and so the Rao test sees this as 'non-uniform' spacing between points

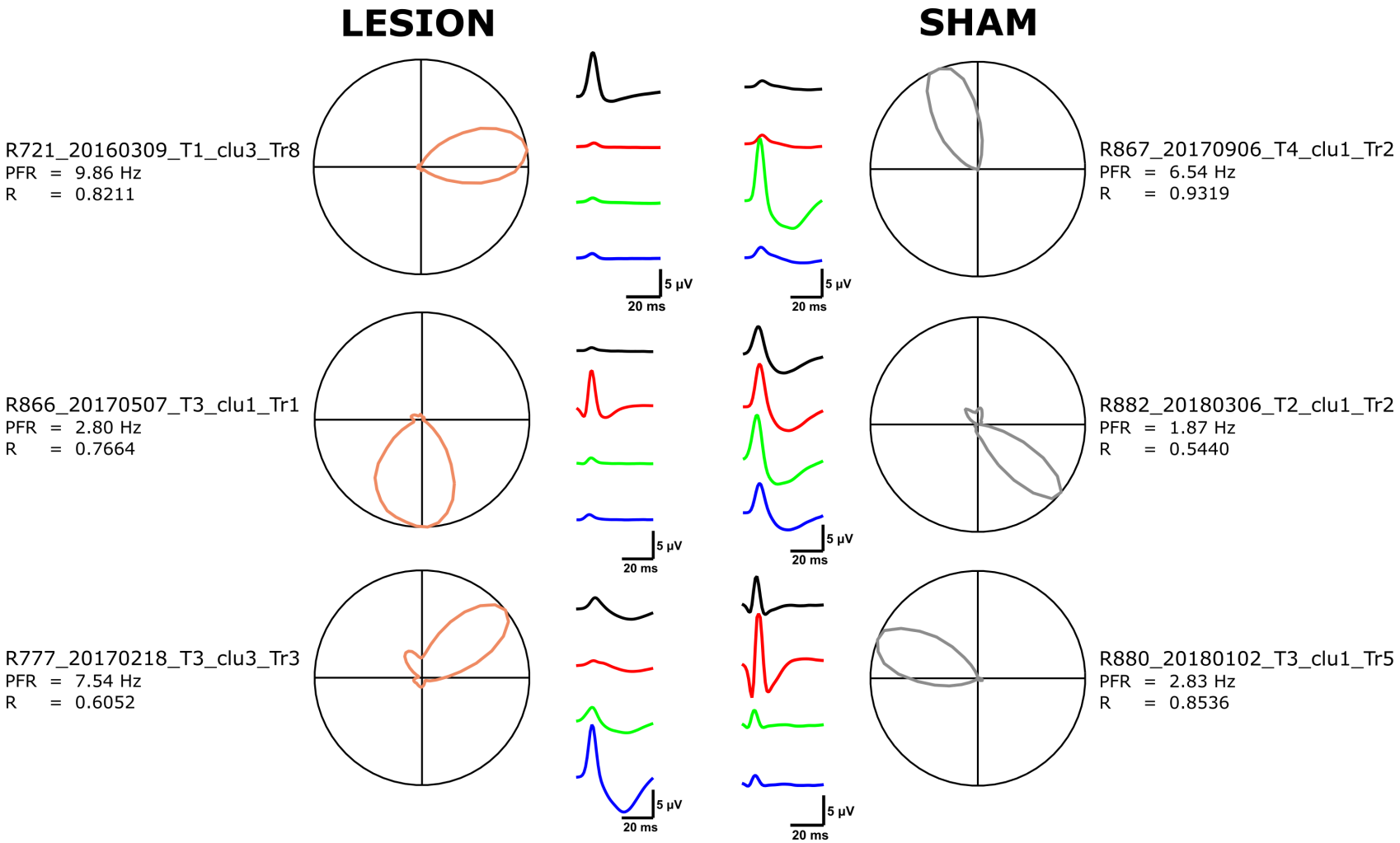

Figure 5.7: Examples of HD cells recorded from Lesion and Sham animals.

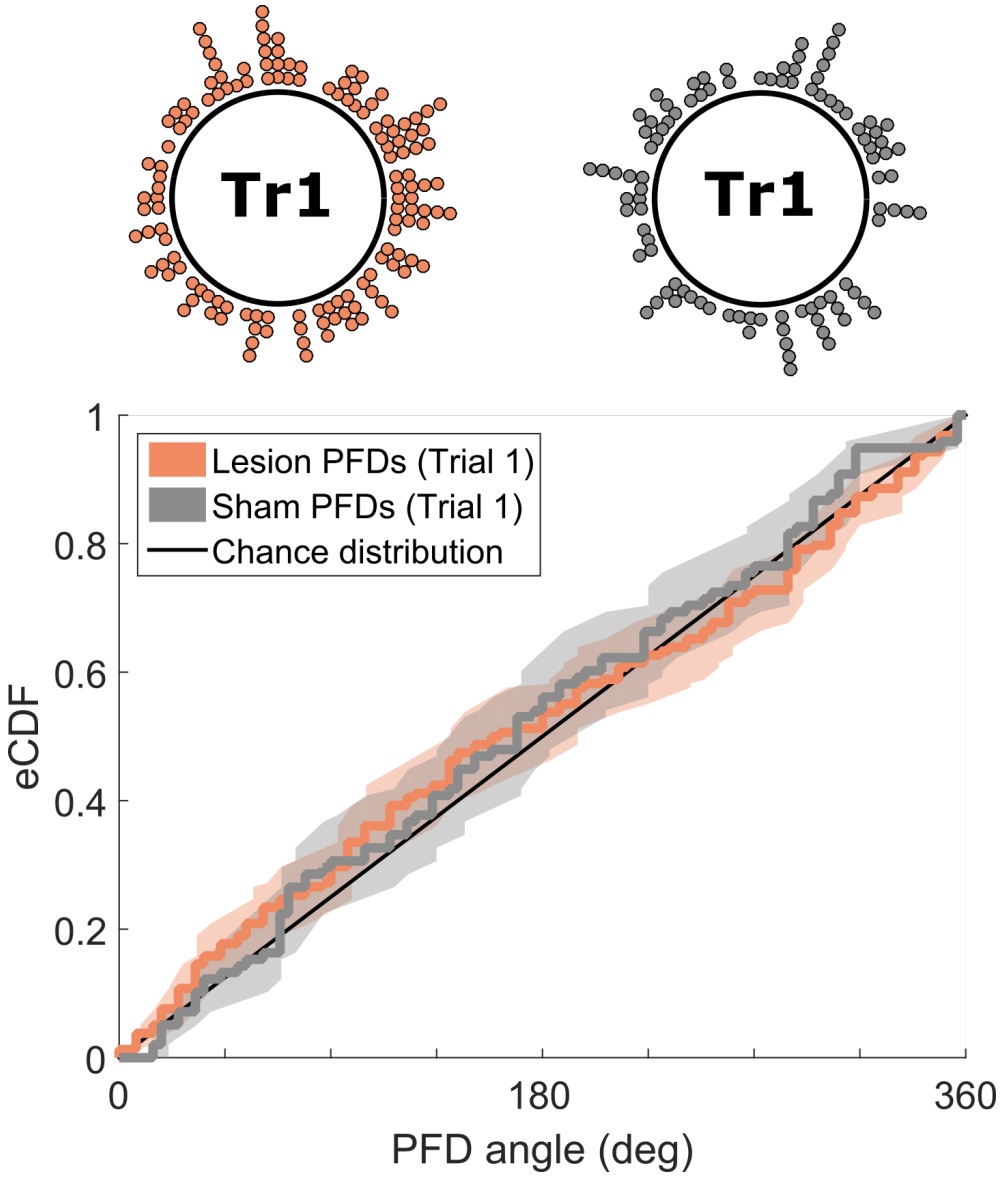

Figure 5.8: Top: circular plots of all HD cell PFDs in the first trial from lesion and sham animals, in the distal reference frame of the room. Bottom: cumulative distribution of PFD angles of all HD cells in the first trial.

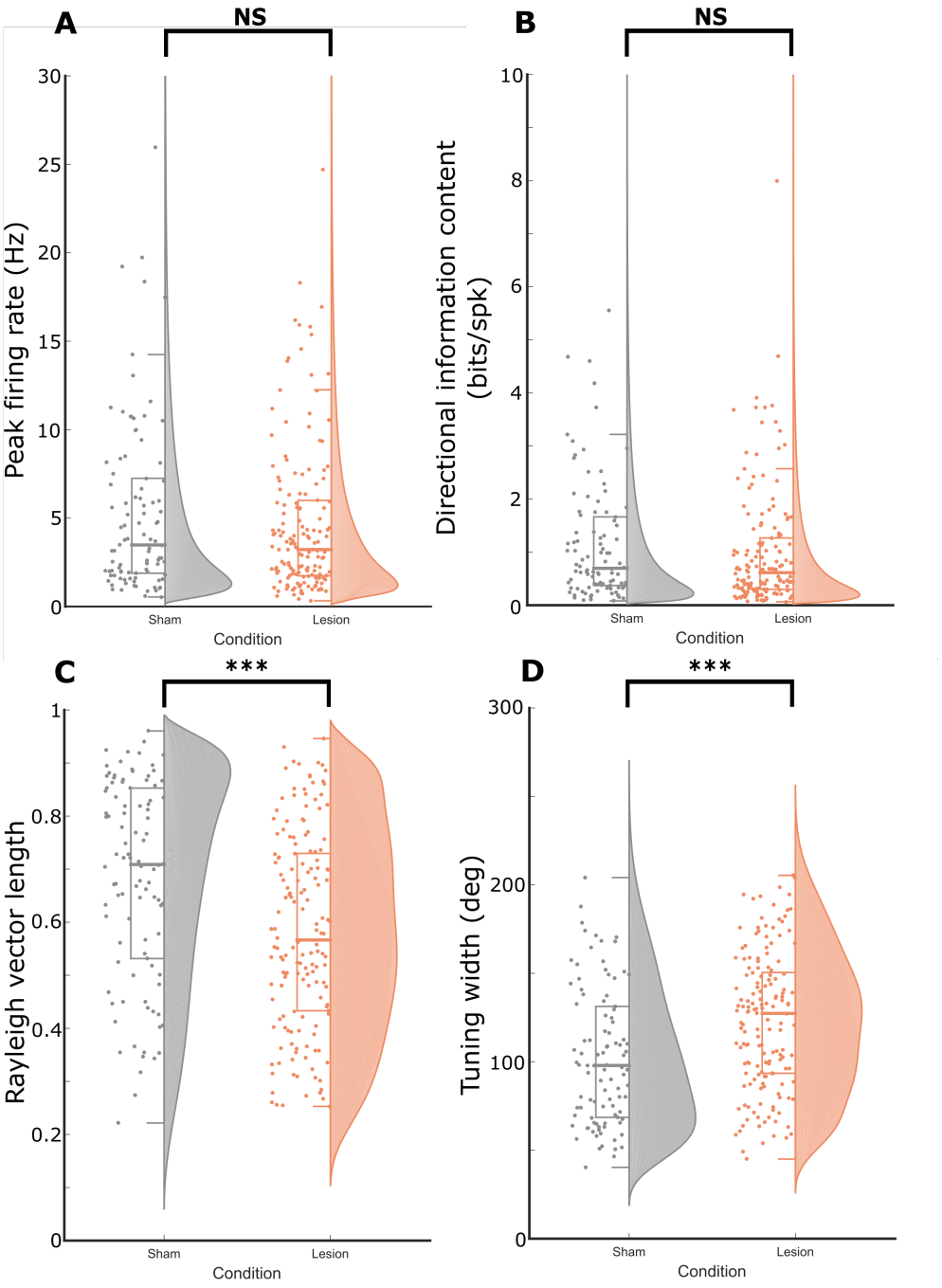

Figure 5.9: Distributions of summary HD cell characteristics. A: . *** indicates $p < 10^{-4}$

To confirm this, we compared the median tuning widths of all recorded HD cells in Lesion and Sham animals. Tuning widths of HD cells were estimated by the mean circular variance of the tuning curves across all trials in a session. For Lesion HD cells, the median tuning with was 127° ($n = 158$), whereas for Sham HD cells the median tuning width was 98.3° ($n = 101$). The tuning width differed significantly between HD cells recorded from Lesion and Sham animals, indicating that animals displayed higher mean tuning widths after dLGN lesions ($z = 4.01$, $p < 10^{-4}$, Wilcoxon ranksum test).

Examples of tuning curves of median width, from Lesion and Sham animals are displayed in Figure 5.10, as well as tuning curves from HD cells at the $25th$ and 75 percentile in each group. In general, it is evident that Lesion HD cells display slightly wider tuning curves than those from Sham animals, and this is reflected in the statistics above.

This finding is consistent with the observation above that the directionality (R vector length) of lesion HD cells is reduced compared with sham cells. This is unsurprising, as the R vector length is negatively correlated with the circular variance of the tuning curve. However this finding strongly implies that the representation of direction in the PoS following LGN lesions was impaired.

This may indicate that the HD cells carry less precise directional information following dLGN lesions. This finding is probed further in Section 5.3.3.

5.3.3 Drift of HD cells

As discussed above, the precision in the directional representation of HD cells is reduced in following LGN lesions. One plausible cause of this is a persistent worsening in the estimated head direction of the animal, manifesting as a consistently broadened tuning curve throughout the trial. Alternatively, a precise tuning curve that slowly drifts over time would appear when averaged over a whole trial as a wider, less directionally precise tuning curve. We wished to assess whether the reduced directionality observed above was due to PFD drift (akin to that observed in darkness), or a permanent reduction in precision.

In order to distinguish these, we looked for evidence of changes in the PFD within a trial. Initially, we binned the trials into two halves (of 4 minutes each), and constructed a tuning curve for each. The PFD of the tuning curves from the first and second halves of the trials were extracted and compared; the PFD change was plotted for each trial on a circular axis and as a CDF (see Figure 5.11).

Although both distributions clustered around 0°, the Rayleigh vector length of these intra-trial shifts was smaller for Lesion HD cells than Sham HD cells (lesion: $R = 0.675$, sham: $R = 0.901$), and a circular Kuiper test showed that the two distributions were significantly

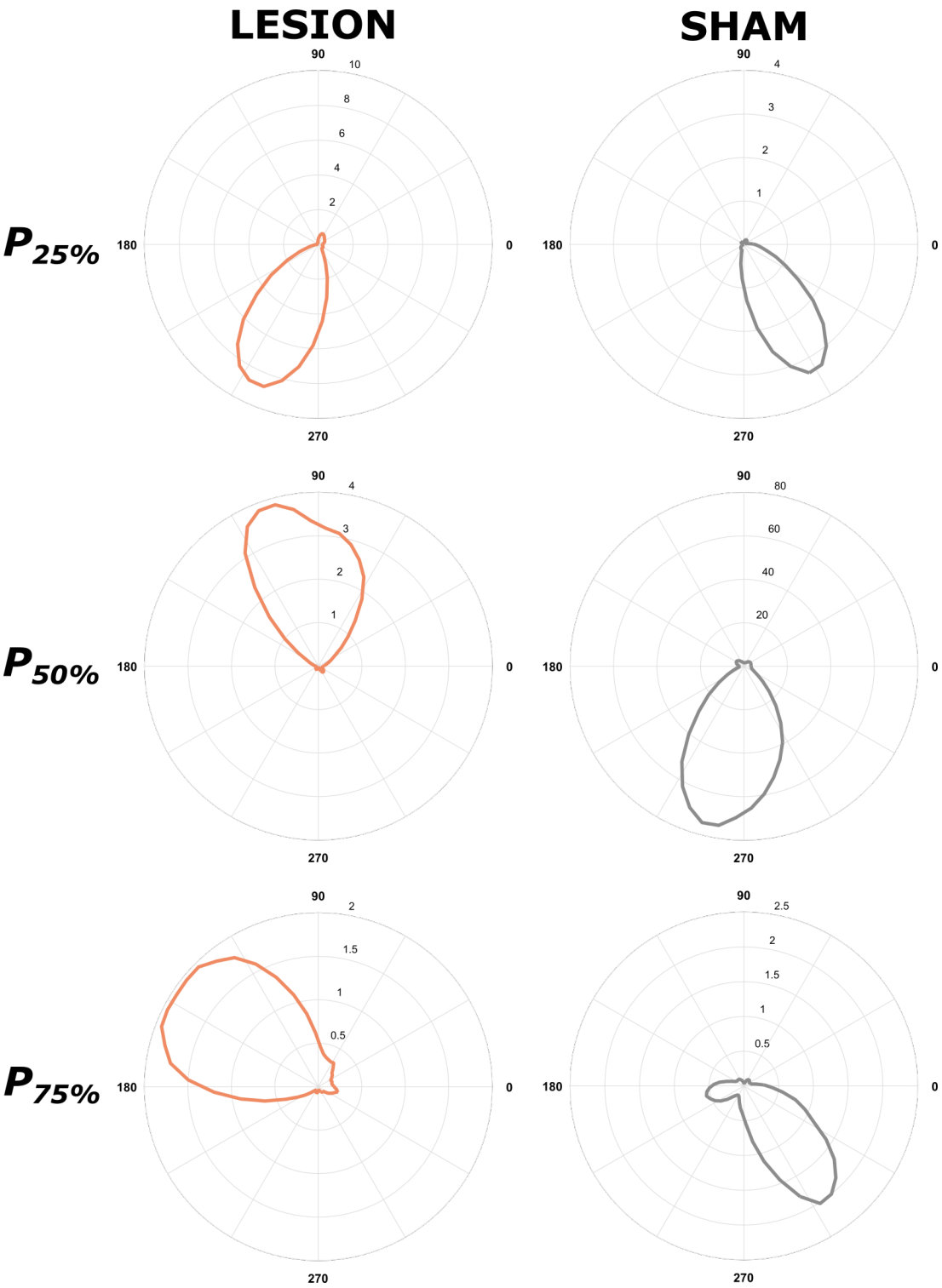

Figure 5.10: Examples of tuning widths of HD cells in Lesion and Sham animals. The HD cells selected display the $25th$ percentile ($P_{25\%}$), $50th$ percentile ($P_{50\%}$), and $75th$ percentile ($P_{75\%}$) tuning curves over all trials.

different ($k = 334550$, $p < 10^{-3}$). This indicates that, in general, Lesion HD cells were less stable over the course of a trial, with their PFDs shifting a larger amount between the first and second halves of the trial.

As we observed an increase in the PFD change between the first and second halves of trials in lesion HD cells relative to sham, we next wished to quantify the rate at which the HD cell representation drifted. In order to do this, we fit a circular-linear regression onto the spike train of each trial to extract an estimate of the linear drift rate across the whole trial, as described in Section 3.5.5.2. The fit equation was kept linear so as to enable ease of interpretation of the parameters: β_1 representing the linear rate of change of PFD over time (in °/min), and β_0 representing the estimated PFD at the beginning of the trial (in °). Moreover, as a substantial portion of lesion HD cell PFDs shifted between the first and second trial halves, we anticipated that a linear equation would suffice to capture the rate of this effect. [2]

To test whether the observed increase in tuning widths was due to attractor drift, we assessed whether the mean tuning curve widths over a whole session, for each cell, was correlated with the absolute linear drift rate for these cells. Over all cells, we saw a notable correlation between mean drift rate and tuning width (Figure 5.13), indicating that cells that drifted more over the course of a trial had greater tuning widths. This indicates that at least some of the wider tuning curves were due to the HD cell attractor drifting over the course of a trial. An example that shows this is seen in Figure 5.12.

We also wished to test whether drift rates were greater in lesioned than sham animals. As anticipated, over all trials, the median absolute drift rate fit to HD cell spike trains was significantly greater for lesion HD cells than sham HD cells (sham: $4.33\,^\circ\,\mathrm{min}^{-1}$, $n = 808$; lesion: $7.00\,^\circ\,\mathrm{min}^{-1}$, $n = 1264$; $z = 8.54$, $p < 10^{-16}$, Wilcoxon ranksum test). This, alongside the evidence that PFDs shifted between the first and second halves of trials, strongly indicates that in lesioned animals HD cells tended to slowly drift over time.

In order to characterise this difference further, we performed a two-way ANOVA over the absolute drift rates, using lesion condition and cue card condition (black-white, vertical-horizontal, or black-black) as categorical predictors. The ANOVA showed significant effects for both lesion condition ($F_{1,1932} = 90.41, p < 10^{-20}$) and cue card condition ($F_{2,1932} = 26.13, p < 10^{-11}$), indicating that both of these session parameters correlated with the HD cell drift rate. The ANOVA also showed a significant interaction between lesion condition and cue condition ($F_{2,1932} = 9.26, p < 10^{-4}$), indicating that the differences in anchoring between lesioned and sham animals depended in some way on cue condition. Correcting for multiple comparisons (Tukey-Kramer),

[2] Also, estimates of instantaneous rate would be complicated by inhomogeneity of directional sampling over time (that is, the animal may not sample all directions equally often, which could skew estimates of instantaneous properties of HD cells).

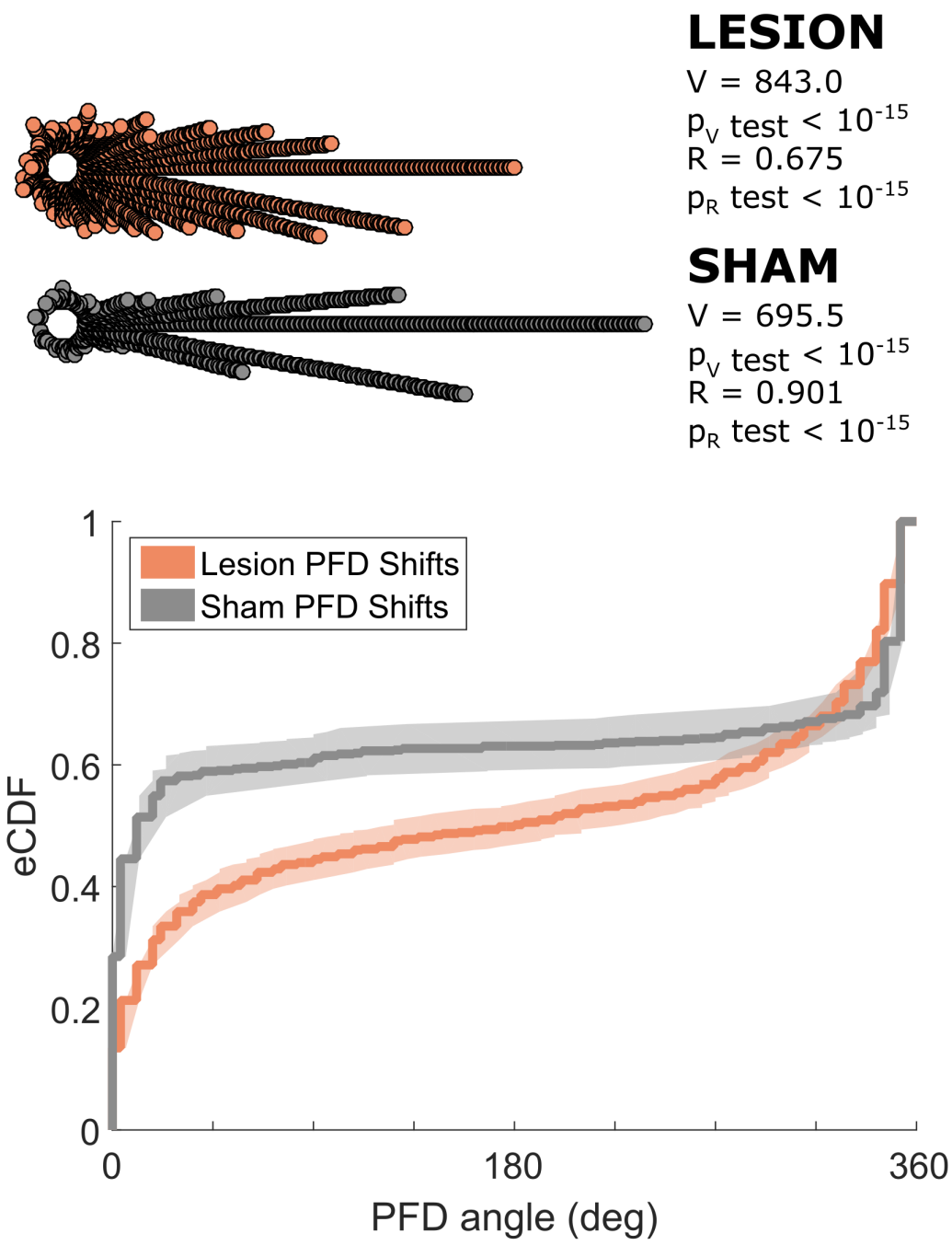

Figure 5.11: Estimated PFD change between the first and second halves of individual trials. Top: circular histogram of cell-x-trial showing the PFD difference between the first and second trial halves. Bottom: empirical cumulative distribution of these shifts for Sham (grey) and Lesion (orange) animals. It is clear from these plots that a larger density of PFD shifts were contained around 0° in Sham than in Lesion animals.

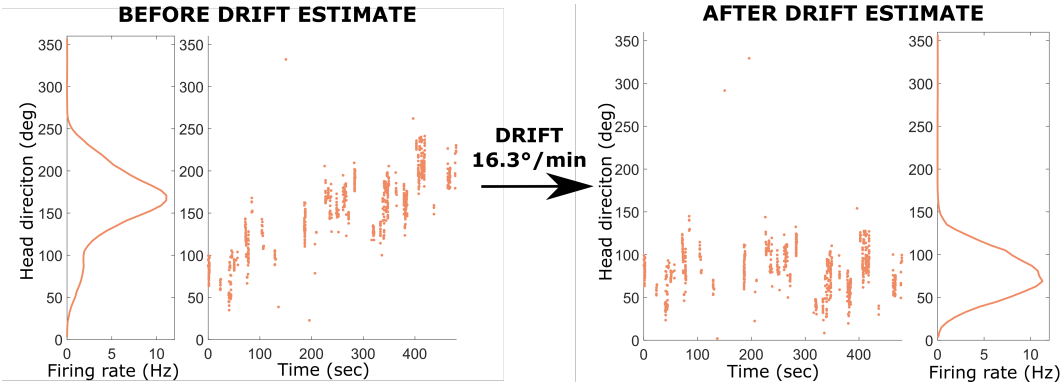

Figure 5.12: An example drifting HD cell recorded from a Lesion animal (cell R866_20170601_T3_clu1_Tr6). On the left, the raw head direction at each spike has been plotted as a scatter plot, alongside the overall HD cell tuning curve for this trial. On the right, the same plots have been made following a correction for the drift as estimated in the way described in Section 3.5.5.2. It can be seen that the head direction at each spike is more consistent across the whole trial, and that the HD tuning curve is less broad.

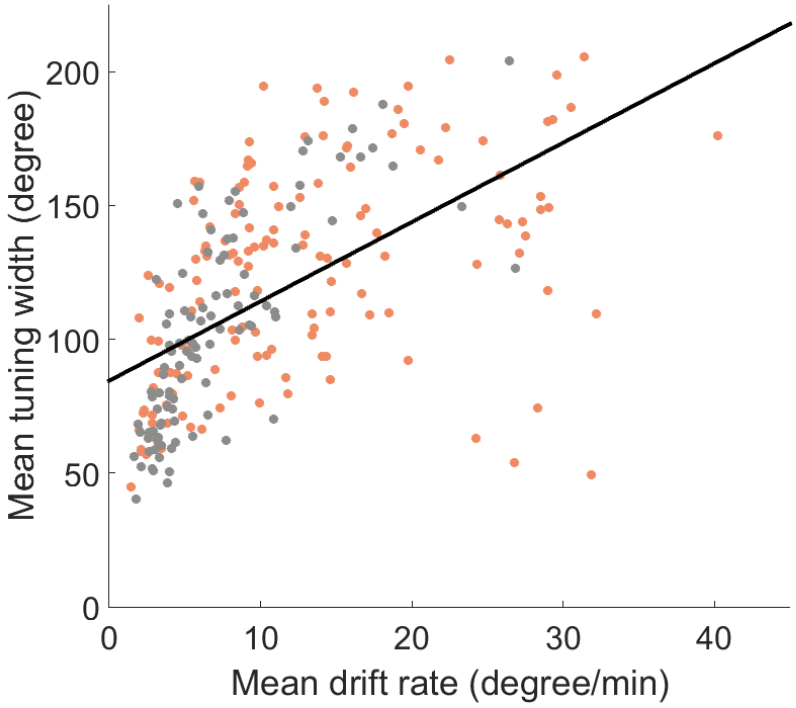

Figure 5.13: Scatter plot of the average attractor drift rate across a session in each cell versus the mean tuning width of each cell in a session, for sham (grey) and lesion (orange) animals. Black line is the least squares regression line through all data, grouped together.

we saw that, in two conditions, the mean cell drift rate was significantly greater in lesioned animals than in sham animals (black-white: $p < 10^{-7}$, vertical-horizontal: $p < 10^{-6}$), however we saw no difference in drift rate between lesioned and sham animals in the black-black condition ($p > 0.2$). As expected, there was no difference in drift rates between any cue card conditions in sham animals, whereas there was a difference between drift rates in cue card conditions in lesioned animals (black-white > vertical-horizontal $p < 0.05$, vertical-horizontal > black-black $p < 10^{-6}$, black-white>black-black $p < 10^{-7}$).

As a final analysis, we compared the net angular turns made by an animal in each trial, to the average drift rate of each HD cell in that trial, for sham and lesioned animals. Net angular turns was defined such that, if an animal turns once clockwise, and once anticlockwise, its net turn would be 0°, whereas if it turned once clockwise and twice anticlockwise the net turn would be 360°. Pearson correlations revealed a significant positive correlation between net turns and drift rate in lesioned animals ($\rho = 0.11, p < 10^{-3}$), whereas there was no significant relationship in sham animals ($\rho = 0.03, p > 0.3$).

5.3.4 HD cell landmark anchoring to local cues

The landmark anchoring of HD cells was tested by assessing whether the normalised PFDs of recorded cells shifted concordantly with rotations of the local visual cues. Examples of HD cells recorded over entire sessions, for each cue condition, are shown in Figure 5.14 for Lesion HD cells, and Figure 5.15 for Sham HD cells. The Lesion cells can be seen to rotate less consistently to follow rotations of the cue than Sham cells, which tended to maintain a consistent preferred direction relative to the cue cards.

Combining all non-ambiguous cue card types (excluding the control black-black condition), a circular histogram of normalised PFD shifts (the deviation from the expected shift if the cells were anchoring to the cue cards) from Sham animals showed significant deviation from uniformity ($R = 0.772$, $p_R < 10^{-53}$, $n = 169$ trial shifts) which on testing showed to be towards the direction zero ($V_{0^\circ} = 130.4$, $p_V < 10^{-51}$). The average absolute deviation from the expected shift (if the cells were anchored to the cue cards) was $26.7^\circ \pm 39.5^\circ$ (mean ± standard deviation). This provides evidence that HD cells in sham animals accurately anchored to the local reference frame and that visual information was successfully integrated into the head direction system. Figure 5.16A shows the distribution of PFD shifts for Sham animals; it is evident that most shifts are clustered around 0°, indicating good cue control.

Figure 5.16A also shows the set of PFD shifts observed in Lesion animals grouped together for black-white and vertical-horizontal sessions. It is clear that these are more broadly distributed around the compass. However, a Rayleigh test on the distribution of normalised PFD

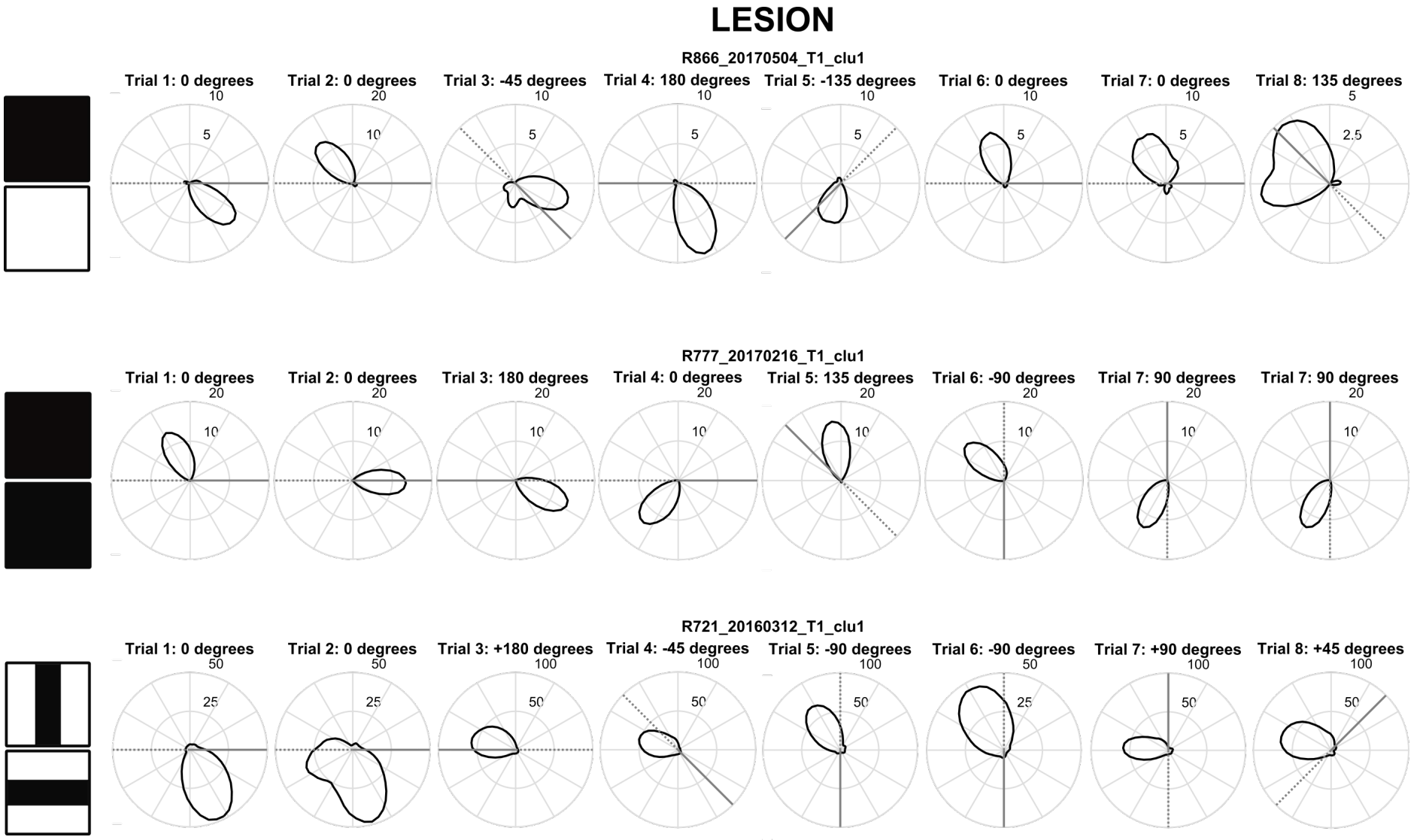

Figure 5.14: Example sessions from Lesion HD cells that display unreliable landmark anchoring to the cue cards. The angle of the cue cards relative to the HD cell tuning curve is indicated by the solid and dashed grey lines superimposed over the tuning curves.

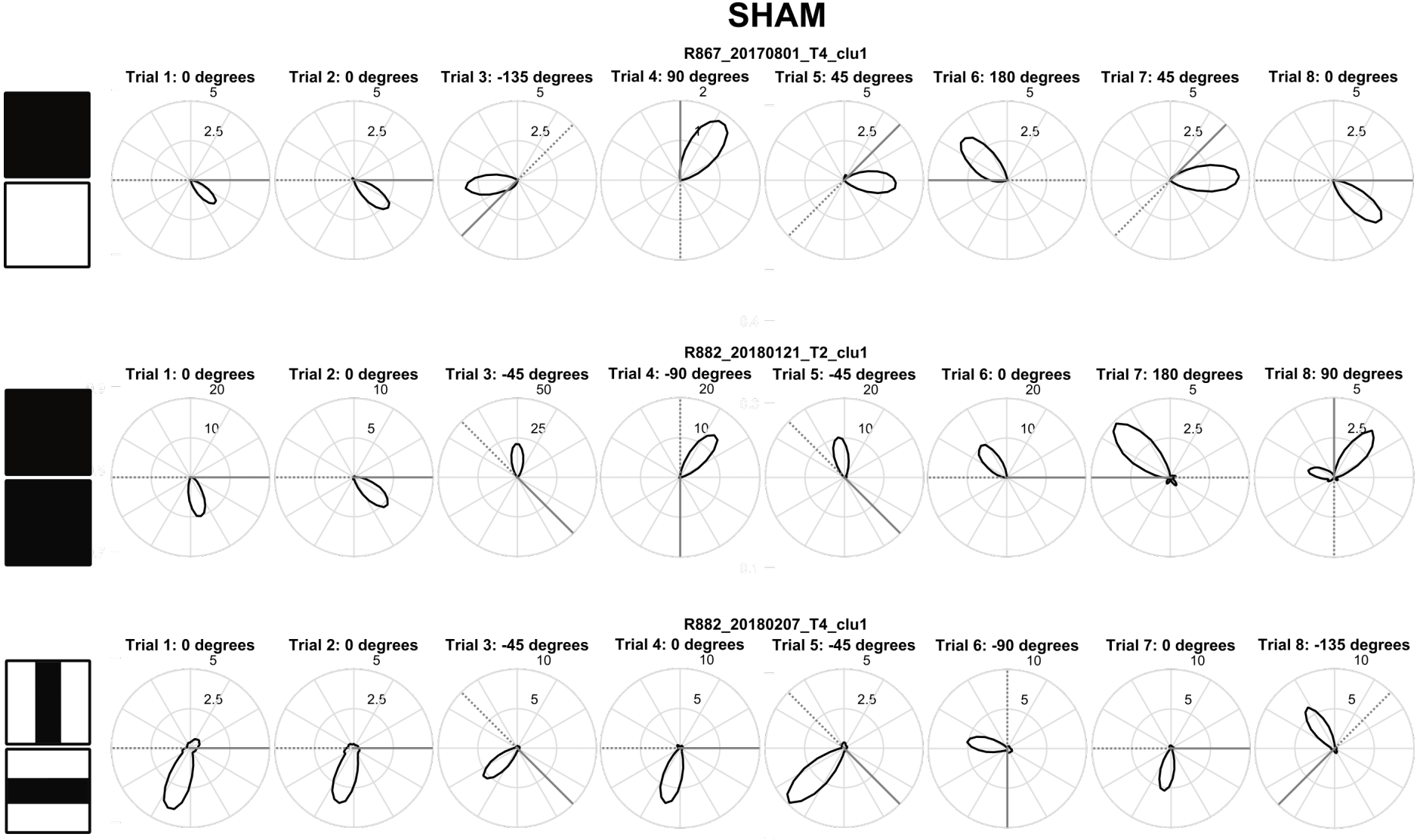

Figure 5.15: Example sessions from Sham HD cells that display good landmark anchoring to the cue cards. The angle of the cue cards relative to the HD cell tuning curve is indicated by the solid and dashed grey lines superimposed over the tuning curves. Note that, for the black-black condition, the cell flipped its preferred direction by 180° between some trials, as would be expected in a visually symmetric environment.

shifts over trials showed significant deviation from uniformity ($R = 0.176$, $p_R < 0.01$, $n = 208$ trial shifts), indicating that the tuning curves of HD cells recorded from lesioned animals did not shift randomly around the circle either. Accordingly, a V test showed this deviation to be towards the predicted direction of 0° ($V_{0°} = 36.5$, $p_V < 10^{-3}$), and the mean (± standard deviation) deviation from the expected shift was $76.5° \pm 61.9°$. This indicated that there was a tendency for HD cells to shift their tuning curves to follow the rotations of the visual cues, although from the larger angular deviation from the expected shift, it is evident this process was not very precise.

Accordingly, the R vector length of PFD shifts in Lesion animals was noticeably smaller than that for sham animals. A Kuiper test of the lesion and sham distribution showed that these distributions were significantly different from each other ($p < 10^{-3}$, $k = 15990$, Figure 5.16B). As such, in visually unambiguous environments, the anchoring of HD cells to visual cues is substantially impaired following LGN lesions, although some evidence of residual anchoring exists.

Assessing landmark anchoring to these cue configurations separately, there was good evidence of landmark anchoring of Sham HD cells to both the black-white ($R = 0.800$, $p_R < 10^{-29}$, $V_{0°} = 67.9$, $p_V < 10^{-51}$, $n = 85$ trial shifts) and vertical-horizontal ($R = 0.745$, $p_R < 10^{-24}$, $V_{0°} = 62.5$, $p_V < 10^{-51}$, $n = 84$ trial shifts) cues. Unlike as has been reported previously (Lozano et al., 2017), we saw no difference in the distributions of PFD shifts between the high-contrast black-white cues and higher complexity vertical-horizontal cues (Kuiper test, $p > 0.9$, $k = 1235$).

In Lesion animals, we saw evidence of some weak cue control in the black-white condition ($R = 0.255$, $p < 10^{-3}$, $V_{0°} = 35.1$, $p_V < 10^{-4}$, $n = 138$ trial shifts), but no evidence of any unimodal deviation from uniformity in the vertical-horizontal cue condition ($R = 0.04$, $p_R = 0.91$, $V_{0°} = -0.92$, $p_V = 0.56$, $n = 70$ trial shifts). This indicates that, in Lesion animals, HD cells could not accurately landmark anchor to vertical-horizontal cues, as the HD cells did not maintain a consistent PFD relative to the local visual scene between trials. However, there was evidence that cells could still anchor (significantly, but mildly) to black-white cues, and therefore might still be able to integrate some visual information in this cue condition. However, the R vector of the PFD shifts was notably smaller than that in Sham animals, and it may be that the accuracy of anchoring was reduced following dLGN lesion.

Comparing lesion and sham sessions, Kuiper tests showed that there was good evidence that the distributions of PFD shifts in lesioned and sham animals were significantly different for both the black-white cue condition ($k = 4817$, $p < 0.001$) and the vertical-horizontal cue condition ($k = 4018$, $p < 0.001$). This indicates that, across of animals, landmark anchoring is

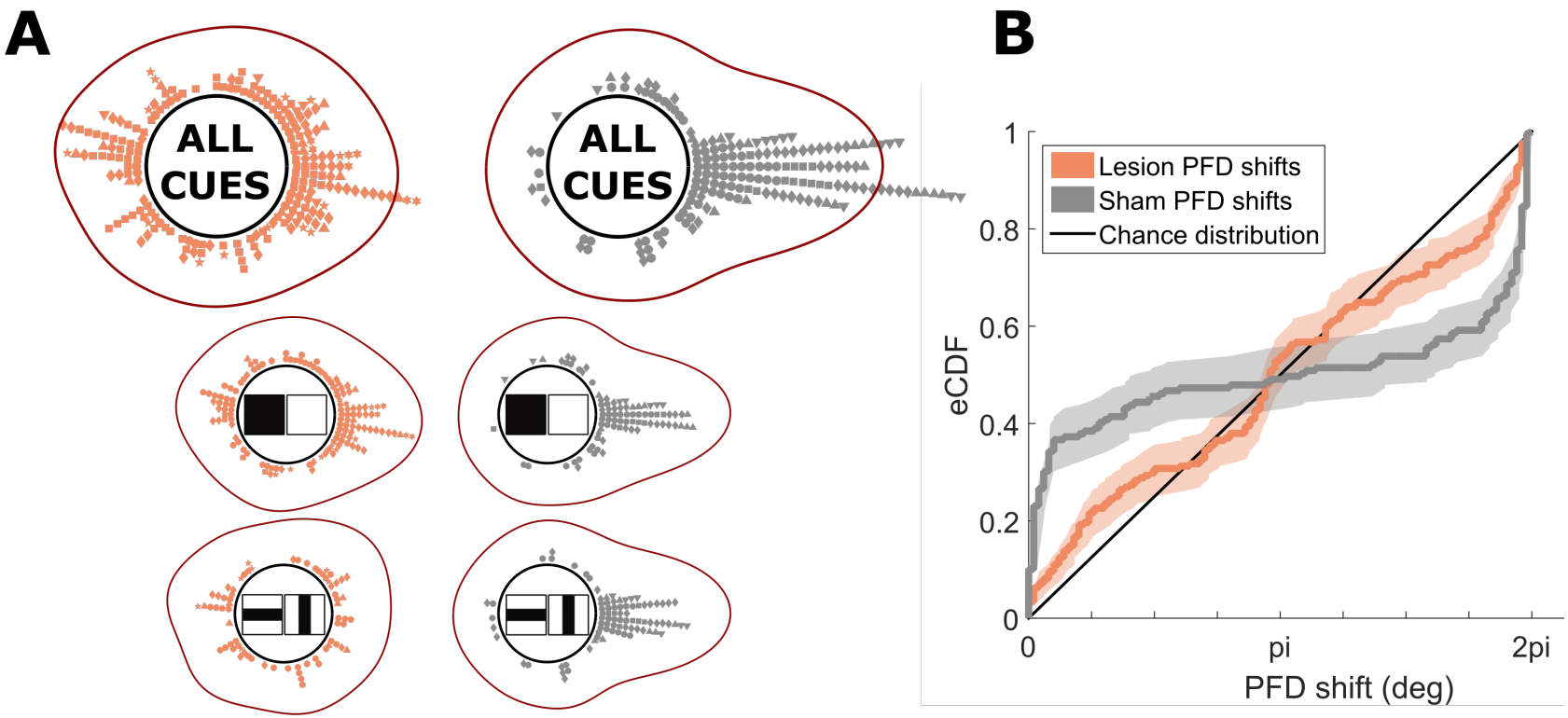

Figure 5.16: Summary of PFD shifts following rotations of all unambiguous cue types. Left: circular distributions of PFD shifts for all rotations for all cues (top), black-white cues (middle) and vertical-horizontal cues (bottom), for lesion (left) and sham (right) animals. Right: empirical cumulative distribution function (eCDF) showing shifts for lesion (orange) and sham (grey) PFD shifts for all cues. It can be observed that, for sham animals, the majority of shifts occur near 0° and 360° (2π radians), whereas the distribution of shifts for lesion HD cells is closer to chance, but still shows some density at 0° and 360°. Confidence intervals were generated using a custom bootstrapping function.

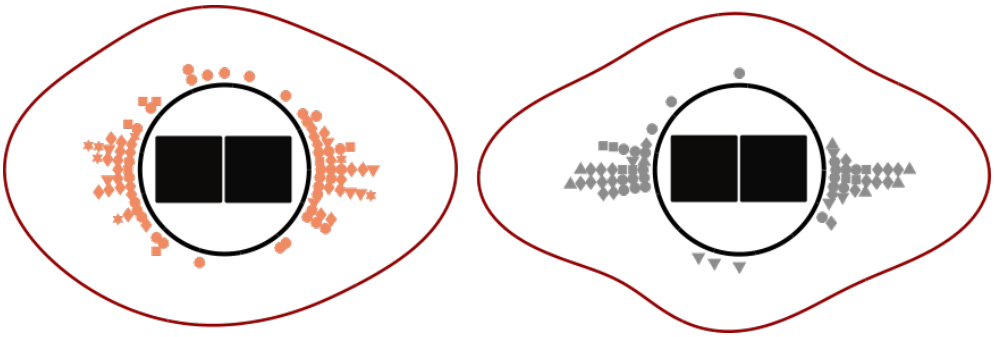

Figure 5.17: PFD shifts for the ambiguous cue-card condition. A general tendency for bimodality is visible with modes at 0° and 180°.

significantly impaired following dLGN lesion. Instead, as is evident from Figure 5.16, HD cells appeared to shift their PFDs randomly between trials, rather than follow the rotations of the local visual scene.

In a two-fold rotationally symmetric environment, such as the black-black condition, normalised PFD shifts would be expected to cluster bimodally about 0° and 180°. In sham animals, visual inspection of the circular histogram of PFD shifts showed the expected bimodal distribution (Figure 5.17), and the corresponding Rayleigh vector length of these shifts was not statistically significant (as would be expected from an axial distribution): sham $R = 0.075, p > 0.5$, lesion $R = 0.042, p > 0.5$. As such, to assess whether the HD cells anchored to visually identical cue cards, an angle doubling procedure was used and is described below (Section 5.3.4.2).

5.3.4.1 HD cells did not anchor to the distal room

HD cells will anchor preferentially to more distal (versus proximal) cues if available (Zugaro et al., 2001), as these cues can provide more stable allothetic directional information to the navigation network. As such, if rats learnt the orientation of the distal room, outside of the enclosing curtain, HD cells would ignore the rotation of the proximal cylinder and remain stable in relation to the reference frame observed by the camera. If lesioned animals were more likely to learn a distal reference frame during recording sessions, this could explain the impairment in landmark anchoring reported above.

To test whether HD cells in either group landmark anchored to the distal room configuration, the normalised PFD shifts of recorded HD cells were correlated against the distal (camera) reference frame instead of the visual scene of the cylinder. The Rayleigh vector of PFD shifts was non-significant in both lesion ($R = 0.005$, $p > 0.99$) and sham ($R = 0.088$, $p > 0.10$) groups, indicating that the HD cells shifted randomly relative to the room between trials and were not stable in the distal reference frame. Similarly, there was no difference between the cumulative distributions of PFD shifts in the lesion and sham groups ($k = 8400$, $p > 0.90$, Kuiper test),

indicating that lesioned animals were not more likely to learn the distal reference frame than sham animals. These findings are shown in Figure 5.18.

5.3.4.2 Angle doubled anchoring

To assess whether HD cells landmark anchored to cues without discriminating them, a similar battery of analyses were performed on angle-doubled PFDs. As the predicted peaks were separated by 180°, doubling PFDs would shift those located at 180° to 0°, allowing for the use of the Rayleigh test and derived statistics (see Section 5.2.6.5). A significant Rayleigh vector test on the angle-doubled dataset (but not on the non-doubled data) would indicate that the PFD shifts were distributed bimodally, and provide evidence that the HD cells significantly landmark anchored to the cue cards but could not discriminate them. This has been observed previously in the black-black condition in animals implanted in PoS and retrosplenial cortex (Lozano et al., 2017).

Circular plots of PFD shifts after the angle-doubling procedure, for each cue configuration, are shown in Figure 5.19. As expected, we observed that, in the black-black cue condition, the R vector of PFD shifts, combined across all animals, was greatly increased for sham animals following the angle-doubling procedure ($R = 0.832$, $p < 10^{-24}$). This was also true for lesion HD cells recorded in the black-black condition ($R = 0.553$, $p < 10^{-12}$), consistent with the interpretation above of some (visual or non-visual) residual landmark anchoring being present following dLGN lesion. Interestingly, as was seen above for black-white cues, the distribution of angle-doubled PFD shifts for black-black cues in lesion animals was significantly different from those for sham animals ($k = 1974$, $p < 0.005$), indicating that the residual anchoring to these cues was impaired relative to sham.

As would be expected for black-white cues, the R vector of angle-doubled PFD shifts was reduced for sham animals ($R = 0.597$) relative to non-doubled R vector above (consider that doubling angles decreases the concentration parameter of a unimodal distribution). This decrease was not seen in lesion PFD shifts ($R = 0.288$), which was approximately equivalent to the value seen before angle-doubling. This indicates that there is little evidence of bimodal landmark anchoring in either sham or lesioned animals to black-white cues.

Of interest, we wished to assess whether the negligible anchoring observed in lesioned animals to vertical-horizontal cues was due to PFD shifts being distributed bimodally or uniformly. Whereas the R vector was reduced following angle-doubling of sham PFD shifts ($R = 0.623$), it was mildly increased following angle-doubling of lesion PFD shifts ($R = 0.125$). This might suggest that the distribution of PFD shifts in the vertical-horizontal condition was mildly bimodal, suggesting the HD cells detected the presence of the cue cards but could not anchor to

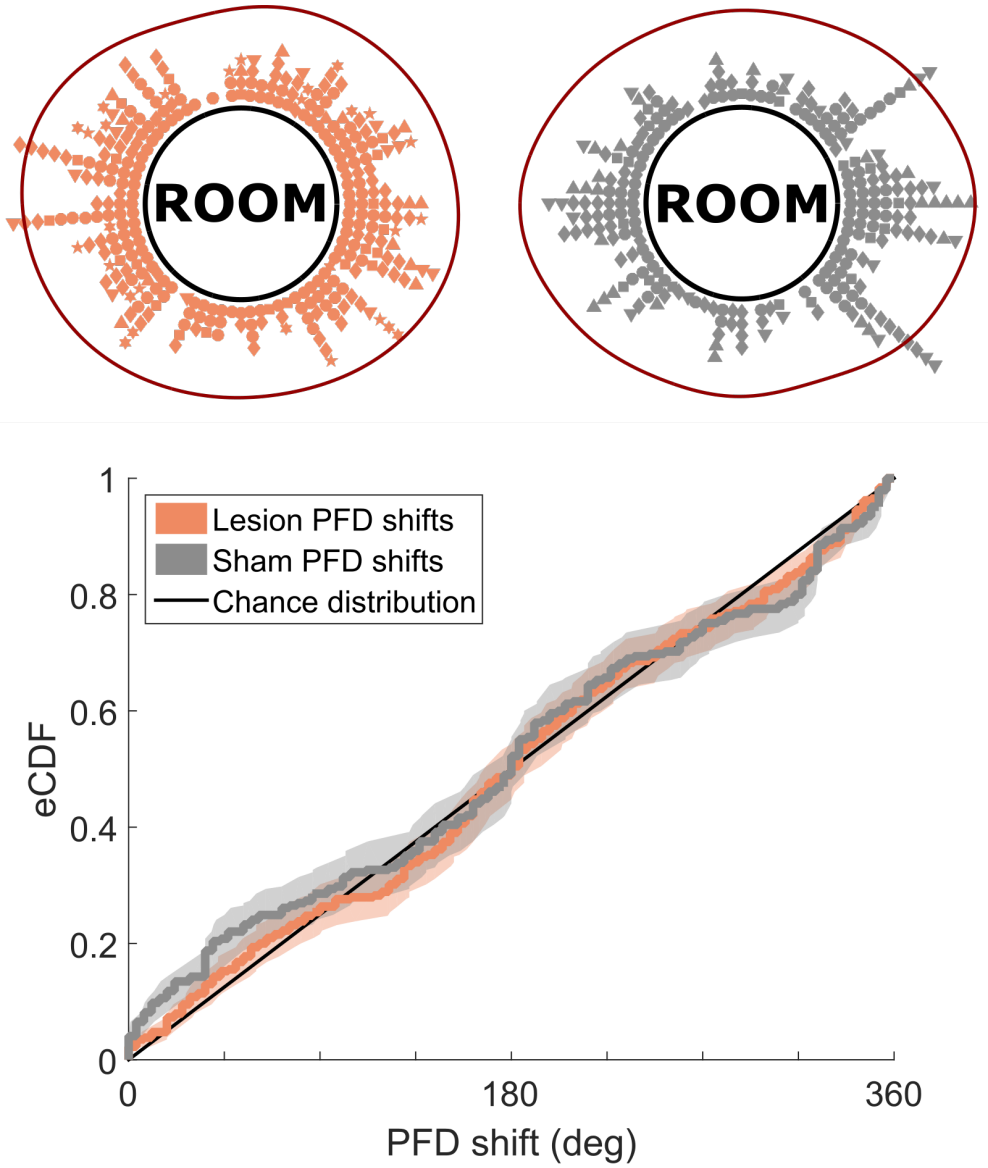

Figure 5.18: Distributions of PFD shifts relative to the distal room for lesion (orange) and sham (grey) sessions. Top: circular plots of PFD shifts, showing little evidence of bias towards the predicted 0°. Bottom: empirical cumulative distribution function (eCDF) of PFD shifts for lesion and sham HD cells, showing considerable overlap with the theoretical chance distribution (black). 95% confidence intervals were generated with a custom bootstrap function.

their visual content. However, for lesion PFD shifts, this R vector still did not reach significance ($p_R > 0.10$), and there was no evidence of a bias in the distribution of PFD shifts towards the predicted direction of 0° ($V_{0°} = 8.84$, $p_V > 0.05$). As such, we could not find evidence that HD cells in lesioned animals were anchoring bimodally to vertical-horizontal cues, and as such there was no evidence that the animals could detect the presence of these cue cards.

5.3.5 Co-rotation of HD tuning curves

As HD cells are modelled as existing within an attractor, it is to be expected that shifts of HD cells between trials are coherent; that is, all recorded HD cells should shift a similar angle between trials (irrespective of whether they anchor to the visual cues), such that all cells maintain a consistent angular relationship to one another.

We assessed the coherence of recorded HD cell pairs by calculating the R vector length for the angle difference between the cell pairs in each trial. A high R vector length indicates that the angle between cell PFDs was consistent across multiple trials, indicating that the cell pair behaved coherently.

The median R vector length for co-recorded Sham HD cells was 0.693 ($n = 298$ pairs), and for Lesion HD cells was 0.557 ($n = 518$ pairs). Both of these were greater than the value generated by a random shuffle ($R = 0.299$, $n = 32633$ pairs), generated by assessing coherence of all pairs of HD cells recorded in different sessions ('extrasession' pairs). As expected, a ranksum test demonstrated that the coherence of 'intrasession' HD cell pairs was significantly greater than 'extrasession' pairs, for both sham ($z = -25.1$, $p < 10^{-138}$) and lesion ($z = -22.9$, $p < 10^{-115}$) HD cell pairs.

This indicates that both Lesion and Sham HD cells tended to rotate coherently between trials, significantly more than chance. This is shown in Figure 5.20, which plots an estimate of the empirical cumulative density functions for sham and lesion cell coherences, alongside the cumulative distribution of the shuffle.

However (as is evident in Figure 5.20), Lesion HD cell pairs were significantly less coherent than Sham HD cell pairs ($z = 8.23$, $p < 10^{-15}$, ranksum test). That HD cells following dLGN lesions behaved less coherently (but were still more coherent than chance) suggests that some degree of error has been introduced into the directionality as encoded in the postsubicular HD system.

A secondary analysis assessing the consistency of HD cell PFDs across a session confirmed these results. Here, we extracted the relative angle between all pairs of co-recorded HD cell pairs in each trial. Across a session, for each pair, this results in eight angles: the (absolute) difference between the maximum and minimum relative angle was computed for each HD cell

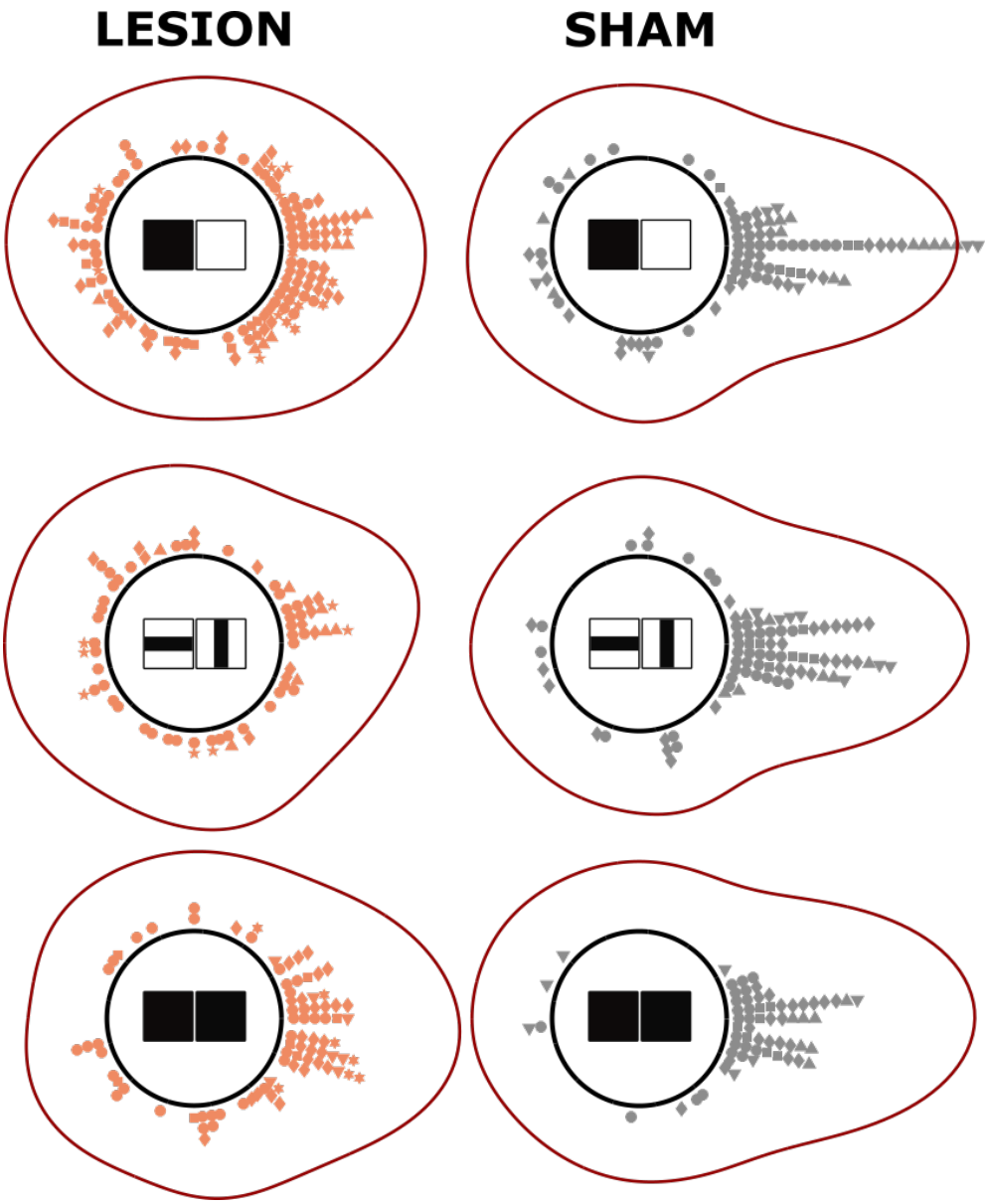

Figure 5.19: Distributions of PFD shifts relative to local cues, for each cue configuration, following the angle-doubling procedure. Note that, for black-black cues, the shifts have been transformed from a bimodal to a unimodal distribution.

pair, and compared between Lesion ($n = 518$ pairs) and Sham ($n = 298$ pairs) groups. Values near 0° indicate consistent relative angles across a session. As can be observed in Figure 5.21, these relative angles between HD cell pairs were more variable in Lesion animals than Sham, as a greater proportion of relative angles were greater than 0°. Accordingly, a KS test showed that these distributions were significantly different ($p < 10^{-14}$ KS statistic = 0.40), indicating that Lesion HD cells were less coherent than Sham HD cells across a recording session.

We wondered whether the reduced coherence in lesion animals was due to a higher variance in estimates of HD cell PFDs, caused by HD cell drift (Section 5.3.3) over the course of a trial. Inhomogeneity in directional sampling by the animal could lead to greater changes in the PFDs of two HD cells in the time between successive trajectories through their PFDs. This may manifest as apparent changes in the angle between their PFDs, leading to decreases in the R vector used to assess coherence.

To test this, we correlated the coherence between HD pairs with the absolute angle between the cell PFDs. Using Pearson correlation, we saw that the coherence between HD cells was negatively correlated with the angle between cell PFDs, for both sham ($\rho = -0.342$, $p < 10^{-8}$) and lesion ($\rho = -0.361$, $p < 10^{-16}$) cell pairs. This indicated that cells with PFDs further apart were generally less coherent between trials. As such, it is plausible that attractor drift could explain this result: the time between sampling of the preferred directions of cells with greater angular separation will also be greater, allowing for more attractor drift between successive samples, and therefore more variance in the PFD estimates.

5.3.6 Individual animal landmark anchoring

There was substantial variation between animals in the extent to which HD cells anchored to the cues. As discussed above, in general HD cells were more able to anchor to the high-contrast black/white cues than to the vertical/horizontal cues.

Indeed, constructing circular histograms of PFD shifts for each animal individually (as in Figures 5.22 and 5.23) illustrates the variance in how well animals anchored to each cue card type. On inspection of these, all lesioned animals display poor anchoring to vertical-horizontal cues, compared with moderate-to-good anchoring to these cues by sham animals. However, whereas some lesioned animals displayed poor anchoring to black-white cues (R777, R866, and R979), other lesioned animals showed some residual anchoring to these cues (R721, R968, R1004, R1005).

To see if anchoring was impaired relative to sham, when present in lesioned animals, we considered only the lesioned animals with residual anchoring to black-white cues. This was indicated by a significant V test in the predicted direction of 0, for PFD shifts following rotations

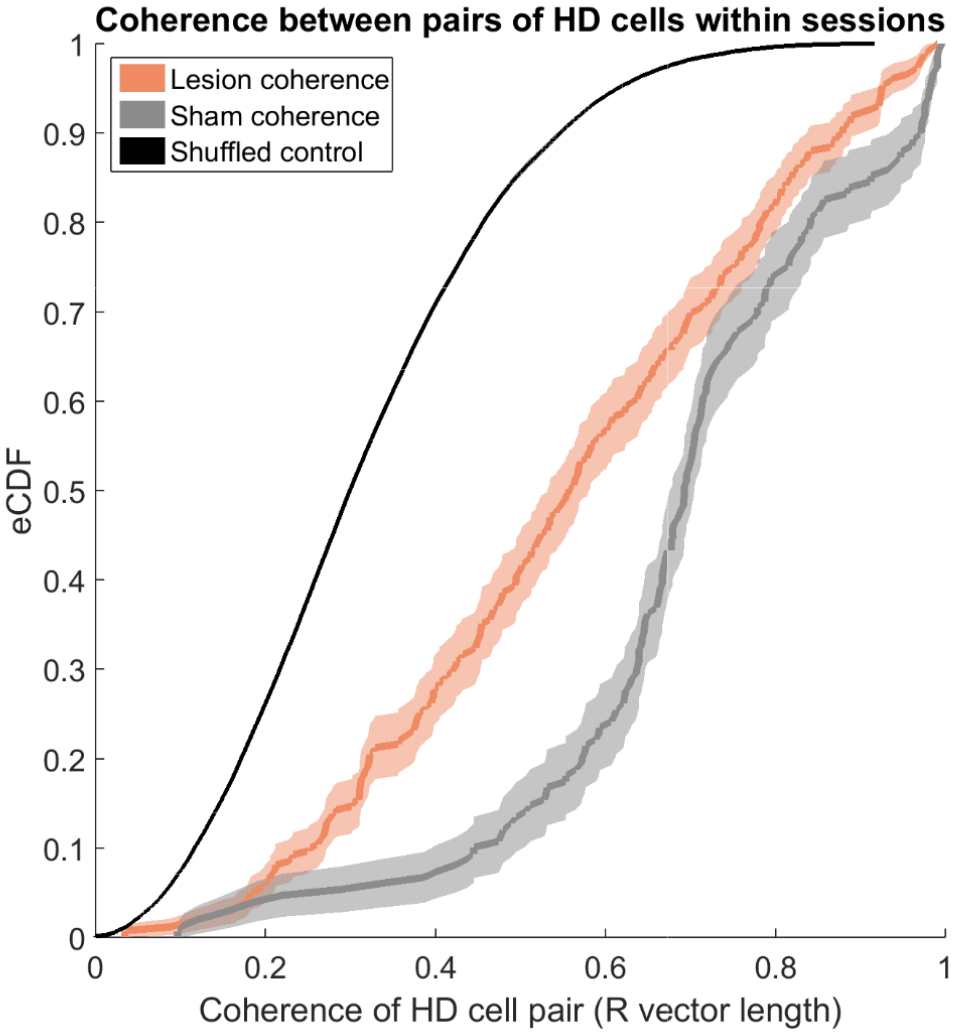

Figure 5.20: Empirical cumulative density plot for estimates of coherence between HD cell pairs in Sham and Lesion animals, compared to a shuffled distribution. Shaded regions represent confidence intervals estimated using Greenwood's formula.

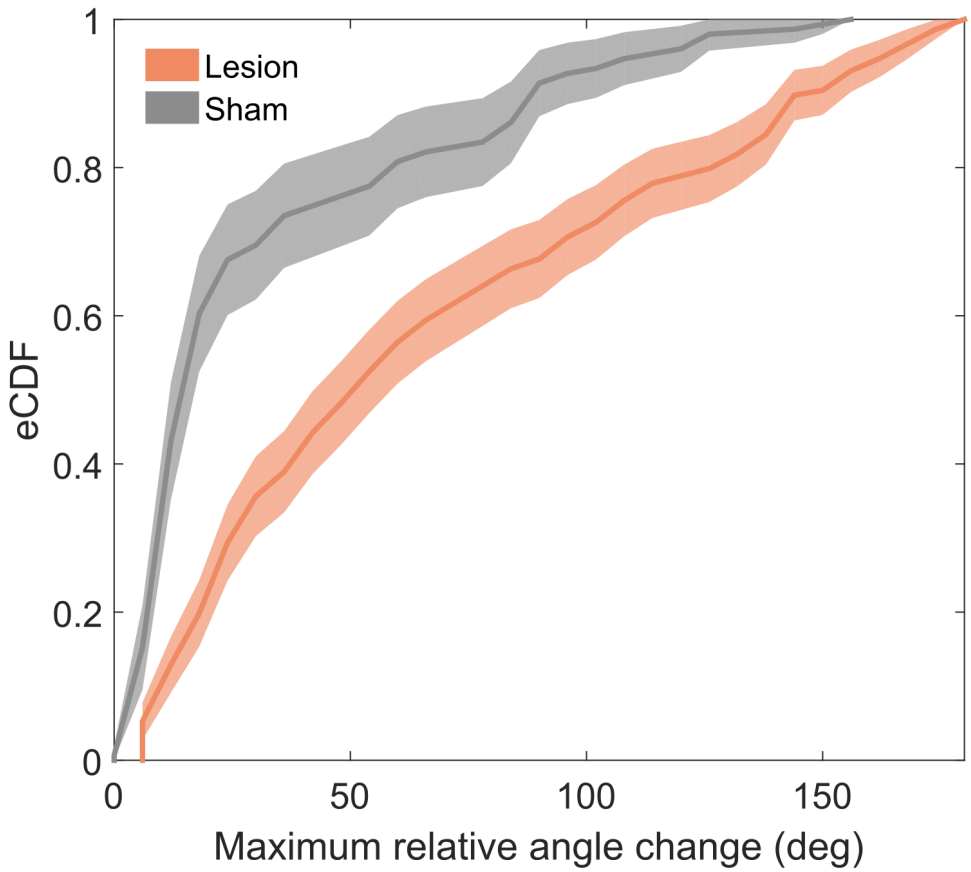

Figure 5.21: Empirical cumulative distribution (eCDF) of relative angle changes between HD cell pairs over the course of a trial for Lesion (orange) and Sham (grey). This is created by subtracting the minimal angle subtended between a HD cell pair over a session from the maximal angle. This provides a metric for how much the relative angle between the two cells changed over the whole session. Confidence intervals generated by Greenwood's formula implemented by MATLAB.

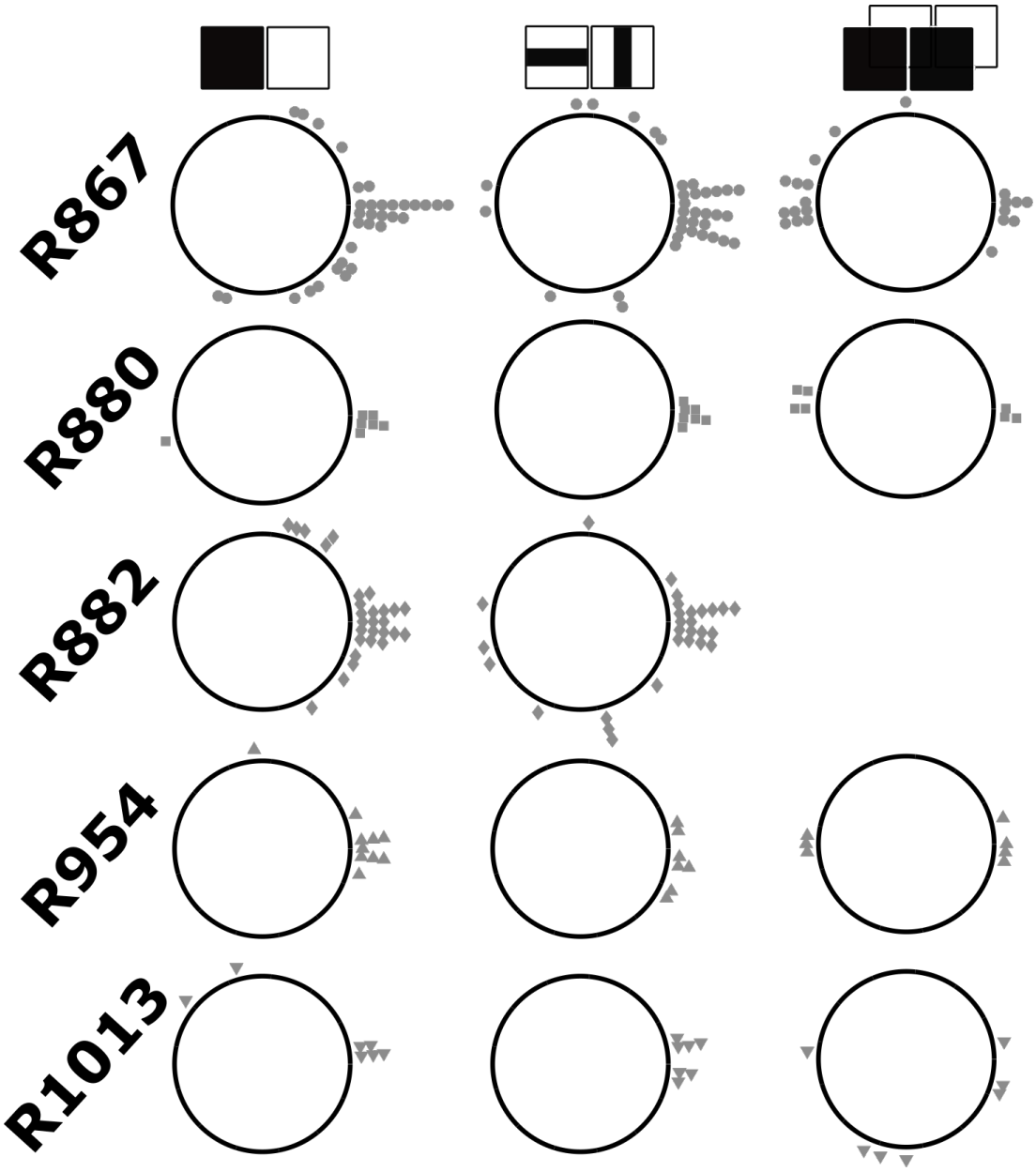

Figure 5.22: Summary of landmark anchoring to each cue condition in each Sham animal.

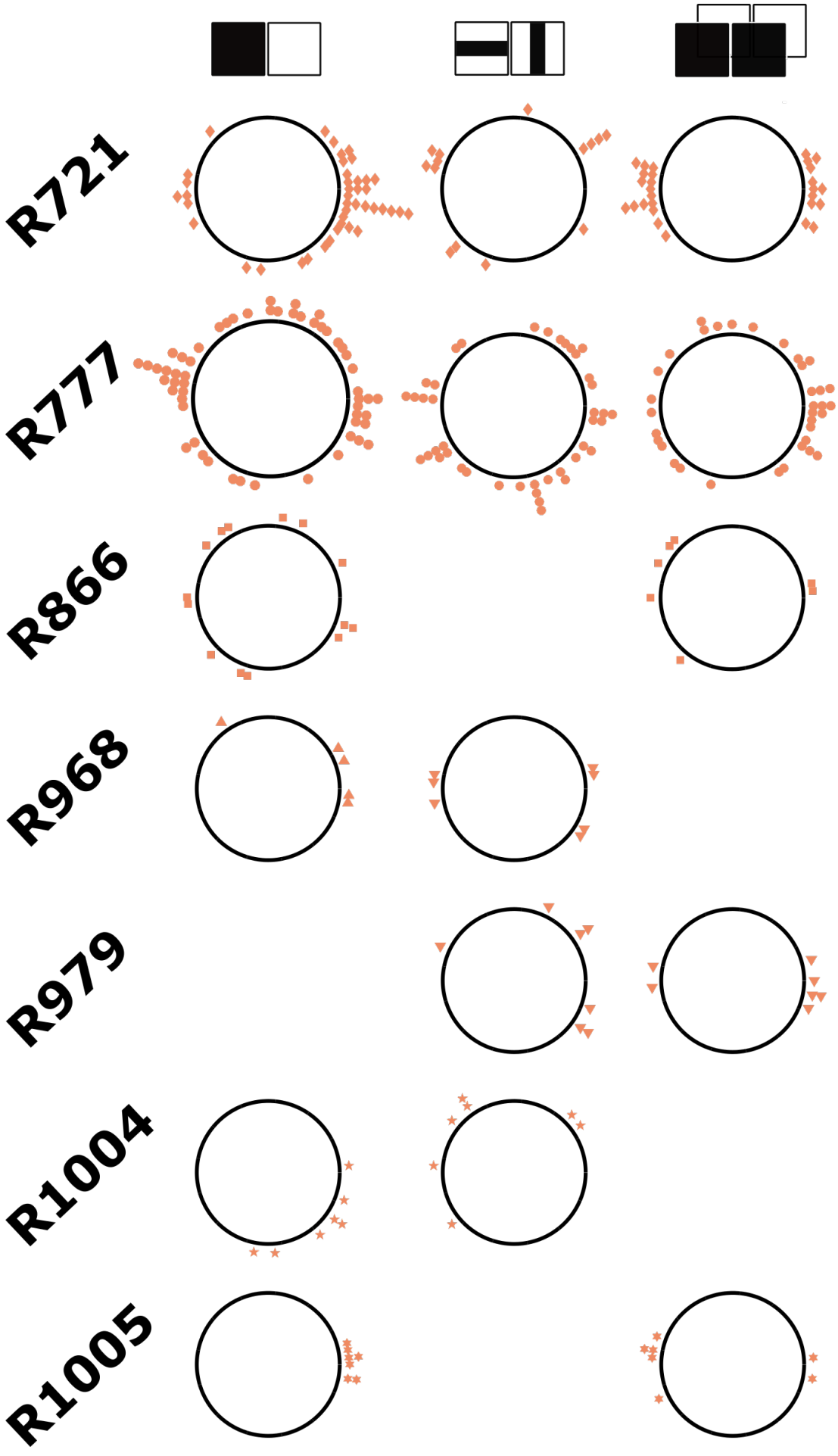

Figure 5.23: Summary of landmark anchoring to each cue condition in each Lesion animal.

Animal name	V	p_V
R721	23.10	$1.84 \times 10{-}7$
R777	-3.21	0.73
R866	-0.91	0.63
R979	1.40	0.23
R968	3.14	0.02
R1004	4.42	0.01
R1005	6.90	1.13×10^{-4}

Table 5.3: Results of V tests on PFD shifts following rotations of cues in black-white sessions only, for all lesioned animals. Whereas some animals show no evidence of anchoring to these cues, some residual – but significant – anchoring exists in a number of rats: R721, R968, R1004, and R1005.

of cues in black-white sessions (summarised in Table 5.3). Considering only these animals, the R vector length of all PFD shifts to black-white cues was reduced in these lesion animals relative to sham (lesion: $R = 0.628$, $n = 61$; sham: $R = 0.800$, $n = 85$), and a Kuiper test shows that the distributions of PFD shifts were significantly different ($k = 1559$, $p < 0.05$). As such, there was evidence of less precise anchoring to black-white cues following dLGN lesions even in animals with evidence of cue control.

To attempt to further quantify the differences between animals, an anchoring metric was designed to compare anchoring success in each cue card condition (see Section 5.2.6.6 in Methods). Using this metric, a 1 would indicate perfect landmark anchoring across all trials, for that cue condition in that animal, whereas values near 0 (or below) would indicate no evidence of anchoring, indicating that PFDs shifted randomly following cue rotations.

A summary of these values, for each individual animal and cue configuration, is shown in Table 5.4. Consistent with the findings discussed above, the anchoring metric for lesioned animals was generally lower than that for sham animals. This was true for all animals in the vertical-horizontal condition, although, as above, for the black-white condition two groups of lesioned animals emerged: one with low anchoring scores (R777, R866, R979), and one with higher anchoring scores (R721, R968, R1004, R1005). The animals generally also showed similar anchoring scores in the angle-doubled black-black cue condition as in the black-white condition. This indicated that these cues exert similar strengths of cue control, and suggested that the residual anchoring following lesions was visual landmark anchoring and not due to input from other modalities.

In order to further probe the effect of dLGN lesions on landmark anchoring precision, we correlated these values (for black-white and vertical-horizontal) with the lesion extent as assessed histologically (Section 5.3.1) using linear regression models in MATLAB. In both models, we saw a significant intercept estimate for the anchoring metric (black-white intercept: 0.83, $p < 10^{-5}$; vertical-horizontal intercept: 0.78, $p < 0.005$), indicating that in the absence of

Animal name	Lesion %	BW	VH	BB	doubled BW	doubled VH	doubled BB
R721	0.539	0.498	−0.116	−0.141	0.436	0.426	0.866
R777	0.831	−0.057	0.064	0.261	0.229	−0.020	0.179
R866	0.913	−0.065	N/A	−0.299	−0.235	N/A	0.338
R979	0.810	0.201	0.532	0.414	−0.070	0.232	−0.132
R968	0.610	0.629	0.099	N/A	0.559	0.671	N/A
R1004		0.632	−0.321	N/A	0.253	−0.086	N/A
R1005		0.986	N/A	−0.405	0.909	N/A	0.890
R882	0.001	0.864	0.612	−0.051	0.522	0.603	0.954
R867	0.000	0.791	0.710	−0.177	0.638	0.567	0.795
R880	0.000	0.719	0.998	−0.141	0.963	0.990	0.988
R954	0.000	0.877	0.961	0.138	0.595	0.733	0.991
R1013	0.000	0.543	0.978	0.192	0.582	0.914	0.132

Table 5.4: Summaries of lesion extent (as percentage of damaged dLGN) and anchoring success metrics for each individual animal. BW: black-white cue condition. VH: vertical-horizontal cue condition. BB: visally identical cue card condition (black-black and white-white).

dLGN lesion this metric is significantly greater than 0, and so HD cells anchor to the cues.

We also saw a significant negative correlation with lesion extent in both the black-white configuration ($\beta_{BW} = -0.955$, confidence interval -0.72 to -1.18, $p < 0.0005$) and vertical-horizontal configuration ($\beta_{VH} = -0.78$, confidence interval -0.09 to -1.48, $p < 0.05$). This indicates that landmark anchoring to non-ambiguous cues is more impaired in animals with larger lesions to the dLGN. This strongly indicates that the nucleus is involved in the processing of landmarks for use by the HD system in maintaining a world-aligned representation of orientation.

5.3.7 Quality of recorded HD cell clusters

A plausible confound that might explain the reported effects is that of the isolation quality of recorded cell clusters. For example, if lesioned animals displayed, in general, poorer cluster quality (and therefore were contaminated with more noise), this could cause HD cell tuning curves to become less clean. This could conceivably lead to reduced directionality (as measured by the Rayleigh vector), wider tuning curve widths, and more variable estimates of the PFD. In turn, greater error in the PFD estimates could cause the observation of worse anchoring across a session, due to an increased error in the estimates of PFD shift.

As such, controlling for cluster quality provides important evidence that the effect described above is not due to such confounding factors. We measured cluster quality using three metrics: L-ratio, isolation distance, and refractory period violations. There was no difference in L-ratio (Sham median: 0.32, Lesion median: 0.23, $z = -1.13$, $p > 0.25$, Wilcoxon ranksum test) or isolation distance (Sham median: 8.37, Lesion median: 10.1, $z = 1.15$, $p > 0.20$) of HD cell clusters between Lesion and Sham animals (see Figure 5.24), however there was evidence that

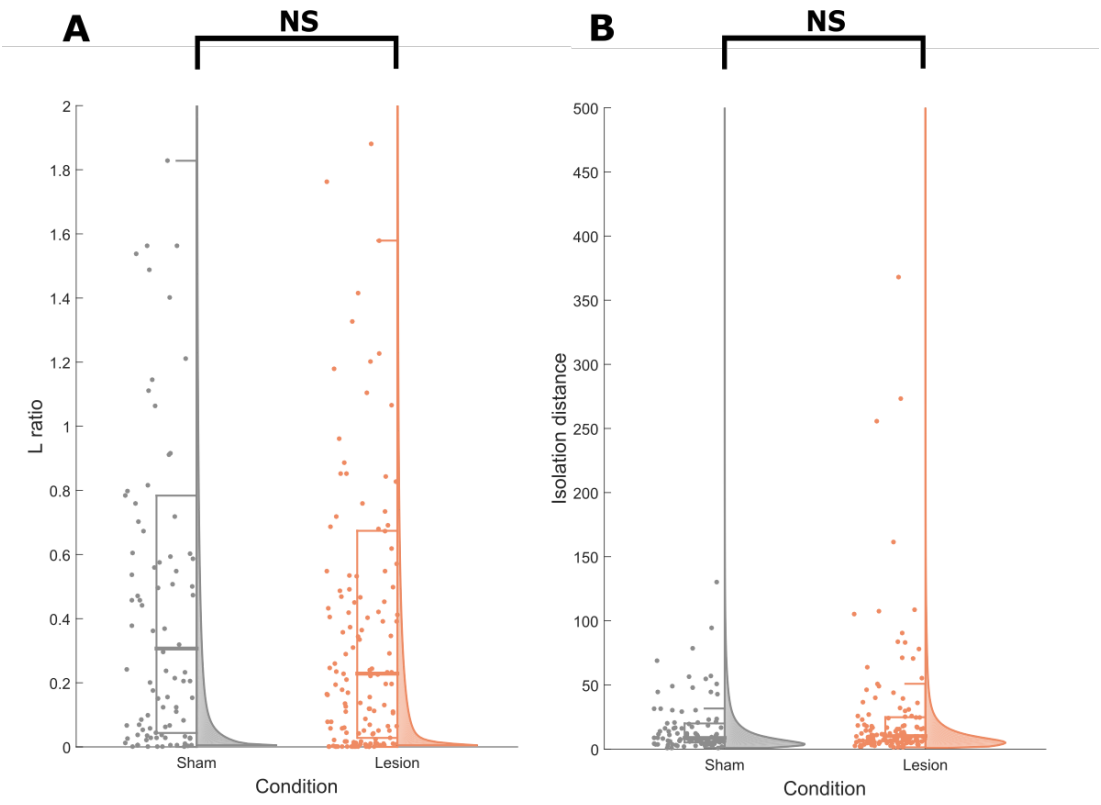

Figure 5.24: Summary of cluster quality statistics for sham and lesion HD cells. A: L ratio distribution. B: Isolation distance distribution.

HD cell clusters in Lesion animals displayed more spikes within the refractory period than clusters from Sham animals (Lesion: 0.168%, Sham: 0.039%, $z = 3.17$, $p < 0.002$). This indicates that, although the cluster isolation quality of HD cells was largely similar between Lesion and Sham animals, HD cell clusters from Lesion animals may have contained more noise spikes than those from Sham animals.

To assess whether this correlated with directional properties of HD cells, we ran Pearson correlations between cluster quality metrics and the HD cell characteristics affected by LGN lesions. In Lesion animals, there was no correlation between the percentage of refractory period spikes and R vector length ($\rho = 0.105, p > 0.30$) or tuning curve width ($\rho = -0.104$, $p > 0.30$), indicating that the differences in HD cell properties are not due to the noise contamination within the Lesion HD cell clusters. Similarly, no significant correlation existed between refractory period violations of Sham HD cells and R vector length ($\rho = -0.057, p > 0.50$) or tuning curve width ($\rho = 0.058, p > 0.50$). The percentage of refractory period violations for a given HD cell did not correlate significantly with its tendency to landmark anchor successfully in either Sham ($\rho = 0.084, p > 0.40$) or Lesion ($\rho = -0.102, p > 0.30$) animals.

As a consequence, we argue that the effects reported above are not confounded by cluster quality, as isolation metrics do not differ between animals and noise contamination is uncorre-

lated with HD cell directional properties.

5.3.8 Animal movement and behaviour

One plausible explanation for a decrease in the precision of the directional code stems from stereotypy in the animal's exploratory behaviour. For example, if HD cell drift is modelled as path integrative error accumulation, then a bias in turning direction (e.g. turning only clockwise), coupled with an inaccuracy in the gain of the transformation from velocity to displacement, may cause the tuning curve to drift.

As such, we extracted and analysed a number of properties of the animal's foraging behaviour from individual trials, to compare lesioned and sham groups. In general, Lesion animals displayed evidence of hyperactivity: the linear path distance travelled by the Lesion group was higher than Sham in both trials and sessions (median path distance per trial: Sham 1800 cm, $n = 258$ trials, Lesion 2510 cm, $n = 422$ trials; median path distance per session: Sham 14 500 cm; Lesion 19 600 cm, $n = 52$ sessions; see Figure 5.25). These path distances were significantly different for both trials ($z = 12.7$, $p < 10^{-36}$, Wilcoxon ranksum test) and sessions ($z = 5.44$, $p < 10^{-7}$, Wilcoxon ranksum test), indicating that Lesion animals moved more during recordings. Accordingly, the median linear speed was consistently higher in Lesion animals, for in both trials (Sham: $0.040\,\mathrm{cm\,s^{-1}}$, Lesion: $0.071\,\mathrm{cm\,s^{-1}}$, $z = 14.1$, $p < 10^{-44}$, Wilcoxon ranksum test) and across sessions (Sham: $0.040\,\mathrm{cm\,s^{-1}}$, Lesion: $0.069\,\mathrm{cm\,s^{-1}}$, $z = 5.67$, $p < 10^{-7}$, Wilcoxon ranksum test, also see Figure 5.25).

Similarly, Lesion animals turned a greater total (absolute) angle than Shams during both trials (median angular distance travelled per trial: Sham $2.22 \times 10^{6\circ}$, Lesion $2.76 \times 10^{6\circ}$, $z = 9.08$, $p < 10^{-18}$, Wilcoxon ranksum test) and sessions (median angular distance travelled per session: Sham $1.69 \times 10^{7\circ}$, Lesion , $2.18 \times 10^{7\circ}$, $z = 3.67$, $p < 10^{-3}$, Wilcoxon ranksum test), and correspondingly displayed a greater median angular head velocity across trials (Sham: $13.6\,^\circ\,\mathrm{s^{-1}}$, Lesion: $26.5\,^\circ\,\mathrm{s^{-1}}$, $z = 14.3$, $p < 10^{-45}$, Wilcoxon ranksum test) and sessions (Sham: $13.9\,^\circ\,\mathrm{s^{-1}}$, Lesion: $25.9\,^\circ\,\mathrm{s^{-1}}$, $z = 5.60$, $p < 10^{-7}$, Wilcoxon ranksum test, see Figure 5.26), further supporting the conclusion of hyperactivity following dLGN lesions.

Finally, there was some evidence that Lesion animals spent slightly more time near the walls than Sham animals over all trials (median percentage of time in inner half of apparatus, Sham: 54%, $n = 282$ trials; Lesion 52%, $n = 422$ trials), which reached statistical significance ($t = 2.33$, $p < 0.05$, two-sample t-test). This is, however, a small absolute difference, and a large variance was seen over all trials. Although the representations of some spatial cells – such as grid cells – may be stabilised by proximity to borders (Giocomo, 2016), it is unclear whether this difference would be sufficient to explain differences in HD cells following dLGN lesions.

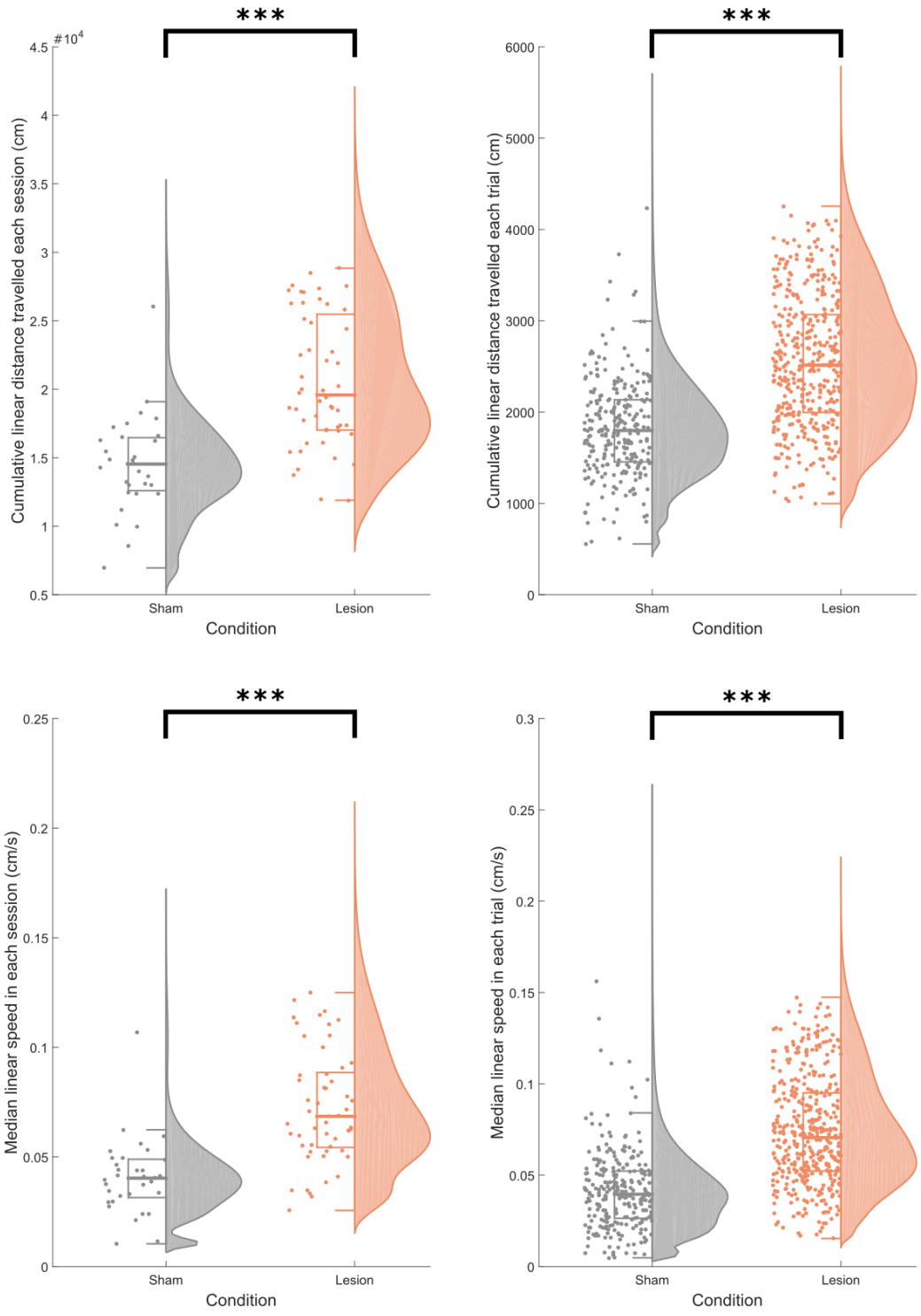

Figure 5.25: Summary of linear movement characteristics of sham and lesioned animals. Top left: Cumulative linear distance travelled in each session. Top right: Linear distance travelled in each trial. Bottom left: Median linear speed in each session. Bottom right: Median linear speed in each trial. *** indicates $p < 10^{-7}$.

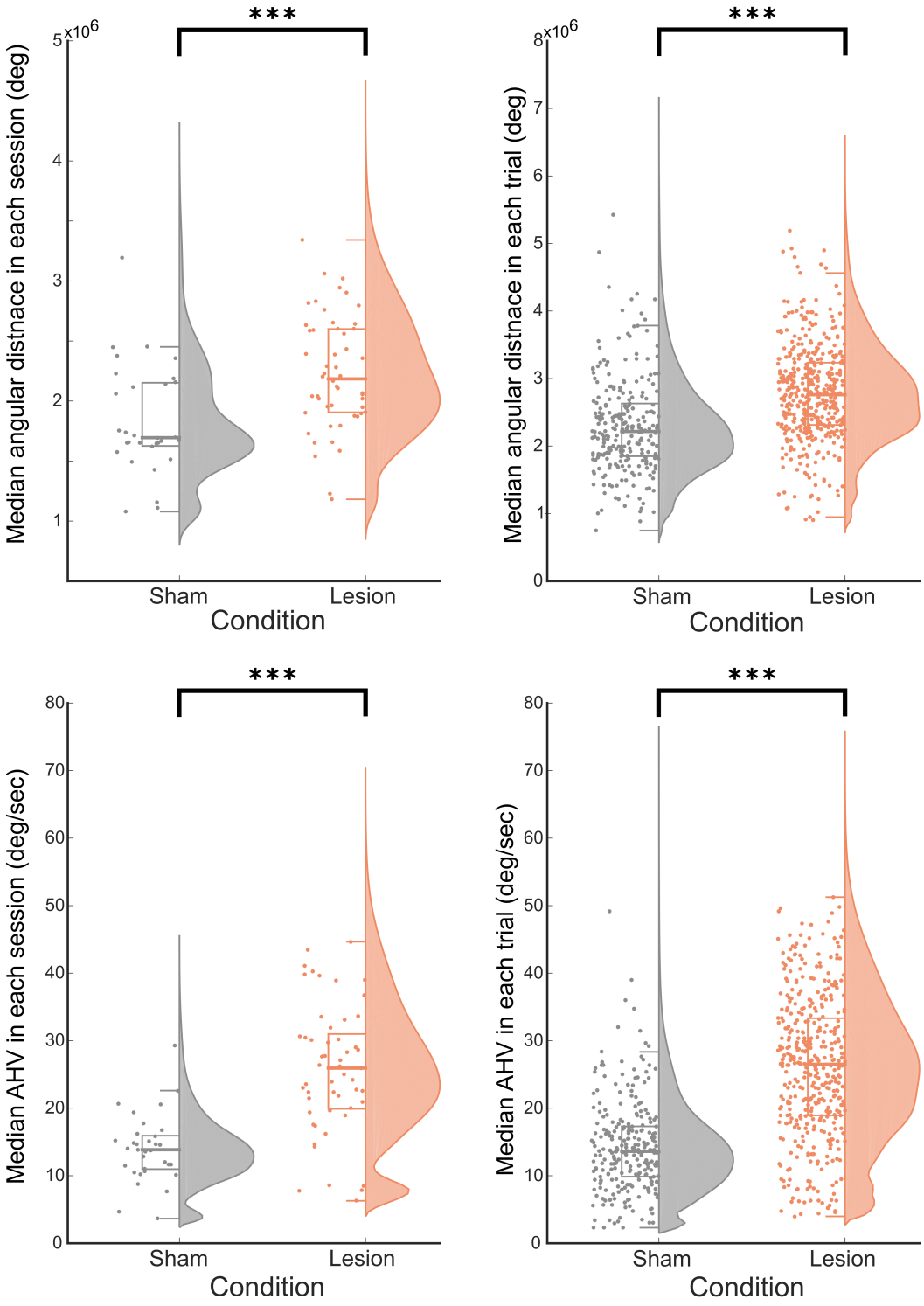

Figure 5.26: Summary of angular movement characteristics of sham and lesioned animals. Top left: Cumulative angular distance travelled in each session. Top right: Angular distance travelled in each trial. Bottom left: Median angular speed in each session. Bottom right: Median angular speed in each trial. *** indicates $p < 10^{-3}$.

5.4 Discussion

Here we present HD cells recorded in a landmark anchoring paradigm following excitotoxic lesions of the dLGN. This paradigm is known to exert good cue control over HD cells (Lozano et al., 2017), and was therefore chosen over the paradigm presented in Chapter 4 (as HD cells from animals recorded in this chapter varied in their anchoring behaviour). As discussed in this chapter, this may be due to the influence of olfactory cues, which may aid visual landmark learning in rats (Lavenex and Schenk, 1997), and that is coupled with the cues here.

Importantly, this paradigm used two cues attached on opposite sides of the cylinder, so as to assess whether the animal could detect the presence of the cues, and differentiate their visual content. As such, although the cues may possess olfactory or tactile content, evidence that HD cells were anchoring to the visual content of the cue cards could be tested using visually identical cards, which would create a 2-fold rotationally symmetric environment.

In animals with sham lesions of the dLGN, we observed a similar set of results to that observed before (Lozano et al., 2017): HD cells significantly anchored to and discriminated high contrast black-white cues and higher-acuity vertical-horizontal cues. Whereas Lozano et al. (2017) observed better anchoring to black-white cues than vertical-horizontal cues, we saw no difference in the precision of landmark anchoring (as assessed by the distributions of normalised PFD shifts) to these two configurations of cues.

We assessed that HD cells were anchoring to the visual content of the cards using two methods. By rotating the vertical-horizontal cards by 90°, we could swap the visual content of the cards. As such, we could assess whether HD cells anchored to the visual scene subtended by the cards, or to the physical cards themselves (which may have unique tactile or olfactory signatures). We also used visually identical cues to assess whether the animals anchored to the visual scene. If so, when placed in the apparatus at the beginning of a trial, an animal would not be able to disambiguate the visual scene from the 180°-rotated scene, due to its rotational symmetry. We observed evidence of a bimodal distribution of HD cell PFD shifts following rotations of these cues, indicating that although HD cells were anchoring to the visual scene, it was not able to disambiguate the cues. We argue this is due to the visual symmetry of the environment, and is evidence for the anchoring to be predominantly visual (Blair and Sharp, 2002).

In animals with lesions of the dLGN, we observed significantly worse landmark anchoring to all cue configurations tested. For high-contrast (black-white) cues, we observed that the distribution of PFD shifts following cue rotations was significantly less directional than that in sham animals, indicating that – averaged over all animals – anchoring to these cues was

disrupted. However, further investigation showed that anchoring to these cues varied between animals: some lesioned animals could still landmark anchor to the black-white cues, whereas some could not. We found that the degree of impairment of landmark anchoring to black-white cues correlated well with the extent of the excitotoxic lesion within the dLGN, indicating that larger disruptions of the geniculo-striate pathway lead to more severe impairments in the integration of vision into the HD signal. Indeed, animals with no evidence of landmark anchoring to black-white cues possessed extensive dLGN lesions.

That regions of intact dLGN following lesions may be sufficient to subtend some residual anchoring in the HD system is not surprising given that the dLGN possesses a weak retinotopy (Reese, 1988). However, demonstrating that the residual anchoring was due to spared dLGN rather than collicular involvement is difficult, and it remains possible that there is a collicular contribution to landmark integration in HD cells. Nevertheless, landmark anchoring was still impaired relative to sham controls in animals with partial dLGN lesions, indicating that visual processing in this region does propagate some information into the HD system.

Interestingly, lesioned animals show no evidence of anchoring to vertical-horizontal cues. As these consist of a single 'grating' oriented horizontally or vertically, these cues contain higher acuity visual information than the black-white cues. As such, smaller disruptions of the dLGN may lead to greater impairments in integrating more complex and higher acuity visual scenes. Angle-doubling of PFD shifts to vertical-horizontal cue rotations did not transform the shifts to a unimodal distribution (there was still no evidence of deviation from uniformity). This provides evidence that the HD cells could not detect the presence of the cue cards at all, and that any olfactory or tactile content of the cards was not sufficient to reorient the HD cell tuning curves. This provides further evidence that landmark anchoring was predominantly visual, consistent with previous studies (Goodridge et al., 1998) and with evidence indicating that visuospatial information is utilised by behaving rats solving spatial tasks, over conflicting local cue information (Lavenex and Schenk, 1995).

Similarly to in sham animals, we saw evidence of bimodal landmark anchoring to black-black cues in those animals that anchored successfully to black-white cues, but little evidence of bimodal anchoring in those animals that showed no anchoring to black-white cues. That the animals showed similar phenotypes of residual anchoring to black-white as to black-black cues is consistent with these cues being large and of similar salience, but indicates that they differ in disciminability (as would be expected for visual anchoring).

A surprising result was that we saw changes in some HD cell tuning curve characteristics following dLGN lesion. Although peak firing rate of HD cells was unchanged following lesions, HD cells in lesioned animals frequently displayed wider tuning curves than those in sham

animals. We found this was due to an increase in PFD drift over time, which caused tuning curves to appear wider when averaged over a whole trial.

In blindfolded rats, HD cells are seen to drift at approximately $23^\circ \pm 6^\circ$ over an 8 minute trial (Goodridge et al., 1998). An explanation for this is that, without visual input to anchor the HD cell firing, the system is likely to accumulate error as a path integrator (Tocker et al., 2018). As we see this drift in lesioned animals, this could be explained by HD cells in these animals not having access to visual information to maintain an anchored representation of direction. This is consistent with the other findings reported above.

A surprising finding was that, in general, HD cells appeared to behave less coherently following the lesion. However, we considered this finding consistent with what would be observed when sampling inhomogeneously from HD cells in a drifting attractor. That is, if HD cells are likely to be drifting over time, then two cells with opposed PFDs will have greater time in between successive trajectories through each PFD – and so observed angle between the cell PFDs will be variable, depending on the animal sampling in that trial. Consistent with this, we saw that cells with closer PFDs were more likely to remain coherent through a session than those with opposed PFDs. Therefore we consider it a possibility that HD cell drift caused decreases in estimated coherence across trials.

Overall, our findings demonstrate that landmark anchoring is severely impaired in PoS HD cells following lesions of the dLGN, with HD cells less consistently shifting their tuning curves to follow rotations of visual cue cards, and increases in attractor drift within individual trials. Although some residual anchoring exists, this is significantly less precise than anchoring in animals with sham lesions, and the observed impairment of landmark anchoring correlated well with the lesion extent. As such, we consider that the dLGN plays an important role in the of visual pathways for landmark processing in the rodent brain.

Chapter 6

General Discussion

> Die allgemeine Form der Wahrheitsfunktion ist: $[\bar{p}, \bar{\xi}, N(\bar{\xi})]$.
>
> The general form of truth-function is: $[\bar{p}, \bar{\xi}, N(\bar{\xi})]$.
>
> TLP 6; Wittgenstein (1922)

In this thesis, two experiments have been presented that aim to elucidate how vision exerts cue control over HD cells in the rodent brain. It is well observed that HD cells can use visual landmarks to reorient and reset their preferred directions, in order to maintain a consistent representation of spatial orientation relative to the outside world. In this thesis, we present two experiments that add to existing literature concerning how vision is integrated into this representation.

Although a substantial body of literature exists that addresses how vestibular information contributes to HD cell activity (Yoder and Taube, 2014; Cullen and Taube, 2017), leading to a large number of models proposed models to explain in some detail how angular head velocity signals are integrated to a representation of direction (Zhang, 1996), the overarching question remains of how HD cells integrate visual information from a scene into a representation of spatial orientation, so as to recalibrate or reset their tuning curves. In particular, does the system need discrete landmarks with distinct visual features, which can be associated with allocentric directions, to orient? Does the system require intact cortical visual processing, or can it rely solely on input from subcortical pathways via the superior colliculus? Although some models exist that aim to explain how visual landmark information could be used by the HD system (Bicanski and Burgess, 2016; Page and Jeffery, 2018), these models often rely on assumptions about how this information reaches HD cells – for example, visual rings of putative landmark cells, that are active whenever a discrete landmark is visible to the rat, could provide a directional input if the landmark is distal enough to occupy a stable location in the animal's

visual field (Page and Jeffery, 2018).

Two broad categories of model have been proposed that describe how visual information could be incorporated into rodent neural spatial representations. In one model (Knierim and Hamilton, 2011), distal sensory information (such as visual features on distal landmarks) set the orientation of HD cells relative to the external world, and local boundary information sets the scales of the spatial maps represented by place and grid cell firing. Together, this information can be used to compute an estimate of self-location.

The other model proposes that the entire visual image on the retina could be used to orient HD cell tuning. In this case, specific features on known landmarks are less important for orienting HD cell activity, but global features in the visual panorama could provide the relevant directional input to the HD system (Zeil, 2012). Indeed, models using view-based scene matching of the current visual panorama with a remembered image accurate emulate rotational errors made by rats when trained to approach a particular corner in a rectangular box (Stürzl et al., 2008), and generates similar search trajectories as behaving rats (Cheung et al., 2008). Some simulations have showed that low resolution visual information is optimal for spatial orienting in ants (Wystrach et al., 2016). Together these models suggest that low spatial frequency information could be integrated into representations of orientation in the rodent brain without the need for feature-based landmarks containing high spatial frequency information.

Our first experiment recorded HD cells in a cue control paradigm, comparing a visual panorama that contained sudden, step-wise changes in contrast (shifts from black-to-grey and grey-to-black), akin to what would be seen if a standard cue card with edges were used, to a continuous visual gradient with no edges. When cue control was achieved in the apparatus, HD cells were able to landmark anchor to both panoramas used. The lack of any discrete, point-landmarks in the gradient cue indicated that the HD system could integrate some visual information from the entirety of the panorama – as would be consistent with a view-based model. However, the anchoring was less precise than that seen with the control gradient. Although this is not inconsistent with a view-based model (e.g. that might scene-match the panorama), it strongly implies that some visual features – such as edges – can provide stronger directional information into the HD system.

In Chapter 5, we assessed whether the geniculo-striate pathway is necessary for the integration of visual information into the HD system. For this, we used a previously published landmark anchoring paradigm (Lozano et al., 2017), which is known to achieve reliable cue control, rather than the method reported in Chapter 4.

We found that, following lesions of the dorsal lateral geniculate nucleus (dLGN), landmark

anchoring of PoS HD cells was significantly impaired to all cue configurations tested. However, in the black-white cue condition, there was still statistically significant evidence of residual cue control; this was not present in sessions using vertical-horizontal cues. Nonetheless this impairment indicates a role for the dLGN and geniculo-striate pathway in the processing of visual landmarks.

That the dLGN is strongly implicated in the processing of vision for landmark integration is surprising given that the superior colliculus is evolutionarily older than the complex organisation of visual cortex in rodents and other mammals (Vanegas, 1984; Northcutt, 2002). HD cells have been recorded and are seen to process visual information in a number of species – such as the fly (Seelig and Jayaraman, 2015) – and so the representation of orientation in space may be expected to have emerged early in the taxonomic hierarchy. This might imply that the structures involved in generating and maintaining this representation, including those that integrate allothetic information into the representation, also was evolved early. The optic tectum (superior colliculus) has been highly conserved through evolution (Northcutt, 2002; Maximino, 2008). One role of the tectum has been summarised as "to localize a stimulus in space and to cause the animal to orient to the stimulus by moving its neck and/or its eyes" (Butler and Hodos, 2005, p. 311). As such, the superior colliculus seems likely to contain visuospatial representations of space, and thereby may be well-positioned to extract spatial components from prominent visual features such as landmarks and panoramas.

We considered two main possibilities to explain the residual anchoring we observed to black-white cues: intact islands of dLGN post-lesion, and contributions of subcortical visual pathways (likely through collicular-pulvinar-extrastriate connections) to HD anchoring. For example, if areas of V2M contributed landmark information to cortical HD areas (such as the postero-medial area), intact projections from the pulvinar or colliculus to here could in principle drive a subset of neurons, that could input this residual information into the HD system. Alternatively, intact dLGN – as it is broadly retinotopic – could contain preserved local circuits that can project visual information from the corresponding part of the retina through the visual pathway and into the HD system.

Although these possibilities are difficult to separate, we note that a subset of animals (with complete or near-complete dLGN lesions) showed no evidence of anchoring to any cue cards tested. We saw that the severity of impairment of landmark anchoring correlated well with lesion extent inside dLGN. As such, we propose that the more likely explanation is that residual anchoring was due to small areas of intact dLGN remaining after the lesion, and that complete destruction of the dLGN obliterated cue control of HD cells.

This interpretation does not rule out any involvement of the superior colliculus. It is known

that the superior colliculus sends a notable projection into dLGN (Bickford et al., 2015). This projection may relay information relevant to landmark processing – and so these data cannot rule out any general contributions of the superior colliculus to landmark integration within the HD system, and future work could test the functional and behavioural significance of this projection using targeted methods such as chemogenetics or optogenetics. There is evidence that visually evoked responses in V1 are modulated by superior colliculus, and that this occurs through gain modulation of dLGN (Ahmadlou et al., 2018). dLGN lesions will similarly disrupt processing through this pathway.

Nonetheless, it appears that any residual anchoring provided by the superior colliculus following dLGN lesions, is small and notably less precise (if present at all). Taking only those animals with significant residual anchoring to black-white cues, HD cells were still significantly less precisely controlled by cue rotations than in sham animals.

The minor role of the superior colliculus in HD cell landmark anchoring is consistent with previous reports that have assessed landmark integration in the HD system. Unpublished observations in the Master's thesis of Rodriguez (2017) showed that unilateral inactivation of the superficial layers of the superior colliculus by infusions of muscimol did not obliterate landmark anchoring of ADN HD cells to rotations of a white cue card in a cylinder. HD cells shifted their tuning curves non-randomly to follow 90° rotations of the cue card in muscimol-infused animals, although with a larger angular dispersion than in saline-infused animals. As such, it appears that any impairment in landmark anchoring following muscimol infusion into sSC is minor. However, it should be noted that in this work, sSC was only unilaterally inactivated, and as such the non-infused hemisphere may subtend enough information to enable cue control. Moreover, histology of the infusion spread was not presented, and so the extent of inactivation cannot be determined.

In other work, lesions of primary visual cortex also appear to disrupt landmark anchoring in place cells (Paz-Villagràn et al., 2002), which are believed to be situated downstream of HD cells. These authors used objects placed against the walls of a cylindrical arena to create a scene with landmarks; rotations of the objects did not cause rotations of the place cell firing fields following V1 lesions, but did in sham animals. Similarly as in our experiment in Chapter 5, this was in spite of some presumed tactile and olfactory content to the objects that could theoretically have provided an anchoring stimulus.

Place cells are considered to receive information from HD cells. Indeed, CA1 place cells and HD cells tend to rotate coherently following rotations of a distal landmark (Zugaro et al., 2001), and lesions of the HD system (ADN or PoS) disrupted the stability of place cells in CA1 (Calton et al., 2003). Importantly, in this study, place cells in animals with lesions of the

HD system did not rotate to follow visual landmark rotations, but shifted randomly between trials. This indicates that the HD system may provide some landmark information into the hippocampus, and thereby implicates the geniculo-striate pathway, through primary visual cortex, in processing this information, and we consider our results to broadly agree with those seen in Paz-Villagràn et al. (2002).

The role of the geniculo-striate pathway in landmark processing can be further investigated in experiments utilising lesions or inactivations downstream in the visual system. For example, the direct projections from V1 into PoS and RSC may convey landmark information. These projections could be targeted using genetic techniques, and inactivated, to assess the contributions of these projections to landmark integration in HD cells. An alternative pathway is via extrastriate cortex, many regions of which project to PoS and RSC, and has been shown to contain HD cells. In a similar way, these regions could be inactivated to test landmark processing by these areas.

Overall, our contributions show that the HD system can use visual panoramas with no discontinuities to reset its orientation, but this process is more precise if visual features like point-landmarks, such as distinct changes in contrast, are present in the scene. Cue integration into the HD system appears to depend on the geniculo-striate visual pathway, with disruptions of the dLGN severely impairing landmark anchoring in HD cells. As such, the rodent brain is able to process a large array of visual scenes to be integrated into spatial representations, although this process may be performed by the evolutionarily newer, and higher-acuity, cortical vision.

> Wovon man nicht sprechen kann, darüber muss man schweigen.
>
> Whereof one cannot speak, thereof one must be silent.
>
> ---
>
> TLP 7; Wittgenstein (1922)

Bibliography

Abbasi, S. and Kumar, S. S. (2013). Electrophysiological and morphological characterization of cells in superficial layers of rat presubiculum. *Journal of Comparative Neurology*, 521(13):3116–3132.

Aggleton, J. P., Hunt, P. R., Nagle, S., and Neave, N. (1996). The effects of selective lesions within the anterior thalamic nuclei on spatial memory in the rat. *Behavioural Brain Research*, 81(1):189–198.

Aggleton, J. P. and Nelson, A. J. D. (2015). Why do lesions in the rodent anterior thalamic nuclei cause such severe spatial deficits? *Neuroscience and biobehavioral reviews*, 54:131–144. 25195980[pmid] PMC4462592[pmcid] S0149-7634(14)00211-5[PII].

Agster, K. L. and Burwell, R. D. (2009). Cortical efferents of the perirhinal, postrhinal, and entorhinal cortices of the rat. *Hippocampus*, 19(12):1159–1186.

Agster, K. L., Tomás Pereira, I., Saddoris, M. P., and Burwell, R. D. (2016). Subcortical connections of the perirhinal, postrhinal, and entorhinal cortices of the rat. ii. efferents. *Hippocampus*, 26(9):1213–1230. 27101786[pmid] PMC5070461[pmcid].

Ahmadlou, M., Tafreshiha, A., and Heimel, J. A. (2017). Visual cortex limits pop-out in the superior colliculus of awake mice. *Cerebral Cortex*, 27(12):5772–5783.

Ahmadlou, M., Zweifel, L. S., and Heimel, J. A. (2018). Functional modulation of primary visual cortex by the superior colliculus in the mouse. *Nature communications*, 9(1):3895–3895. 30254324[pmid] PMC6156231[pmcid] 10.1038/s41467-018-06389-6[PII] Nat Commun.

Albo, Z., Viana Di Prisco, G., and Vertes, R. (2006). Anterior thalamic unit discharge profiles and coherence with hippocampal theta rhythm. *Thalamus & Related Systems*, 2(2):133–144.

Alexander, A. S., Carstensen, L. C., Hinman, J. R., Raudies, F., Chapman, G. W., and Hasselmo, M. E. (2019). Egocentric boundary vector tuning of the retrosplenial cortex. *bioRxiv*, page 702712.

Allen, A. E., Procyk, C. A., Howarth, M., Walmsley, L., and Brown, T. M. (2016). Visual input to the mouse lateral posterior and posterior thalamic nuclei: photoreceptive origins and retinotopic order. *The Journal of physiology*, 594(7):1911–1929. 26842995[pmid] PMC4818601[pmcid] J Physiol.

Allen, M., Poggiali, D., Whitaker, K., Marshall, T., and Kievit, R. (2019). Raincloud plots: a multi-platform tool for robust data visualization [version 1; peer review: 2 approved]. *Wellcome Open Research*, 4(63).

Alyan, S. and Jander, R. (1994). Short-range homing in the house mouse, mus musculus: stages in the learning of directions. *Animal Behaviour*, 48(2):285–298.

Amaral, D. G., Dolorfo, C., and Alvarez-Royo, P. (1991). Organization of ca1 projections to the subiculum: A pha-l analysis in the rat. *Hippocampus*, 1(4):415–435.

Amaral, D. G. and Witter, M. P. (1995). *Hippocampal formation*, pages 247–291. Academic Press, New York.

American Psychiatric Association (2013). *Diagnostic and statistical manual of mental disorders*. Author, Arlington, VA, 5th ed. edition.

Barker, G. R. and Warburton, E. C. (2018). A critical role for the nucleus reuniens in long-term, but not short-term associative recognition memory formation. *The Journal of Neuroscience*, 38(13):3208–3217.

Barry, C. and Burgess, N. (2017). To be a grid cell: Shuffling procedures for determining "gridness". *bioRxiv*, page 230250.

Barry, C., Lever, C., Hayman, R., Hartley, T., Burton, S., O'Keefe, J., Jeffery, K., and Burgess, N. (2006). The boundary vector cell model of place cell firing and spatial memory. *Reviews in the neurosciences*, 17(1-2):71–97.

Bassett, J. P. and Taube, J. S. (2001). Neural correlates for angular head velocity in the rat dorsal tegmental nucleus. *The Journal of Neuroscience*, 21(15):5740–5751.

Bassett, J. P., Tullman, M. L., and Taube, J. S. (2007). Lesions of the tegmentomammillary circuit in the head direction system disrupt the head direction signal in the anterior thalamus. *The Journal of Neuroscience*, 27(28):7564–7577.

Beltramo, R. and Scanziani, M. (2019). A collicular visual cortex: Neocortical space for an ancient midbrain visual structure. *Science*, 363(6422):64–69.

Benhamou, S. (1997). Path integration by swimming rats. *Animal Behaviour*, 54(2):321–327.

Bennett, C., Gale, S. D., Garrett, M. E., Newton, M. L., Callaway, E. M., Murphy, G. J., and Olsen, S. R. (2019). Higher-order thalamic circuits channel parallel streams of visual information in mice. *Neuron*, 102(2):477–492.e5.

Bennett, M. and Hacker, P. (2003). *Philosophical Foundations of Neuroscience*. Wiley-Blackwell.

Berens, P. (2009). Circstat: A matlab toolbox for circular statistics. *2009*, 31(10):21.

Berezovskii, V. K., Nassi, J. J., and Born, R. T. (2011). Segregation of feedforward and feedback projections in mouse visual cortex. *The Journal of comparative neurology*, 519(18):3672–3683. 21618232[pmid] PMC3219532[pmcid].

Berkowitz, L. E., Ybarra, I., Jones, J. A., Amato, M. E., Rodriguez, A. M., and Calton, J. L. (2015). Nmda blockade inhibits experience-dependent modification of anterior thalamic head direction cells. *Behavioral Neuroscience*, 129(2):113–128.

Berman, D., Golomb, J. D., and Walther, D. B. (2017). Scene content is predominantly conveyed by high spatial frequencies in scene-selective visual cortex. *PLOS ONE*, 12(12):e0189828.

Bett, D., Wood, E. R., and Dudchenko, P. A. (2012). The postsubiculum is necessary for spatial alternation but not for homing by path integration. *Behavioral Neuroscience*, 126(2):237–248.

Biazoli Jr, C. E., Goto, M., Campos, A. M. P., and Canteras, N. S. (2006). The supragenual nucleus: A putative relay station for ascending vestibular signs to head direction cells. *Brain Research*, 1094(1):138–148.

Bicanski, A. and Burgess, N. (2016). Environmental anchoring of head direction in a computational model of retrosplenial cortex. *The Journal of Neuroscience*, 36(46):11601–11618.

Bickford, M. E., Zhou, N., Krahe, T. E., Govindaiah, G., and Guido, W. (2015). Retinal and tectal "driver-like" inputs converge in the shell of the mouse dorsal lateral geniculate nucleus. *The Journal of neuroscience : the official journal of the Society for Neuroscience*, 35(29):10523–10534. 26203147[pmid] PMC4510292[pmcid] 35/29/10523[PII].

Bishop, P. O., Kozak, W., Levick, W. R., and Vakkur, G. J. (1962). The determination of the projection of the visual field on to the lateral geniculate nucleus in the cat. *The Journal of physiology*, 163(3):503–539. 13971234[pmid] PMC1359721[pmcid].

Bjerknes, T. L., Langston, R. F., Kruge, I. U., Moser, E. I., and Moser, M.-B. (2015). Coherence among head direction cells before eye opening in rat pups. *Current biology : CB*, 25(1):103–108. 25466682[pmid] PMC4291142[pmcid] S0960-9822(14)01436-5[PII].

Blair, H. and Sharp, P. (1995). Anticipatory head direction signals in anterior thalamus: evidence for a thalamocortical circuit that integrates angular head motion to compute head direction. *The Journal of Neuroscience*, 15(9):6260–6270.

Blair, H. and Sharp, P. (2002). *Functional Organisation of the Rat Head-Direction Circuit*, book section 9, pages 163–182. Springer, New York.

Blair, H. T., Cho, J., and Sharp, P. E. (1998). Role of the lateral mammillary nucleus in the rat head direction circuit: A combined single unit recording and lesion study. *Neuron*, 21(6):1387–1397.

Blair, H. T., Cho, J., and Sharp, P. E. (1999). The anterior thalamic head-direction signal is abolished by bilateral but not unilateral lesions of the lateral mammillary nucleus. *The Journal of Neuroscience*, 19(15):6673–6683.

Boccara, C. N., Sargolini, F., Thoresen, V. H., Solstad, T., Witter, M. P., Moser, E. I., and Moser, M.-B. (2010). Grid cells in pre- and parasubiculum. *Nature Neuroscience*, 13:987.

Boucheny, C., Brunel, N., and Arleo, A. (2005). A continuous attractor network model without recurrent excitation: Maintenance and integration in the head direction cell system. *Journal of Computational Neuroscience*, 18(2):205–227.

Bovet, J. (1984). Strategies of homing behavior in the red squirrel, tamiasciurus hudsonicus. *Behavioral Ecology and Sociobiology*, 16(1):81–88.

Brandon, M., Koenig, J., Leutgeb, J., and Leutgeb, S. (2014). New and distinct hippocampal place codes are generated in a new environment during septal inactivation. *Neuron*, 82(4):789–796.

Brandon, M. P., Bogaard, A. R., Libby, C. P., Connerney, M. A., Gupta, K., and Hasselmo, M. E. (2011). Reduction of theta rhythm dissociates grid cell spatial periodicity from directional tuning. *Science*, 332(6029):595–599.

Brandon, M. P., Bogaard, A. R., Schultheiss, N. W., and Hasselmo, M. E. (2013). Segregation of cortical head direction cell assemblies on alternating theta cycles. *Nature Neuroscience*, 16:739.

Brown, J. E., Card, J. P., and Yates, B. J. (2005). Polysynaptic pathways from the vestibular nuclei to the lateral mammillary nucleus of the rat: substrates for vestibular input to head direction cells. *Experimental Brain Research*, 161(1):47–61.

Brown, J. E. and Rojas, J. A. (1965). Rat retinal ganglion cells: Receptive field organization and maintained activity. *Journal of Neurophysiology*, 28(6):1073–1090.

Burgess, N. (2006). *Computational Models of the Spatial and Mnemonic Functions of the Hippocampus*. Oxford University Press, New York.

Burgess, N. and O'Keefe, J. (1996). Neuronal computations underlying the firing of place cells and their role in navigation. *Hippocampus*, 6(6):749–762.

Burwell, R. D. and Amaral, D. G. (1998). Cortical afferents of the perirhinal, postrhinal, and entorhinal cortices of the rat. *Journal of Comparative Neurology*, 398(2):179–205.

Burwell, R. D. and Hafeman, D. M. (2003). Positional firing properties of postrhinal cortex neurons. *Neuroscience*, 119(2):577–588.

Burwell, R. D., Witter, M. P., and Amaral, D. G. (1995). Perirhinal and postrhinal cortices of the rat: A review of the neuroanatomical literature and comparison with findings from the monkey brain. *Hippocampus*, 5(5):390–408.

Bush, D., Barry, C., and Burgess, N. (2014). What do grid cells contribute to place cell firing? *Trends in Neurosciences*, 37(3):136–145.

Butler, A. and Hodos, W. (2005). *Comparative vertebrate neuroanatomy: evolution and adaptation*. John Wiley & Sons, Hoboken, NJ.

Butler, W. N., Smith, K. S., van der Meer, M. A. A., and Taube, J. S. (2017). The head-direction signal plays a functional role as a neural compass during navigation. *Current Biology*, 27(9):1259–1267.

Butler, W. N. and Taube, J. S. (2015). The nucleus prepositus hypoglossi contributes to head direction cell stability in rats. *The Journal of Neuroscience*, 35(6):2547–2558.

Cacucci, F., Lever, C., Wills, T. J., Burgess, N., and O'Keefe, J. (2004). Theta-modulated place-by-direction cells in the hippocampal formation in the rat. *The Journal of neuroscience : the official journal of the Society for Neuroscience*, 24(38):8265–8277. 15385610[pmid] PMC2683733[pmcid] 24/38/8265[PII] J Neurosci.

Calton, J. L., Stackman, R. W., Goodridge, J. P., Archey, W. B., Dudchenko, P. A., and Taube, J. S. (2003). Hippocampal place cell instability after lesions of the head direction cell network. *The Journal of Neuroscience*, 23(30):9719.

Calton, J. L., Turner, C. S., Cyrenne, D.-L. M., Lee, B. R., and Taube, J. S. (2008). Landmark control and updating of self-movement cues are largely maintained in head direction cells after lesions of the posterior parietal cortex. *Behavioral Neuroscience*, 122(4):827–840.

Canto, C. B., Koganezawa, N., Beed, P., Moser, E. I., and Witter, M. P. (2012). All layers of medial entorhinal cortex receive presubicular and parasubicular inputs. *The Journal of Neuroscience*, 32(49):17620–17631.

Chen, L. L., Lin, L.-H., Barnes, C. A., and McNaughton, B. L. (1994a). Head-direction cells in the rat posterior cortex ii. contributions of visual and ideothetic information to the directional firing. *Experimental Brain Research*, 101(1):24–34.

Chen, L. L., Lin, L.-H., Green, E. J., Barnes, C. A., and McNaughton, B. L. (1994b). Head-direction cells in the rat posterior cortex i. anatomical distribution and behavioral modulation. *Experimental Brain Research*, 101(1):8–23.

Cheng, K. (1986). A purely geometric module in the rat's spatial representation. *Cognition*, 23(2):149–178.

Cheung, A., Stürzl, W., Zeil, J., and Cheng, K. (2008). The information content of panoramic images ii: View-based navigation in nonrectangular experimental arenas. *Journal of Experimental Psychology: Animal Behavior Processes*, 34(1):15–30.

Cho, J. and Sharp, P. E. (2001). Head direction, place, and movement correlates for cells in the rat retrosplenial cortex. *Behavioral Neuroscience*, 115(1):3–25.

Choi, D. W. (1992). Excitotoxic cell death. *Journal of Neurobiology*, 23(9):1261–1276.

Cisek, P. (2012). Making decisions through a distributed consensus. *Current Opinion in Neurobiology*, 22(6):927–936.

Clark, B. J., Bassett, J. P., Wang, S. S., and Taube, J. S. (2010). Impaired head direction cell representation in the anterodorsal thalamus after lesions of the retrosplenial cortex. *The Journal of Neuroscience*, 30(15):5289–5302.

Clark, B. J., Brown, J. E., and Taube, J. S. (2012a). Head direction cell activity in the anterodorsal thalamus requires intact supragenual nuclei. *Journal of neurophysiology*, 108(10):2767–2784. 22875899[pmid] PMC3545120[pmcid] jn.00295.2012[PII].

Clark, B. J., Harris, M. J., and Taube, J. S. (2012b). Control of anterodorsal thalamic head direction cells by environmental boundaries: Comparison with conflicting distal landmarks. *Hippocampus*, 22(2):172–187.

Clark, B. J., Sarma, A., and Taube, J. S. (2009). Head direction cell instability in the anterior dorsal thalamus after lesions of the interpeduncular nucleus. *The Journal of Neuroscience*, 29(2):493–507.

Clark, B. J. and Taube, J. S. (2011). Intact landmark control and angular path integration by head direction cells in the anterodorsal thalamus after lesions of the medial entorhinal cortex. *Hippocampus*, 21(7):767–782.

Clark, B. J. and Taube, J. S. (2012). Vestibular and attractor network basis of the head direction cell signal in subcortical circuits. *Frontiers in Neural Circuits*, 6(7).

Clemens, L. E., Jansson, E. K. H., Portal, E., Riess, O., and Nguyen, H. P. (2014). A behavioral comparison of the common laboratory rat strains lister hooded, lewis, fischer 344 and wistar in an automated homecage system. *Genes, Brain and Behavior*, 13(3):305–321.

Coleman, K. A. and Mitrofanis, J. (1996). Organization of the visual reticular thalamic nucleus of the rat. *European Journal of Neuroscience*, 8(2):388–404.

Conrad, C. D. and Stumpf, W. E. (1975). Direct visual input to the limbic system: Crossed retinal projections to the nucleus anterodorsalis thalami in the tree shrew. *Experimental Brain Research*, 23(2):141–149.

Coogan, T. and Burkhalter, A. (1993). Hierarchical organization of areas in rat visual cortex. *The Journal of Neuroscience*, 13(9):3749–3772.

Crabtree, J. W. (2018). Functional diversity of thalamic reticular subnetworks. *Frontiers in Systems Neuroscience*, 12(41).

Cressant, A., Muller, R. U., and Poucet, B. (1997). Failure of centrally placed objects to control the firing fields of hippocampal place cells. *The Journal of Neuroscience*, 17(7):2531–2542.

Cruz-Martín, A., El-Danaf, R. N., Osakada, F., Sriram, B., Dhande, O. S., Nguyen, P. L., Callaway, E. M., Ghosh, A., and Huberman, A. D. (2014). A dedicated circuit links direction-selective retinal ganglion cells to the primary visual cortex. *Nature*, 507(7492):358–361. 24572358[pmid] PMC4143386[pmcid] nature12989[PII].

Cullen, K. E. and Taube, J. S. (2017). Our sense of direction: progress, controversies and challenges. *Nature Neuroscience*, 20:1465.

Darwin, C. (1873). Origin of certain instincts. *Nature*, 7(179):417–418.

De Franceschi, G. and Solomon, S. G. (2018). Visual response properties of neurons in the superficial layers of the superior colliculus of awake mouse. *The Journal of physiology*, 596(24):6307–6332. 30281795[pmid] PMC6292807[pmcid] J Physiol.

Dean, P. (1978). Visual acuity in hooded rats: Effects of superior collicular or posterior neocortical lesions. *Brain Research*, 156(1):17–31.

Dean, P. (1981a). Grating detection and visual acuity after lesions of striate cortex in hooded rats. *Experimental Brain Research*, 43(2):145–153.

Dean, P. (1981b). Visual pathways and acuity in hooded rats. *Behavioural Brain Research*, 3(2):239–271.

Derdikman, D. (2009). Are the boundary-related cells in the subiculum boundary-vector cells? *The Journal of Neuroscience*, 29(43):13429–13431.

Deshmukh, S. S. and Knierim, J. J. (2011). Representation of non-spatial and spatial information in the lateral entorhinal cortex. *Frontiers in behavioral neuroscience*, 5:69–69. 22065409[pmid] PMC3203372[pmcid].

Dillingham, C. M., Frizzati, A., Nelson, A. J. D., and Vann, S. D. (2015). How do mammillary body inputs contribute to anterior thalamic function? *Neuroscience and biobehavioral reviews*, 54:108–119. 25107491[pmid] PMC4462591[pmcid] S0149-7634(14)00190-0[PII].

Dima, D. C., Perry, G., and Singh, K. D. (2018). Spatial frequency supports the emergence of categorical representations in visual cortex during natural scene perception. *NeuroImage*, 179:102–116.

Dreher, B., Sefton, A. J., Ni, S. Y. K., and Nisbett, G. (1985). The morphology, number, distribution and central projections of class i retinal ganglion cells in albino and hooded rats (part 1 of 3). *Brain, Behavior and Evolution*, 26(1):10–22.

Dudchenko, P. A., Goodridge, J. P., and Taube, J. S. (1997). The effects of disorientation on visual landmark control of head direction cell orientation. *Experimental Brain Research*, 115(2):375–380.

Dudchenko, P. A. and Taube, J. S. (1997). Correlation between head direction cell activity and spatial behavior on a radial arm maze. *Behavioral Neuroscience*, 111(1):3–19.

Dudchenko, P. A., Wood, E. R., and Smith, A. (2019). A new perspective on the head direction cell system and spatial behavior. *Neuroscience & Biobehavioral Reviews*, 105:24–33.

Dudchenko, P. A. and Zinyuk, L. E. (2005). The formation of cognitive maps of adjacent environments: Evidence from the head direction cell system. *Behavioral Neuroscience*, 119(6):1511–1523.

Eacott, M. J. and Gaffan, E. A. (2005). The roles of perirhinal cortex, postrhinal cortex, and the fornix in memory for objects, contexts, and events in the rat. *The Quarterly Journal of Experimental Psychology Section B*, 58(3-4b):202–217.

Elduayen, C. and Save, E. (2014). The retrosplenial cortex is necessary for path integration in the dark. *Behavioural Brain Research*, 272:303–307.

Ellis, E. M., Gauvain, G., Sivyer, B., and Murphy, G. J. (2016). Shared and distinct retinal input to the mouse superior colliculus and dorsal lateral geniculate nucleus. *Journal of neurophysiology*, 116(2):602–610. 27169509[pmid] PMC4982907[pmcid] jn.00227.2016[PII] J Neurophysiol.

Erişir, A., Van Horn, S., and Sherman, S. (1997). Relative numbers of cortical and brainstem inputs to the lateral geniculate nucleus. *Proceedings of the National Academy of Sciences*, 94(4):1517–1520.

Erlich, J. C., Bialek, M., and Brody, C. D. (2011). A cortical substrate for memory-guided orienting in the rat. *Neuron*, 72(2):330–343. 22017991[pmid] PMC3212026[pmcid] S0896-6273(11)00607-6[PII] Neuron.

Espinoza, S. G. (1983). Single unit studies in the visual cortex of rodents. *Archivos de biologia y medicina experimentales*, 16 3-4:305–15.

Espinoza, S. G. and Thomas, H. C. (1983). Retinotopic organization of striate and extrastriate visual cortex in the hooded rat. *Brain Research*, 272(1):137–144.

Etienne, A. S. (1980). The orientation of the golden hamster to its nest-site after the elimination of various sensory cues. *Experientia*, 36(9):1048–1050.

Etienne, A. S. and Jeffery, K. J. (2004). Path integration in mammals. *Hippocampus*, 14(2):180–192.

Etienne, A. S., Maurer, R., Saucy, F., and Teroni, E. (1986). Short-distance homing in the golden hamster after a passive outward journey. *Animal Behaviour*, 34(3):696–715.

Etienne, A. S., Teroni, E., Hurni, C., and Portenier, V. (1990). The effect of a single light cue on homing behaviour of the golden hamster. *Animal Behaviour*, 39(1):17–41.

Etienne, A. S., Teroni, E., Maurer, R., Portenier, V., and Saucy, F. (1985). Short-distance homing in a small mammal: the role of exteroceptive cues and path integration. *Experientia*, 41(1):122–125.

Evangelio, M., García-Amado, M., and Clascá, F. (2018). Thalamocortical projection neuron and interneuron numbers in the visual thalamic nuclei of the adult c57bl/6 mouse. *Frontiers in Neuroanatomy*, 12(27).

Felleman, D. J. (2001). *Visual System in the Brain*, pages 16278–16285. Pergamon, Oxford.

Finkelstein, A., Ulanovsky, N., Tsodyks, M., and Aljadeff, J. (2018). Optimal dynamic coding by mixed-dimensionality neurons in the head-direction system of bats. *Nature communications*, 9(1):3590–3590. 30181554[pmid] PMC6123463[pmcid] 10.1038/s41467-018-05562-1[PII] Nat Commun.

Fodor, J. A. (1983). *The Modularity of Mind*. The MIT Press, Cambridge, MA.

Foo, P., Warren, W. H., Duchon, A., and Tarr, M. J. (2005). Do humans integrate routes into a cognitive map? map- versus landmark-based navigation of novel shortcuts. *Journal of Experimental Psychology: Learning, Memory, and Cognition*, 31(2):195–215.

Frisch, S. (2014). How cognitive neuroscience could be more biological—and what it might learn from clinical neuropsychology. *Frontiers in Human Neuroscience*, 8(541).

Frohardt, R. J., Bassett, J. P., and Taube, J. S. (2006). Path integration and lesions within the head direction cell circuit: Comparison between the roles of the anterodorsal thalamus and dorsal tegmental nucleus. *Behavioral Neuroscience*, 120(1):135–149.

Fukuda, Y., Sumitomo, I., Sugitani, M., and Iwama, K. (1979). Receptive-field properties of cells in the dorsal part of the albino rat's lateral geniculate nucleus. *The Japanese Journal of Physiology*, 29(3):283–307.

Funahashi, M. and Stewart, M. (1997a). Presubicular and parasubicular cortical neurons of the rat: Electrophysiological and morphological properties. *Hippocampus*, 7(2):117–129.

Funahashi, M. and Stewart, M. (1997b). Presubicular and parasubicular cortical neurons of the rat: Functional separation of deep and superficial neurons in vitro. *The Journal of Physiology*, 501(2):387–403.

Furtak, S. C., Wei, S., Agster, K. L., and Burwell, R. D. (2007). Functional neuroanatomy of the parahippocampal region in the rat: The perirhinal and postrhinal cortices. *Hippocampus*, 17(9):709–722.

Fyhn, M., Molden, S., Witter, M. P., Moser, E. I., and Moser, M.-B. (2004). Spatial representation in the entorhinal cortex. *Science*, 305(5688):1258–1264.

Gale, S. D. and Murphy, G. J. (2014). Distinct representation and distribution of visual information by specific cell types in mouse superficial superior colliculus. *The Journal of neuroscience : the official journal of the Society for Neuroscience*, 34(40):13458–13471. 25274823[pmid] PMC4180477[pmcid] 34/40/13458[PII] J Neurosci.

Gallardo, L., Mottles, M., Vera, L., Carrasco, M. A., Torrealba, F., Montero, V. M., and Pinto-Hamuy, T. (1979). Failure by rats to learn a visual conditional discrimination after lateral peristriate cortical lesions. *Physiological Psychology*, 7(2):173–177.

Gao, E., DeAngelis, G. C., and Burkhalter, A. (2010). Parallel input channels to mouse primary visual cortex. *The Journal of Neuroscience*, 30(17):5912–5926.

Giocomo, L., Moser, M.-B., and Moser, E. (2011). Computational models of grid cells. *Neuron*, 71(4):589–603.

Giocomo, L., Stensola, T., Bonnevie, T., Van Cauter, T., Moser, M.-B., and Moser, E. (2014). Topography of head direction cells in medial entorhinal cortex. *Current Biology*, 24(3):252–262.

Giocomo, L. M. (2016). Environmental boundaries as a mechanism for correcting and anchoring spatial maps. *The Journal of Physiology*, 594(22):6501–6511.

Girman, S. and Lund, R. (2010). Orientation-specific modulation of rat retinal ganglion cell responses and its dependence on relative orientations of the center and surround gratings. *Journal of Neurophysiology*, 104(6):2951–2962.

Girman, S. V. and Lund, R. D. (2007). Most superficial sublamina of rat superior colliculus: Neuronal response properties and correlates with perceptual figure–ground segregation. *Journal of Neurophysiology*, 98(1):161–177.

Golob, E. J., Stackman, R. W., Wong, A. C., and Taube, J. S. (2001). On the behavioral significance of head direction cells: Neural and behavioral dynamics during spatial memory tasks. *Behavioral Neuroscience*, 115(2):285–304.

Golob, E. J. and Taube, J. S. (1997). Head direction cells and episodic spatial information in rats without a hippocampus. *Proceedings of the National Academy of Sciences*, 94(14):7645–7650.

Golob, E. J., Wolk, D. A., and Taube, J. S. (1998). Recordings of postsubiculum head direction cells following lesions of the laterodorsal thalamic nucleus. *Brain Research*, 780(1):9–19.

Goodale, M. A. and Murison, R. C. C. (1975). The effects of lesions of the superior colliculus on locomotor orientation and the orienting reflex in the rat. *Brain Research*, 88(2):243–261.

Goodridge, J. P., Dudchenko, P. A., Worboys, K. A., Golob, E. J., and Taube, J. S. (1998). Cue control and head direction cells. *Behavioral Neuroscience*, 112(4):749–761.

Goodridge, J. P. and Taube, J. S. (1995). Preferential use of the landmark navigational system by head direction cells in rats. *Behavioral Neuroscience*, 109(1):49–61.

Goodridge, J. P. and Taube, J. S. (1997). Interaction between the postsubiculum and anterior thalamus in the generation of head direction cell activity. *The Journal of Neuroscience*, 17(23):9315–9330.

Grieves, R. M., Duvelle, E., and Dudchenko, P. A. (2018). A boundary vector cell model of place field repetition. *Spatial Cognition & Computation*, 18(3):217–256.

Grieves, R. M. and Jeffery, K. J. (2017). The representation of space in the brain. *Behavioural Processes*, 135:113–131.

Grieves, R. M., Jenkins, B. W., Harland, B. C., Wood, E. R., and Dudchenko, P. A. (2016). Place field repetition and spatial learning in a multicompartment environment. *Hippocampus*, 26(1):118–134. 26190393[pmid] PMC4745022[pmcid].

Grubb, M. S. and Thompson, I. D. (2003). Quantitative characterization of visual response properties in the mouse dorsal lateral geniculate nucleus. *Journal of Neurophysiology*, 90(6):3594–3607.

Grubb, M. S. and Thompson, I. D. (2004). Biochemical and anatomical subdivision of the dorsal lateral geniculate nucleus in normal mice and in mice lacking the beta-2 subunit of the nicotinic acetylcholine receptor. *Vision Research*, 44(28):3365–3376.

Güler, A. D., Ecker, J. L., Lall, G. S., Haq, S., Altimus, C. M., Liao, H.-W., Barnard, A. R., Cahill, H., Badea, T. C., Zhao, H., Hankins, M. W., Berson, D. M., Lucas, R. J., Yau, K.-W., and Hattar, S. (2008). Melanopsin cells are the principal conduits for rod–cone input to non-image-forming vision. *Nature*, 453:102.

Hafting, T., Fyhn, M., Molden, S., Moser, M.-B., and Moser, E. I. (2005). Microstructure of a spatial map in the entorhinal cortex. *Nature*, 436(7052):801–806.

Hall, C. A. and Chilcott, R. P. (2018). Eyeing up the future of the pupillary light reflex in neurodiagnostics. *Diagnostics (Basel, Switzerland)*, 8(1):19. 29534018[pmid] PMC5872002[pmcid].

Hardcastle, K., Maheswaranathan, N., Ganguli, S., and Giocomo, L. M. (2017). A multiplexed, heterogeneous, and adaptive code for navigation in medial entorhinal cortex. *Neuron*, 94(2):375–387.e7.

Harland, B., Grieves, R. M., Bett, D., Stentiford, R., Wood, E. R., and Dudchenko, P. A. (2017). Lesions of the head direction cell system increase hippocampal place field repetition. *Current biology : CB*, 27(17):2706–2712.e2. 28867207[pmid] PMC5607353[pmcid] S0960-9822(17)31009-6[PII].

Harland, B., Wood, E. R., and Dudchenko, P. A. (2015). The head direction cell system and behavior: The effects of lesions to the lateral mammillary bodies on spatial memory in a novel landmark task and in the water maze. *Behavioral Neuroscience*, 129(6):709–719.

Harris, K. D., Henze, D. A., Csicsvari, J., Hirase, H., and Buzsáki, G. (2000). Accuracy of tetrode spike separation as determined by simultaneous intracellular and extracellular measurements. *Journal of Neurophysiology*, 84(1):401–414.

Hayakawa, T. and Zyo, K. (1985). Afferent connections of gudden's tegmental nuclei in the rabbit. *Journal of Comparative Neurology*, 235(2):169–181.

Hayakawa, T. and Zyo, K. (1989). Retrograde double-labeling study of the marnmillothalamic and the mammillotegmental projections in the rat. *Journal of Comparative Neurology*, 284(1):1–11.

Heine, W. F. and Passaglia, C. L. (2011). Spatial receptive field properties of rat retinal ganglion cells. *Visual neuroscience*, 28(5):403–417. 21944166[pmid] PMC5130229[pmcid] S0952523811000307[PII].

Hofbauer, A. and Dräger, U. C. (1985). Depth segregation of retinal ganglion cells projecting to mouse superior colliculus. *Journal of Comparative Neurology*, 234(4):465–474.

Hok, V., Jacob, P.-Y., Bordiga, P., Truchet, B., Poucet, B., and Save, E. (2018). A spatial code in the dorsal lateral geniculate nucleus. *bioRxiv*, page 473520.

Hopkins, D. A. (2005). *Neuroanatomy of head direction cell circuits*, book section 2. The MIT Press, Cambridge, MA.

Horne, M. R., Iordanova, M. D., Albasser, M. M., Aggleton, J. P., Honey, R. C., and Pearce, J. M. (2010). Lesions of the perirhinal cortex do not impair integration of visual and geometric information in rats. *Behavioral Neuroscience*, 124(3):311–320.

Housh, A. A., Berkowitz, L. E., Ybarra, I., Kim, E. U., Lee, B. R., and Calton, J. L. (2014). Impairment of the anterior thalamic head direction cell network following administration of the nmda antagonist mk-801. *Brain research bulletin*, 109:77–87. 25307435[pmid] PMC4266603[pmcid] S0361-9230(14)00148-8[PII].

Høydal, Ø. A., Skytøen, E. R., Andersson, S. O., Moser, M.-B., and Moser, E. I. (2019). Object-vector coding in the medial entorhinal cortex. *Nature*, 568(7752):400–404.

Huang, L.-W., Simonnet, J., Nassar, M., Richevaux, L., Lofredi, R., and Fricker, D. (2017). Laminar localization and projection-specific properties of presubicular neurons tar-

geting the lateral mammillary nucleus, thalamus, or medial entorhinal cortex. *eNeuro*, 4(2):ENEURO.0370–16.2017. 28508034[pmid] PMC5430300[pmcid] eNeuro.

Huberman, A. D. and Niell, C. M. (2011). What can mice tell us about how vision works? *Trends in Neurosciences*, 34(9):464–473.

Hughes, H. C. (1977). Anatomical and neurobehavioral investigations concerning the thalamocortical organization of the rat's visual system. *The Journal of Comparative Neurology*, 175(3):311–335.

Humphrey, N. K. (1968). Responses to visual stimuli of units in the superior colliculus of rats and monkeys. *Experimental Neurology*, 20(3):312–340.

Itaya, S. K., Van Hoesen, G. W., and Benevento, L. A. (1986). Direct retinal pathways to the limbic thalamus of the monkey. *Experimental Brain Research*, 61(3):607–613.

Itaya, S. K., Van Hoesen, G. W., and Jenq, C. B. (1981). Direct retinal input to the limbic system of the rat. *Brain Research*, 226(1):33–42.

Ito, S. and Feldheim, D. A. (2018). The mouse superior colliculus: An emerging model for studying circuit formation and function. *Frontiers in Neural Circuits*, 12(10).

Jacob, P.-Y., Casali, G., Spieser, L., Page, H., Overington, D., and Jeffery, K. (2017). An independent, landmark-dominated head-direction signal in dysgranular retrosplenial cortex. *Nature neuroscience*, 20(2):173–175. 27991898[pmid] PMC5274535[pmcid] nn.4465[PII].

Jankowski, M. M., Islam, M. N., Wright, N. F., Vann, S. D., Erichsen, J. T., Aggleton, J. P., and O'Mara, S. M. (2014). Nucleus reuniens of the thalamus contains head direction cells. *eLife*, 3:e03075.

Jankowski, M. M. and O'Mara, S. M. (2015). Dynamics of place, boundary and object encoding in rat anterior claustrum. *Frontiers in Behavioral Neuroscience*, 9(250).

Jankowski, M. M., Passecker, J., Islam, M. N., Vann, S., Erichsen, J. T., Aggleton, J. P., and O'Mara, S. M. (2015). Evidence for spatially-responsive neurons in the rostral thalamus. *Frontiers in Behavioral Neuroscience*, 9(256).

Jankowski, M. M., Ronnqvist, K. C., Tsanov, M., Vann, S. D., Wright, N. F., Erichsen, J. T., Aggleton, J. P., and O'Mara, S. (2013). The anterior thalamus provides a subcortical circuit supporting memory and spatial navigation. *Frontiers in Systems Neuroscience*, 7(45).

Jeffery, K. J. (2007). Integration of the sensory inputs to place cells: What, where, why, and how? *Hippocampus*, 17(9):775–785.

Jeffery, K. J., Donnett, J. G., and O'Keefe, J. (1995). Medial septal control of theta-correlated unit firing in the entorhinal cortex of awake rats. *NeuroReport*, 6(16):2166–2170.

Jeffery, K. J., Grieves, R., and Donnett, J. (2018). *Chapter 5 - Recording the Spatial Mapping Cells: Place, Head Direction, and Grid Cells*, volume 28, pages 95–121. Elsevier.

Jeffery, K. J., Page, H. J. I., and Stringer, S. M. (2016). Optimal cue combination and landmark-stability learning in the head direction system. *The Journal of physiology*, 594(22):6527–6534. 27479741[pmid] PMC5108898[pmcid].

Ji, W., Gămănuţ, R., Bista, P., D'Souza, R., Wang, Q., and Burkhalter, A. (2015). Modularity in the organization of mouse primary visual cortex. *Neuron*, 87(3):632–643.

Jones, B. F. and Witter, M. P. (2007). Cingulate cortex projections to the parahippocampal region and hippocampal formation in the rat. *Hippocampus*, 17(10):957–976.

Kaas, J. H., Krubitzer, L. A., and Johanson, K. L. (1989). Cortical connections of areas 17 (v-i) and 18 (v-ii) of squirrels. *Journal of Comparative Neurology*, 281(3):426–446.

Kamishina, H., Conte, W. L., Patel, S. S., Tai, R. J., Corwin, J. V., and Reep, R. L. (2009). Cortical connections of the rat lateral posterior thalamic nucleus. *Brain Research*, 1264:39–56.

Kamishina, H., Yurcisin, G. H., Corwin, J. V., and Reep, R. L. (2008). Striatal projections from the rat lateral posterior thalamic nucleus. *Brain Research*, 1204:24–39.

Kauffmann, L., Ramanoël, S., and Peyrin, C. (2014). The neural bases of spatial frequency processing during scene perception. *Frontiers in Integrative Neuroscience*, 8(37).

Keinath, A. T. (2016). The preferred directions of conjunctive grid x head direction cells in the medial entorhinal cortex are periodically organized. *PloS one*, 11(3):e0152041–e0152041. 27003407[pmid] PMC4803195[pmcid] PONE-D-16-03391[PII].

Kerschensteiner, D. and Guido, W. (2017). Organization of the dorsal lateral geniculate nucleus in the mouse. *Visual neuroscience*, 34:E008–E008. 28965501[pmid] PMC6380502[pmcid] S0952523817000062[PII].

Khabbaz, A., Fee, M., Tsien, J., and Tank, D. (2000). A compact convergingelectrode micro-drive for recording head direction cells in mice. *Soc Neurosci Abstr*, 26:984.

Khibnik, L. A., Tritsch, N. X., and Sabatini, B. L. (2014). A direct projection from mouse primary visual cortex to dorsomedial striatum. *PLOS ONE*, 9(8):e104501.

Kim, I.-J., Zhang, Y., Meister, M., and Sanes, J. R. (2010). Laminar restriction of retinal ganglion cell dendrites and axons: subtype-specific developmental patterns revealed with transgenic markers. *The Journal of neuroscience : the official journal of the Society for Neuroscience*, 30(4):1452–1462. 20107072[pmid] PMC2822471[pmcid] 30/4/1452[PII] J Neurosci.

Kim, N., Barter, J. W., Sukharnikova, T., and Yin, H. H. (2014). Striatal firing rate reflects head movement velocity. *European Journal of Neuroscience*, 40(10):3481–3490.

Kirby, E. D., Jensen, K., Goosens, K. A., and Kaufer, D. (2012). Stereotaxic surgery for excitotoxic lesion of specific brain areas in the adult rat. *Journal of visualized experiments : JoVE*, (65):e4079–e4079. 22847556[pmid] PMC3476400[pmcid] 4079[PII].

Kirk, I. J. and McNaughton, N. (1991). Supramammillary cell firing and hippocampal rhythmical slow activity. *NeuroReport*, 2(11):723.

Knierim, J. J. (2002). Dynamic interactions between local surface cues, distal landmarks, and intrinsic circuitry in hippocampal place cells. *The Journal of Neuroscience*, 22(14):6254–6264.

Knierim, J. J. and Hamilton, D. A. (2011). Framing spatial cognition: neural representations of proximal and distal frames of reference and their roles in navigation. *Physiological reviews*, 91(4):1245–1279.

Knierim, J. J. and Rao, G. (2003). Distal landmarks and hippocampal place cells: Effects of relative translation versus rotation. *Hippocampus*, 13(5):604–617.

Knight, R., Hayman, R., Lin Ginzberg, L., and Jeffery, K. (2011). Geometric cues influence head direction cells only weakly in nondisoriented rats. *The Journal of neuroscience : the official journal of the Society for Neuroscience*, 31(44):15681–15692. 22049411[pmid] PMC3242014[pmcid] 31/44/15681[PII].

Knight, R., Piette, C. E., Page, H., Walters, D., Marozzi, E., Nardini, M., Stringer, S., and Jeffery, K. J. (2014). Weighted cue integration in the rodent head direction system. *Philosophical transactions of the Royal Society of London. Series B, Biological sciences*, 369(1635):20120512–20120512. 24366127[pmid] PMC3866437[pmcid] rstb.2012.0512[PII].

Kocsis, B. and Vertes, R. (1994). Characterization of neurons of the supramammillary nucleus and mammillary body that discharge rhythmically with the hippocampal theta rhythm in the rat. *The Journal of Neuroscience*, 14(11):7040–7052.

Koenig, J., Linder, A. N., Leutgeb, J. K., and Leutgeb, S. (2011). The spatial periodicity of grid cells is not sustained during reduced theta oscillations. *Science*, 332(6029):592–595.

Kolb, B. (1990). *Posterior parietal and temporal association cortex*, pages 459–471. The MIT Press, Cambridge, MA.

Kolb, B. and Walkey, J. (1987). Behavioural and anatomical studies of the posterior parietal cortex in the rat. *Behavioural Brain Research*, 23(2):127–145.

Kondo, S. and Ohki, K. (2015). Laminar differences in the orientation selectivity of geniculate afferents in mouse primary visual cortex. *Nature Neuroscience*, 19:316.

Kornienko, O., Latuske, P., Bassler, M., Kohler, L., and Allen, K. (2018). Non-rhythmic head-direction cells in the parahippocampal region are not constrained by attractor network dynamics. *eLife*, 7:e35949. 30222110[pmid] PMC6158010[pmcid] Elife.

Kraft, P., Evangelista, C., Dacke, M., Labhart, T., and Srinivasan, M. V. (2011). Honeybee navigation: following routes using polarized-light cues. *Philosophical transactions of the Royal Society of London. Series B, Biological sciences*, 366(1565):703–708. 21282174[pmid] PMC3049011[pmcid] 366/1565/703[PII].

Kravitz, D. J., Saleem, K. S., Baker, C. I., and Mishkin, M. (2011). A new neural framework for visuospatial processing. *Nature reviews. Neuroscience*, 12(4):217–230. 21415848[pmid] PMC3388718[pmcid] nrn3008[PII].

Krieg, W. J. S. (1946). Connections of the cerebral cortex. i. the albino rat. a. topography of the cortical areas. *Journal of Comparative Neurology*, 84(2):221–275.

Kropff, E., Carmichael, J. E., Moser, M.-B., and Moser, E. I. (2015). Speed cells in the medial entorhinal cortex. *Nature*, 523:419.

Krubitzer, L., Campi, K. L., and Cooke, D. F. (2011). All rodents are not the same: a modern synthesis of cortical organization. *Brain, behavior and evolution*, 78(1):51–93. 21701141[pmid] PMC3182045[pmcid] 000327320[PII].

Kuiper, N. H. (1960). Tests concerning random points on a circle. *Proceedings of the Koninklijke Nederlandse Akademie van Wetenschappen, Series A*, 63:38–47.

Kuruvilla, M. V. and Ainge, J. A. (2017). Lateral entorhinal cortex lesions impair local spatial frameworks. *Frontiers in Systems Neuroscience*, 11(30).

LaChance, P. A., Todd, T. P., and Taube, J. S. (2019). A sense of space in postrhinal cortex. *Science*, 365(6449):eaax4192.

Lamprea, M., Cardenas, F., Setem, J., and Morato, S. (2008). Thigmotactic responses in an open-field. *Brazilian Journal of Medical and Biological Research*, 41:135–140.

Lannou, J., Cazin, L., Precht, W., and Le Taillanter, M. (1984). Responses of prepositus hypoglossi neurons to optokinetic and vestibular stimulations in the rat. *Brain Research*, 301(1):39–45.

Laramée, M.-E. and Boire, D. (2015). Visual cortical areas of the mouse: comparison of parcellation and network structure with primates. *Frontiers in Neural Circuits*, 8(149).

Lashley, K. S. (1939). The mechanism of vision. xvi. the functioning of small remnants of the visual cortex. *Journal of Comparative Neurology*, 70(1):45–67.

Laurens, J., Abrego, A., Cham, H., Popeney, B., Yu, Y., Rotem, N., Aarse, J., Dickman, D., and Angelaki, D. (2019). Multiplexed code of navigation variables in the anterior limbic system. *bioRxiv*, page 684464.

Laurens, J. and Angelaki, D. E. (2018). The brain compass: A perspective on how self-motion updates the head direction cell attractor. *Neuron*, 97(2):275–289. 29346751[pmid] PMC5777220[pmcid] S0896-6273(17)31165-0[PII].

Lavenex, P. and Schenk, F. (1995). Influence of local environmental olfactory cues on place learning in rats. *Physiology & Behavior*, 58(6):1059–1066.

Lavenex, P. and Schenk, F. (1997). Olfactory cues potentiate learning of distant visuospatial information. *Neurobiology of Learning and Memory*, 68(2):140–153.

Lee, I., Yoganarasimha, D., Rao, G., and Knierim, J. J. (2004). Comparison of population coherence of place cells in hippocampal subfields ca1 and ca3. *Nature*, 430(6998):456–459.

Leinweber, M., Ward, D. R., Sobczak, J. M., Attinger, A., and Keller, G. B. (2017). A sensorimotor circuit in mouse cortex for visual flow predictions. *Neuron*, 95(6):1420–1432.e5.

Lennie, P. and Perry, V. H. (1981). Spatial contrast sensitivity of cells in the lateral geniculate nucleus of the rat. *The Journal of Physiology*, 315(1):69–79.

Lever, C., Burton, S., Jeewajee, A., Keefe, J., and Burgess, N. (2009). Boundary vector cells in the subiculum of the hippocampal formation. *The Journal of Neuroscience*, 29(31):9771.

LeVere, T. E. (1978). The primary visual system of the rat: A primer of its anatomy. *Physiological Psychology*, 6(2):142–169.

Levick, W. R. and Thibos, L. N. (1982). Analysis of orientation bias in cat retina. *The Journal of physiology*, 329:243–261. 7143249[pmid] PMC1224778[pmcid].

Levin, H., Benton, A., and Grossman, R. (1982). *Neurobehavioral Consequences of Closed Head Injury*. Oxford University Press, Oxford.

Linden, R. and Perry, V. H. (1983). Massive retinotectal projection in rats. *Brain Research*, 272(1):145–149.

Liu, R., Chang, L., and Wickern, G. (1984). The dorsal tegmental nucleus: an axoplasmic transport study. *Brain Research*, 310(1):123–132.

Llinas, R. R. and Alonso, A. (1992). Electrophysiology of the mammillary complex in vitro. i. tuberomammillary and lateral mammillary neurons. *Journal of Neurophysiology*, 68(4):1307–1320.

Long, X. and Zhang, S.-J. (2018). A novel somatosensory spatial navigation system outside the hippocampal formation. *bioRxiv*, page 473090.

Lozano, Y. R., Page, H., Jacob, P.-Y., Lomi, E., Street, J., and Jeffery, K. (2017). Retrosplenial and postsubicular head direction cells compared during visual landmark discrimination. *Brain and Neuroscience Advances*, 1:2398212817721859.

Lund, R. D. (1969). Synaptic patterns of the superficial layers of the superior colliculus of the rat. *Journal of Comparative Neurology*, 135(2):179–207.

Lund, R. D. (1972). Anatomic studies on the superior colliculus. *Investigative Ophthalmology & Visual Science*, 11(6):434–441.

Lund, R. D., Land, P. W., and Boles, J. (1980). Normal and abnormal uncrossed retinotectal pathways in rats: An hrp study in adults. *Journal of Comparative Neurology*, 189(4):711–720.

Malach, R. (1989). Patterns of connections in rat visual cortex. *The Journal of Neuroscience*, 9(11):3741–3752.

Mankin, E. A., Thurley, K., Chenani, A., Haas, O. V., Debs, L., Henke, J., Galinato, M., Leutgeb, J. K., Leutgeb, S., and Leibold, C. (2019). The hippocampal code for space in mongolian gerbils. *Hippocampus*, 0(0).

Marshel, J. H., Garrett, M. E., Nauhaus, I., and Callaway, E. M. (2011). Functional specialization of seven mouse visual cortical areas. *Neuron*, 72(6):1040–1054. 22196338[pmid] PMC3248795[pmcid] S0896-6273(11)01046-4[PII].

Martin, P. R. (1986). The projection of different retinal ganglion cell classes to the dorsal lateral geniculate nucleus in the hooded rat. *Experimental Brain Research*, 62(1):77–88.

Martinet, L., Servière, J., and Peytevin, J. (1992). Direct retinal projections of the "non-image forming" system to the hypothalamus, anterodorsal thalamus and basal telencephalon of mink (mustela vison) brain. *Experimental Brain Research*, 89(2):373–382.

Mason, R. and Groos, G. A. (1981). Cortico-recipient and tecto-recipient visual zones in the rat's lateral posterior (pulvinar) nucleus: An anatomical study. *Neuroscience Letters*, 25(2):107–112.

Maximino, C. (2008). Evolutionary changes in the complexity of the tectum of nontetrapods: A cladistic approach. *PLOS ONE*, 3(10):e3582.

May, P. J. (2006). *The mammalian superior colliculus: laminar structure and connections*, volume 151, pages 321–378. Elsevier.

McDaniel, W. F., Coleman, J., and Lindsay Jr, J. F. (1982). A comparison of lateral peristriate and striate neocortical ablations in the rat. *Behavioural Brain Research*, 6(3):249–272.

McDonald, A. J. and Mascagni, F. (1996). Cortico-cortical and cortico-amygdaloid projections of the rat occipital cortex: a phaseolus vulgaris leucoagglutinin study. *Neuroscience*, 71(1):37–54.

Mehlman, M. L., Winter, S. S., and Taube, J. S. (2019a). Functional and anatomical relationships between the medial precentral cortex, dorsal striatum, and head direction cell circuitry. ii. neuroanatomical studies. *Journal of Neurophysiology*, 121(2):371–395.

Mehlman, M. L., Winter, S. S., Valerio, S., and Taube, J. S. (2019b). Functional and anatomical relationships between the medial precentral cortex, dorsal striatum, and head direction cell circuitry. i. recording studies. *Journal of Neurophysiology*, 121(2):350–370.

Menzel, R., Greggers, U., Smith, A., Berger, S., Brandt, R., Brunke, S., Bundrock, G., Hülse, S., Plümpe, T., Schaupp, F., Schüttler, E., Stach, S., Stindt, J., Stollhoff, N., and Watzl, S. (2005). Honey bees navigate according to a map-like spatial memory. *Proceedings of the National Academy of Sciences of the United States of America*, 102(8):3040.

Michael, C. R. (1972). Visual receptive fields of single neurons in superior colliculus of the ground squirrel. *Journal of Neurophysiology*, 35(6):815–832.

Miller, M. W. and Vogt, B. A. (1984). Direct connections of rat visual cortex with sensory, motor, and association cortices. *Journal of Comparative Neurology*, 226(2):184–202.

Minini, L. and Jeffery, K. J. (2006). Do rats use shape to solve "shape discriminations"? *Learning & memory (Cold Spring Harbor, N.Y.)*, 13(3):287–297. 16705141[pmid] PMC1475809[pmcid] lm.84406[PII].

Mink, J. W., Sinnamon, H. M., and Adams, D. B. (1983). Activity of basal forebrain neurons in the rat during motivated behaviors. *Behavioural Brain Research*, 8(1):85–108.

Mishkin, M., Ungerleider, L. G., and Macko, K. A. (1983). Object vision and spatial vision: two cortical pathways. *Trends in Neurosciences*, 6:414–417.

Mitchell, A. S., Czajkowski, R., Zhang, N., Jeffery, K., and Nelson, A. J. D. (2018). Retrosplenial cortex and its role in spatial cognition. *Brain and Neuroscience Advances*, 2:2398212818757098.

Mittelstaedt, M. L. and Mittelstaedt, H. (1980). Homing by path integration in a mammal. *Naturwissenschaften*, 67(11):566–567.

Mizumori, S. and Williams, J. (1993). Directionally selective mnemonic properties of neurons in the lateral dorsal nucleus of the thalamus of rats. *The Journal of Neuroscience*, 13(9):4015–4028.

Mizumori, S. J. Y., Miya, D. Y., and Ward, K. E. (1994). Reversible inactivation of the lateral dorsal thalamus disrupts hippocampal place representation and impairs spatial learning. *Brain Research*, 644(1):168–174.

Mizumori, S. J. Y., Ragozzino, K. E., and Cooper, B. G. (2000). Location and head direction representation in the dorsal striatum of rats. *Psychobiology*, 28(4):441–462.

Mohamed, W. (2008). The edwin smith surgical papyrus: Neuroscience in ancient egypt.

Monavarfeshani, A., Sabbagh, U., and Fox, M. A. (2017). Not a one-trick pony: Diverse connectivity and functions of the rodent lateral geniculate complex. *Visual Neuroscience*, 34:E012.

Montero, V. M. (1993). Retinotopy of cortical connections between the striate cortex and extrastriate visual areas in the rat. *Experimental Brain Research*, 94(1):1–15.

Montero, V. M., Bravo, H., and Ferna´ndez, V. (1973a). Striate-peristriate cortico-cortical connections in the albino and gray rat. *Brain Research*, 53(1):202–207.

Montero, V. M. and Guillery, R. W. (1968). Degeneration in the dorsal lateral geniculate nucleus of the rat following interruption of the retinal or cortical connections. *The Journal of Comparative Neurology*, 134(2):211–241.

Montero, V. M., Rojas, A., and Torrealba, F. (1973b). Retinotopic organization of striate and peristriate visual cortex in the albino rat. *Brain Research*, 53(1):197–201.

Morgan, J. L. and Lichtman, J. W. (2019). An individual interneuron participates in many kinds of inhibition and spans much of the mouse visual thalamus. *bioRxiv*, page 683276.

Mort, E., Cairns, S., Hersch, H., and Finlay, B. (1980). The role of the superior colliculus in visually guided locomotion and visual orienting in the hamster. *Physiological Psychology*, 8(1):20–28.

Moser, M.-B., Rowland, D. C., and Moser, E. I. (2015). Place cells, grid cells, and memory. *Cold Spring Harbor Perspectives in Biology*, 7(2).

Muir, G. M., Brown, J. E., Carey, J. P., Hirvonen, T. P., Della Santina, C. C., Minor, L. B., and Taube, J. S. (2009). Disruption of the head direction cell signal after occlusion of the semicircular canals in the freely moving chinchilla. *The Journal of Neuroscience*, 29(46):14521–14533.

Muller, R. U., Kubie, J. L., Bostock, E. M., Taube, J. S., and Quirk, G. J. (1991). *Spatial firing correlates of neurons in the hippocampal formation of freely moving rats*, pages 296–333. Oxford University Press, New York, NY, US.

Musel, B., Kauffmann, L., Ramanoël, S., Giavarini, C., Guyader, N., Chauvin, A., and Peyrin, C. (2014). Coarse-to-fine categorization of visual scenes in scene-selective cortex. *Journal of Cognitive Neuroscience*, 26(10):2287–2297.

Nauta, W. J. H. and Bucher, V. M. (1954). Efferent connections of the striate cortex in the albino rat. *Journal of Comparative Neurology*, 100(2):257–285.

Nilsson, D.-E. (2009). The evolution of eyes and visually guided behaviour. *Philosophical Transactions of the Royal Society B: Biological Sciences*, 364(1531):2833–2847.

Nitz, D. A. (2006). Tracking route progression in the posterior parietal cortex. *Neuron*, 49(5):747–756.

Nitz, D. A. (2012). Spaces within spaces: rat parietal cortex neurons register position across three reference frames. *Nature Neuroscience*, 15:1365.

Northcutt, R. G. (2002). Understanding vertebrate brain evolution1. *Integrative and Comparative Biology*, 42(4):743–756.

Noseda, R., Kainz, V., Jakubowski, M., Gooley, J. J., Saper, C. B., Digre, K., and Burstein, R. (2010). A neural mechanism for exacerbation of headache by light. *Nature neuroscience*, 13(2):239–245. 20062053[pmid] PMC2818758[pmcid] nn.2475[PII] Nat Neurosci.

O'Keefe, J. and Burgess, N. (1996). Geometric determinants of the place fields of hippocampal neurons. *Nature*, 381(6581):425–428.

O'Keefe, J. and Dostrovsky, J. (1971). The hippocampus as a spatial map. preliminary evidence from unit activity in the freely-moving rat. *Brain Research*, 34(1):171–175.

O'Keefe, J. and Nadel, L. (1978). *The Hippocampus as a Cognitive Map*. Oxford University Press, Oxford.

Olavarria, J. and Montero, V. M. (1981). Reciprocal connections between the striate cortex and extrastriate cortical visual areas in the rat. *Brain Research*, 217(2):358–363.

Olavarria, J. and Montero, V. M. (1984). Relation of callosal and striate-extrastriate cortical connections in the rat: Morphological definition of extrastriate visual areas. *Experimental Brain Research*, 54(2):240–252.

Olavarria, J. and Montero, V. M. (1989). Organization of visual cortex in the mouse revealed by correlating callosal and striate-extrastriate connections. *Visual Neuroscience*, 3(1):59–69.

Olavarria, J. and Van Sluyters, R. C. (1982). The projection from striate and extrastriate cortical areas to the superior colliculus in the rat. *Brain Research*, 242(2):332–336.

Olsen, S. R., Bortone, D. S., Adesnik, H., and Scanziani, M. (2012). Gain control by layer six in cortical circuits of vision. *Nature*, 483:47.

Olson, J. M., Tongprasearth, K., and Nitz, D. A. (2016). Subiculum neurons map the current axis of travel. *Nature Neuroscience*, 20:170.

O'Mara, S. M., Sanchez-Vives, M. V., Brotons-Mas, J. R., and O'Hare, E. (2009). Roles for the subiculum in spatial information processing, memory, motivation and the temporal control of behaviour. *Progress in Neuro-Psychopharmacology and Biological Psychiatry*, 33(5):782–790.

Page, H. J. I. and Jeffery, K. J. (2018). Landmark-based updating of the head direction system by retrosplenial cortex: A computational model. *Frontiers in Cellular Neuroscience*, 12(191).

Page, H. J. I., Walters, D. M., Knight, R., Piette, C. E., Jeffery, K. J., and Stringer, S. M. (2014). A theoretical account of cue averaging in the rodent head direction system. *Philosophical Transactions of the Royal Society B: Biological Sciences*, 369(1635):20130283.

Page, H. J. I., Wilson, J. J., and Jeffery, K. J. (2018). A dual-axis rotation rule for updating the head direction cell reference frame during movement in three dimensions. *Journal of neurophysiology*, 119(1):192–208. 29021391[pmid] PMC5866468[pmcid] jn.00501.2017[PII].

Park, E. H., Keeley, S., Savin, C., Ranck, J. B., and Fenton, A. A. (2019). How the internally organized direction sense is used to navigate. *Neuron*, 101(2):285–293.e5.

Parron, C. and Save, E. (2004). Evidence for entorhinal and parietal cortices involvement in path integration in the rat. *Experimental Brain Research*, 159(3):349–359.

Partridge, L. D. and Brown, J. E. (1970). Receptive fields of rat retinal ganglion cells. *Vision Research*, 10(6):455–460.

Paxinos, G. and Watson, C. (2007). *The Rat Brain in Stereotaxic Coordinates*. Academic Press, 6th edition edition.

Paz-Villagràn, V., Lenck-Santini, P.-P., Save, E., and Poucet, B. (2002). Properties of place cell firing after damage to the visual cortex. *European Journal of Neuroscience*, 16(4):771–776.

Peck, J. R. and Taube, J. S. (2017). The postrhinal cortex is not necessary for landmark control in rat head direction cells. *Hippocampus*, 27(2):156–168. 27860052[pmid] PMC5235971[pmcid] Hippocampus.

Peckford, G., Dwyer, J. A., Snow, A. C., Thorpe, C. M., Martin, G. M., and Skinner, D. M. (2014). The effects of lesions to the postsubiculum or the anterior dorsal nucleus of the thalamus on spatial learning in rats. *Behavioral Neuroscience*, 128(6):654–665.

Pegel, U., Pfeiffer, K., Zittrell, F., Scholtyssek, C., and Homberg, U. (2019). Two compasses in the central complex of the locust brain. *The Journal of Neuroscience*, 39(16):3070–3080.

Peters, A. and Feldman, M. L. (1976). The projection of the lateral geniculate nucleus to area 17 of the rat cerebral cortex. i. general description. *Journal of Neurocytology*, 5(1):63–84.

Peters, A. and Saldanha, J. (1976). The projection of the lateral geniculate nucleus to area 17 of the rat cerebral cortex. iii. layer vi. *Brain Research*, 105(3):533–537.

Petrof, I. and Sherman, S. M. (2009). Synaptic properties of the mammillary and cortical afferents to the anterodorsal thalamic nucleus in the mouse. *The Journal of Neuroscience*, 29(24):7815–7819.

Petrof, I. and Sherman, S. M. (2013). Functional significance of synaptic terminal size in glutamatergic sensory pathways in thalamus and cortex. *The Journal of physiology*, 591(13):3125–3131. 23359668[pmid] PMC3717215[pmcid] jphysiol.2012.247619[PII].

Peyrache, A., Lacroix, M. M., Petersen, P. C., and Buzsáki, G. (2015). Internally organized mechanisms of the head direction sense. *Nature Neuroscience*, 18:569.

Peyrache, A., Schieferstein, N., and Buzsáki, G. (2017). Transformation of the head-direction signal into a spatial code. *Nature Communications*, 8(1):1752.

Philippides, A., Baddeley, B., Cheng, K., and Graham, P. (2011). How might ants use panoramic views for route navigation? *The Journal of Experimental Biology*, 214(3):445–451.

Pinto-Hamuy, T., Montero, V. M., and Torrealba, F. (2004). Neurotoxic lesion of anteromedial/posterior parietal cortex disrupts spatial maze memory in blind rats. *Behavioural Brain Research*, 153(2):465–470.

Pinto-Hamuy, T., Olavarria, J., Guic-Robles, E., Morgues, M., Nassal, O., and Petit, D. (1987). Rats with lesions in anteromedial extrastriate cortex fail to learn a visuosomatic conditional response. *Behavioural Brain Research*, 25(3):221–231.

Piscopo, D. M., El-Danaf, R. N., Huberman, A. D., and Niell, C. M. (2013). Diverse visual features encoded in mouse lateral geniculate nucleus. *The Journal of Neuroscience*, 33(11):4642–4656.

Powers, M. K. and Green, D. G. (1978). Single retinal ganglion cell responses in the dark-reared rat: Grating acuity, contrast sensitivity, and defocusing. *Vision Research*, 18(11):1533–1539.

Prasad, J. A. and Chudasama, Y. (2013). Viral tracing identifies parallel disynaptic pathways to the hippocampus. *The Journal of Neuroscience*, 33(19):8494–8503.

Preston-Ferrer, P., Coletta, S., Frey, M., and Burgalossi, A. (2016). Anatomical organization of presubicular head-direction circuits. *eLife*, 5:e14592.

Prévost, F., Lepore, F., and Guillemot, J.-P. (2007). Spatio-temporal receptive field properties of cells in the rat superior colliculus. *Brain Research*, 1142:80–91.

Purves, D., Augustine, G., Fitzpatrick, D., Katz, L. C., LaMantia, A.-S., McNamara, J., and Williams, S. (2001). *Neuroscience*. Sinauer Associates, Sunderland (MA).

Ragozzino, K. E., Leutgeb, S., and Mizumori, S. J. (2001). Dorsal striatal head direction and hippocampal place representations during spatial navigation. *Experimental Brain Research*, 139(3):372–376.

Ramanathan, K. R., Ressler, R. L., Jin, J., and Maren, S. (2018). Nucleus reuniens is required for encoding and retrieving precise, hippocampal-dependent contextual fear memories in rats. *The Journal of Neuroscience*, 38(46):9925–9933.

Raudies, F., Brandon, M. P., Chapman, G. W., and Hasselmo, M. E. (2015). Head direction is coded more strongly than movement direction in a population of entorhinal neurons. *Brain Research*, 1621:355–367.

Redish, A. D., Elga, A. N., and Touretzky, D. S. (1996). A coupled attractor model of the rodent head direction system. *Network: Computation in Neural Systems*, 7(4):671–685.

Reese, B. E. (1988). 'hidden lamination' in the dorsal lateral geniculate nucleus: the functional organization of this thalamic region in the rat. *Brain Research Reviews*, 13(2):119–137.

Reese, B. E. and Cowey, A. (1983). Projection lines and the ipsilateral retino-geniculate pathway in the hooded rat. *Neuroscience*, 10(4):1233–1247.

Reese, B. E. and Jeffery, G. (1983). Crossed and uncrossed visual topography in dorsal lateral geniculate nucleus of the pigmented rat. *Journal of Neurophysiology*, 49(4):877–885.

Ribak, C. E. and Peters, A. (1975). An autoradiographic study of the projections from the lateral geniculate body of the rat. *Brain Research*, 92(3):341–368.

Robertson, R. G., Rolls, E. T., Georges-François, P., and Panzeri, S. (1999). Head direction cells in the primate pre-subiculum. *Hippocampus*, 9(3):206–219.

Rodriguez, A. (2017). *Role of the superior colliculus on the functioning of head direction cells.* Master's thesis.

Rosa, M. G. P. and Krubitzer, L. A. (1999). The evolution of visual cortex: where is v2? *Trends in Neurosciences*, 22(6):242–248.

Rossier, J. and Schenk, F. (2003). Olfactory and/or visual cues for spatial navigation through ontogeny: Olfactory cues enable the use of visual cues. *Behavioral Neuroscience*, 117(3):412–425.

Rubin, A., Yartsev, M. M., and Ulanovsky, N. (2014). Encoding of head direction by hippocampal place cells in bats. *The Journal of Neuroscience*, 34(3):1067–1080.

Ryszka, A. and Heger, M. (1979). Afferent connections of the laterodorsal thalamic nucleus in the rat. *Neuroscience Letters*, 15(1):61–64.

Sagdullaev, B. T. and McCall, M. A. (2005). Stimulus size and intensity alter fundamental receptive-field properties of mouse retinal ganglion cells in vivo. *Visual Neuroscience*, 22(5):649–659.

Sánchez, R. F., Montero, V. M., Espinoza, S. G., Díaz, E., Canitrot, M., and Pinto-Hamuy, T. (1997). Visuospatial discrimination deficit in rats after ibotenate lesions in anteromedial visual cortex. *Physiology & Behavior*, 62(5):989–994.

Sarel, A., Finkelstein, A., Las, L., and Ulanovsky, N. (2017). Vectorial representation of spatial goals in the hippocampus of bats. *Science*, 355(6321):176–180.

Sargolini, F., Fyhn, M., Hafting, T., McNaughton, B. L., Witter, M. P., Moser, M.-B., and Moser, E. I. (2006). Conjunctive representation of position, direction, and velocity in entorhinal cortex. *Science*, 312(5774):758.

Save, E., Cressant, A., Thinus-Blanc, C., and Poucet, B. (1998). Spatial firing of hippocampal place cells in blind rats. *The Journal of Neuroscience*, 18(5):1818–1826.

Save, E., Nerad, L., and Poucet, B. (2000). Contribution of multiple sensory information to place field stability in hippocampal place cells. *Hippocampus*, 10(1):64–76.

Save, E., Paz-Villagran, V., Alexinsky, T., and Poucet, B. (2005). Functional interaction between the associative parietal cortex and hippocampal place cell firing in the rat. *European Journal of Neuroscience*, 21(2):522–530.

Save, E. and Poucet, B. (2009). Role of the parietal cortex in long-term representation of spatial information in the rat. *Neurobiology of Learning and Memory*, 91(2):172–178.

Savelli, F., Yoganarasimha, D., and Knierim, J. J. (2008). Influence of boundary removal on the spatial representations of the medial entorhinal cortex. *Hippocampus*, 18(12):1270–1282. 19021262[pmid] PMC3007674[pmcid] Hippocampus.

Schindelin, J., Arganda-Carreras, I., Frise, E., Kaynig, V., Longair, M., Pietzsch, T., Preibisch, S., Rueden, C., Saalfeld, S., Schmid, B., Tinevez, J.-Y., White, D. J., Hartenstein, V., Eliceiri, K., Tomancak, P., and Cardona, A. (2012). Fiji: an open-source platform for biological-image analysis. *Nature Methods*, 9:676.

Schmitzer-Torbert, N., Jackson, J. L., Henze, D., Harris, K. I., and Redish, A. D. (2005). Quantitative measures of cluster quality for use in extracellular recordings. *Neuroscience*, 131:1–11.

Scholl, B., Tan, A. Y. Y., Corey, J., and Priebe, N. J. (2013). Emergence of orientation selectivity in the mammalian visual pathway. *The Journal of neuroscience : the official journal of the Society for Neuroscience*, 33(26):10616–10624. 23804085[pmid] PMC3693051[pmcid] 33/26/10616[PII].

Schuett, S., Bonhoeffer, T., and Hübener, M. (2002). Mapping retinotopic structure in mouse visual cortex with optical imaging. *The Journal of Neuroscience*, 22(15):6549–6559.

Schwarz, S., Mangan, M., Zeil, J., Webb, B., and Wystrach, A. (2017). How ants use vision when homing backward. *Current Biology*, 27(3):401–407.

Seelig, J. D. and Jayaraman, V. (2015). Neural dynamics for landmark orientation and angular path integration. *Nature*, 521(7551):186–191. 25971509[pmid] PMC4704792[pmcid] nature14446[PII].

Sefton, A. J., Dreher, B., Harvey, A. R., and Martin, P. R. (2015). *Chapter 30 - Visual System*, pages 947–983. Academic Press, San Diego.

Séguinot, V., Maurer, R., and Etienne, A. S. (1993). Dead reckoning in a small mammal: the evaluation of distance. *Journal of Comparative Physiology A*, 173(1):103–113.

Seki, M. and Zyo, K. (1984). Anterior thalamic afferents from the mamillary body and the limbic cortex in the rat. *Journal of Comparative Neurology*, 229(2):242–256.

Semm, P. (1978). Antidromically activated direction selective ganglion cells of the rabbit. *Neuroscience Letters*, 9(2):207–211.

Sharp, P. and Green, C. (1994). Spatial correlates of firing patterns of single cells in the subiculum of the freely moving rat. *The Journal of Neuroscience*, 14(4):2339–2356.

Sharp, P. E. (1999). Subicular place cells expand or contract their spatial firing pattern to fit the size of the environment in an open field but not in the presence of barriers: Comparison with hippocampal place cells. *Behavioral Neuroscience*, 113(4):643–662.

Sharp, P. E. (2005). *Regional distribution and variation in the firing properties of head direction cells*, book section 1. The MIT Press, Cambridge, MA.

Sharp, P. E., Blair, H. T., and Cho, J. (2001a). The anatomical and computational basis of the rat head-direction cell signal. *Trends in Neurosciences*, 24(5):289–294.

Sharp, P. E., Tinkelman, A., and Cho, J. (2001b). Angular velocity and head direction signals recorded from the dorsal tegmental nucleus of gudden in the rat: Implications for path integration in the head direction cell circuit. *Behavioral Neuroscience*, 115(3):571–588.

Sherman, S. M. (2007). The thalamus is more than just a relay. *Current opinion in neurobiology*, 17(4):417–422. 17707635[pmid] Curr Opin Neurobiol.

Shibata, H. (1987). Ascending projections to the mammillary nuclei in the rat: A study using retrograde and anterograde transport of wheat germ agglutinin conjugated to horseradish peroxidase. *Journal of Comparative Neurology*, 264(2):205–215.

Shibata, H. (1992). Topographic organization of subcortical projections to the anterior thalamic nuclei in the rat. *Journal of Comparative Neurology*, 323(1):117–127.

Shimizu, T. and Bowers, A. N. (1999). Visual circuits of the avian telencephalon: evolutionary implications. *Behavioural Brain Research*, 98(2):183–191.

Shipp, S. (2003). The functional logic of cortico-pulvinar connections. *Philosophical Transactions of the Royal Society B: Biological Sciences*, 358(1438):1605–1624. 14561322[pmid] Philos Trans R Soc Lond B Biol Sci.

Shrager, Y., Kirwan, C. B., and Squire, L. R. (2008). Neural basis of the cognitive map: Path integration does not require hippocampus or entorhinal cortex. *Proceedings of the National Academy of Sciences*, 105(33):12034–12038.

Siminoff, R., Schwassmann, H. O., and Kruger, L. (1966). An electrophysiological study of the visual projection to the superior colliculus of the rat. *Journal of Comparative Neurology*, 127(4):435–444.

Simon, P., Dupuis, R., and Costentin, J. (1994). Thigmotaxis as an index of anxiety in mice. influence of dopaminergic transmissions. *Behavioural Brain Research*, 61(1):59–64.

Simonnet, J., Eugène, E., Cohen, I., Miles, R., and Fricker, D. (2013). Cellular neuroanatomy of rat presubiculum. *European Journal of Neuroscience*, 37(4):583–597.

Sinnamon, H. M. and Galer, B. S. (1984). Head movements elicited by electrical stimulation of the anteromedial cortex of the rat. *Physiology & Behavior*, 33(2):185–190.

Skaggs, W. E., Knierim, J. J., Kudrimoti, H. S., and McNaughton, B. L. (1995). A model of the neural basis of the rat's sense of direction. In Tesauro, G., Touretzky, D. S., and Leen, T. K., editors, *Advances in Neural Information Processing Systems 7*, pages 173–180. MIT Press.

Skaggs, W. E., McNaughton, B. L., and Gothard, K. M. (1993). An information-theoretic approach to deciphering the hippocampal code. In Hanson, S. J., Cowan, J. D., and Giles, C. L., editors, *Advances in Neural Information Processing Systems 5*, pages 1030–1037. Morgan-Kaufmann.

Smythies, J. R., Edelstein, L. R., and Ramachandran, V. S. (2014). *Chapter 13 - Hypotheses Relating to the Function of the Claustrum*, pages 299–352. Academic Press, San Diego.

Solstad, T., Boccara, C. N., Kropff, E., Moser, M.-B., and Moser, E. I. (2008). Representation of geometric borders in the entorhinal cortex. *Science*, 322(5909):1865.

Solstad, T., Moser, E. I., and Einevoll, G. T. (2006). From grid cells to place cells A mathematical model. *Hippocampus*, 16(12):1026–1031.

Song, P. and Wang, X.-J. (2005). Angular path integration by moving "hill of activity": A spiking neuron model without recurrent excitation of the head-direction system. *The Journal of Neuroscience*, 25(4):1002–1014.

Sparks, D. L. and Hartwich-Young, R. (1989). The deep layers of the superior colliculus. *Reviews of oculomotor research*, 3:213–55.

Spiers, H. J., Hayman, R. M. A., Jovalekic, A., Marozzi, E., and Jeffery, K. J. (2015). Place field repetition and purely local remapping in a multicompartment environment. *Cerebral cortex (New York, N.Y. : 1991)*, 25(1):10–25. 23945240[pmid] PMC4400414[pmcid] bht198[PII].

Stackman, R. W., Clark, A. S., and Taube, J. S. (2002). Hippocampal spatial representations require vestibular input. *Hippocampus*, 12(3):291–303.

Stackman, R. W. and Taube, J. S. (1997). Firing properties of head direction cells in the rat anterior thalamic nucleus: dependence on vestibular input. *The Journal of neuroscience : the official journal of the Society for Neuroscience*, 17(11):4349–4358. 9151751[pmid] PMC1489676[pmcid].

Stackman, R. W. and Taube, J. S. (1998). Firing properties of rat lateral mammillary single units: Head direction, head pitch, and angular head velocity. *The Journal of Neuroscience*, 18(21):9020–9037.

Stensola, H., Stensola, T., Solstad, T., Frøland, K., Moser, M.-B., and Moser, E. I. (2012). The entorhinal grid map is discretized. *Nature*, 492:72.

Stewart, S., Jeewajee, A., Wills Thomas, J., Burgess, N., and Lever, C. (2014). Boundary coding in the rat subiculum. *Philosophical Transactions of the Royal Society B: Biological Sciences*, 369(1635):20120514.

Stringer, S. M., Trappenberg, T. P., Rolls, E. T., and Araujo, I. E. T. d. (2002). Self-organizing continuous attractor networks and path integration: one-dimensional models of head direction cells. *Network: Computation in Neural Systems*, 13(2):217–242.

Stürzl, W., Cheung, A., Cheng, K., and Zeil, J. (2008). The information content of panoramic images i: The rotational errors and the similarity of views in rectangular experimental arenas. *Journal of Experimental Psychology: Animal Behavior Processes*, 34(1):1–14.

Su, H.-S. and Bentivoglio, M. (1990). Thalamic midline cell populations projecting to the nucleus accumbens, amygdala, and hippocampus in the rat. *Journal of Comparative Neurology*, 297(4):582–593.

Takahashi, T. (1985). The organization of the lateral thalamus of the hooded rat. *The Journal of Comparative Neurology*, 231(3):281–309.

Tang, J., Ardila Jimenez, S. C., Chakraborty, S., and Schultz, S. R. (2016). Visual receptive field properties of neurons in the mouse lateral geniculate nucleus. *PLOS ONE*, 11(1):e0146017.

Taube, J. (1995a). Head direction cells recorded in the anterior thalamic nuclei of freely moving rats. *The Journal of Neuroscience*, 15(1):70–86.

Taube, J., Muller, R., and Ranck, J. (1990a). Head-direction cells recorded from the postsubiculum in freely moving rats. i. description and quantitative analysis. *The Journal of Neuroscience*, 10(2):420–435.

Taube, J., Muller, R., and Ranck, J. (1990b). Head-direction cells recorded from the postsubiculum in freely moving rats. ii. effects of environmental manipulations. *The Journal of Neuroscience*, 10(2):436–447.

Taube, J. S. (1995b). Place cells recorded in the parasubiculum of freely moving rats. *Hippocampus*, 5(6):569–583.

Taube, J. S. (2007). The head direction signal: Origins and sensory-motor integration. *Annual Review of Neuroscience*, 30(1):181–207.

Taube, J. S. and Burton, H. L. (1995). Head direction cell activity monitored in a novel environment and during a cue conflict situation. *Journal of Neurophysiology*, 74(5):1953–1971.

Taube, J. S., Kesslak, J. P., and Cotman, C. W. (1992). Lesions of the rat postsubiculum impair performance on spatial tasks. *Behavioral and Neural Biology*, 57(2):131–143.

Taube, J. S. and Muller, R. U. (1998). Comparisons of head direction cell activity in the postsubiculum and anterior thalamus of freely moving rats. *Hippocampus*, 8(2):87–108.

Tees, R. C. (1999). The effects of posterior parietal and posterior temporal cortical lesions on multimodal spatial and nonspatial competencies in rats. *Behavioural Brain Research*, 106(1):55–73.

Tocker, G., Borodach, E., Bjerknes, T. L., Moser, M.-B., Moser, E. I., and Derdikman, D. (2018). Head-direction drift in rat pups is consistent with an angular path-integration process. *bioRxiv*, page 212852.

Tohmi, M., Meguro, R., Tsukano, H., Hishida, R., and Shibuki, K. (2014). The extrageniculate visual pathway generates distinct response properties in the higher visual areas of mice. *Current Biology*, 24(6):587–597.

Tolman, E. (1948). Cognitive maps in rats and men. *The Psychological Review*, 55(4):189–208.

Tomás Pereira, I., Agster, K. L., and Burwell, R. D. (2016). Subcortical connections of the perirhinal, postrhinal, and entorhinal cortices of the rat. i. afferents. *Hippocampus*, 26(9):1189–1212. 27119220[pmid] PMC5070464[pmcid].

Torrealba, F. and Valdés, J. L. (2008). The parietal association cortex of the rat. *Biological Research*, 41:369 – 377.

Tsanov, M., Chah, E., Vann, S. D., Reilly, R., Erichsen, J. T., Aggleton, J. P., and O'Mara, S. M. (2011a). Theta-modulated head-direction cells in the rat anterior thalamus. *The Journal of neuroscience : the official journal of the Society for Neuroscience*, 31(26):10.1523/JNEUROSCI.0353–11.2011. 21715614[pmid] J Neurosci.

Tsanov, M., Chah, E., Wright, N., Vann, S. D., Reilly, R., Erichsen, J. T., Aggleton, J. P., and O'Mara, S. M. (2011b). Oscillatory entrainment of thalamic neurons by theta rhythm in freely moving rats. *Journal of Neurophysiology*, 105(1):4–17.

Tukker, J. J., Tang, Q., Burgalossi, A., and Brecht, M. (2015). Head-directional tuning and theta modulation of anatomically identified neurons in the presubiculum. *The Journal of Neuroscience*, 35(46):15391–15395.

Ungerleider, L. G. and Haxby, J. V. (1994). 'what' and 'where' in the human brain. *Current Opinion in Neurobiology*, 4(2):157–165.

Usrey, W. M. and Alitto, H. J. (2015). Visual functions of the thalamus. *Annual Review of Vision Science*, 1(1):351–371.

Valerio, S. and Taube, J. S. (2012). Path integration: how the head direction signal maintains and corrects spatial orientation. *Nature neuroscience*, 15(10):1445–1453.

Valerio, S. and Taube, J. S. (2016). Head direction cell activity is absent in mice without the horizontal semicircular canals. *The Journal of neuroscience : the official journal of the Society for Neuroscience*, 36(3):741–754. 26791205[pmid] PMC4719012[pmcid] 36/3/741[PII].

Van Cauter, T., Poucet, B., and Save, E. (2008). Unstable ca1 place cell representation in rats with entorhinal cortex lesions. *European Journal of Neuroscience*, 27(8):1933–1946.

van der Meer, M. A. A., Richmond, Z., Braga, R. M., Wood, E. R., and Dudchenko, P. A. (2010). Evidence for the use of an internal sense of direction in homing. *Behavioral Neuroscience*, 124(1):164–169.

van Groen, T. and Wyss, J. M. (1990a). The connections of presubiculum and parasubiculum in the rat. *Brain Research*, 518(1):227–243.

van Groen, T. and Wyss, J. M. (1990b). Connections of the retrosplenial granular a cortex in the rat. *Journal of Comparative Neurology*, 300(4):593–606.

van Groen, T. and Wyss, J. M. (1990c). The postsubicular cortex in the rat: characterization of the fourth region of the subicular cortex and its connections. *Brain Research*, 529(1):165–177.

van Groen, T. and Wyss, J. M. (1992). Connections of the retrosplenial dysgranular cortex in the rat. *Journal of Comparative Neurology*, 315(2):200–216.

Van Groen, T. and Wyss, J. M. (2003). Connections of the retrosplenial granular b cortex in the rat. *Journal of Comparative Neurology*, 463(3):249–263.

van Strien, N. M., Cappaert, N. L. M., and Witter, M. P. (2009). The anatomy of memory: an interactive overview of the parahippocampal–hippocampal network. *Nature Reviews Neuroscience*, 10:272.

Vanegas, H. (1984). *Comparative Neurology of the Optic Tectum*. Springer US, 1 edition.

Vann, S. D. and Aggleton, J. P. (2004). The mammillary bodies: two memory systems in one? *Nature Reviews Neuroscience*, 5(1):35–44.

Vertes, R. P., Albo, Z., and Viana Di Prisco, G. (2001). Theta-rhythmically firing neurons in the anterior thalamus: implications for mnemonic functions of papez's circuit. *Neuroscience*, 104(3):619–625.

Viskontas, I. V., Ekstrom, A. D., Wilson, C. L., and Fried, I. (2007). Characterizing interneuron and pyramidal cells in the human medial temporal lobe in vivo using extracellular recordings. *Hippocampus*, 17(1):49–57.

Wagor, E., Mangini, N. J., and Pearlman, A. L. (1980). Retinotopic organization of striate and extrastriate visual cortex in the mouse. *Journal of Comparative Neurology*, 193(1):187–202.

Wallace, D. G., Hines, D. J., Pellis, S. M., and Whishaw, I. Q. (2002). Vestibular information is required for dead reckoning in the rat. *The Journal of Neuroscience*, 22(22):10009–10017.

Wang, C., Chen, X., Lee, H., Deshmukh, S. S., Yoganarasimha, D., Savelli, F., and Knierim, J. J. (2018). Egocentric coding of external items in the lateral entorhinal cortex. *Science*, 362(6417):945–949.

Wang, L., Sarnaik, R., Rangarajan, K., Liu, X., and Cang, J. (2010). Visual receptive field properties of neurons in the superficial superior colliculus of the mouse. *The Journal of neuroscience : the official journal of the Society for Neuroscience*, 30(49):16573–16584. 21147997[pmid] PMC3073584[pmcid] 30/49/16573[PII] J Neurosci.

Wang, Q. and Burkhalter, A. (2007). Area map of mouse visual cortex. *Journal of Comparative Neurology*, 502(3):339–357.

Wang, Q., Gao, E., and Burkhalter, A. (2011). Gateways of ventral and dorsal streams in mouse visual cortex. *The Journal of neuroscience : the official journal of the Society for Neuroscience*, 31(5):1905–1918. 21289200[pmid] J Neurosci.

Wang, Q., Sporns, O., and Burkhalter, A. (2012). Network analysis of corticocortical connections reveals ventral and dorsal processing streams in mouse visual cortex. *The Journal of Neuroscience*, 32(13):4386–4399.

Wehner, R. (2003). Desert ant navigation: how miniature brains solve complex tasks. *Journal of Comparative Physiology A*, 189(8):579–588.

Westheimer, G. (2001). The fourier theory of vision. *Perception*, 30(5):531–541.

Weyand, Theodore, G. (2016). The multifunctional lateral geniculate nucleus.

Whitlock, J. R. and Derdikman, D. (2012). Head direction maps remain stable despite grid map fragmentation. *Frontiers in neural circuits*, 6:9–9. 22479237[pmid] PMC3314958[pmcid] Front Neural Circuits.

Whitlock, J. R., Sutherland, R. J., Witter, M. P., Moser, M.-B., and Moser, E. I. (2008). Navigating from hippocampus to parietal cortex. *Proceedings of the National Academy of Sciences of the United States of America*, 105(39):14755–14762. 18812502[pmid] 4715[PII] Proc Natl Acad Sci U S A.

WHO Patient Safety and World Health Organization (2009). Who guidelines for safe surgery : 2009 :safe surgery saves lives.

Wiener, S. (1993). Spatial and behavioral correlates of striatal neurons in rats performing a self-initiated navigation task. *The Journal of Neuroscience*, 13(9):3802–3817.

Wilber, A. A., Clark, B. J., Demecha, A. J., Mesina, L., Vos, J. M., and McNaughton, B. L. (2015). Cortical connectivity maps reveal anatomically distinct areas in the parietal cortex of the rat. *Frontiers in Neural Circuits*, 8(146).

Wilber, A. A., Clark, B. J., Forster, T. C., Tatsuno, M., and McNaughton, B. L. (2014). Interaction of egocentric and world-centered reference frames in the rat posterior parietal cortex. *The Journal of Neuroscience*, 34(16):5431–5446.

Wilton, L. A. K., Baird, A. L., Muir, J. L., Honey, R. C., and Aggleton, J. P. (2001). Loss of the thalamic nuclei for "head direction" impairs performance on spatial memory tasks in rats. *Behavioral Neuroscience*, 115(4):861–869.

Winter, S. S., Clark, B. J., and Taube, J. S. (2015). Disruption of the head direction cell network impairs the parahippocampal grid cell signal. *Science*, 347(6224):870–874.

Winter, S. S. and Taube, J. S. (2014). *Head Direction Cells: From Generation to Integration*, pages 83–106. Springer Vienna, Vienna.

Wittgenstein, L. (1922). *Tractatus Logico-Philosophicus*. KEGAN PAUL, TRENCH, TRUBNER & CO., LTD., London. [C.K. Ogden, Trans. (2010)].

Woodward, W. R., Chiaia, N., Teyler, T. J., Leong, L., and Coull, B. M. (1990). Organization of cortical afferent and efferent pathways in the white matter of the rat visual system. *Neuroscience*, 36(2):393–401.

Woodward, W. R. and Coull, B. M. (1984). Localization and organization of geniculocortical and corticofugal fiber tracts within the subcortical white matter. *Neuroscience*, 12(4):1089–1099.

Wyss, J. M. and Van Groen, T. (1992). Connections between the retrosplenial cortex and the hippocampal formation in the rat: A review. *Hippocampus*, 2(1):1–11.

Wystrach, A., Dewar, A., Philippides, A., and Graham, P. (2016). How do field of view and resolution affect the information content of panoramic scenes for visual navigation? a computational investigation. *Journal of comparative physiology. A, Neuroethology, sensory, neural, and behavioral physiology*, 202(2):87–95. 26582183[pmid] PMC4722065[pmcid] 10.1007/s00359-015-1052-1[PII].

Yoder, R. M., Clark, B. J., and Taube, J. S. (2011). Origins of landmark encoding in the brain. *Trends in Neurosciences*, 34(11):561–571.

Yoder, R. M., Peck, J. R., and Taube, J. S. (2015). Visual landmark information gains control of the head direction signal at the lateral mammillary nuclei. *The Journal of Neuroscience*, 35(4):1354–1367.

Yoder, R. M. and Taube, J. S. (2009). Head direction cell activity in mice: robust directional signal depends on intact otolith organs. *The Journal of neuroscience : the official journal of the Society for Neuroscience*, 29(4):1061–1076. 19176815[pmid] PMC2768409[pmcid] 29/4/1061[PII].

Yoder, R. M. and Taube, J. S. (2011). Projections to the anterodorsal thalamus and lateral mammillary nuclei arise from different cell populations within the postsubiculum: implications for the control of head direction cells. *Hippocampus*, 21(10):1062–1073. 20575008[pmid] PMC2975049[pmcid] Hippocampus.

Yoder, R. M. and Taube, J. S. (2014). The vestibular contribution to the head direction signal and navigation. *Frontiers in Integrative Neuroscience*, 8(32).

Yoganarasimha, D. and Knierim, J. J. (2005). Coupling between place cells and head direction cells during relative translations and rotations of distal landmarks. *Experimental Brain Research*, 160(3):344–359.

Yoganarasimha, D., Yu, X., and Knierim, J. J. (2006). Head direction cell representations maintain internal coherence during conflicting proximal and distal cue rotations: Comparison with hippocampal place cells. *The Journal of Neuroscience*, 26(2):622–631.

Youngstrom, I. A. and Strowbridge, B. W. (2012). Visual landmarks facilitate rodent spatial navigation in virtual reality environments. *Learning & memory*, 19(3):84–90. 22345484[pmid] PMC3293517[pmcid] 19/3/84[PII].

Zar, J. H. (2010). *Biostatistical Analysis*. Pearson, Northern Illinois University, 5th edition edition.

Zeil, J. (2012). Visual homing: an insect perspective. *Current Opinion in Neurobiology*, 22(2):285–293.

Zhang, K. (1996). Representation of spatial orientation by the intrinsic dynamics of the head-direction cell ensemble: a theory. *The Journal of Neuroscience*, 16(6):2112–2126.

Zhao, X., Chen, H., Liu, X., and Cang, J. (2013). Orientation-selective responses in the mouse lateral geniculate nucleus. *The Journal of neuroscience : the official journal of the Society for Neuroscience*, 33(31):12751–12763. 23904611[pmid] PMC3728687[pmcid] 33/31/12751[PII].

Zhou, N., Masterson, S. P., Damron, J. K., Guido, W., and Bickford, M. E. (2018). The mouse pulvinar nucleus links the lateral extrastriate cortex, striatum, and amygdala. *The Journal of Neuroscience*, 38(2):347–362.

Zhou, N. A., Maire, P. S., Masterson, S. P., and Bickford, M. E. (2017). The mouse pulvinar nucleus: Organization of the tectorecipient zones. *Visual Neuroscience*, 34:E011.

Zilli, E. (2012). Models of grid cell spatial firing published 2005–2011. *Frontiers in Neural Circuits*, 6(16).

Zugaro, M. B., Berthoz, A., and Wiener, S. I. (2001). Background, but not foreground, spatial cues are taken as references for head direction responses by rat anterodorsal thalamus neurons. *The Journal of Neuroscience*, 21(14):RC154–RC154.

Zugaro, M. B., Tabuchi, E., and Wiener, S. I. (2000). Influence of conflicting visual, inertial and substratal cues on head direction cell activity. *Experimental Brain Research*, 133(2):198–208.